Faculty of
Aerospace Engineering

A Cybernetic Analysis of Biodynamic Effects in Turbulence on Touchscreen Continuous-Dragging Tasks

X. R. I. Mobertz

21 September 2017

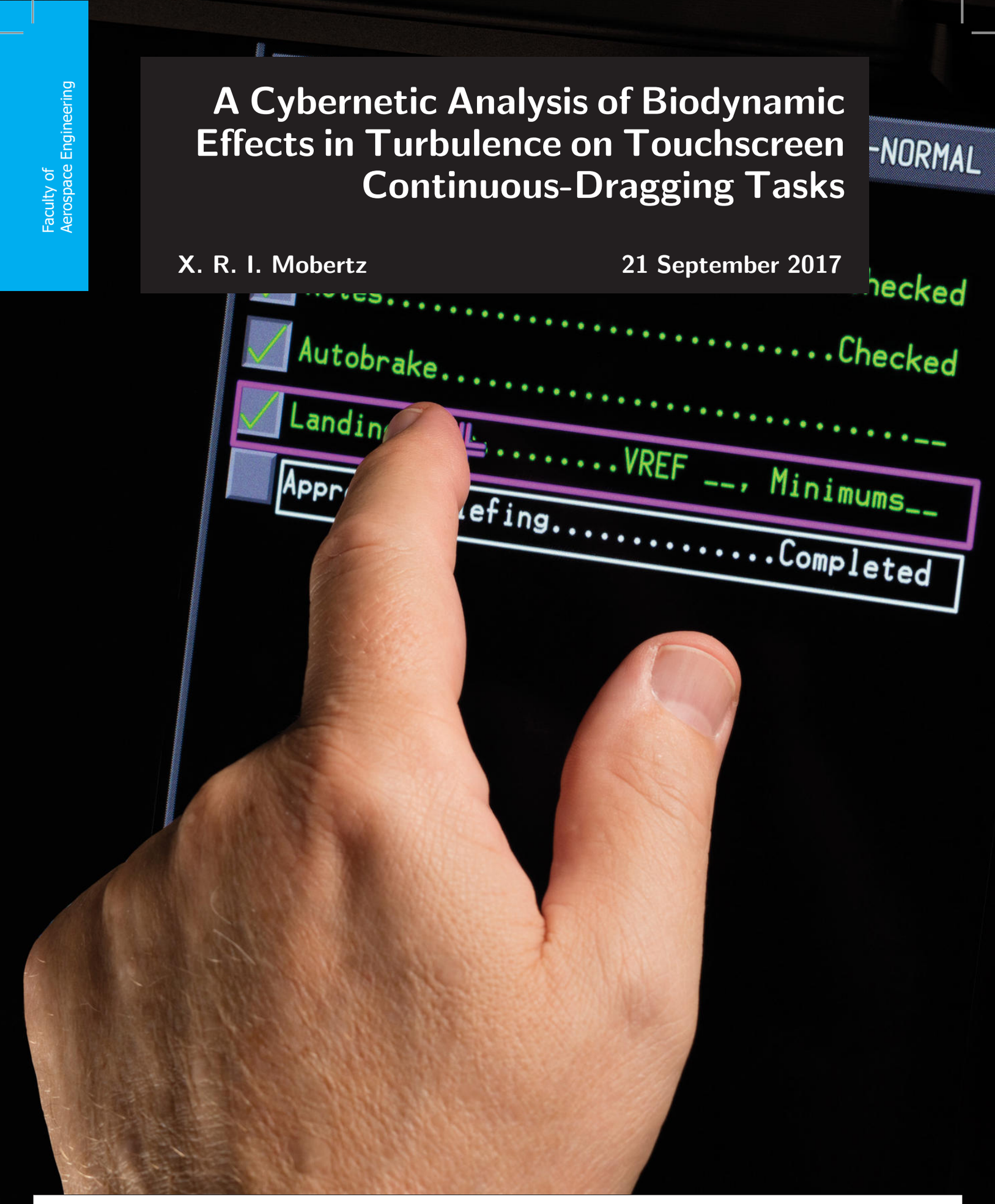

TU Delft Delft University of Technology

Challenge the future

A Cybernetic Analysis of Biodynamic Effects in Turbulence on Touchscreen Continuous-Dragging Tasks

Master of Science Thesis

For obtaining the degree of Master of Science in Aerospace Engineering at Delft University of Technology

X. R. I. Mobertz

21 September 2017

Cover Image [1]

Delft University of Technology

Copyright © X. R. I. Mobertz
All rights reserved.

Delft University Of Technology
Department Of
Control and Simulation

The undersigned hereby certify that they have read and recommend to the Faculty of Aerospace Engineering for acceptance a thesis entitled **"A Cybernetic Analysis of Biodynamic Effects in Turbulence on Touchscreen Continuous-Dragging Tasks"** by **X. R. I. Mobertz** in partial fulfillment of the requirements for the degree of **Master of Science**.

Dated: 21 September 2017

Readers:

dr.ir. D. M. Pool

prof.dr.ir. M. Mulder

dr.ir. M. M. van Paassen

dr.ir. J. C. F. de Winter

Acknowledgements

This Thesis Report marks the end of a remarkable chapter in my life during which aerospace knowledge was gained, many friendships were born and valuable life lessons were learned. Especially the final stages of this study were memorable, and it is because of the enthusiasm and dedication of my supervisors that university started to feel more like a hobby, rather than school. Of course, this all started with Max who enthused me for the department of Control & Simulation and provided me with the incredible opportunity to put all this knowledge into use at NASA. Daan, thank you for the many meetings that we had during my work, in which you provided so much guidance and support. I am sure that my thesis wouldn't have reached half the quality it has now, if it weren't for you. René, thank you for helping me out with the DUECA simulations and the valuable inputs you made during the experiment design. Although he may not have been my supervisor, I would also like to express my gratitude towards Olaf, who helped me many times prior and during my experiment with (his) SIMONA.

Then, I would like to thank my roomies in SIM 0.08 for providing the needed and not-needed diversions from work, the many laughs during breaks and the memorable drinks at the Atmosfeer. Graduating wouldn't have been the same without you guys, and you always motivated me to come in and work together with you.

All of this, however, wouldn't have been possible without the support of my parents. You allowed me to start with this incredible adventure in the first place and supported me with whatever decision I made. I am truly forever grateful for this opportunity you gave me.

Finally I want to thank you Rowie, for being patient with me after coming home so late for these last few months. I am sure that my time here in Delft wouldn't have been as enjoyable without you, and I look forward to the many adventures together in the future.

Xander
Delft, 21 September 2017

Contents

Acknowledgements v

List of Figures xiv

List of Tables xv

Nomenclature xvii

1 Report Introduction 1
- 1-1 Problem Statement . . . 3
- 1-2 Methodology . . . 4
- 1-3 Thesis Report Outline . . . 4

I AIAA Paper 5

II Preliminary Report 29

2 Preliminary Research Questions 31

3 Turbulence 33
- 3-1 Definition of Turbulence . . . 33
  - 3-1-1 Mechanisms for Atmospheric Turbulence . . . 34
  - 3-1-2 Examples of Atmospheric Turbulence . . . 35
- 3-2 Intensity of Turbulence . . . 35
- 3-3 Effects of vibration on Human Performance . . . 37
  - 3-3-1 Visual Impairment . . . 37
  - 3-3-2 Neuromuscular Interference . . . 37
  - 3-3-3 Central Effects . . . 38
  - 3-3-4 Vibration Feedthrough . . . 38
- 3-4 Summary . . . 39

4 Touch Sensitive Displays **41**
4-1 Advantages of Touchscreen Technology . . . 41
4-2 Disadvantages of Touchscreen Technology . . . 42
4-3 Display Interaction Methods . . . 43
4-3-1 Interaction Methods . . . 43
4-3-2 Activation Methods . . . 46
4-4 Current Implementations and Future Visions . . . 47
4-5 Effects of BDFT on the use of Touchscreens . . . 48
4-5-1 Effects of BDFT with varying controller postures . . . 48
4-5-2 Effects of BDFT with varying TSC gestures and vibration levels . . . 49
4-6 Summary . . . 50

5 Conclusion and Recommendations **51**
5-1 Answers to Research Questions . . . 51
5-2 Literature Study Recommendations . . . 53

6 Preliminary Experiment Setup **55**
6-1 Experiment Objective . . . 55
6-2 Control Task . . . 56
6-3 Forcing Functions . . . 57
6-4 Apparatus . . . 58
6-5 Implementation . . . 59
6-6 Participants and Procedures . . . 60

7 Preliminary Experiment Results **61**
7-1 Power Spectral Densities . . . 61
7-1-1 PSD: Horizontal input . . . 62
7-1-2 PSD: Vertical input . . . 62
7-2 Biodynamic Feedthrough Estimation . . . 64
7-3 Performance . . . 65
7-4 Experiment Discussions & Recommendations . . . 67
7-4-1 Results Discussion . . . 67
7-4-2 Experiment Conclusion and Recommendations . . . 69

8 Research Proposal **71**
8-1 Research Question . . . 71
8-2 Experimental Setup . . . 71
8-2-1 Control Variables . . . 72
8-2-2 Independent Variables . . . 72
8-2-3 Dependent Variables . . . 73
8-2-4 Participants . . . 74
8-2-5 Experimental Procedure . . . 74
8-2-6 Apparatus . . . 75
8-3 Results, Outcome and Relevance . . . 75

9 Conclusions & Future Steps **77**
9-1 Conclusions . . . 77
9-2 Future Steps . . . 78

III Appendices **79**

A Motion Disturbance **81**

B Experiment Briefing **85**

C BDFT Parameter Estimation Results **89**
Parameters Estimates: Participant 2 . . . 90
Parameters Estimates: Participant 3 . . . 94
Parameters Estimates: Participant 4 . . . 98
Parameters Estimates: Participant 5 . . . 102
Parameters Estimates: Participant 6 . . . 106
Parameters Estimates: Participant 7 . . . 110
Parameters Estimates: Participant 8 . . . 114
Parameters Estimates: Participant 9 . . . 118
Parameters Estimates: Participant 10 . . . 122
Parameters Estimates: Participant 11 . . . 126
Parameters Estimates: Participant 12 . . . 130
Parameters Estimates: Participant 13 . . . 134
Parameters Estimates: Participant 14 . . . 138
Parameters Estimates: Participant 15 . . . 142
Parameters Estimates: Participant 16 . . . 146
Parameters Estimates: Participant 17 . . . 150

D Performance **155**
Performance: Participant 2 . . . 156
Performance: Participant 3 . . . 156
Performance: Participant 4 . . . 157
Performance: Participant 5 . . . 157
Performance: Participant 6 . . . 158
Performance: Participant 7 . . . 158
Performance: Participant 8 . . . 159
Performance: Participant 9 . . . 159
Performance: Participant 10 . . . 160
Performance: Participant 11 . . . 160
Performance: Participant 12 . . . 161
Performance: Participant 13 . . . 161
Performance: Participant 14 . . . 162
Performance: Participant 15 . . . 162
Performance: Participant 16 . . . 163
Performance: Participant 17 . . . 163

E Experiment Curiosities **165**

Bibliography **172**

List of Figures

1-1 Evolution of the flight deck. 1
1-2 Touch screen controllers in the flight deck environment. 2

3-1 A breakdown of 'Turbulence'. 33
3-2 Cross-section of conditions associated with mountain waves. 34
3-3 Turbulence vector reference system. 35
3-4 Turbulence reporting classifications of turbulence. 36
3-5 ISO2631 Co-ordinate system for mechanical vibration influencing humans. . . 37
3-6 Variables associated with BDFT. 38

4-1 Example of non-intuitive control interface for display interaction. 41
4-2 Example of glare effects when using TSCs on the flight deck. 42
4-3 A selection of TSC Gestures. 45
4-4 Example of a waypoint modification gesture. 47
4-5 Estimate of ETW, as a function of vibration frequency and target location. . 48
4-6 TSC locations evaluated by Dodd 49

6-1 Visual representation of the preliminary experiment interface. 55
6-2 Visual representation of motion disturbance directions. 56
6-3 Motion disturbance signal $f_{d_{faded}}$ 58
6-4 The SIMONA Research Simulator and the preliminary experiment setup. . . . 59

7-1 PSDs of the target and motion disturbance signals 62
7-2 Horizontal input PSD, averaged over all participants. 63

7-3 Vertical input PSD, averaged over all participants. 63
7-4 Estimated Biodynamic Feedthrough, averaged over all participants. 64
7-5 Tracking error variance decomposition for horizontal inputs. 65
7-6 Vertical tracking error variance decomposition 66
7-7 Vertical tracking error variance decomposition, detailed image of baseline, sway and heave conditions. 66

8-1 Visual representation of the experiment control interface. 72
8-2 A schematic representation of the experiment. 73
8-3 The SIMONA Research Simulator and the experiment setup 75

A-1 Estimated Boeing 747 turbulence model. 82
A-2 Determining realistic turbulence 83

C-1 Parameters Estimates: Participant 2, Horizontal Inputs on CDU 90
C-2 Parameters Estimates: Participant 2, Vertical Inputs on CDU 91
C-3 Parameters Estimates: Participant 2, Horizontal Inputs on PFD 92
C-4 Parameters Estimates: Participant 2, Vertical Inputs on PFD 93
C-5 Parameters Estimates: Participant 3, Horizontal Inputs on CDU 94
C-6 Parameters Estimates: Participant 3, Vertical Inputs on CDU 95
C-7 Parameters Estimates: Participant 3, Horizontal Inputs on PFD 96
C-8 Parameters Estimates: Participant 3, Vertical Inputs on PFD 97
C-9 Parameters Estimates: Participant 4, Horizontal Inputs on CDU 98
C-10 Parameters Estimates: Participant 4, Vertical Inputs on CDU 99
C-11 Parameters Estimates: Participant 4, Horizontal Inputs on PFD 100
C-12 Parameters Estimates: Participant 4, Vertical Inputs on PFD 101
C-13 Parameters Estimates: Participant 5, Horizontal Inputs on CDU 102
C-14 Parameters Estimates: Participant 5, Vertical Inputs on CDU 103
C-15 Parameters Estimates: Participant 5, Horizontal Inputs on PFD 104
C-16 Parameters Estimates: Participant 5, Vertical Inputs on PFD 105
C-17 Parameters Estimates: Participant 6, Horizontal Inputs on CDU 106
C-18 Parameters Estimates: Participant 6, Vertical Inputs on CDU 107
C-19 Parameters Estimates: Participant 6, Horizontal Inputs on PFD 108
C-20 Parameters Estimates: Participant 6, Vertical Inputs on PFD 109
C-21 Parameters Estimates: Participant 7, Horizontal Inputs on CDU 110
C-22 Parameters Estimates: Participant 7, Vertical Inputs on CDU 111

C-23 Parameters Estimates: Participant 7, Horizontal Inputs on PFD 112
C-24 Parameters Estimates: Participant 7, Vertical Inputs on PFD 113
C-25 Parameters Estimates: Participant 8, Horizontal Inputs on CDU 114
C-26 Parameters Estimates: Participant 8, Vertical Inputs on CDU 115
C-27 Parameters Estimates: Participant 8, Horizontal Inputs on PFD 116
C-28 Parameters Estimates: Participant 8, Vertical Inputs on PFD 117
C-29 Parameters Estimates: Participant 9, Horizontal Inputs on CDU 118
C-30 Parameters Estimates: Participant 9, Vertical Inputs on CDU 119
C-31 Parameters Estimates: Participant 9, Horizontal Inputs on PFD 120
C-32 Parameters Estimates: Participant 9, Vertical Inputs on PFD 121
C-33 Parameters Estimates: Participant 10, Horizontal Inputs on CDU 122
C-34 Parameters Estimates: Participant 10, Vertical Inputs on CDU 123
C-35 Parameters Estimates: Participant 10, Horizontal Inputs on PFD 124
C-36 Parameters Estimates: Participant 10, Vertical Inputs on PFD 125
C-37 Parameters Estimates: Participant 11, Horizontal Inputs on CDU 126
C-38 Parameters Estimates: Participant 11, Vertical Inputs on CDU 127
C-39 Parameters Estimates: Participant 11, Horizontal Inputs on PFD 128
C-40 Parameters Estimates: Participant 11, Vertical Inputs on PFD 129
C-41 Parameters Estimates: Participant 12, Horizontal Inputs on CDU 130
C-42 Parameters Estimates: Participant 12, Vertical Inputs on CDU 131
C-43 Parameters Estimates: Participant 12, Horizontal Inputs on PFD 132
C-44 Parameters Estimates: Participant 12, Vertical Inputs on PFD 133
C-45 Parameters Estimates: Participant 13, Horizontal Inputs on CDU 134
C-46 Parameters Estimates: Participant 13, Vertical Inputs on CDU 135
C-47 Parameters Estimates: Participant 13, Horizontal Inputs on PFD 136
C-48 Parameters Estimates: Participant 13, Vertical Inputs on PFD 137
C-49 Parameters Estimates: Participant 14, Horizontal Inputs on CDU 138
C-50 Parameters Estimates: Participant 14, Vertical Inputs on CDU 139
C-51 Parameters Estimates: Participant 14, Horizontal Inputs on PFD 140
C-52 Parameters Estimates: Participant 14, Vertical Inputs on PFD 141
C-53 Parameters Estimates: Participant 15, Horizontal Inputs on CDU 142
C-54 Parameters Estimates: Participant 15, Vertical Inputs on CDU 143
C-55 Parameters Estimates: Participant 15, Horizontal Inputs on PFD 144
C-56 Parameters Estimates: Participant 15, Vertical Inputs on PFD 145

C-57 Parameters Estimates: Participant 16, Horizontal Inputs on CDU 146
C-58 Parameters Estimates: Participant 16, Vertical Inputs on CDU 147
C-59 Parameters Estimates: Participant 16, Horizontal Inputs on PFD 148
C-60 Parameters Estimates: Participant 16, Vertical Inputs on PFD 149
C-61 Parameters Estimates: Participant 17, Horizontal Inputs on CDU 150
C-62 Parameters Estimates: Participant 17, Vertical Inputs on CDU 151
C-63 Parameters Estimates: Participant 17, Horizontal Inputs on PFD 152
C-64 Parameters Estimates: Participant 17, Vertical Inputs on PFD 153

D-1 Error variance components for Participant 1 156
D-2 Error variance components for Participant 2 156
D-3 Error variance components for Participant 3 157
D-4 Error variance components for Participant 4 157
D-5 Error variance components for Participant 5 158
D-6 Error variance components for Participant 6 158
D-7 Error variance components for Participant 7 159
D-8 Error variance components for Participant 8 159
D-9 Error variance components for Participant 9 160
D-10 Error variance components for Participant 10 160
D-11 Error variance components for Participant 11 161
D-12 Error variance components for Participant 12 161
D-13 Error variance components for Participant 13 162
D-14 Error variance components for Participant 14 162
D-15 Error variance components for Participant 15 163
D-16 Error variance components for Participant 16 163

List of Tables

4-1 A selection of TSC gestures 45
4-2 Touch locations used by Rider. 48

6-1 Latin square used for the preliminary experiment. 56
6-2 Target and Disturbance forcing function properties. 58
6-3 Motion limits of the SIMONA Research Simulator 58

8-1 Experimental conditions used for the experiment. 73

A-1 Parameters of the estimated multisine Boeing 747 motion disturbance signal. 83

Nomenclature

List of Abbreviations

BDFT	Biodynamic Feedthrough
CAT	Clear Air Turbulence
CB	Cumulonimbus
CDU	Control Display Unit
CLS	Control Loading System
C&S	Control & Simulation
DUECA	Delft University Environment for Communication and Activation
EASA	European Aviation Safety Agency
ECI	Experiment Control Interface
EICAS	Engine-indicating and crew-alerting system
ETW	Effective Target Width
FFT	Fast Fourier Transform
FMS	Flight Management System
GA	Genetic Algorithm
GUI	Graphic User Interface
HMI	Human Machine Interaction
IAS	Indicated Air Speed
ICR	Instantaneous Center of Rotation
MLE	Maximum Likelihood Estimation
ND	Navigation Display
NMS	Neuromuscular System
PFD	Primary Flight Display
PSD	Power Spectral Density
RMS	Root Mean Square
SIMONA	SImulation, MOtion and NAvigation Institute
SNR	Signal to Noise Ratio
SRS	SIMONA Research Simulator
TSC	Touch Screen Controller

List of Symbols

A	Sinusoid amplitude	[deg]
b_{BDFT}	BDFT damping coefficient	[kg/sec]
e_x	Error from target in horizontal direction	[deg]
e_y	Error from target in vertical direction	[deg]
f_{d_x}	Disturbance forcing function (surge)	[deg]
f_{d_y}	Disturbance forcing function (sway)	[deg]
f_{d_z}	Disturbance forcing function (heave)	[deg]
f_{t_x}	Horizontal target forcing function	[deg]
f_{t_y}	Vertical target forcing function	[deg]
$g_{d,t}$	Fade-in function	[-]
G_{BDFT}	BDFT gain	[-]
H_{BDFT}	Transfer function describing BDFT dynamics	[-]
$\hat{H}_{BDFT}$	Estimate of transfer function describing BDFT dynamics	[-]
H_{NM}	Neuromuscular dynamics	[-]
H_P	Transfer function describing pilot model	[-]
i_r	Run number	[-]
k	Sinusoid index	[-]
k_{BDFT}	BDFT stiffness	[kg/sec^2]
m_{BDFT}	BDFT mass	[kg]
n_{loss}	TSC loss of contact instances	[-]
$n_{d,t}$	Sinusoid frequency integer factor	[-]
s	Laplace operator	[-]
t	Time	[sec]
t_{loss}	TSC loss of contact duration	[sec]
$\bar{u}_g$	Longitudinal gust velocity	$[m/sec]$
u_x	Screen input in horizontal direction	[deg]
u_y	Screen input in vertical direction	[deg]
$\bar{v}_g$	Side gust velocity	$[m/sec]$
$\bar{w}_g$	Vertical gust velocity	$[m/sec]$

$\sigma^2_{e_x}$	Variance of the horizontal input error	[deg^2]
$\sigma^2_{e_y}$	Variance of the vertical input error	[deg^2]
$\sigma^2_{u_x}$	Variance of horizontal control activity	[deg^2]
$\sigma^2_{u_y}$	Variance of vertical control activity	[deg^2]
$\sigma_{\bar{u}_g}$	Standard deviation of longitudinal gust velocity	$[m/sec]$
$\sigma_{\bar{v}_g}$	Standard deviation of side gust velocity	$[m/sec]$
$\sigma_{\bar{w}_g}$	Standard deviation of vertical gust velocity	$[m/sec]$
ω	Sinusoid frequency	$[rad/sec]$

Chapter 1

Report Introduction

Aircraft are becoming progressively more complex ever since the first heavier-than-air flight on December 17th in 1903, with increasing amounts of subsystems that are to be monitored from the flight deck. This is reflected by the increased cockpit complexity of these aircraft. Early-day aircraft such as the Douglas DC2 only required control interfaces for the basic flight controls (Figure 1-1a). The introduction of jets with multiple engines demanded for more dials to monitor engine parameters (Figure 1-1b). By the end of the 1970's, the number of controls and mechanical instruments in commercial aircraft already surpassed one hundred [2]. It was found that more information could be provided to the pilots with the introduction of displays (Figure 1-1c). The trend to increase the amount of information that is presented to the pilots continues with modern-era aircraft such as the Airbus A380 (Figure 1-1d).

(a) Douglas DC2 cockpit [3]

(b) Boeing 707-329 cockpit [4]

(c) Boeing 737-300 cockpit [5]

(d) Airbus A380-800 cockpit [6]

Figure 1-1: Evolution of the flight deck.

Adequate design of human-machine interfaces is required in order to keep insight in the automation and working principles of all these systems. Navigation through the sheer amount of information without affecting this insight, however, is a challenge. Current methods to accommodate all information using non-intuitive controls are already leading to pilot's loss of situation awareness [7, 8]. The solution might be to provide pilots with an interface that allows for direct manipulation of the data, which can be achieved with a touch screen controller (TSC). The idea is not new, as the use of touch screen technology in the aviation industry has already been proposed in a paper from 1965 [9].

More than fifty years later, the use is widespread and TSCs are integrated in consumer products varying from smartphones and industrial controllers to ATMs and Point of Sales (POS) kiosks. Within the flight deck environment, however, TSCs are still not common due to a number of unsolved challenges and the high safety requirements as posed by governing authorities [10].

First initiatives for the integration of TSCs in flightdecks were introduced by Garmin and Rockwell Collins for the General Aviation (GA) and business-jet markets in 2009 and 2011, respectively [11, 12], but TSCs for the commercial markets have been announced only recently by Boeing for the 777X series aircraft (Figure 1-2a)[13]. The continuation of the trend to introduce TSCs is underlined by Thales, who envisioned the future flightdeck to consist of a single, large touchscreen (Figure 1-2b)[14].

Although the implementation of TSCs has clear advantages over conventional systems, such as the improvement of situation awareness [15], there are also disadvantages that have to be considered. The lack of haptic feedback, effects of glare and worse input accuracy [16] are only some of these disadvantages. However, especially the influences of motion accelerations and vibrations caused by turbulence affects input performance for TSCs when implemented in the flightdeck [17]. In order to ensure acceptable piloting performance, flight integrity and airworthiness with this relatively new control system, it is important that the effects of motion disturbances on the use of TSCs are understood. Efforts towards quantitatively measuring TSC input errors resulting from biodynamic effects have been made before [18, 19]. Research that aims to model the biodynamic effects is however lacking.

This Thesis Report presents the research that was performed to measure and model these biodynamic effects on the use of TSCs in a cockpit environment as a result from motion disturbances, during continuous-dragging tasks. The AIAA paper is the result of this research and presented in Part I. The preliminary research is included in Part II and explains in detail how the main research question came to be. It also describes a preliminary experiment that was performed and presents its results. The Thesis Report concludes with appendices in Part III.

(a) Boeing 777-X cockpit [1] **(b)** Thales flightdeck of the future [14]

Figure 1-2: Touch screen controllers in the flight deck environment.

1-1 Problem Statement

The current section serves to motivate the research at hand and to present the scope of this Thesis Report. Furthermore, the research question is defined which is to be answered in the remainder of this Thesis Report.

Motivation The integration of TSC on the flight deck shows clear advantages over traditional systems. It can provide for a higher information density [20] whilst greatly improving intuitivity and situation awareness [17], especially when more natural gestures are used, e.g. zooming by pinching or dragging [21].

But with the introduction of TSCs in the flight deck of commercial aircraft, the disadvantages of this particular use are to be understood and possibly modeled as well, in order to warrant acceptable piloting performance, flight integrity and airworthiness. Previous work describing the effects of turbulence onto the use of TSCs does exist and has already shown a degradation in performance [19, 18, 22, 21, 23]. However, the process behind the reason why these errors occur, BDFT, has not been modeled before for such tasks. A model could help to mitigate the effects of BDFT through model-based signal cancellation [24].

Scope The scope of this Thesis Report is to present the research that was performed in three parts. Each has its own scope;

1. *AIAA paper:* Scope of the AIAA paper presented in Part I is to provide an answer to the research question as posed below in Section 8-1. Furthermore, it describes the human-in-the-loop experiment that was conducted in the SIMONA Research Simulator for this research, its results and the conclusions that can be drawn.
2. *Preliminary Report:* Scope of the Preliminary Report presented in Part II is to present an overview of current research in the field of TSC usage on the flightdeck, the advantages and disadvantages of this use, and in particular how motion disturbances affect the ability to perform piloting tasks. Based on the preliminary research question and its subquestions in Chapter 2, gaps in the present state of knowledge are identified to form the final research question posed below in Section 8-1. Feasibility of the research was tested by means of a preliminary experiment, and its setup and results are described in this part as well.
3. *Appendices:* Scope of the Appendices presented in Part III is to provide additional information on the experiment setup and its findings described in the AIAA paper in Part I.

Research Question The main research question followed from the preliminary research, presented in Part II and serves as a basis for the remainder of the research and the AIAA paper in I. This research question reads:

> **Research Question:** "How do motion disturbances influence pilot control skills and biodynamic feedthrough whilst performing a dragging task on flightdeck-based touch screen positioned at the PFD and FMS locations?"

1-2 Methodology

Prior to the main answering the main research question, a preliminary research was carried out. This preliminary research consisted of a literature review and a preliminary experiment- both are presented in Part II. In order to conduct the literature review, the preliminary research question was decomposed to two main categories; touch screen technology and turbulence. Each of those categories was reviewed by finding appropriate literature using Google Scholar, Scopus, AIAA, IEEE Xplore, the Delft University of Technology central library and the Delft UT Control & Simulation references database. The following keywords have been used during the research in various combinations;

> *Touchscreen, Turbulence, Display Location, Glass Cockpit, Flight Deck, Biodynamic Feedthrough, Human Vibration*

From the recommendations and research question that followed from the literature study, a preliminary research was carried out using the SRS at the Delft University of Technology. The data resulting from this experiment was analyzed using MATLAB.

The same methodology was used for the main experiment for purpose of the AIAA paper. Results of the MATLAB analysis were subsequently subject to statistical analysis using the SPSS software package.

1-3 Thesis Report Outline

This Thesis Report consists of three parts. Part I follows after this introduction and presents the AIAA paper which is the product of the final reseach experiment that was carried out. The paper describes a human-in-the-loop experiment that was performed and its results in order to answer the main research question at hand.

The basis for this research question was laid down in the preliminary research which is documented in the preliminary report in Part II. The first chapter in this preliminary report poses a preliminary research question with several subquestions. Using these questions, gaps in the present state of knowledge were identified using both a literature study and preliminary experiment to form the final research question.

Part III presents a set of appendices to provide information on efforts that have been taken to improve experimental design. Furthermore, additional results not given in the AIAA paper are presented.

Part I

AIAA Paper

A Cybernetic Analysis of Biodynamic Effects in Turbulence on Touchscreen Continuous-Dragging Tasks

Xander R.I. Mobertz*
Delft University of Technology
Delft, Netherlands

Although implementation of touchscreen controllers in the cockpit would offer many advantages over traditional interfaces, unsolved challenges such as unwanted inputs due to turbulence still stand in the way of large scale implementation. The study presented in this paper investigates the effects of biodynamic feedtrough on the execution of a way point dragging task on touch screens located in a turbulent cockpit. Two touch screens, located at positions similar to the Primary Flight Display (PFD) and Control Display Unit (CDU), were used by participants during the experiment whilst being perturbed by either surge, sway, heave or no disturbances.

Results show a highly significant increase in finger loss of contact using the CDU display when Heave disturbance was added to the control task. Highly significant differences between the PFD and CDU regarding finger loss of contact during the no motion condition reveal that participants have more trouble providing continuous inputs onto a PFD when compared to the CDU, due to lacking passive support with the use of PFDs. However, evidence was also found that target signals are more accurately tracked on PFD displays rather than CDU screens due to effects of parallax. Results furthermore indicate that effects of biodynamic feedthrough predominantly manifest themselves when motion disturbances act in the direction of touchscreen control inputs. Effects of biodynamic feedthrough are however also measured during off-axis disturbances, but to a limited extent.

Finally, a biodynamic feedthrough model was proposed. Parameters were fitted onto this model for the different motion conditions. Validation of the biodynamic feedthrough model with its parameters show that the suggested model accounts for at least 70% of the biodynamic feedthrough dynamics for those cases where sufficient biodynamic feedthrough was detected, which potentially allows for mitigation of BDFT through model-based signal cancellation[1].

Nomenclature

A	Sinusoid amplitude, [deg]
b_{BDFT}	BDFT damping coefficient, [kg/sec]
e_x	Error from target in horizontal direction, [deg]
e_y	Error from target in vertical direction, [deg]
f_{d_x}	Disturbance forcing function (surge), [deg]
f_{d_y}	Disturbance forcing function (sway), [deg]
f_{d_z}	Disturbance forcing function (heave), [deg]
f_{t_x}	Horizontal target forcing function, [deg]
f_{t_y}	Vertical target forcing function, [deg]
$g_{d,t}$	Fade-in function, [-]
G_{BDFT}	BDFT gain, [-]
H_{BDFT}	Measured BDFT dynamics, [-]
H_{NM}	Neuromuscular dynamics, [-]
$\hat{H}_{BDFT}$	Estimated BDFT dynamics, [-]
i_r	Run number, [-]
k	Sinusoid index, [-]
k_{BDFT}	BDFT stiffness, [kg/sec^2]
m_{BDFT}	BDFT mass, [kg]
n_{loss}	TSC loss of contact instances, [-]
$n_{d,t}$	Sinusoid frequency integer factor, [-]
s	Laplace operator
t_{loss}	TSC loss of contact duration, [sec]
t	time, [sec]
T_m	measurement time, [sec]
u_x	finger position, horizontal direction, [deg]
u_y	finger position, vertical direction, [deg]
σ_e^2	Variance of the error signal, [deg^2]
σ_u^2	Variance of the input signal, [deg^2]
ω	sinusoid frequency, [rad/sec]

Abbreviations

CDU	Command Display Unit
GA	Genetic Algorithm
MLE	Maximum Likelihood Estimation
PFD	Primary Flight Display
RMS	Root Mean Square
SIMONA	SImulation, MOtion and NAvigation Institute
SRS	SIMONA Research Simulator
TSC	Touch Screen Controller

*MSc Student, Supervised by Dr. ir. D.M. Pool, Prof. Dr. ir. M. Mulder, Dr. ir. M. M. van Paassen, Control and Simulation Division, Delft University of Technology, Kluyverweg 1, 2629 HS Delft, Netherlands; xander@mobertz.com.

I. Introduction

Although some examples of the implementations of touch screen controllers (TSCs) on the flightdeck exist,[2,3] a number of unsolved challenges still stand in the way of large scale implementation of touchscreens in the cockpit. From an interface design perspective, the direct manipulation offered by touchscreens has shown to be capable of improving certain in-flight tasks,[4] while perhaps being less suitable as a replacement for hardware input devices in others.[5] Another critical challenge comes from using touchscreens as input devices in a possibly highly dynamic and turbulent environment as an aircraft.[6] Resulting loss of finger contact with, and involuntary inputs given on a touchscreen through BioDynamic FeedThrough (BDFT) may significantly complicate any task that is to be performed on a touch sensitive cockpit display.

The effects of multiple variables, including display location, turbulence frequency and vibration levels on BDFT and its resulting impact on the use of TSCs in dynamic environments have been researched before.[4–10] Mitigation of the effects of BDFT, however, currently only takes place in the form of passive support systems. Mitigation of BDFT using noise signal cancellation was proposed in literature,[1] but it requires a good model of the BDFT. Efforts to build such a model for the use of touch screens in a turbulent environment have not been found in existing literature.

This paper describes the results of a human-in-the-loop experiment, conducted in the SIMONA Research Simulator (SRS) at Delft University of Technology, aimed to gain understanding of the influence of BDFT on performing a 'dragging' task (e.g., waypoint repositioning) on a touch sensitive cockpit display. Participants in the experiment performed a screen position pursuit tracking task on a touchscreen display, while being perturbed by a forward (surge), a lateral (sway), or a vertical (heave) motion disturbance in different experimental conditions. This allows for observation of the effects of BDFT whilst the finger is in contact with the TSC. The motion disturbance spectrum was identical in all axes to allow for direct comparison. Furthermore, the spectrum approximated a realistic (low-pass) turbulence signal similar to those used in previous investigations.[11–14] The use of independent multisine (visual) target and motion disturbance signals enable direct quantitative measurements of BDFT effects, by comparing the Power Spectral Densities (PSDs) of the touchscreen input data over the different experiment conditions. In turn, these measurements allowed for development of a model that describes the effects of BDFT when performing a continuous dragging task.

Section II and Section III provide the details of the experiment methods. The results of the experiment are presented in Section IV, after which the paper ends with a discussion and recommendations in Section V.

II. Control Task

A target-following disturbance-rejection experiment was performed to measure the effects of biodynamic feedthrough when performing a continuous dragging tasks on a TSC. The diagram of the experiment control task is depicted in Fig. 1. The human controller's task was to minimize both horizontal and vertical tracking errors, e_x and e_y, respectively. The errors were defined as the difference between the output of target functions (f_{t_x} and f_{t_y}), and the input positions of the finger, u_x and u_y. The actual position of the target was determined directly by the output of the target forcing functions, and depicted by a white triangle on Fig. 2. The input position of the finger was confirmed by a magenta circle. The white horizontal and vertical lines always moved with the target, to prevent that its location could not be determined due to visual obstruction by the participant's hand.

Whilst performing the control task, subjects were either exposed to one of three motion conditions (pure surge, pure sway, pure heave) or to no motion disturbance (baseline condition), Fig. 3. The disturbance signal was identical for all motion directions and directly determined by the output of the disturbance forcing function $f_{d_{x,y,z}}$.

The presence of this disturbance forcing function allowed for identification of the controller's biodynamic feedthrough model, H_{BDFT}. Inputs that were made on the TSC did not influence the motion disturbances. Inputs were directly made on a vertically oriented TSC located in front of the controller ('PFD') or on a horizontally oriented TSC located on the right side of the controller ('CDU') using the index finger of the controller only.

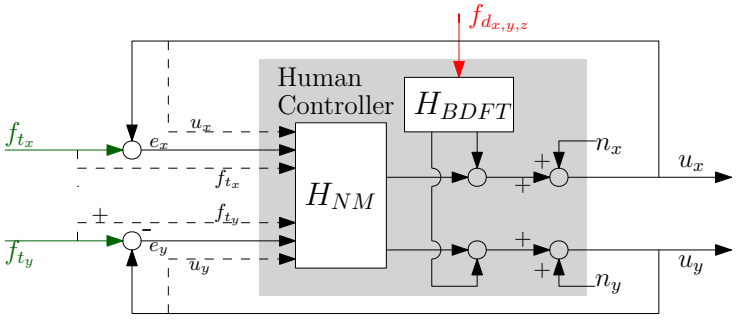

Figure 1. Multi-axis closed loop control task.

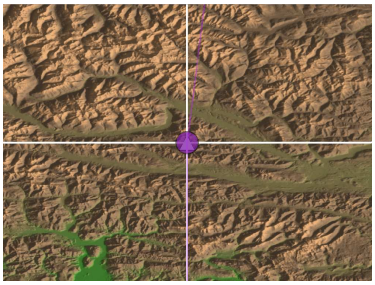

Figure 2. Experiment interface.

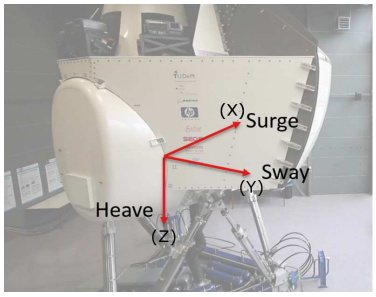

Figure 3. Motion directions in the SRS.

II.A. Forcing Functions

The aim of this research is to both measure and model BDFT for a continuous dragging task under varying motion conditions. In order to do this, use was made of fully deterministic target- and motion disturbance signals with sines at unique and known frequencies, amplitudes and phases. Although this yields a motion disturbance signal which is seemingly random in the time domain, it is easy to analyze the different components in the frequency domain. The Power Spectral Density in Fig. 4 shows the power and frequency locations of target and disturbance components that were presented to the participant. These sum-of-sines signals were defined by Eq. (1). $A_{d,t}[k]$, $\omega_{d,t}[k]$, and $\phi_{d,t}[k]$ indicate the amplitude, frequency and phase of the k^{th} sine in f_d or f_t respectively, where subscripts d and t are used to distinguish between the disturbance and target forcing functions. Primes $n_{d,t}$ were used as integer multiple of the measurement time base frequency, $\omega_m = 2\pi/T_m = 0.0767$ rad/s, to obtain a frequency for that particular wave. For this experiment, a measurement time of $T_m = 81.92$ s was used. A cresting technique was used such to determine the phases, preventing peaks in the time domain.[15]

$$f_{d,t}(t) = \sum_{k=1}^{N_{d,t}} A_{d,t}[k] \sin\left(\omega_{d,t}[k]t + \phi_{d,t}[k]\right) \tag{1}$$

For the target signals in both horizontal and vertical directions (f_{t_x} and f_{t_y}, respectively), the sum-of-sines signals consisted of three sines, each with different amplitudes, frequencies, and phases. The amplitudes were scaled such that the standard deviation of the signal was 13 cm in horizontal direction, and 9.75 cm in vertical direction. This ensured that the entire surface of the TSC devices was used. With only three low frequency sines, the 'randomness' in the time domain signal was questionable. To maintain signal characteristics that resembled a smooth dragging task whilst preventing signal recognition by the participant, the target signal was either displayed normally, mirrored over the horizontal axis, mirrored over the vertical axis, or mirrored over both axes.

The position signals for the motion disturbances $f_{d_{x,y,z}}$ were obtained in a similar way. This sum-of-sines signal consisted of ten sines. The selected primes have been used in a number of earlier experiments,[11,12,14] ensuring that the frequencies in the disturbance signal covered a wide frequency range of human control at regular intervals on a logarithmic scale. Due to the higher number of sines present in this signal, recognition of the disturbance signal by the participant was not likely. This prevented the need to invert the signal, resulting in an identical motion disturbance signal for all runs.

The forcing functions f_{t_x} and f_{t_y} were obtained using Eq. (1) with properties of the second and third columns in Table 1, respectively. To prevent nonzero starting values a fade-in function was applied, indicated in Eq. (2). This fade-in function was multiplied with the forcing function from equation Eq. (1).

$$g_{d,t}(t) = 1 - \frac{1}{2}\cos\left(\frac{\pi t}{t_{fade}}\right) \tag{2}$$

The motion disturbance signal f_d too, was obtained using Eq. (1) with properties from the first column in Table 1. This resulted in a position signal for disturbance. The apparatus described in Section III.A.1, however, required acceleration inputs and fade-in on the motion disturbance. Differentiating a faded position signal

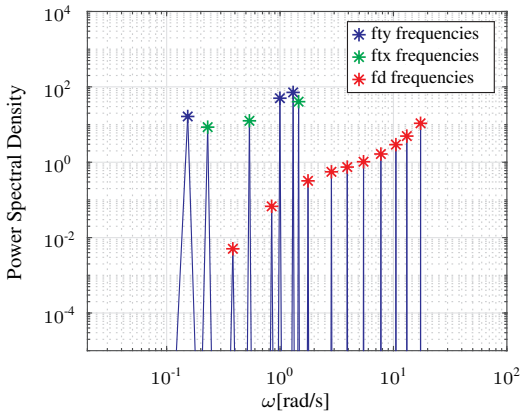

Figure 4. Power Spectral Densities of the forcing functions.

twice to obtain acceleration inputs for the hexapod simulator would yield motion commands that drift the simulator to the edge of its motion bounds due to a nonzero mean. Using Equations 1 and 2 in combination with the chain rule as in Eq. (3) prevented such drift and yielded an acceleration signal that was properly faded whilst preventing a nonzero starting acceleration.

$$f_{d_{faded}}(t) = f_d(t) \cdot g_d''(t) + 2 \cdot g_d'(t) \cdot f_d'(t) + f_d''(t) \cdot g_d(t) \tag{3}$$

Table 1. Forcing function properties.

	Disturbance, $f_{d_{xyz}}$				Target, f_{t_x}				Target, f_{t_y}			
k	n_d	ω_d	A_d	ϕ_d	n_{t_x}	ω_{t_x}	A_{t_x}	ϕ_{t_x}	n_{t_y}	ω_{t_y}	A_{t_y}	ϕ_{t_y}
–	–	rad s^{-1}	deg	rad	–	rad s^{-1}	deg	rad	–	rad s^{-1}	deg	rad
1	5	0.3835	$1.067 \cdot 10^{-1}$	-0.269	3	0.230	0.646	1.445	2	0.153	0.894	0.308
2	11	0.8437	$8.069 \cdot 10^{-2}$	4.016	7	0.537	0.784	0.000	13	0.997	1.562	-0.431
3	23	1.7641	$4.019 \cdot 10^{-2}$	-0.806	19	1.457	1.406	-1.825	17	1.304	1.866	-1.591
4	37	2.8379	$2.048 \cdot 10^{-2}$	4.938								
5	51	3.9117	$1.246 \cdot 10^{-2}$	5.442								
6	71	5.4456	$7.568 \cdot 10^{-3}$	2.274								
7	101	7.7466	$4.735 \cdot 10^{-3}$	1.636								
8	137	10.5078	$3.424 \cdot 10^{-3}$	2.973								
9	171	13.1155	$2.856 \cdot 10^{-3}$	3.429								
10	226	17.3340	$2.416 \cdot 10^{-3}$	3.486								

II.B. BDFT Model

The inputs that participants make on the TSC during the experiment are recorded, and converted to the frequency domain. If power of the disturbance feeds through onto the input signals, peaks are observed in the PSDs of TSC input signals u_x and u_y. Fig. 5 shows an example in which a PSD of u_y is visualized. Target signal power is clearly observed at frequencies corresponding with locations of the vertical target. Furthermore, the presence of power at f_d frequencies suggests that BDFT is present for this particular condition.

Presence of disturbance power at frequencies of the motion disturbance in the input signal, however, does in itself not quantify the extent to which BDFT takes place at these frequencies. After all, a large motion disturbance power at a certain frequency is almost guaranteed to cause a large input power for that specific frequency in the TSC input signal. Instead, the ratio between the disturbance power to which the participant is exposed and the power observed in the TSC input is used as BDFT estimate, Eq. (4).[1] Transfer function $H_{BDFT}(j\omega)$ is used to obtain such estimate, which yields a BDFT response for the ten disturbance frequencies.

$$H_{BDFT}(j\omega) = \frac{S_{f_d,u_{x,y}}(j\omega_d)}{S_{f_d,f_d}(j\omega_d)} \tag{4}$$

Fig. 6 shows an example of the BDFT dynamics that was estimated for a particular run. Red stars indicate the BDFT that was measured. Based on the response that was observed over the different frequencies, a second-order transfer function with additional gain was used to model these dynamics. An additional delay term was considered for the phase differences at the higher frequencies. Based on the observed magnitude dynamics the effect would have been negligible.

$$\hat{H}_{BDFT}(s) = G_{BDFT} \cdot \frac{1}{m_{BDFT} \cdot s^2 + b_{BDFT} \cdot s + k_{BDFT}} \tag{5}$$

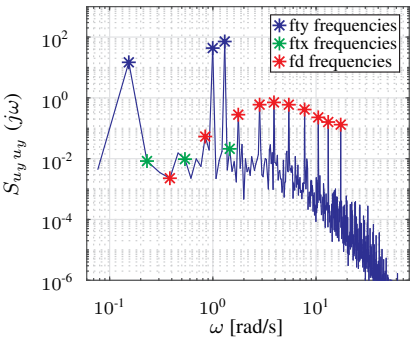

Figure 5. PSD example of TSC input

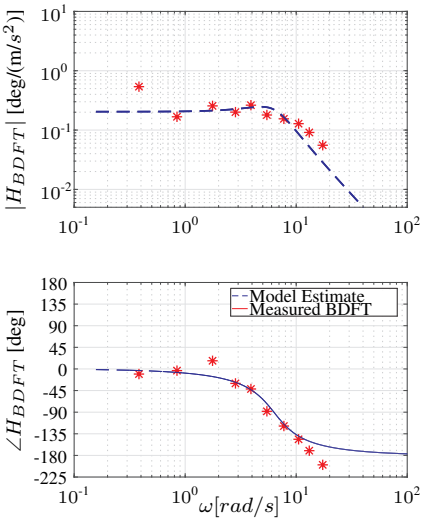

Figure 6. Measured and estimated BDFT sample

This yielded a BDFT model based on a mass, spring and damper system as proposed in Eq. (5), in which G_{BDFT} corresponds with the BDFT model gain, m_{BDFT} with mass, b_{BDFT} with damping, k_{BDFT} with stiffness. To subsequently estimate these BDFT model parameters, the time-domain parameter estimation routine of Pool[16] was used. In case of the example shown, this resulted in a model that is represented with the blue dashed line.

III. Experiment

To measure the effects of BDFT when performing continuous dragging tasks during motion disturbances, the task as described in Section II was conducted. This section provides details of the experimental setup; it elaborates on the experimental conditions, apparatus, and dependent measures that were used, and explains the methods used to analyze the obtained data. The section concludes with the hypotheses.

III.A. Method

III.A.1. Apparatus

The experiment was conducted in the SIMONA Reseach Simulator (SRS), located in the faculty of Aerospace Engineering at Delft University of Technology. The SRS is equipped with a hydraulic motion system, capable of providing motion cues in six degrees-of-freedom. Time delays of the motion system for all degrees of freedom are in the order of 20 msec.[17] Stroosma et al.[18] provide more information. Participants did not have influence on the motion cues they received, but instead received motion disturbances defined by the forcing functions. Participants were seated at the left side of the pedestal, from where two TSCs were to be controlled. The vertical TSC, referred to as 'PFD', was a 15-inch Iiyama ProLite TF1534MC-B1X. The screen was tilted from the vertical plane with an angle of 18° (Fig. 8). The second TSC, a 23-inch Dell P2314Tt, was horizontally mounted on the pedestal and is referred to as 'CDU'. Published response times of both screens was 8ms.[19,20] Markers on the floor of the simulator ensured a fixed seating position for participants with respect to the TSCs. Although participants were restrained using a five-point-harness, there was freedom to lean forward and backward. The following TSC positions were used, with respect to the center of the seat lumbar support:

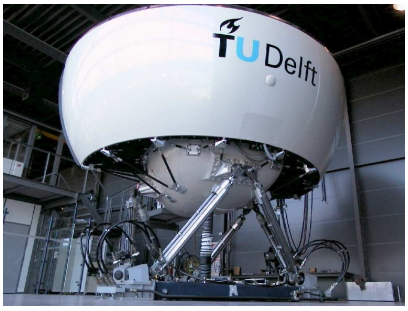

Figure 7. SIMONA Research Simulator.

- the PFD was located approximately 75 cm in front of the reference point.
- the CDU was located approximately 25 cm in front, and 40 cm right of the reference point.

The experiment display had dimensions of 30 cm width and 22.5 cm height. For the PFD, these dimensions covered the whole screen. On the CDU, the interface only used the top-left corner such that the same physical interface dimensions were maintained for both screens. An impression of the setup can be observed in Fig. 10. Anti-static electronics touchscreen gloves were used by the participants at all times throughout the experiment (EN338 performance level 2242, NEN-EN-IEC 61340-5-1 ESD rated).[21]

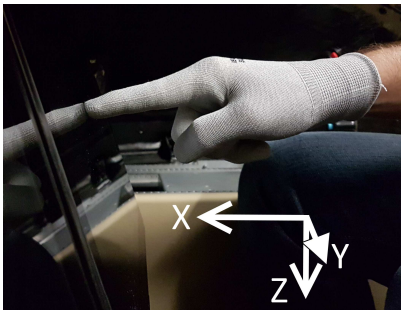

Figure 8. Control of the PFD.

Figure 9. Control of the CDU.

Figure 10. Cockpit setup.

III.A.2. Experimental Conditions

Participants were exposed to four different motion disturbance scenarios during the experiment: heave, sway, surge and a baseline condition without motion disturbance. Furthermore, two TSC locations were used for the experiment; one at the Primary Flight Display (PFD) location, the other at a location comparable to the Control Display Unit (CDU). This results in a total of eight experimental conditions. With 64 runs, this resulted in a eight repetitions per condition. To avoid target pattern recognition, the target was either displayed normally, mirrored over the horizontal axis, mirrored over the vertical axis, or mirrored over both axes.

III.A.3. Participants

Sixteen participants conducted the experiment, fifteen male and one female. All participants were right-handed and had experience with TSCs. The age of this group was recorded (M = 28.7, SD = 10.8 years), as well as length (M = 182.0, SD = 6.9 centimeters) and mass (M = 76.7, SD = 12.7 kilograms). All participants were fit to conduct an experiment in the SRS whilst being subjected to motion disturbances.

III.A.4. Procedures

Participants received a written briefing prior to the experiment with an explanation of the control task and the procedures. This briefing was covered again prior to the experiment. After signing a consent form, a safety briefing of the simulator was given prior to adjusting the seat to a predefined position. Participants wore noise-cancelling over-the-ear headphones, with additional masking sounds representing aircraft engine noise to prevent distraction from sound coming from the SRS pistons. A two-way radio communications link was present during the experiment. The main cabin lights were dimmed, but two reading lights were turned on to alleviate strain on the eyes whilst preventing visual distractions. Participants were instructed to wear a touchscreen glove (as specified in Section III.A.1) to ensure smooth continuous finger inputs and to limit strain on the controller's finger. Furthermore, the target was only touched with the index finger. The participants were prevented from supporting their hand on the screen, as multiple touch inputs resulted in a rejected measurement. Participants were instructed to continuously try to improve their performance, which was done by verbally indicating the sum of their root mean square (RMS) scores of both the the horizontal and vertical screen inputs after each run. A lower score indicated a better performance for a particular run. Before starting each run, participants were asked if they were ready. If desired, they could take a small break whilst remaining seated in the SRS. The total experiment consisted of 64 runs lasting 90 seconds each. After 32 runs, a larger break of approximately 20 minutes was given in which participants left the SRS. In total, the experiment lasted 2.5 hours per subject.

III.A.5. Dependent measures

In order to gain insight in the effect of biodynamic feedthrough during TSC dragging tasks, touchscreen inputs were recorded. From these recorded inputs, a number of dependent measures were calculated:

- *Loss of Screen Contact.* The loss of contact count n_{loss} is the number of samples for which no inputs were registered due to finger loss of contact with the TSC. The loss of contact time t_{loss} indicates the sum of the time during which no inputs were registered.
- *Tracking Performance.* To assess the performance of the participants, variances of both the horizontal ($\sigma^2_{e_x}$) and vertical ($\sigma^2_{e_y}$) error signals were determined, from which contributions of the target disturbances (f_{t_x} and f_{t_y}), motion disturbance frequency (f_d) and remnant (n) were calculated as measures of performance.
- *BDFT Model Estimate.* To obtain an estimate for the BDFT model (Eq. (5)), four dependent measures were required: BDFT gain G_{BDFT}, BDFT mass m_{BDFT}, BDFT damping b_{BDFT}, and BDFT stiffness k_{BDFT}. These variables were determined per participant for each condition, and for both the horizontal and vertical input signals. However, parameters could only be estimated in case of sufficient feedthrough of f_d. To assess whether this was the case, variances of both the horizontal ($\sigma^2_{u,x}$) and vertical ($\sigma^2_{u,y}$) control signals were determined, from which contributions of the motion disturbance frequency (f_d) were calculated.

In this paper, these dependent measures are presented with their sample means and 95% confidence intervals using box plots, over the dataset consisting of sixteen participants.

III.A.6. Data Analysis

Controllers performed 64 runs during the experiment, of which the first half was treated as training. The final thirty runs were used for the data analysis. The horizontal and vertical input over each screen were separately logged at 100Hz. Each analysis was performed for both the horizontal and vertical input signals separately.

To investigate the effects of motion disturbances on the ability for participants to maintain in contact with the TSC throughout each run, input signals were checked for missing inputs. Loss of contact was registered when at least ten consecutive samples (i.e., 0.1 seconds) were detected with a zero derivative for both the horizontal and vertical input signals. Both the number of times that contact loss occurred, and the sum of the duration of contact loss, were recorded for each run. Normality checks indicated that non-parametric testing methods had to be used for statistic analysis. Friedman's ANOVA was therefore used, after which follow-up tests were performed using Wilcoxon tests.[22]

To obtain a quantitative measure for the control performance of the participant, the TSC input error was determined. This error was determined for each direction by simply subtracting the target signal for each corresponding direction with the TSC input signals, as can be derived from Fig. 1. The variance was directly determined from this error signal, which served as measure for performance of the participants. With the total error variance obtained, it was possible to account parts of the total error variance to the known disturbances as the frequencies of those components were known.[23] This allowed to identify participant's sources of tracking error.

To verify whether motion disturbance signals actually fed through the participant's body to the TSC device, the Power Spectral Densities (PSDs) of the input data were determined subsequently. Since the motion disturbance signals were fully deterministic with power at known frequencies (Fig. 4), inputs signals on the TSC devices were expected to contain power at these same frequencies if sufficient BDFT occurred. PSDs were determined using the half-sided Fast Fourier Transform (FFT) of the output signals u_x and u_y, and their complex conjugate. These FFTs were calculated per individual run, after which all FFTs belonging to a certain condition were averaged. An averaged FFT was used to obtain the PSD. Presence of disturbance signals frequencies in these PSDs could subsequently be quantified, as power at the disturbance frequencies could be expressed as a percentage of the total power in the PSD.

If sufficient power from the motion disturbance signal was available in the control signal, an estimate for the biodynamic feedthrough dynamics was determined using Eq. (4) at the disturbance frequencies. To obtain an estimate for a full BDFT model ($\hat{H}_{BDFT}$), BDFT model parameters were estimated using a time-domain Maximum Likelihood Estimation (MLE) method. For all signals, initial parameters were estimated using a Genetic Algorithm, after which they were refined using a Gauss-Newton optimization.[24]

III.B. Hypotheses

The following hypotheses were formulated for the current experiment based on earlier findings and a literature search:

H1: *Loss of contact between the TSC and finger will significantly increase with motion, when compared to the baseline condition.*

Applying constant pressure to ensure smooth dragging and preventing accidental touches with finger are only some of the fine skills needed to operate a TSC. Effects of vibration, of which neuromuscular interference and BDFT are only two examples,[25] can interfere with these skills causing longer task completion time and reduced accuracy.[6–10] Reduced sense of pressure and inertia of participant's limbs are expected to cause loss of contact with the TSC.

H2: *Without motion disturbance, the target signals are more accurately tracked on the PFD than on the CDU.*

A known disadvantage of the use of TSCs is parallax,[26] which causes participants to perceive a different target location as a result of the viewing position if the participant is not directly in front of the screen.

H3: *Effects of BDFT will cause larger errors with the use of the PFD in comparison to the CDU.*

Since BDFT can be mitigated by providing passive support systems,[1,25] it is expected that the combination of lack of support and increased inertia of the operator's limbs lead to increased BDFT when using the PFD.

H4: *Effects of BDFT manifest predominantly when motion disturbances act in the direction of TSC control inputs.*

Earlier research suggested that touch errors are largest in the direction of the motion disturbance.[8] No significant results were found at that time. However, unpublished results of a preliminary research for this experiment do suggest that this effect indeed exists.

IV. Results

This section presents the results of the experiment based on the input signals of sixteen participants. Results for the CDU inputs are presented in blue, whereas results for the PFD inputs are presented in red.

IV.A. Input Loss

Fig. 11 shows the input loss data, and indicates to which extent participants were able to keep their finger on the TSC for the duration of the experiment. The number of instances that this 'contact loss' occurred is represented by Fig. 11a.

Friedman's ANOVA, with Wilcoxon Signed-ranks post-hoc tests were used to determine whether loss of contact count and duration increased with motion disturbance conditions, when compared to the baseline. These tests reveal that, indeed, significant differences were found between both the input loss count (n_{loss}) and input loss duration (t_{loss}) during the baseline condition and the disturbance conditions when using the CDU (blue boxplots), with most significant effects for the heave disturbance (Z). This matches expectations, as the screen moves 'away' from the hand, whilst the participant's limbs lag behind the movement due to inertia (Fig. 9).

Table 2. Friedman 's ANOVA with Wilcoxon Signed-ranks test results for input loss (sig^b), where ** is highly significant (p <.00143), * significant (.00143 ≤ p < .0072) and – not significant (p >.0072). Results indicated at sig. are without Bonferroni correction, where ** is highly significant (p <.01), * significant (.01 ≤ p < .05) and – not significant (p >.05)

Compared Conditions		Dependent measures							
		Count				Duration			
Friedman χ^2 *(7)*		46.309, p <.001				27.872, p <.001			
Wilcoxon α *= .0072*		z	r	sig^b.	sig.	z	r	sig^b.	sig.
CDU (NM)	x CDU (X)	-2.025	-.506	–	*	-2.192	-.548	–	*
CDU (NM)	x CDU (Y)	-2.825	-.706	*	**	-2.981	-.745	*	**
CDU (NM)	x CDU (Z)	-3.213	-.803	**	**	-3.180	-.795	**	**
PFD (NM)	x PFD (X)	-2.135	-.533	–	*	-1.448	-.362	–	–
PFD (NM)	x PFD (Y)	-1.450	-.362	–	–	-0.682	-.170	–	–
PFD (NM)	x PFD (Z)	-1.821	-.455	–	–	-1.422	-.355	–	–
CDU (NM)	x PFD (NM)	-3.319	-.830	**	**	-3.235	-.809	**	**

Using the same logic it can be reasoned that for the PFD, input loss count and duration would be highest for the forward (surge) motion disturbance (X). Results in Fig. 11a (red boxplots) show that this, indeed, is true. Friedman's ANOVA, with Wilcoxon Signed-ranks post-hoc tests, however, reveal that no statistical significant differences exist between the baseline and motion conditions. This can be explained by the fact that participants already lost contact with the PFD during the baseline condition without motion, on average 0.5 times per run.

An additional finding from these results is that in general, the number of times that participants lost contact with the TSC was increased whilst using the PFD, as compared to the CDU under same motion conditions. Although no hypothesis was developed for this phenomenon, a post-hoc Wilcoxon signed-ranks test between the two TSCs during baseline (NM) condition was performed to check for significance, which proved to be highly significant. It could be hypothesized that the passive support provided by the CDU helps the participant in maintaining contact with the screen. Such support is not given by the PFD, as the forward pointing arm has the freedom to move around.

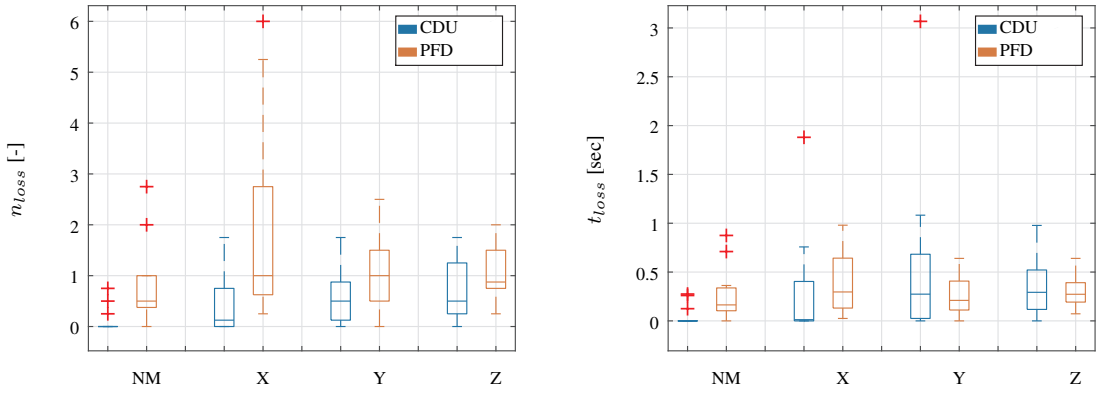

(a) Instances of TSC input loss, per disturbance

(b) Duration of TSC input loss, per disturbance

Figure 11. TSC input loss, count and duration.

IV.B. Tracking Performance

Variance of the error signal was used as quantitative measure for the performance of the participant. Results of this analysis are given in Figure 12, in which higher values indicate worse tracking performance. Once again, blue boxplots represent results for the CDU, whereas PFD results are given by red boxplots.

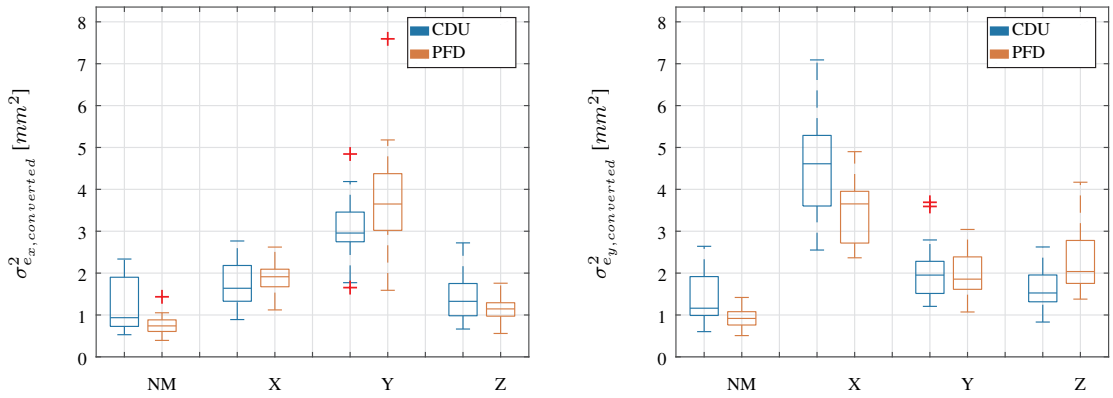

(a) Variance of horizontal input error e_x, converted to mm.

(b) Variance of vertical input error e_y, converted to mm.

Figure 12. Variance of the horizontal and vertical input errors.

From figure Fig. 12a, in which the error variance was converted from (deg^2) to physical screen input error variance (mm^2) for easier interpretation, it becomes evident that sway (Y) motion disturbances cause the largest errors for both the CDU and PFD displays when looking at horizontal inputs. This corresponds with findings in earlier research stating that feedthrough of disturbance motions are largest when acting in the same plane as the control inputs,[8] as horizontal inputs on the CDU correspond with the sway motion direction (Fig. 9).

Results for the vertical input in Fig. 12b support these findings as well, as surge (X) disturbances cause the error to be largest when using the CDU. Indeed, forward (surge) motion aligns with the vertical screen input of the CDU. The results show that when using the PFD too, surge leads to largest errors in the vertical input direction. This can be explained by the fact that the PFD was tilted by 18° from the vertical plane, as described in Section III.A.1 (Fig. 8). Accelerations in the negative X direction (surge) will cause the finger to slide upward, causing vertical offset from the target.

Table 3. Friedman 's ANOVA with Wilcoxon Signed-ranks test results error variance $\sigma^2_{e_x}$ and $\sigma^2_{e_y}$, where ** is highly significant (p <.0025), * significant (.0025 ≤ p < .0125) and – not significant (p >.0125).

Compared Conditions		Dependent measures					
		$\sigma^2_{e_x}$			$\sigma^2_{e_y}$		
Friedman $\chi^2(7)$		95.583, p <.001			91.729, p <.001		
Wilcoxon α = *.0125*		z	r	sig.	z	r	sig.
CDU (NM)	x PFD (NM)	-3.102	-.775	**	-3.361	-.840	**
CDU (X)	x PFD (X)	-1.086	-.272	–	-2.999	-.750	*
CDU (Y)	x PFD (Y)	-2.172	-.543	–	-0.052	-.013	–
CDU (Z)	x PFD (Z)	-2.275	-.569	–	-3.206	-.802	**

Friedman 's ANOVA followed up by Wilcoxon Signed-ranks tests (Table 3) reveal that, both for the vertical and horizontal input directions, a highly significant difference between input error exists when using the CDU and the PFD for the baseline (NM) condition. The use of the CDU leads in both cases to more error.

The following subsections cover the error variance components of the disturbance signal f_d, targets f_{t_x} and f_{t_y} and the remaining remnant n, in order to determine sources of error.

IV.B.1. Tracking performance: Horizontal Target

The f_{t_x} components of the total variance of the horizontal and vertical error signal ($\sigma^2_{e_{x,f_{t_x}}}$ and $\sigma^2_{e_{y,f_{t_x}}}$, respectively) are given in Fig. 13 as percentage of the total variance. For each motion disturbance, the target component was most strongly present in the error variance when using the CDU display when compared to the PFD. This difference was found to be highly significant (Table 4).

Table 4. Friedman 's ANOVA with Wilcoxon Signed-ranks test results for horizontal target components in $\sigma^2_{e_x}$ and $\sigma^2_{e_y}$, where ** is highly significant (p <.0025), * significant (.0025 $\leq$ p < .0125) and – not significant (p >.0125).

Compared Conditions		Dependent measures					
		$\sigma^2_{e_{x,f_{t_x}}}/\sigma^2_{e_x}$			$\sigma^2_{e_{y,f_{t_x}}}/\sigma^2_{e_y}$		
Friedman $\chi^2(7)$		95.583, p <.001			31.125, p <.001		
Wilcoxon α = *.0125*		z	r	sig.	z	r	sig.
CDU (NM)	x PFD (NM)	-3.464	-.866	**	-2.896	-.724	*
CDU (X)	x PFD (X)	-3.464	-.866	**	-.672	-.168	–
CDU (Y)	x PFD (Y)	-3.464	-.866	**	-.569	-.142	–
CDU (Z)	x PFD (Z)	-3.464	-.866	**	-.569	-.142	–

Note that f_{t_x} components are mainly observed in the horizontal input error e_x as expected. However, components of the horizontal target signal f_{t_x} are also detected in the vertical input error, which can be explained by mechanical coupling of participant's arm. The participant is unable to steer perfectly in a single axis, causing horizontal target frequencies to appear in vertical inputs.[14] Another reason for detection could be noise that is located at frequencies of the target component f_{t_x}.

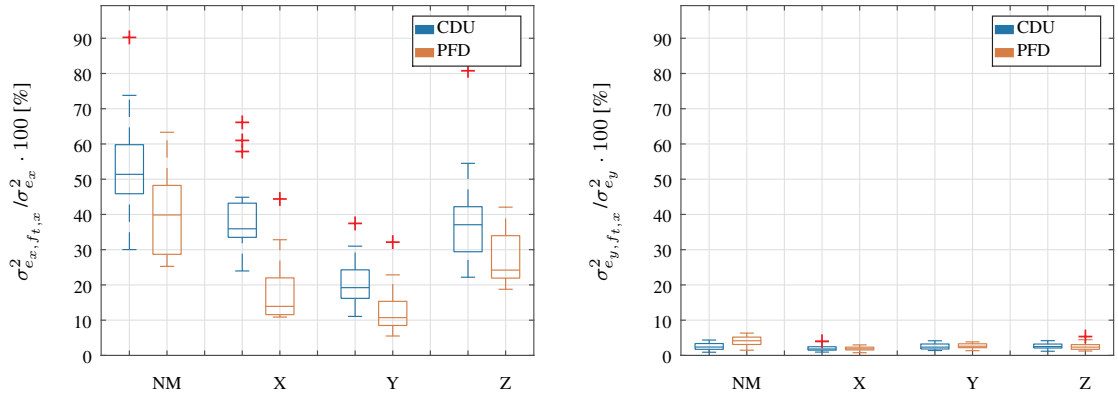

(a) Horizontal target signal components in $\sigma^2_{e_x}$

(b) Horizontal target signal components in $\sigma^2_{e_y}$

Figure 13. Horizontal Target components in the variance of error signals e_x and e_y.

IV.B.2. Tracking performance: Vertical Target

The f_{t_y} components of the total variance of the horizontal and vertical error signal ($\sigma^2_{e_{x,f_{t_y}}}$ and $\sigma^2_{e_{y,f_{t_y}}}$, respectively) are given in Fig. 14 as a percentage of the total variance. Similar to what was observed with the horizontal target components, vertical target components were most present in the error variance when using the CDU display. This difference between the CDU and PFD displays was again highly significant for the baseline (NM), sway (Y) and heave (Z) conditions (Table 5), and significant for surge (X).

Table 5. Friedman 's ANOVA with Wilcoxon Signed-ranks test results for vertical target components in $\sigma^2_{e_x}$ and $\sigma^2_{e_y}$, where ** is highly significant (p <.0025), * significant (.0025 $\leq$ p < .0125) and – not significant (p >.0125).

Compared Conditions		Dependent measures					
		$\sigma^2_{e_{x,f_{t_y}}}/\sigma^2_{e_x}$			$\sigma^2_{e_{y,f_{t_y}}}/\sigma^2_{e_y}$		
Friedman $\chi^2(7)$		20.375, p = .005			94.104, p <.001		
Wilcoxon α = *.0125*		z	r	sig.	z	r	sig.
CDU (NM)	x PFD (NM)	-.414	-.104	–	-3.516	-.879	**
CDU (X)	x PFD (X)	-.621	-.155	–	-2.637	-.659	*
CDU (Y)	x PFD (Y)	-.724	-.181	–	-3.258	-.815	**
CDU (Z)	x PFD (Z)	-1.086	-.272	–	-3.516	-.879	**

Note that this time, f_{t_y} components are mainly observed in the vertical input error e_y as expected. However, f_{t_y} components are also observed in the horizontal input direction for reasons noted in Section IV.B.1.

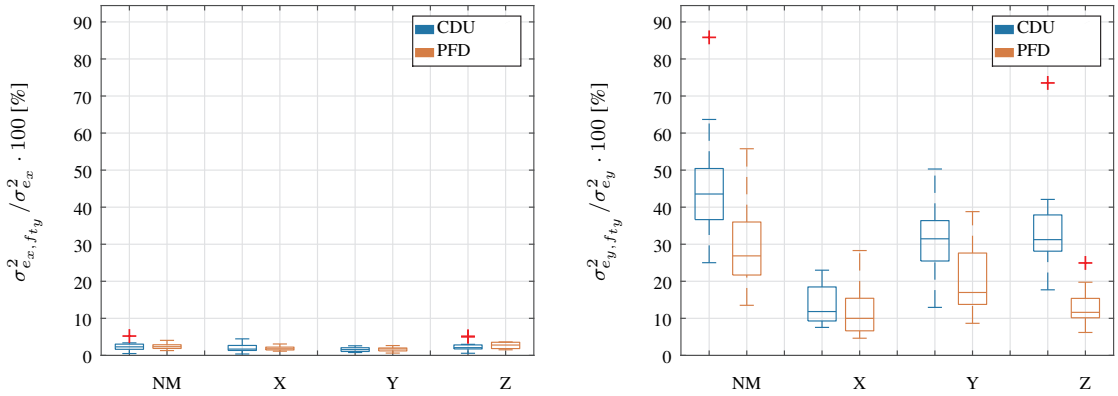

(a) Vertical target signal components in $\sigma^2_{e_x}$

(b) Vertical target signal components in $\sigma^2_{e_y}$

Figure 14. Vertical Target components in the variance of error signals e_x and e_y.

IV.B.3. Tracking performance: Motion Disturbance

The f_d components in the total variance of both the horizontal and vertical error signal ($\sigma^2_{e_{x,f_d}}$ and $\sigma^2_{e_{y,f_d}}$, respectively), are given in Fig. 15 as a percentage of the total variance. Little power is observed during the NM condition for both input directions, which is easily explained by the fact that no motion disturbance power was present. The components visible simply originate from noise at the f_d frequencies.

Table 6. Friedman 's ANOVA with Wilcoxon Signed-ranks test results for motion disturbance components in $\sigma^2_{e_x}$ and $\sigma^2_{e_y}$, where ** is highly significant (p <.0025), * significant (.0025 ≤ p < .0125) and – not significant (p >.0125).

Compared Conditions		Dependent measures					
		$\sigma^2_{e_{x,f_d}}/\sigma^2_{e_x}$			$\sigma^2_{e_{y,f_d}}/\sigma^2_{e_y}$		
Friedman $\chi^2(7)$		98.521, p <.001			99.167, p <.001		
Wilcoxon α = *.0125*		z	r	sig.	z	r	sig.
CDU (NM)	x PFD (NM)	-1.965	-.491	–	-1.810	-.453	–
CDU (X)	x PFD (X)	-3.309	-.827	**	-3.206	-.802	**
CDU (Y)	x PFD (Y)	-1.655	-.414	–	-0.827	-.207	–
CDU (Z)	x PFD (Z)	-3.516	-.879	**	-3.413	-.853	**

For the horizontal input direction, Fig. 15a, it can be observed that largest components of $\sigma^2_{e_{x,f_d}}$ are measured during sway (Y), followed by surge (X). With sway (Y) acting in the same direction as the horizontal TSC input for both the CDU and PFD screens, large values components were to be expected. However, for both displays it can be seen that forward surge (X) motion also influences horizontal screen input. During heave (Z), f_d only contributes minimally.

For the vertical input direction, Fig. 15b, it can be observed that the largest components of $\sigma^2_{e_{y,f_d}}$ are measured during surge (X) for both screens, and heave (Z) for the PFD. According to hypothesis H4, this can be explained by the fact that the motion disturbance acts in the same direction as the screen input. This might be less intuitive for the forward (surge, X) disturbance in case of the PFD, but remember that this particular screen was tilted slightly causing the finger to slide up and down with forward and backward disturbance motions.

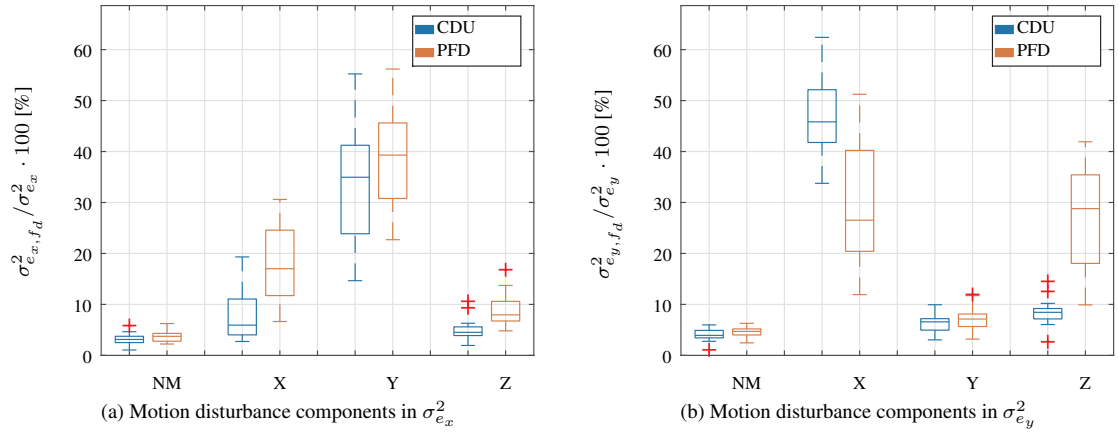

(a) Motion disturbance components in $\sigma^2_{e_x}$

(b) Motion disturbance components in $\sigma^2_{e_y}$

Figure 15. Motion Disturbance components in the variance of error signals e_x and e_y.

IV.B.4. Tracking performance: Remnant

Power at frequencies that is not accounted for are referred to as remnant, and may include effects ranging from simulator motion dynamics to non-linearities in participant control behavior. The remnant components in the horizontal error signal are given in Fig. 16a, whereas remnant for the vertical error signal are given in Fig. 16b, both expressed as percentage of $\sigma^2_{e_x}$ and $\sigma^2_{e_x}$ respectively. Both for the horizontal and vertical directions, it can be observed that the use of PFD leads to higher remnant components when compared to the use of the CDU for the same motion disturbance. This indicates that participants have more trouble operating the PFD for reasons other than target or disturbance frequencies. Examples may include physical effects such as nonlinear neuromuscular effects or fatigue. This difference is highly significant for the baseline condition and significant for surge (X) and heave (Z) in the horizontal direction. For the vertical direction, the difference is highly significant for the baseline (NM), surge (X) and sway (Y) conditions.

Table 7. Friedman 's ANOVA with Wilcoxon Signed-ranks test results for remnant components in $\sigma^2_{e_x}$ and $\sigma^2_{e_y}$, where ** is highly significant (p <.0025), * significant (.0025 ≤ p < .0125) and – not significant (p >.0125).

		$\sigma^2_{e_{x,n}}/\sigma^2_{e_x}$			$\sigma^2_{e_{y,n}}/\sigma^2_{e_y}$		
Friedman $\chi^2(7)$		57.188, p <.001			57.208, p <.001		
Wilcoxon α = *.0125*		z	r	sig.	z	r	sig.
CDU (NM)	x PFD (NM)	-3.464	-.866	**	-3.516	-.879	**
CDU (X)	x PFD (X)	-2.999	-.750	*	-3.309	-.827	**
CDU (Y)	x PFD (Y)	-.982	-.246	–	-3.154	-.789	**
CDU (Z)	x PFD (Z)	-2.844	-.711	*	-1.396	-.349	–

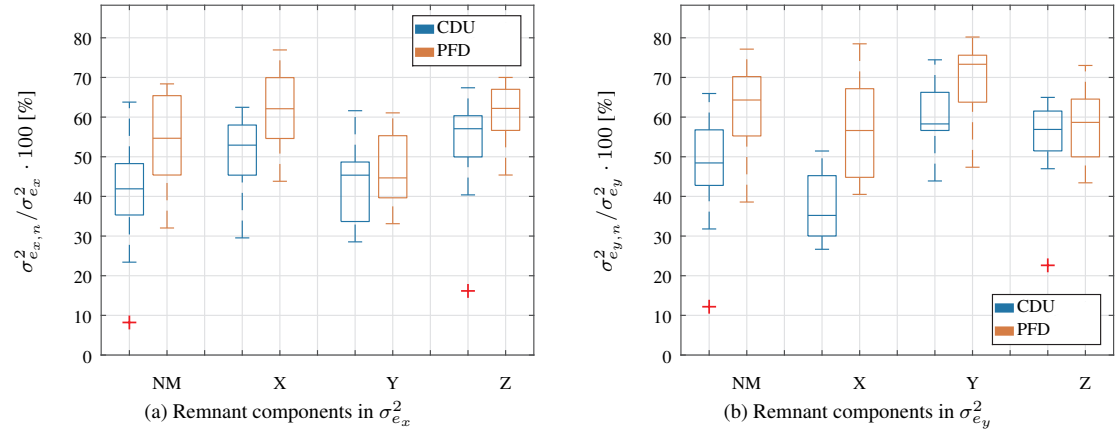

(a) Remnant components in $\sigma^2_{e_x}$

(b) Remnant components in $\sigma^2_{e_y}$

Figure 16. Remnant components in the variance of error signals e_x and e_y.

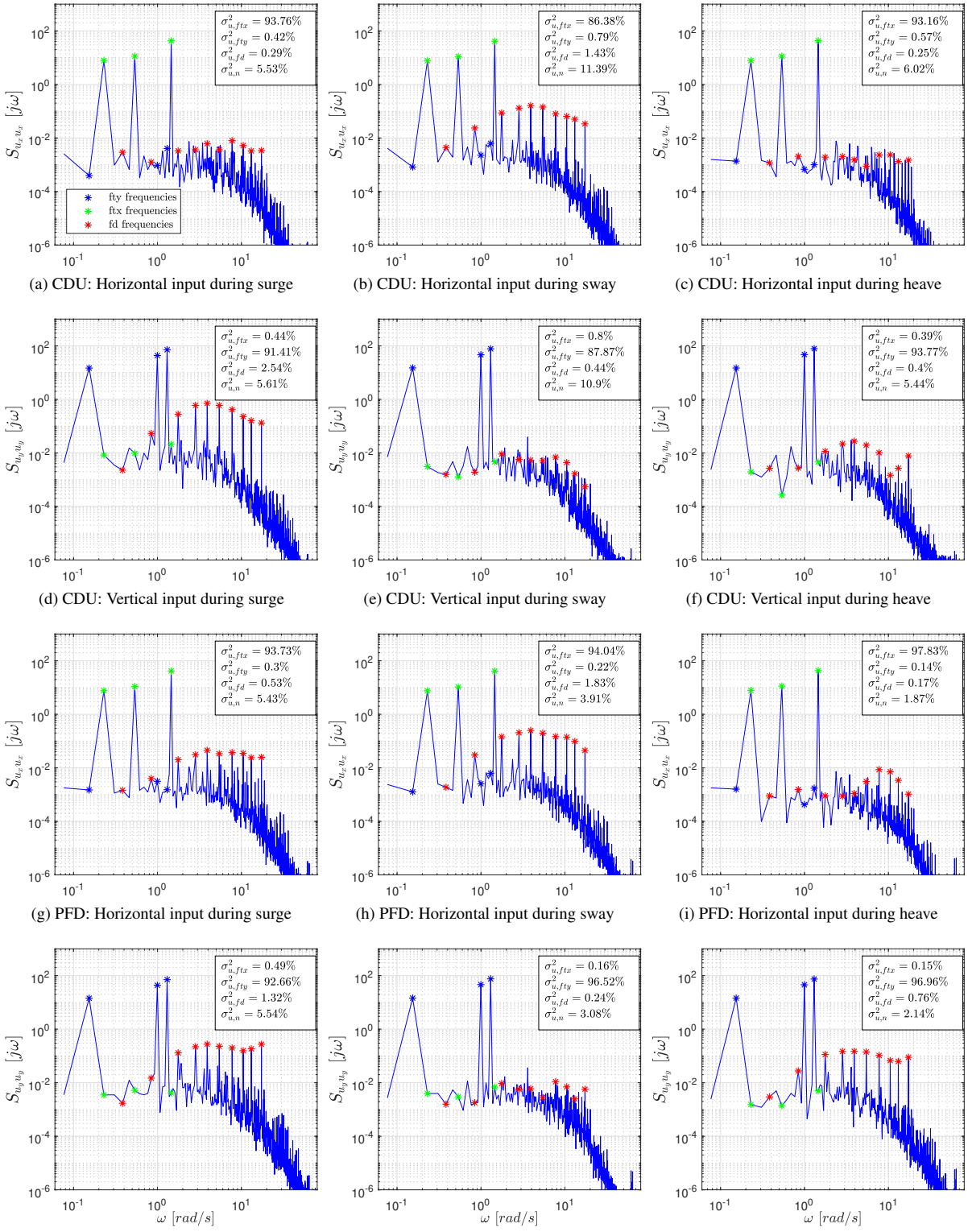

(a) CDU: Horizontal input during surge (b) CDU: Horizontal input during sway (c) CDU: Horizontal input during heave

(d) CDU: Vertical input during surge (e) CDU: Vertical input during sway (f) CDU: Vertical input during heave

(g) PFD: Horizontal input during surge (h) PFD: Horizontal input during sway (i) PFD: Horizontal input during heave

(j) PFD: Vertical input during surge (k) PFD: Vertical input during sway (l) PFD: Vertical input during heave

Figure 17. Power Spectral Densities of the TSC inputs.

IV.C. Disturbance Feedthrough

Fig. 17 shows the Power Spectral Density (PSD) for both the horizontal and vertical TSC input signals u_x and u_y for the motion conditions surge, sway and heave, averaged over all participants. If BDFT occurs, peaks should be observed at frequency locations of the motion disturbance f_d. Subsequently, the extent to which the motion disturbance frequencies are present in the TSC input signal can be calculated by quantification of the presence of σ^2_{u,f_d} components in σ^2_u. Fig. 18 shows to what extent the disturbance signal contributes to the TSC input signals u_x and u_y, as percentage of the total TSC input signal variance. As is clear from Fig. 18, these percentages are generally very low as most energy in the input signals originates from the target signals. Fig. 20 shows an example of an input signal with separated motion component to illustrate this. Note that results for the baseline condition are omitted for the upcoming sections as no BDFT can occur without motion.

Table 8. Friedman 's ANOVA with Wilcoxon Signed-ranks test results for disturbance components in $\sigma^2_{u_x}$ and $\sigma^2_{u_y}$, where ** is highly significant (p <.0033), * significant (.0033 ≤ p < .0167) and – not significant (p >.0167).

Compared Conditions		Dependent measures					
		$\sigma^2_{u_{x,f_d}}/\sigma^2_{u_x}$			$\sigma^2_{u_{y,f_d}}/\sigma^2_{u_y}$		
Friedman χ^2 *(7)*		93.063, p <.001			89.938, p <.001		
Wilcoxon α = *.0125*		z	r	sig.	z	r	sig.
CDU (X)	x PFD (X)	-2.223	-.556	–	-3.361	-.840	**
CDU (Y)	x PFD (Y)	-1.965	-.491	–	-2.017	-.504	–
CDU (Z)	x PFD (Z)	-0.982	-.246	–	-2.534	-.634	*

Fig. 17a to Fig. 17c show the PSDs of the horizontal input on the CDU screen during surge, sway and heave, respectively. Although all figures show at least some presence of power at the disturbance frequencies (indicated by red stars), strongest responses are observed when sway disturbances are present. Responses to f_d for the surge and heave conditions contain barely more power than noise at other frequencies. This corresponds with the findings in Fig. 18a, where f_d components are only significantly present for sway (Y) when using the CDU.

Fig. 17d to Fig. 17f show the PSDs of the vertical input on the CDU screen during surge, sway and heave, respectively. Strongest responses to disturbance motions are observed when the motion acts in the forward direction (surge). Responses to sway and heave are minimal. This is confirmed by the data in Fig. 18b, where surge (X) is the only disturbance with significant feedthrough when using the CDU.

Fig. 17g to Fig. 17i show the PSDs of the horizontal input on the PFD screen under varying disturbances. Strong responses are observed when the motion acts in both the forward (surge) and lateral (sway) directions, although the sway response is significantly stronger. This also follows from Fig. 18a, where the red boxplots representing the PFD results shows strong responses to sway (Y) and less (but still significantly) strong response during sway.

Finally, Fig. 17j to Fig. 17l show the PSDs of the vertical input on the PFD screen during surge, sway and heave, respectively. The largest contributions are observed when the motion acts in both the forward (surge) and vertical (heave) direction. The effect of sway is negligible. Fig. 18a confirms these findings, where the red boxplots representing PFD results are showing strong response to both surge (X) and heave (Z).

For the vertical input direction, a significant difference between the PFD and CDU was found during the heave (Z) disturbance. A highly significant difference was observed between the two input methods for surge (X). Significant differences for the horizontal input direction between both screens were not found, for any disturbance.

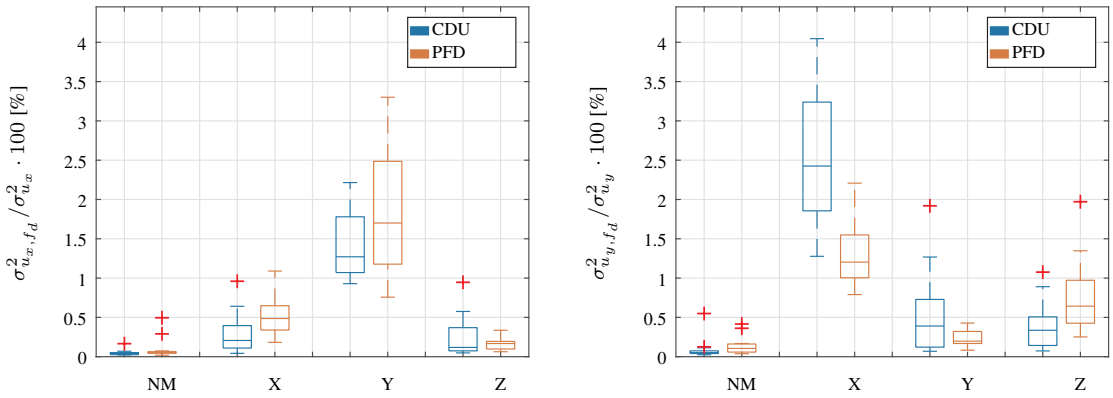

(a) Motion disturbance components in $\sigma^2_{u_x}$

(b) Motion disturbance components in $\sigma^2_{u_y}$

Figure 18. Motion disturbance components in the variance of input signals u_x and u_y.

IV.D. Biodynamic Feedthrough Dynamics

IV.D.1. Examples of BDFT

Table 9. f_d components of σ_u^2

TSC	Input Direction	Disturbance	$\sigma^2_{u,f_d}/\sigma^2_u$ ·100 [%]	Possibility of Accurate BDFT Estimation
CDU	Horizontal	Surge (X)	0.3	✗
CDU	Horizontal	Sway (Y)	1.4	✓
CDU	Horizontal	Heave (Z)	0.3	✗
CDU	Vertical	Surge (X)	2.5	✓
CDU	Vertical	Sway (Y)	0.4	✗
CDU	Vertical	Heave (Z)	0.4	✗
PFD	Horizontal	Surge (X)	0.5	✓
PFD	Horizontal	Sway (Y)	1.8	✓
PFD	Horizontal	Heave (Z)	0.2	✗
PFD	Vertical	Surge (X)	1.3	✓
PFD	Vertical	Sway (Y)	0.2	✗
PFD	Vertical	Heave (Z)	0.8	✓

Section II.B elaborated on how the BDFT dynamics were measured and modeled. In order to determine a reliable BDFT response, however, sufficient motion disturbance power should be observed in the input signals u_x and u_y as the BDFT response would otherwise be based on noise.[1]

Fig. 19a shows a representative example of identified BDFT response of horizontal input on the PFD during surge (forward) disturbance for a single participant. Red bars indicate the spread over the four BDFT responses that were identified from four runs for a single condition. The four responses obtained were initially fitted using a Genetic Algorithm (GA), after which the results were refined using a Gauss-Newton estimation to obtain four sets of model parameters. The averaged model, thus composed with the average of these parameters, is indicated with the blue line. The Variance Accounted For, a measure described in Section IV.D.2 which is used to estimate the accuracy of the estimated model, showed that model estimates with an average accuracy of 70% could be made when at least 0.5% of the horizontal input variance $\sigma^2_{u_x}$ was composed of feedthrough from f_d.

Fig. 19b on the other hand shows a representative example of identified BDFT response of horizontal input on the CDU during surge (forward) disturbance for a single participant. From Table 9 it can be seen that the horizontal input variance $\sigma^2_{u_x}$ is only composed of 0.3% feedthrough from f_d. This also follows from Fig. 17a, where power at the f_d frequencies barely exceeds noise levels. This causes BDFT measurements with a wide spread, which makes estimation of the BDFT model unreliable.

In general it was observed that at least 0.5% of the input variance σ^2_u needed to be composed of feedthrough from f_d, before reliable BDFT measurements and estimates could be made. It is for this reason that BDFT estimations were performed only for conditions in which $\sigma^2_{u.f_d}$ exceeded 0.5 %.

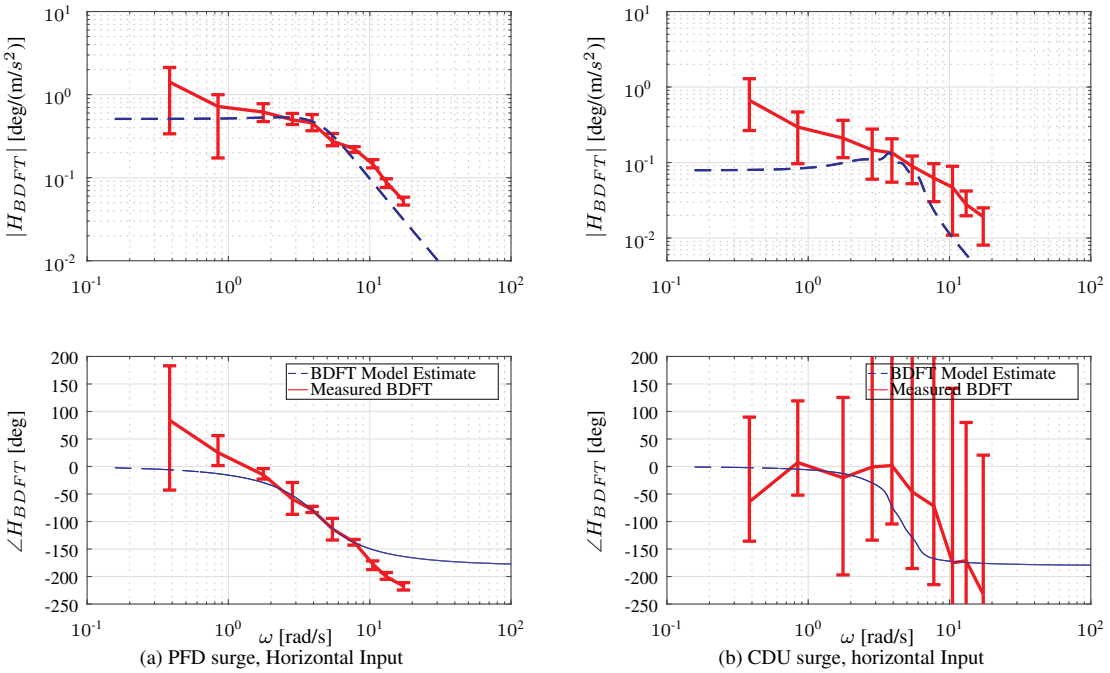

(a) PFD surge, Horizontal Input

(b) CDU surge, horizontal Input

Figure 19. BDFT Model Estimation Examples.

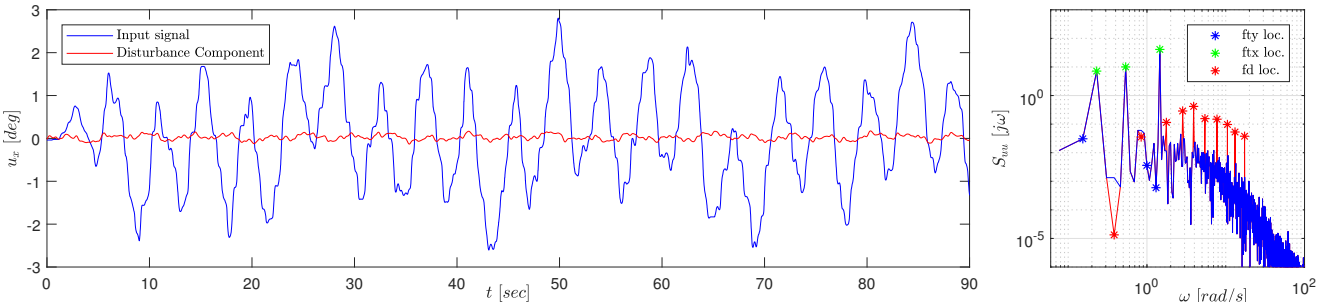

Figure 20. Example timetrace of input signal, with separate motion disturbance feedthrough component.

IV.D.2. BDFT Model Validation using VAF

Although the model proposed in Section II.B modeled the example BDFT dynamics in Fig. 6 reasonably well, it is possible that each condition with different motion disturbance has to be modelled by a different BDFT model. After all, BDFT is a complex mechanism that involves many variables.[1,25] Its results might not be easily captured by a single model with varying parameters. To evaluate whether the model proposed in Section II.B can be used for all conditions in this experiment, the model is validated using Variance Accounted For (VAF). The VAF describes the extent to which the motion disturbance components in the touchscreen input signals u_{x,f_d} and u_{y,f_d} can be accounted for by the model and is expressed as a percentage.

Fig. 21 shows the VAF results for all conditions, for both horizontal and vertical inputs, where the values have been averaged over all participants. The conditions for which the disturbance feedtrough was determined to be too weak, as determined in Section IV.D.1, have been presented with a grey background. One can clearly observe that a good model cannot be determined if there is not enough feedthrough of motion disturbances to the TSC, as all grey columns contain boxplots with low VAFs. For the remainder of the conditions, a mean VAF of 70% or higher was obtained. This indicates that the model as suggested in Section II.B is capable of modelling BDFT accurately for especially the conditions with notable BDFT.

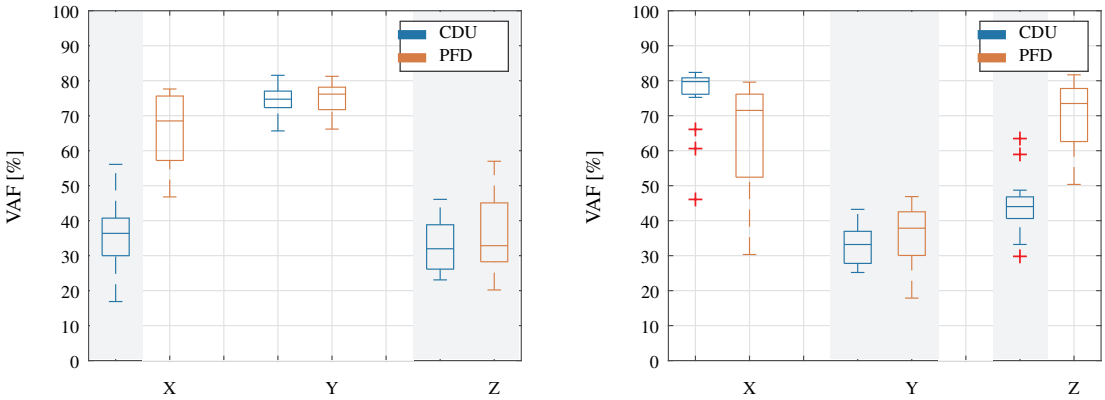

(a) VAF, Horizontal Input

(b) VAF, Vertical Input

Figure 21. Average VAF of the BDFT Model Estimation.

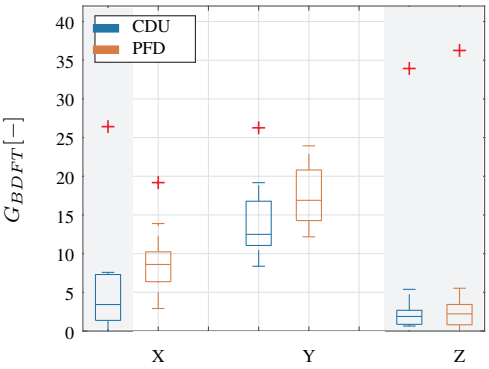

(a) BDFT model estimation of G_{BDFT}, horizontal input

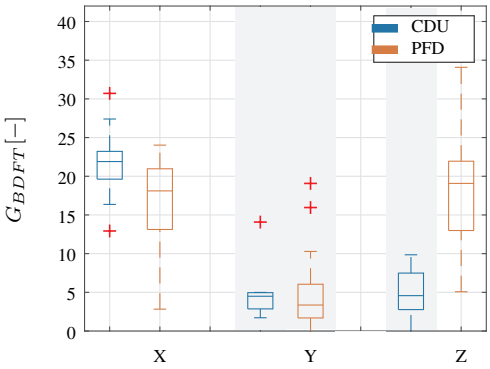

(b) BDFT model estimation of G_{BDFT}, vertical input

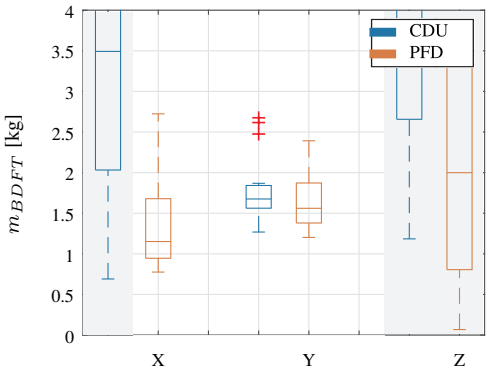

(c) BDFT model estimation of m_{BDFT}, horizontal input

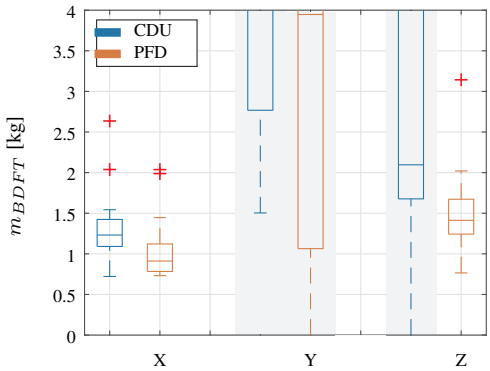

(d) BDFT model estimation of m_{BDFT}, vertical input

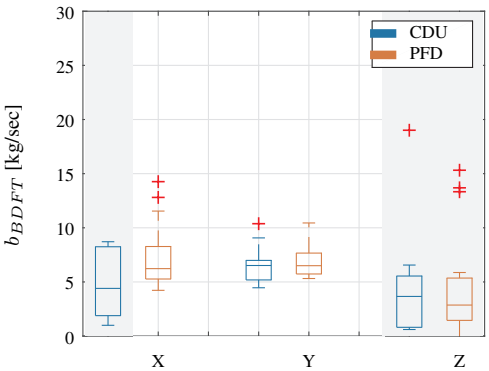

(e) BDFT model estimation of B_{BDFT}, horizontal input

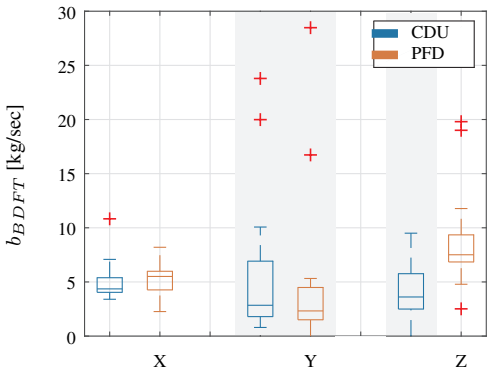

(f) BDFT model estimation of B_{BDFT}, vertical input

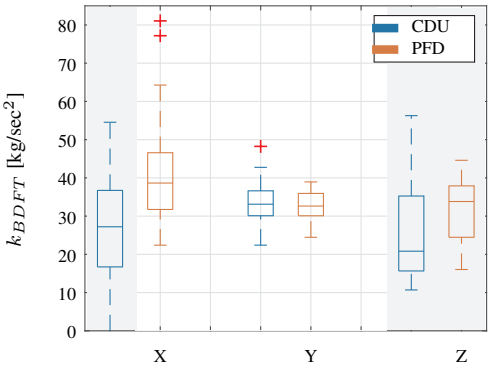

(g) BDFT model estimation of k_{BDFT}, horizontal input

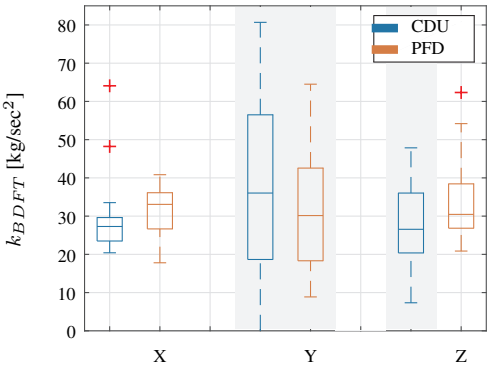

(h) BDFT model estimation of k_{BDFT}, vertical input

Figure 22. BDFT model parameter estimation results.)

IV.D.3. Parameter estimation: G_{BDFT}

The first row of Fig. 22 shows results of the BDFT model gain (G_{BDFT}). Note that the figures for both the horizontal (Fig. 22a) and vertical (Fig. 22b) control signals also show the unreliable estimation results for the BDFT gain as explained in Section IV.D.1. These results are indicated with a grey background and, as can be verified from Fig. 22, their values are generally low when compared to the gains of conditions that are accurately describing BDFT.

Fig. 22a indicates a notable difference between the gains of surge (X) and sway (Y) for the PFD. A possible explanation is that BDFT mainly acts in the direction of the control input. Therefore, less BDFT is present in the horizontal input of the PFD when a forward disturbance (surge, X) is present. For both the PFD and the CDU, the sway (Y) motion is in plane with the horizontal control inputs. For the same sway disturbance, the PFD gain is slightly larger when compared to the gain of the CDU. This matches expectations, as increased limb inertia and reduced arm support will increase effects of BDFT.

Fig. 22b shows that the BDFT gains for surge (X) and heave (Z) are comparable with those for vertical inputs on the PFD. Note, however, that the spread for heave is large, which may be caused by the low feedthrough into the input signal, resulting in less accurate estimations. Comparing the CDU and PFD G_{BDFT} values for surge (X), it can be seen that the CDU gain is clearly higher. This is expected, as forward disturbance (surge) acts in the same plane as the vertical inputs over the CDU. As the PFD is tilted, the same effect occurs to a limited degree, as explained in Section III.A.1 (Fig. 8). Acceleration toward the forward direction (surge) might cause the finger to slide upward, causing vertical offset from the target.

IV.D.4. Parameter estimation: m_{BDFT}

The second row of Fig. 22 shows results of the BDFT model's mass parameter (m_{BDFT}) estimation. Again, unreliable estimation results for BDFT frequency are indicated with a grey background. These values for m_{BDFT} have a huge spread, which can be attributed to the fact that the GA and MLE algorithms were fitting models to noise. The figures do not show the entire spread of these values in order to visualize m_{BDFT} values that have been estimated accurately.

Looking at the horizontal inputs in Fig. 22c during sway (Y), m_{BDFT} parameters are comparable for the CDU and PFD with values around 1.5 kg. Note that BDFT consists of many variables and this mass figure should therefore be seen as a system equivalent mass rather than just the typical mass of an arm. When the PFD is compared between the surge (X) and sway (Y) motion conditions it can be seen that m_{BDFT} is slightly, but not significantly, larger for sway.

For the vertical inputs in Fig. 22d with surge (X) disturbance motion, an increase of approximately 30% is observed for m_{BDFT} parameters when using the CDU, when compared to use of the PFD. When the PFD values for m_{BDFT} are compared between the surge (X) and heave (Z) conditions, one can see that these values are approximately 50% higher for heave (Z).

IV.D.5. Parameter estimation: B_{BDFT}

The third row of Fig. 22 shows results of the BDFT model's damping parameter (B_{BDFT}) estimation. Again, unreliable results are indicated with a grey background. Larger spreads and increased numbers of outliers for these conditions indicate that, indeed, the GA and MLE algorithms could not determine consistent parameter estimates.

For the horizontal inputs in Fig. 22e, no significant differences can be observed for values of B_{BDFT} over surge (X) and sway (Y) using the PFD. Furthermore, no significant differences were found between CDU and PFD values of B_{BDFT} during sway (Y). The results for vertical inputs in Fig. 22f indicate slightly higher values of B_{BDFT} during heave (Z) than during surge (X) when using the PFD, but this difference is not significant. Pairwise comparisons of the CDU and PFD for surge (X) show no statistical relevant differences.

IV.D.6. Parameter estimation: k_{BDFT}

The final row of Fig. 22 shows results of the BDFT model's stiffness parameter (k_{BDFT}) estimation. For the horizontal inputs in Fig. 22g, results show that use of the PFD during surge (X) results in 20% higher stiffness coefficients when compared to the use of the PFD during sway (Y). Although these differences are not significant, they can be attributed to the fact that participants' arms were supported by the PFD during surge (X), which allows the participant to increase arm stiffness. This support lacks during sway (Y), as the arm is moved left and right due to effects of BDFT. No significant differences were found between CDU and PFD values of k_{BDFT} during sway (Y).

The results for vertical inputs in Fig. 22f show similar values of k_{BDFT} during surge (X) and heave (Z) for use of the PFD. Comparing the CDU with the PFD for surge (X), it can be seen that stiffness values with the use of PFD are approximately 20% higher. This too, can likely be explained by the added support of the PFD during forward (surge, X) disturbance. The CDU does not offer such support during surge.

V. Discussion

In this paper, a cybernetic approach was used to set up and analyze results of a human-in-the-loop experiment, aimed to gain understanding on the influence of BDFT on performing a waypoint dragging task on a touch-sensitive cockpit display. Participants in the experiment performed a position pursuit tracking task on a touchscreen display, either without motion or while being perturbed by forward (surge), lateral (sway), or vertical (heave) motion disturbances.

Data were first analyzed for loss of contact between the TSC and participant's finger. **H1** hypothesized that loss of contact between the TSCs and finger would significantly increase with motion, when compared to the baseline condition. Results showed that, indeed, loss of contact count increased from an average of 0.09 counts per run during the no motion condition to 0.56 counts during motion disturbances for the CDU, and from 0.75 to 1.32, respectively, for the PFD. This increase was highly significant for the CDU when comparing the baseline (NM) with heave (Z) conditions, both for contact loss count and contact loss duration. For sway (Y) too, significant effects were found when compared to the baseline condition on the CDU. For surge (X), results were not significant due to a large Bonferonni correction. For the PFD, however, no significant differences were found between the baseline (NM) and motion conditions. One can conclude that TSC contact loss depends on more variables than motion disturbance alone. **Hypothesis H1 therefore only holds partially**. An additional finding from the input loss analysis was that the number of times that participant lost contact with the TSC was increased when the PFD was used when compared to the CDU under the same motion conditions. This suggests that it is easier for participants to apply a consistent control strategy on a system that supports the human finger, rather than on a system where the participant is required to hold his or her arm suspended in the air. This might also explain why PFD contact loss already occurred for an average of 0.5 times per run when no motion disturbance was present.

After analyzing data for loss of contact, performance was measured using the variance of the error signal σ_e^2. Due to the known frequency locations of the target signals, it was possible to determine to what extent the these signal contributed to the total error variance σ_e^2. On average, around 30% of the error variances is inherently explained by the target signals. **H2** hypothesized that target signals are more accurately tracked on the PFD than on the CDU as a result of parallax, a known problem with the use of TSCs.[26] Pairwise comparison between the two TSCs for each disturbance condition showed highly significant differences for target component present in error signals. Participants were in all cases able to track the target more accurately on the PFD, suggesting that hypothesis H2 holds. However, it has to be noted that participants observed a slightly higher delay with the use of the CDU compared to the PFD, i.e., the magenta position indicator 'lagged' behind the actual finger position. Such errors would produce higher components of target error in the error variance, invalidating results. Although specifications of both TSCs show the same response rate (8ms), it might be possible that touch registration time differs. Quantification of this registration time was, however, outside the scope of this research. **Hypothesis H2 therefore holds conditionally**.

Similarly, it can be determined to what extent f_d components contribute to the total error variance σ_e^2. **H3** hypothesized that effects of BDFT will cause larger control errors with the use of the PFD in comparison to the CDU. If this hypothesis holds, larger components of $\sigma^2_{e_x f_d}$ should be observed for the PFD than for the CDU. Since sway (Y) is critical for the horizontal inputs at both TSCs, that condition will be used for comparison. It was shown that for sway (Y), indeed, use of the PFD resulted in higher components (15% on average) of $\sigma^2_{e_x f_d}$ than the CDU. This difference, however, is not significant (Table 6). The total variance of the error $\sigma^2_{e_x}$ in general, did not show significantly higher values for the PFD than the CDU during sway (Y) disturbance. Therefore, it cannot be concluded that control errors are larger when using the PFD in comparison to the CDU for similar motion conditions in general, and **Hypothesis H3 is rejected**. Note, however, that increased remnant components in the error variance for the PFD with respect to the CDU, do suggest that the PFD is more susceptible to errors which cannot be attributed to either target or disturbance frequencies.

H4 hypothesized that effects of BDFT manifest predominantly when motion disturbances act in the direction of TSC control inputs. For the CDU, this means that sway (Y) was expected to generate most feedthrough for horizontal inputs, and surge (X) for vertical inputs. This was visually confirmed in the PSDs (Fig. 17b and Fig. 17d, respectively). Furthermore Fig. 18 showed that for the CDU, the f_d component in $\sigma^2_{u_x}$ was highest during sway (Y) disturbance whereas the f_d component in $\sigma^2_{u_y}$ was highest during the surge (X) condition. If the hypothesis were to hold, sway (Y) should generate the most feedthrough for the horizontal PFD inputs, whereas both surge (X) and heave (Z) should generate most feedthrough for the vertical PFD inputs, due to the fact that the screen was tilted. Indeed, the PSD in Fig. 17h visually confirm that most feedthrough in the horizontal direction of the PFD occurred during sway (Y). Analysis of the disturbance variance components also confirmed that sway (Y) causes most feedthrough. For the vertical inputs on the PFD the PSDs showed strong feedthrough for both the surge (X) and heave (Z) conditions as expected. This was confirmed by the f_d components in $\sigma^2_{u_y}$, showing strongest feedthrough for surge (X)

(1.32% $u^2_{y,f_{d_x}}$), and less strong, but still significant (0.76% $u^2_{y,f_{d_z}}$) for heave (Z) (Fig. 18b). As the results therefore corresponded fully with the hypothesis, it can be concluded that **Hypothesis H4 holds**.

Finally, the BDFT model parameters were fit onto the model using a Genetic Algorithm method in conjunction with a Gauss-Newton optimization. Beforehand, an analysis was performed which evaluated PSDs and disturbance components in the variance of the control signal. This analysis indicated that sufficient feedthrough of motion signals for accurate BDFT modeling was only observed for six out of twelve conditions. Feedthrough for the remainder of the conditions might be determined if all the repetitions for a single participant and motion condition were to be averaged in an attempt to cancel out noise. Such attempt an was not made during this research due to complexities of mirrored target signals (see Section III.A.2).

To overcome this problem, it is suggested that parts of this experiment are repeated with an increased number of participants. This would allow for more accurate analysis and modeling of the BDFT for conditions in which the TSC inputs were out-of-plane with the motion disturbance. With the increased accuracy, research could be performed on the dependencies of the model parameters on varying factors including pilot seating position and display location. Pairwise comparisons between different conditions often hinted at a difference, but could not be statistically proven. The input loss for the PFD during the baseline and motion conditions is only one example. Results are expected to be more statistical significant with an increased participant pool. This especially holds when multiple pairwise comparisons are made, which affects the Bonferonni correction.

Furthermore, it is recommended to use a single touchscreen brand and type if multiple TSC locations are evaluated. Even though this experiment made use of touchscreen with similar specifications, undocumented system delays are suspected to influence results.

The final recommendation is to increase the realism of the task. This experiment aimed to observe and model BDFT for varying frequencies using a single, continuous way-point dragging task lasting 90 seconds, which simplified analysis of the results in the frequency domain. To improve realism, shorter dragging tasks should be performed by dragging a waypoint to a stationary target. Realism can furthermore be increased by adapting the turbulence profile such, that it corresponds to turbulence typically experienced in the cockpit of a commercial airliner.

As TSCs allow for higher information density[27] and increased situation awareness,[28] the increased use of TSC devices in the cockpit environment is a given fact. One of the main disadvantage of such integration comes from the dynamic environment in which these systems are used.[5] Mitigation of resulting BDFT through model-based signal cancellation has shown to be effective if the BDFT model is adapted to the human operator and the control task.[1] A foundation for such a model was provided in this research.

VI. Conclusions

A cybernetic approach gave insight into the effects of BDFT, occurring when pilots perform a way point dragging task on a Touch Screen Controller (TSC) located in a turbulent cockpit. TSC locations comparable to CDU and FMS positions were evaluated during pure surge (X), pure sway (Y), pure heave (Z) and baseline (No Motion) conditions. Results, based on the TSC input signals, showed a highly significant increase in finger loss of contact using the CDU display when heave (Z) disturbance was added to the control task. Highly significant differences between the PFD and CDU regarding finger loss of contact during the baseline (NM) condition reveal that participants have less trouble providing continuous inputs onto the CDU rather than the PFD. Tracking performance results, based on variances of the error and their components,[23] indicated that effects of BDFT predominantly manifest themselves when motion disturbances act in the direction of TSC control inputs. Components of target signals in the error provided evidence that target signals are more accurately tracked on PFD displays (for all motion conditions) rather than on CDU screens. Components of disturbance signals in the error revealed no significant evidence that BDFT affects a particular screen more than another under comparable motion conditions. Higher remnant components for the PFD relative to the CDU, suggest that the PFD is more susceptible to non linear errors. Neuromuscular effects and fatigue of the human controller are examples that could lead to such errors. BDFT model parameters were fit onto a linear mass, spring and damper model with additional gain. Sufficient feedthrough of motion signals for accurate BDFT modeling was observed for six out of twelve conditions. Results of the parameter estimation were therefore only valid for those conditions. Validation of the BDFT model with its parameters showed that the suggested model can account for at least 70% of the BDFT dynamics for those cases where sufficient BDFT was detected. This potentially allows for mitigation of BDFT through model-based signal cancellation.

References

[1]Venrooij, J., *Measuring, modeling and mitigating biodynamic feedthrough*, Ph.D. thesis, Delft University of Technology, March 2014.

[2]Garmin, "Garmins G3000 Integrated Flightdeck Brings Touchscreen and Widescreens to the Cockpit," October 2009, http://newsroom.garmin.com/press-release/aviation/garmins-g3000-integrated-flightdeck-brings-touchscreen-and-widescreens-cockpi [Online; accessed January 30, 2017].

[3]Rockwell Collins, "Rockwell Collins unveils touch-control flight displays to enable natural eyes-forward operation," http://www.airframer.com/news_story.html?release=13937, July 2011, [Online; accessed January 30, 2017].

[4]Bjørneseth, F. B., Dunlop, M. D., and Hornecker, E., "Assessing the effectiveness of direct gesture interaction for a safety critical maritime application," *International Journal of Human Computer Studies*, Vol. 70, No. 10, 2012, pp. 729–745.

[5]Bauersfeld, K., "Effects of turbulence and activation method on touchscreen performance in aviation environments," 1992.

[6]Dodd, S. R., Lancaster, J., Grothe, S., DeMers, B., Rogers, B., and Miranda, A., "Touch on the flight deck: The impact of display location, size, touch technology and turbulence on pilot performance," *Proceedings of the IEEE/AIAA 33rd Digital Avionics Systems Conference (DASC)*, 2014, pp. 2C3–1–2C3–13.

[7]Rider, K. A., "Effects of ride motion perturbations on the speed and accuracy of in-vehicle reaching tasks," 2006, pp. 1–180.

[8]Bisschop, J. F., *The effects of motion induced interference on the use of touch interfaces in a cockpit*, Master's thesis, Delft University of Technology, Faculty of Aerospace Engineering, July 2012.

[9]van den Berg, R., Damveld, H. J., Borst, C., van Paassen, M. M., and Mulder, M., "Investigating the Effects of Turbulence and Spatial Gesture Thresholds on Multi-Touch Interaction," .

[10]N. Goode, M. G. Lenn and P. Salmon, "The impact of on-road motion on BMS touch screen device operation," *Ergonomics*, Vol. 55, No. 9, 2012, pp. 986–996.

[11]Zaal, P. M. T., Pool, D. M., de Bruin, J., Mulder, M., and van Paassen, M. M., "Use of Pitch and Heave Motion Cues in a Pitch Control Task," *Journal of Guidance, Control, and Dynamics*, Vol. 32, No. 2, 2009, pp. 366–377.

[12]Van Wieringen, A. T., Pool, D. M., van Paassen, M. M., and Mulder, M., "Effects of Heave Washout Filtering on Motion Fidelity and Pilot Control Behavior for a Large Commercial Airliner," *Proceedings of the AIAA Modeling and Simulation Technologies Conference, Portland, Oregon, Aug. 8-11*, No. AIAA-2011-6323, 2011.

[13]Zaal, P. M. T. and Pool, D. M., "Multimodal Pilot Behavior in Multi-Axis Tracking Tasks with Time-Varying Motion Cueing Gains," *Proceedings of the AIAA Modeling and Simulation Technologies Conference, National Harbor (MD)*, No. AIAA-2014-0810, Jan. 2014.

[14]Barendswaard, S., Pool, D. M., and Mulder, M., "Human Crossfeed in Dual-Axis Manual Control with Motion Feedback," *Proceedings of the 13th IFAC/IFIP/IFORS/IEA Symposium on Analysis, Design, and Evaluation of Human-Machine Systems, Kyoto, Japan*, 2016.

[15]Pintelon, R. and Schoukens, J., *System identification: A frequency domain approach*, IEEE Press, 2001.

[16]Pool, D. M., Zaal, P. M. T., Mulder, M., van Paassen, M. M., and Mulder, J. A., "Parameter Estimation of Multimodal Pilot Models for Manual Target-following Tasks," *Proceedings of the 27th European Annual Conference on Human Decision-Making and Manual Control*, 2008.

[17]Field, E. J., Rossitto, K. F., and Hodgkinson, J., "Identification of Frequency Responses from Flight Data and Their Application for Flying Qualities Analyses," *Proceedings of the AIAA Atmospheric Flight Mechanics Conference and Exhibit, Austin (TX)*, No. AIAA-2003-5537, 2003.

[18]Stroosma, O., van Paassen, M. M., and Mulder, M., "Using the SIMONA Research Simulator for Human-machine Interaction Research," *Proceedings of the AIAA Modeling and Simulation Technologies Conference and Exhibit, Austin, Texas, Aug. 11-14, 2003*, No. AIAA-2003-5525, Aug. 2003, pp. 1–8.

[19]Iiyama, "PROLITE TF1534MC-B1X," https://iiyama.com/us_en/products/prolite-tf1534mc-b1x/, 2016, [Online; accessed August 26, 2017].

[20]Dell, "Dell 23 Touch Monitor P2314T," http://www.dell.com/ed/business/p/dell-p2314t/pd, 2016, [Online; accessed August 26, 2017].

[21]Guide, "Guide - The Right Gloves - EN388," http://www.guide.eu/en/info/EN/en388.html, [Online; accessed August 26, 2017].

[22]Field, A. and Hole, G., *How to Design and Report Experiments*, Sage, 2003.

[23]Jex, H. R. and Magdaleno, R. E., "Roll Tracking Effects of G-vector Tilt and Various Types of Motion Washout," *Fourteenth Annual Conference on Manual Control*, University of Southern California, Los Angeles (CA), 25–27 April 1978, pp. 463–502.

[24]Zaal, P. M. T., Pool, D. M., Chu, Q. P., van Paassen, M. M., Mulder, M., and Mulder, J. A., "Modeling Human Multimodal Perception and Control Using Genetic Maximum Likelihood Estimation," *Journal of Guidance, Control, and Dynamics*, Vol. 32, No. 4, July–Aug. 2009, pp. 1089–1099.

[25]Griffin, M., *Handbook of Human Vibration*, 988 p, Academic Press, 1996.

[26]Sears, A. and Shneiderman, B., "High Precision Touchscreens: Design Strategies and Comparisons with a Mouse," *Int. J. Man-Mach. Stud.*, Vol. 34, No. 4, April 1991, pp. 593–613.

[27]Bonelli, S. et all, "The usability evaluation of a touch screen in the flight deck," *Cases on Usability Engineering*, Vol. 53, IGI Global, 2013, p. 270297.

[28]Albinsson, P.-A. and Zhai, S., "High Precision Touch Screen Interaction," *Proceedings of the SIGCHI Conference on Human Factors in Computing Systems*, CHI '03, ACM, New York, NY, USA, 2003, pp. 105–112.

Part II

Preliminary Report

Note:
Part II has already been graded
under AE4020.

Chapter 2

Preliminary Research Questions

In order to obtain insight in the literature research that is to be performed, a research question is posed which is broken down into several sub-questions. Answering these questions might lead to finding gaps in the present state of knowledge regarding the topic of TSC use in the flightdeck environment. Furthermore, the sub-questions provide guidance in the literature that is to be studied.

Note that once gaps in the present state of knowledge have been identified, this research question will be adapted and narrowed down. The updated research question serving for the remainder of the research will be presented in the conclusion of the literature study and serves as basis for the main experiment that will be performed. The general research question for the literature study reads:

Research Question: "What is the present state of research in the field of touch screen use in the cockpit environment and how can the understanding of flight deck motion disturbances contribute to the mitigation of challenges associated with this particular use of touch screen technology?"

Two main topics can be derived from the research question; **Touch Screen technology** and motion disturbance or **turbulence**. First it needs to be determined how TSC devices are currently implemented in the cockpit environment and what developments can be expected for the future, in order to conduct meaningful research.

Sub-question 1: "How are touch sensitive displays currently implemented in the flightdeck environment and what developments are to be expected?"

However, if such developments are found in literature they do not necessarily correspond to tasks that are theoretically best suited for touch screens. To find out for what purposes TSCs are well suitable, and which tasks are better to be conducted using traditional input devices, the next question is posed:

Sub-question 2: "For what applications in the cockpit are touch screen displays best used, and which for which tasks are TSCs not suitable?"

With integration of TSCs in the most common objects such as satellite navigation systems in cars, even the general consumer knows that vibrations can affect the use of such systems. Gaining a deeper knowledge behind the principles behind the effects of vibration are important, leading to the following sub-question:

Sub-question 3: "How do vibrations present in the cockpit affect the human controller?"

With the knowledge of both topics, the following question is posed that connects both the aspects of turbulence and TSCs.

Sub-question 4: "How does turbulence affect the controllability of touch screens in a flightdeck environment?"

Chapter 3

Turbulence

Anyone who has ever tried to operate a satellite navigation system with touchscreen whilst driving over an uneven road surface knows how hard it can be to prevent wrong inputs. Bumps in the road cause accelerations onto the car which translate onto the human body. That these body accelerations can interfere with the ability of a controller to perform his or her task has been known for a long time [25], and as such a lot of research has already been performed onto these effects of these accelerations. The effects of body accelerations (or vibrations) on the execution of a task are, however, very specific to the nature of such task. Furthermore, the effects are also specific to the variable nature of environmental turbulence, making it even harder to extrapolate data from a laboratory setting to a flightdeck situation [26]. In order to fully understand the effects these motion perturbations for the use of TSCs in a dynamic flightdeck environment, the concept of turbulence, perhaps the dominant source of vibrations in an airliner, is to be understood.

Section 3-1 provides a short definition of what atmospheric turbulence actually is. Section 3-2 elaborates on the components and magnitude of typical turbulence. This allows to determine for which frequencies, directions and other components of turbulence the effects of the use of TSCs are to be evaluated. Section 3-3 presents known effects of vibrations on the human body. Note that the terms vibration and body accelerations are used interchangeably in this chapter.

3-1 Definition of Turbulence

Turbulence is often seen as a stochastic process, i.e. a random process which Griffin [27] defines as "*an ensemble of time functions that can be characterized through statistical properties.*" The reason for the 'randomness' lies in the fact that turbulence is the product of a complex mechanism involving atmospheric processes and aircraft dynamic responses. In order to gain a basic understanding of this mechanism, a fundamental introduction follows.

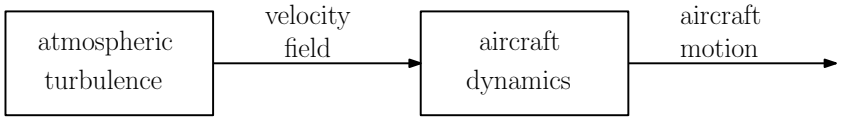

Figure 3-1: A breakdown of 'Turbulence', adapted [28]

3-1-1 Mechanisms for Atmospheric Turbulence

The type of turbulence that is referred to throughout this report is atmospheric turbulence, which mainly finds its origin in thermal mechanisms where parcels of air undergo adiabatic ascent through the atmosphere. This adiabatic ascent takes place due to the geometric temperature lapse rate. For the lower parts of Earth's atmosphere up to 11 km altitude, this lapse rate is defined by ICAO at λ_{dry} = -0.0065 $°C/m$ [29]. If the earlier mentioned packet of air experiences a displacement, temperature differences between the air particles cause a different density under equal pressure. This change of density causes the parcel of air to experience an upward force until density and temperature of the air equal its surroundings. This process also takes place in an opposite way, causing parcels of air to descend [30].

This process especially occurs on sunny days over land, at lower altitudes. During nights, the air is considerably more stable - especially when skies are clear. Stability of the air over water depends on several factors, but mainly relies on differential temperature between the body of water and the temperature of the air [28].

Atmospheric turbulence is, however, not only caused by thermal processes. Mechanical mechanisms can also contribute to the occurrence of turbulence, of which windshear is an example. Windshear refers to the magnitude of rate of change of the wind velocity vector, and can occur in both vertical and horizontal directions, thereby creating atmospheric turbulence by friction between the layers of air. More types of turbulence are discussed in the subsection 3-1-2. Note that most often, atmospheric turbulence is a combination of the two aforementioned mechanisms.

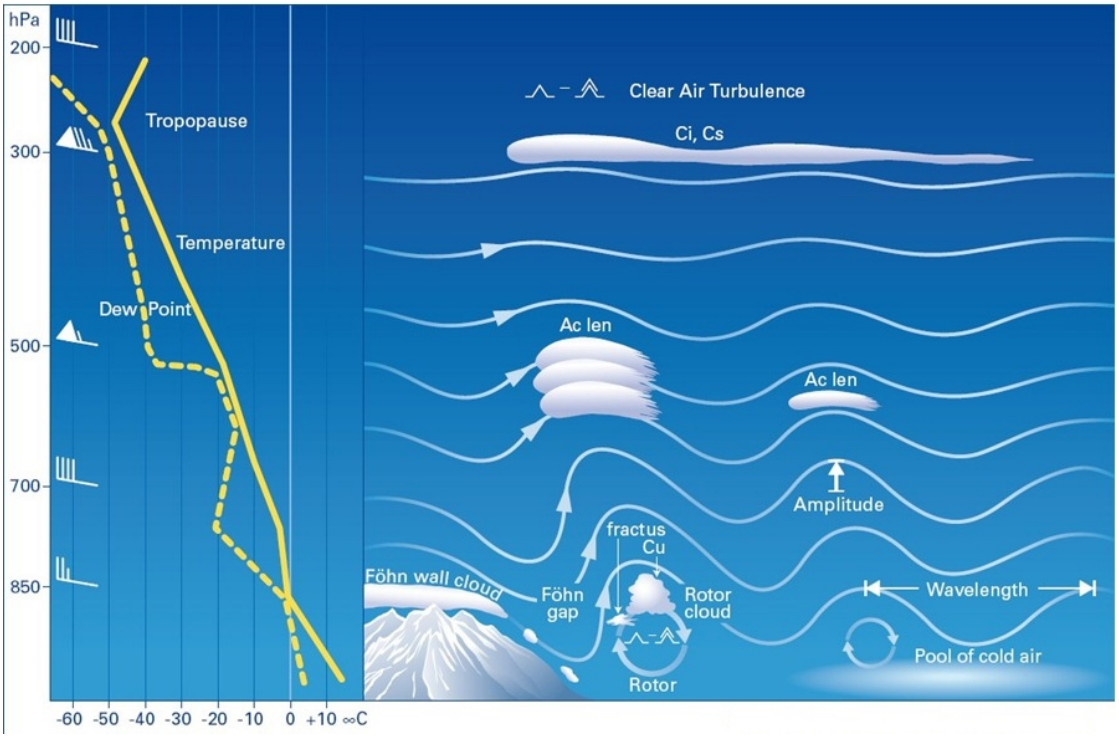

Figure 3-2: Cross-section of conditions associated with mountain waves [31].

3-1-2 Examples of Atmospheric Turbulence

Mountain waves can cause some of the strongest turbulence, and occur when a body of air crosses a mountain or mountain ridge at the right angle. This is depicted in Figure 3-2. Especially the rotor clouds downstream at lower altitudes are of turbulent nature.

Clear-air turbulence (CAT) is used to describe turbulence that occurs outside of clouds and away from the ground, usually occurring in the higher troposphere levels at cruise altitudes from around 7 to 12 kilometers altitude. They often occur near jet-streams, but the mechanical friction from the jet-stream is rarely the only cause for CAT. Often temperature gradients are a contributing cause. Mountain waves can also cause CAT, provided a strong perpendicular wind on a mountain range in combination with temperature inversion at the top of the mountain range is present, as depicted in Figure 3-2.

Turbulence in clouds, and especially in cumulonimbus (CB) exists due to unstable, saturated air. Although CBs initially form turbulence with thermal mechanisms, shear can occur once a circulation has developed. Especially in the region between updrafts and the rain-producing downdrafts the turbulence tends to be severe, where most severe turbulence is to be expected in the top of the clouds.

Wake air turbulence is caused by aircraft that fly through the air. Differential pressure between the lower and upper wing cause vortices and turbulent air, which spread out and descend behind the aircraft over time. Aircraft flying below and behind another aircraft at an angle may experience this type turbulence.

3-2 Intensity of Turbulence

For this literature study it is important to know what kind of accelerations pilots experience in the flightdeck whilst operating a TSC. Figure 3-1 showed that these perceived accelerations are dependent on both the velocity field of the turbulence and aircraft dynamics. Turbulence that is observed in the cockpit therefore depends on the type of aircraft. A description of the typical turbulence that is experienced on the flight deck is given by the United States Federal Aviation Administration "Aeronautical Information Manual" [32], see Figure 3-4.

A more accurate method to describe the intensity of turbulence by means of standard deviations of gust velocities. Usually turbulence velocity vectors are broken down into three separate components, each for every perpendicular direction in the stability reference frame. The velocity vector $\bar{w}_g$ denounces the vertical gust velocity, and is defined positive upward (Figure 3-3). Vertical gusts can, next to accelerating the aircraft vertically, induce pitching moments which are due to the length of the cabin with respect to the Instantaneous Center of Rotation (ICR) most severely felt in both ends of the cabin. The side gust velocity $\bar{v}_g$ is positive

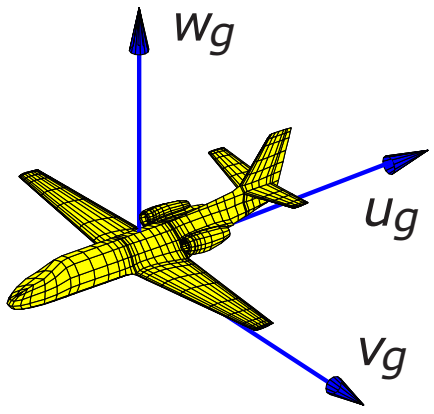

Figure 3-3: Turbulence vector reference system, adapted [28].

towards the left and causes the airplane to yaw and roll under influence of aerodynamic forces on the vertical tail and fuselage. The longitudinal component $\bar{u}_g$ is defined as positive towards the back and is usually of less importance during flight at cruising altitude but can be important for low-speed flight near proximity of the ground [28].

Pritchard[33] experimentally found that the vertical gust velocity standard deviation $\sigma_{\bar{w}_g}$ was a function of wind velocity, terrain factor, height and atmospheric stability, although wind speed and stability of the atmosphere primarily proved to be the major contributors. If isentropic turbulence is assumed, both $\sigma_{\bar{u}_g}$ and $\sigma_{\bar{v}_g}$ are equal to $\sigma_{\bar{w}_g}$ for heights above 250 meters [34]. Typical variances for vertical turbulence velocity rate 1 m^2/sec^2 in ordinary cumulus clouds.

Intensity	Aircraft Reaction	Reaction Inside Aircraft	Reporting Term–Definition
Light	Turbulence that momentarily causes slight, erratic changes in altitude and/or attitude (pitch, roll, yaw). Report as **Light Turbulence;** [1] or Turbulence that causes slight, rapid and somewhat rhythmic bumpiness without appreciable changes in altitude or attitude. Report as **Light Chop.**	Occupants may feel a slight strain against seat belts or shoulder straps. Unsecured objects may be displaced slightly. Food service may be conducted and little or no difficulty is encountered in walking.	Occasional–Less than $^1/_3$ of the time. Intermittent–$^1/_3$ to $^2/_3$. Continuous–More than $^2/_3$.
Moderate	Turbulence that is similar to Light Turbulence but of greater intensity. Changes in altitude and/or attitude occur but the aircraft remains in positive control at all times. It usually causes variations in indicated airspeed. Report as **Moderate Turbulence;** [1] or Turbulence that is similar to Light Chop but of greater intensity. It causes rapid bumps or jolts without appreciable changes in aircraft altitude or attitude. Report as **Moderate Chop.**[1]	Occupants feel definite strains against seat belts or shoulder straps. Unsecured objects are dislodged. Food service and walking are difficult.	**NOTE** 1. Pilots should report location(s), time (UTC), intensity, whether in or near clouds, altitude, type of aircraft and, when applicable, duration of turbulence. 2. Duration may be based on time between two locations or over a single location. All locations should be readily identifiable.
Severe	Turbulence that causes large, abrupt changes in altitude and/or attitude. It usually causes large variations in indicated airspeed. Aircraft may be momentarily out of control. Report **as Severe Turbulence.** [1]	Occupants are forced violently against seat belts or shoulder straps. Unsecured objects are tossed about. Food Service and walking are impossible.	**EXAMPLES:** a. Over Omaha. 1232Z, Moderate Turbulence, in cloud, Flight Level 310, B707.
Extreme	Turbulence in which the aircraft is violently tossed about and is practically impossible to control. It may cause structural damage. Report as **Extreme Turbulence.** [1]		b. From 50 miles south of Albuquerque to 30 miles north of Phoenix, 1210Z to 1250Z, occasional Moderate Chop, Flight Level 330, DC8.
[1] High level turbulence (normally above 15,000 feet ASL) not associated with cumuliform cloudiness, including thunderstorms, should be reported as CAT (clear air turbulence) preceded by the appropriate intensity, or light or moderate chop.			

Figure 3-4: Turbulence reporting classifications of turbulence [32].

3-3 Effects of vibration on Human Performance

The human body is a complex, dynamic structure that does not always behave in a predictable way when exposed to motion. Vibrations can cause annoyance, discomfort, but it can also be exhilarating. It can impair health or induce motion sickness, but it can also cause interference with activities. The whole human body can be brought in vibration through either local vibrations, e.g. when a head or hand touch a vibrating object, or through whole-body vibration in which the controller stands, sits or lies on a vibrating object [27]. Due to the nature of the task that is researched, only whole-body vibrations are considered.

The responsiveness of the human body to whole-body vibrations varies with the direction of the acceleration of these vibrations. In the Z-direction (Figure 3-5), frequencies around 5 Hz affect humans most as the body parts start to resonance [35]. For accelerations in the horizontal axes, most response was found to occur around 2 Hz [36]. Once the human body has been brought into vibration, four effects are observed [37]: Visual Impairment, Neuromuscular interference, Central Effects and Vibration Feed-through. Each of these are elaborated upon in the following subsections.

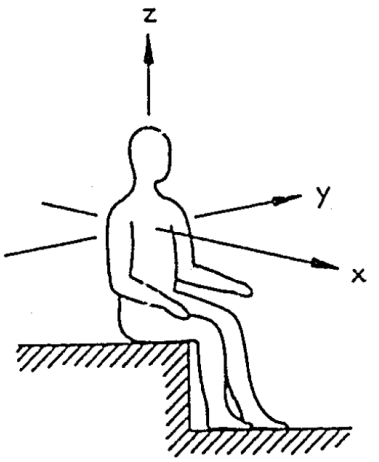

Figure 3-5: ISO2631 Co-ordinate system for mechanical vibration influencing humans, adapted [27]

3-3-1 Visual Impairment

Only a small part of the human eye is capable of capturing a detailed image, the so-called fovea. When a display and operator are moving with respect to one other, it becomes harder for the operator to maintain the information on the display in the foveal vision which impairs the ability to resolve visual detail. The human controller can compensate for relative movement between the eyes and the target by means of pursuit eye movements, but only for frequencies up to 2 Hz. With compensatory eye movements in response to head movements this increases to over 10 Hz [37].

3-3-2 Neuromuscular Interference

The human brain receives feedback of the current whereabouts of the operator's limbs from muscular sensors such as the Golgi-tendon organ and muscle spindles. Vibration can interfere with these feedback processes, reducing the signal to noise ratio (SNR) between intentional and random muscle activity feedback. The effects of neuromuscular interference can be compensated by supporting the limbs, such that the relative movement between them is limited.

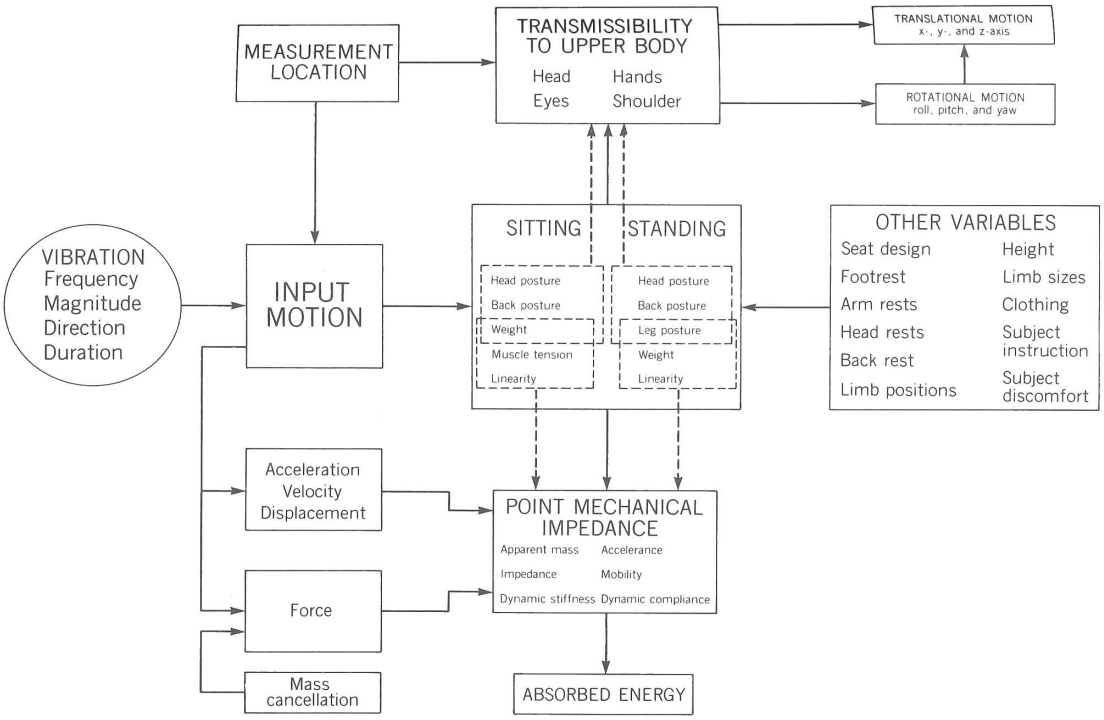

Figure 3-6: Variables associated with BDFT [27].

3-3-3 Central Effects

Central effects refer to cognitive processes that are affected due to the presence of vibrations. Central effects can be both voluntary and involuntary. Examples of voluntary central effects include, but are not limited to changes of control strategy and behavior adaptations to minimize the interference effects. Examples of involuntary central effects include distraction from the task, arousal or anxiety.

3-3-4 Vibration Feedthrough

Vibration Feedthrough, also referred to as Biodynamic Feedtrough (BDFT), is defined by Venrooij as "*The transfer of accelerations through the human body during the execution of a manual control task, causing involuntary forces being applied to the control device, which may result in involuntary control device deflections*" [24].

Several methods to mitigate BDFT were investigated by Venrooij, but only two methods were deemed promising. The first method involves noise signal cancellation, in which a BDFT model is used to cancel out unwanted perturbations. This is, however, only possible if a good model is available of the task that is executed, which is challenging as this model would depend on many variables. Figure 3-6 gives an impression of some of these variables. A second mitigation method involves implementation of passive support systems. Traditional input devices such as switches and knobs already allow for such support, as the operator can hold on to these protrusions. The reduced support of a TSC when performing an input task therefore means that the effects of motion perturbation differ when compared to traditional input means.

3-4 Summary

Being responsible for many of the vibration on board of an aircraft, the fundamental working principles of turbulence were discussed in this chapter. Furthermore, typical values for the intensity of the resulting accelerations were found which helps to determine for which magnitudes of body acceleration research may have to be conducted [28]. Resulting vibrations impact the human body in several ways, causing visual impairment, neuromuscular interference, central effects and vibration feed-trough (BDFT) [37].

Chapter 4

Touch Sensitive Displays

This chapter presents an overview of the research that has been performed in the area of touch sensitive displays and aims to answer the subquestions as posed in Section 1-1 related to TSCs. The advantages of the use of touch screen technology are presented in Section 4-1, after which the disadvantages are discussed in in Section 4-2. Interaction methods and previous findings of the effect of turbulence on these methods are discussed in Section 4-3, before concluding the chapter with examples of current implementation in Section 4-4.

4-1 Advantages of Touchscreen Technology

Touch screen controllers used to be a fancy method to control devices not too long ago. Even though the technology was already proposed in the 60's [9], cost and inaccuracy of the controller prevented widespread implementation at the time. Nowadays, touch screens controllers are integrated in even the most common devices such as thermostats and mobile telephones for good reasons. Use of Touch Screen Controllers brings several advantages:

- Intuitiveness
- Less space occupancy
- Easy adaptation
- Reducing operational effort
- Increased situation awareness

Figure 4-1: Example of non-intuitive control interface to interact with information on a display [38].

The use of TSCs allows to make interaction very intuitive. Information can be accessed on the exact same interface as where control inputs are to be made. This prevents the design of a control interface that does not correspond to information on a screen. One dear example is the scrolling through information on a screen using a round knob (Figure 4-1). Performing control inputs on the same interface as where the information is presented has another advantage of requiring less physical space, which is especially important in a control-interface dense environment like the flight deck [20].

The fact that any part of a touch screen controller can be made responsive to touch inputs allows for easy redesign in case of future updates or improvements of a system. This means that TSCs are essentially adaptable to any configuration, simply by changing the underlying software. The need to remove or reconfigure physical physical control input devices is therefore mitigated. The freedom to assign any part of a TSC to a function allows for the creation of sliders, icons or other forms of buttons to input new information which attributes to "intuitivity" of the controls [17]. As there exists no displacement between the location of information output and control input, attention is maintained. This not only reduces both physical and cognitive effort, but also reduces search time whilst helping users to keep their attention [15]. Whilst an erroneous input on a traditional input device can go unnoticed, a touch screen input is likely observed immediately. Previous studies revealed that TSCs are considered the most effective control method for navigation through subsystems [10], especially for the selection of stationary targets when compared to other peripherals such as joysticks, keyboards and mice [39].

4-2 Disadvantages of Touchscreen Technology

There are, however, also some good reasons to be careful with the implementation of TSCs in a cockpit environment, as disadvantages of its use when compared to conventional controllers exist:

- Absence of tactile feedback
- Parallax errors
- Glare effects
- Increased fatigue
- Accidental inputs

Figure 4-2: Example of glare effects of TSCs on the flight deck. [40].

In previous studies that involved the use of TSCs in a flightdeck environment, criticism that was most often given by pilots was the absence of tactile feedback [41]. The absence of such feedback prevents inputs that can usually be made without visual confirmation of the control action. Example of such control input is turning on the lights of a car whilst driving, which would become significantly harder should such control action be made using a touch screen, as it demands operators to focus solely on the screen.

Sears et al. [42] indicated that another major disadvantage of TSCs susceptibility to parallax errors, the perceived change of a target's location as a result of the operators viewing position. This causes the pilot to make touches that are offset from the target location. Observation of the target may further be complicated due to glare effects of the screen due to high reflection of the smooth surface 4-2. As airplanes are typically exposed to direct sunlight when flying above the clouds, this is especially a problem for the use of TSCs in a flight deck environment. The high reflectivity also causes visibility of smudges due to residual skin fats, limiting visibility of on-screen targets.

Another disadvantage mentioned is increased fatigue. The TSC generally cannot provide support for the hand during operation, as it would result in unwanted inputs. This forces the operator to hold the hand actively in free space whilst using one or more fingers for TSC inputs. The emittance of light from the screen in a dark environment can furthermore fatigue eyes of the controller [43].

The biggest drawback of when compared to physical counterparts, however, are unwanted and accidental touches that can activate or trigger a control action [44]. Whereas physical force is required to switch a button, a TSC can already be activated by an accidental touch. Activation methods described in Subsection 4-3-2 seek to address this issue.

4-3 Display Interaction Methods

As indicated in Section 4-1, TSCs allow for direct interaction with the information that is indicated on the screen. Some of the most used methods to interact with the information are discussed in this Section. A distinction is made between activation- and interaction methods. Whilst activation methods are used to activate a certain target marked on the TSC to select a single option, interaction methods allow for more complex interplay with the information that is displayed on the TSC.

4-3-1 Interaction Methods

Different methods of interaction with a TSC exist to perform a different sorts tasks. From here on, these methods of interaction are referred to as *gestures*. Gestures include both *touch mechanics* defining what your fingers do on the screen, and *touch activities*, i.e. the results of specific gestures. Apple, an electronics manufacturer relying heavily on the integration of TSCs in its products and Google's Android, a mobile operating system, specify gestures in its developer manuals [45, 46]. A distinction will be made between Single Touch (ST) and Multi Touch (MT) gestures, where ST gesture inputs are made with a single finger, whilst MT gestures are to be made with multiple fingers. Furthermore, a difference is made between Discrete (D) and Continuous (C) inputs. Discrete gestures either succeed or fail, and are therefore used for non-quantifiable actions only. On the other hand, continuous gestures provide continuous feedback as long as inputs are registered by the TSC. They are therefore used for quantifiable actions [45].

A selection of the gestures most often used from [45], [46] are specified in the following paragraphs. A summary of these gestures is to be found in Table 4-1.

Tap Tapping and is a discrete input in which the target on the screen is shortly touched. Sometimes it is used to open a certain application or window, but more often tapping is used to activate or select an option on the TSC, comparable to *clicking* when using a peripheral such as a computer mouse. It involves the use of a single finger only. A multitude of these activation methods are discussed in the following subsection 4-3-2. A representation of a tap gesture is given in Figure 4-3a.

Double Tap Double taps too are discrete inputs in which two taps are made with a short interval, typically within 0.5 seconds [45]. This gesture is mainly used open an application or window on a TSC. Both of the taps have to land on the same target in order to launch a specific application or window, and are to be made with a single finger only. A representation of a tap gesture is given in Figure 4-3b.

Hold Hold inputs can be made by providing a maintained, stationary touch at a single target on the TSC. This discrete interaction method is often used to unlock more options of the target that is selected, which can be selected consecutively by a tap. The gesture is to be made by a single finger only. A representation of a tap gesture is given in Figure 4-3c.

Drag Dragging gestures demand for continuous input and can be made, unlike swiping gestures, in more than one direction during the execution of the gesture. Typically a dragging action is made using a single finger only, but it is possible to use multiple fingers as well. Dragging gestures are considered a fine gesture, made to perform a more controlled task and typically have an on-screen target [46]. A practical example for the use of this gesture in a flight deck environment is the moving of route points when interacting with a FMS. Such purpose has been proposed in literature before [47, 48]. A representation of a drag gesture is given in Figure 4-3d.

Swipe Swiping is an example of a discrete gesture that can be made using both a single and multiple fingers, and involves holding fingers on the screen for a short time whilst simultaneously moving in a single, specified direction. Examples of swipe gestures range from scrolling through a page and dismiss messages to revealing hidden information upon swiping and opening a menu. A representation of a swipe gesture is given in Figure 4-3e.

Zoom A zooming gesture is by default a continuous MT event. During the gesture, the controller can zoom the information on the TSC in and out by altering the distance between two touches, as indicated in Figure 4-3f. As proposed in the aforementioned literature [47, 48], zoom gestures can for example be used to display either more of the route on the FMS by zooming out, or get a more detailed representation of the current surroundings by zooming in.

Rotate A representation of a rotation gesture is given in Figure 4-3g. Similar to a zoom gesture, this is a MT event in which at least two fingers are to contact the TSC. Unlike the zooming gesture, however, the distance between the touches is to remain equidistant whilst changing the mutual angle. The rotation gesture is continuous meaning that the rotation angle of the screen can be continuously adapted whilst performing a single gesture, as long as the touches are maintained. A practical example of this gesture would be to change orientation of the map. A combination of the zoom and rotation gestures is possible, resulting in map that simultaneously changes in orientation and level of detail [45].

Table 4-1: A selection of TSC gestures, adapted from [22]

Gesture name	Description	ST	MT	D	C
Tap	Short touch	·		·	
Double Tap	Two consecutive taps	·		·	
Hold	Maintained touch, stationary	·		·	
Swipe	Short touch in specific direction	·	·	·	
Drag	Prolonged touch in multiple directions	·	·		·
Zoom	Changing distance between touches		·		·
Rotate	Changing angle between touches		·		·

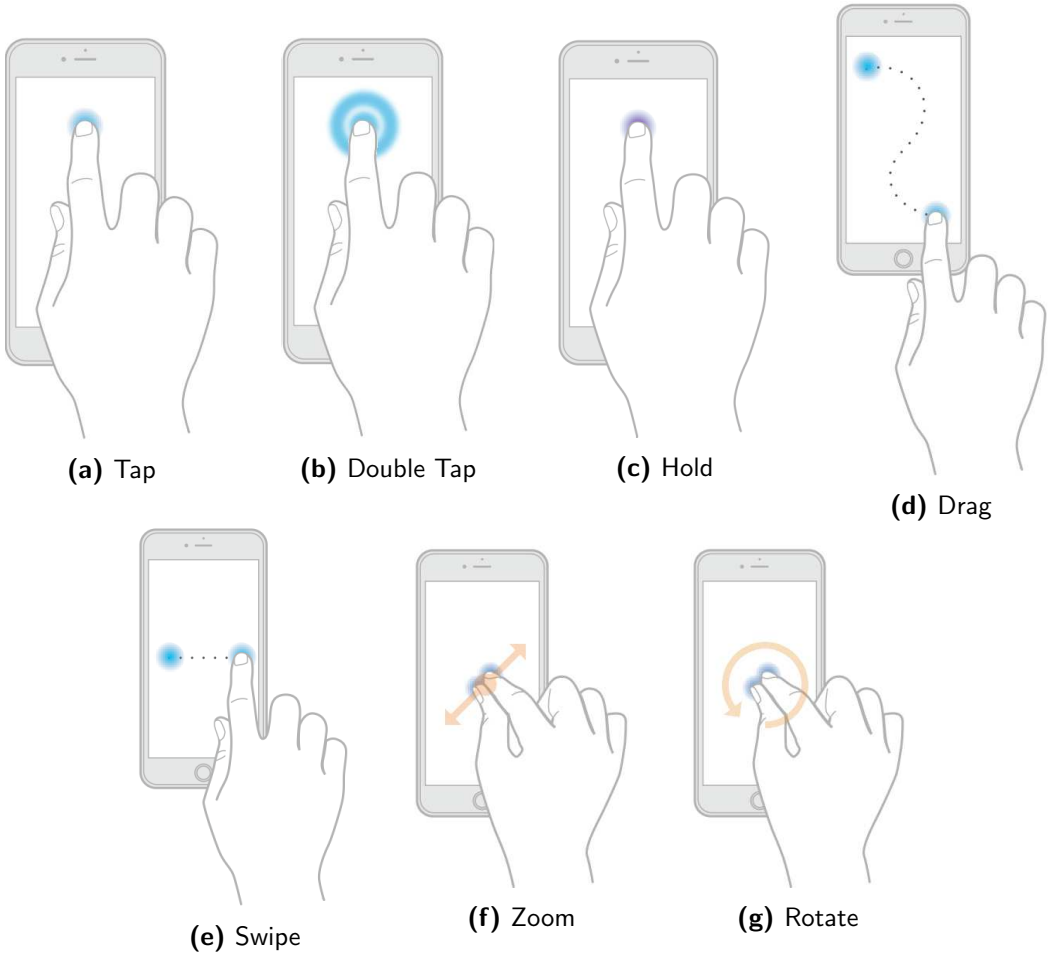

Figure 4-3: A selection of TSC Gestures, adapted [45].

4-3-2 Activation Methods

Whereas Subsection 4-3-1 described the interaction methods with a TSC which are used to input data, activation methods refer to the manner how the target on the TSC is activated. One example is the activation of a target as soon as the finger touches this target location on the screen. There are, however, five methods that are commonly used; land-on, lift-off, land-on – lift off, first contact and sequential touch [42]. Each of these are elaborated in the following paragraphs.

Land On This method ensures that the exact location where the operator's finger lands is activated. If a target is missed, the operator will have to remove the finger and try again. Also, if the finger lands at the wrong target, the erroneous target will be activated. For dynamic environments this interaction method is undesirable, since the controller is unable to correct for the errors once an erroneous touch has been made.

Lift Off This method is similar to the land-on method, but now the exact location where the operator's finger lifts-off the screen is activated. Here too if a target is missed, the operator will have to remove the finger and try again. This method, however, is more suitable for a dynamic environment as the controller is able to correct mistakes. If the finger lands next to the intended target, the operator can drag the finger to the correct location after which lifting the finger ensures the correct target is activated.

Land On – Lift Off is a method that combines both of the previous activation methods. A finger has to land- and lift-off on a target in order to activate it, which makes this method most error-proof.

First Contact This method activates the first target that the finger touches. If a finger lands on a zone that is no valid target, nothing happens. The operator has the ability, however, to drag the finger towards a target. As soon as a target gets in contact with the finger, it is then activated. Although this method increases task completion time [49], it only allows for a correction if a target was initially missed.

Sequential Touch With sequential touch, a series of touches has to be performed in order to activate a function. For example, a confirmation button has to be touched in order to activate a previous selection. This method can be combined with other activation methods such as Land on - Lift off to improve safety even more which would definitely be recommendable for irreversible operations such as engine shut-off, but this would require more time and attention than a regular switch which possibly defies the purpose of incorporating a TSC in the cockpit.

4-4 Current Implementations and Future Visions

Current implementation of TSCs on the flight decks is limited, mainly due to long-term lack of legislation and concerns arising regarding the sensitivity to vehicle motion perturbations.

Garmin was one of the first to announce TSCs in its G3000® cockpit for the business market in 2009 [11], with PA47 Piper Jet and HA-420 HondaJet being the first aircraft to be equipped with this particular cockpit in 2012. In this system, tapping gestures allow for navigation through menus and data entry, whereas panning and zooming of maps is possible using a separate, on-screen touchpad.

Rockwell Collins followed soon in 2011 with implementation of TSCs in its Pro Line Fusion® avionics system, also destined for the business market [12]. This system allowed for dragging gestures to move charts and tapping gestures for navigation through menus and data entry. Rockwell Collins now cooperates with Boeing for implementation of its TSCs in the upcoming Boeing 777X series aircraft, which will support Multi-Touch gestures [1]. Exact uses of these multi-touch gestures were not published at the time of writing.

Honeywell could not stay behind, and it introduced touchscreens in its Symmetry™flightdeck that were to be implemented in some of Gulfstreams larger G500 and G600 business jets [50]. The ten TSCs that are implemented in these cockpits allow for tapping, swiping and dragging gestures to control system controls, flight management, communications, checklists, and monitoring weather and flight information. [51]

For the future, Thales announced the Avionics 2020 cockpit concept [52]. The concept shows intuitive interaction with the system, in which tapping and swiping gestures are used to navigate through the menus. Furthermore, MT gestures are used to zoom in- and out of maps, whilst single finger dragging gestures are used to interact with routes.

More detailed proposals for the use of TSCs in a cockpit environment are available as well. One example is the work of Stuyven et al., who proposes the use of certain gestures for the purpose of interacting with flight routes. In this work, pilots can zoom using the pinch gesture, pan using two finger drag, moving routes using one-finger drag and creation of new intermediate way points by one-finger touches [48]. Mertens and Damveld proposed the same gestures for these tasks [47], an example of their setup is displayed in Figure 4-4.

Figure 4-4: Example of a waypoint modification gesture [47].

4-5 Effects of BDFT on the use of Touchscreens

Chapter 3 explained how turbulence can result in body vibrations. These vibrations caused several effects on the human controller: visual impairment, neuromuscular interference, central effects and vibration feedthrough (BDFT) which results in involuntary movement of controller limbs [27]. Subsequently, this chapter discussed the advantages and disadvantages of the use of TSCs. Especially in combination with the effects of BDFT, accidental inputs are a serious disadvantage to the use of TSCs in a dynamic environments [35].

The purpose of this section is to connect the topics of BDFT and TSCs in order to be able to answer the fourth research sub-question, which asks how turbulence affects controllability of TSCs in a flightdeck environment. Subsection 4-5-1 evaluates previous findings with respect to BDFT effects for different postures. Subsection 4-5-2 looks at the BDFT effects on the execution of different types of TSC gestures and vibration intensity.

4-5-1 Effects of BDFT with varying controller postures

Figure 3-6 showed that many variables affect BDFT. The effect of the controller's posture is one of these key variables. In an attempt to investigate the effects of BDFT on end-point accuracy of reaching tasks in a dynamic environment, Rider [18] conducted an experiment in which locations of the end point targets were differed (Table 4-2).

Table 4-2: Touch locations used by Rider [18].

Button Name	Description	Dist. [m]
Overhead	Above right shoulder	1.2
Radio	Elbow height arm at rest	0.8
Floor	On floor, 45 deg right	0.6
Glove Box	Hip height, 45 deg right	1.0
Steering Column	Fwd of elbow, arm at rest	0.5
Speedometer	Fwd of right shoulder	1.0

Additionally, the frequency of the vertical sinusoidal vibrations was varied. The location of the end point targets affected BDFT effects significantly, as expected. Figure 4-5 shows that a disturbance between 4-6 Hz whilst reaching toward the "Radio" position, the location corresponding to a traditional CDU position, caused the most significant performance degradation. This performance was measured using Effective Target Widths (ETW), an exact quantification of the hypothetical target size should 95% of the touches be successful.

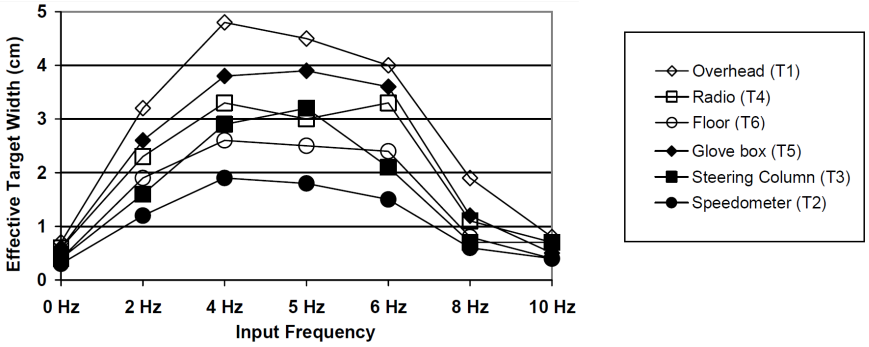

Figure 4-5: Estimate of ETW, as a function of vibration frequency and target location. Adapted [18].

Research in which the target location was varied has also been performed by Dodd et al. [17]. Four TSC locations were used during this experiment; inboard, outboard, forward panel and overhead (Figure 4-6). The inboard and forward located TSCs were found to be least prone to data entry errors. However, increased errors for the other display locations were possibly explained by handedness of the participants and could not necessarily be contributed to effects from BDFT.

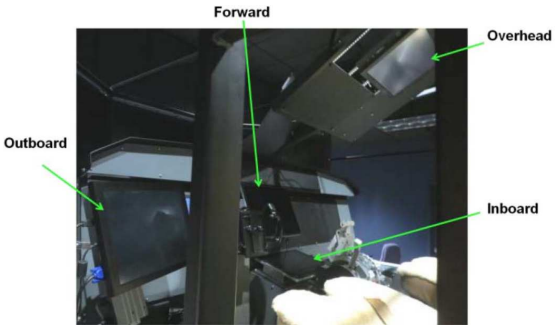

Figure 4-6: TSC locations evaluated by Dodd [17].

4-5-2 Effects of BDFT with varying TSC gestures and vibration levels

Section 4-3 showed that several forms of interaction and activation methods exist for TSCs, each requiring different controller postures. Furthermore, each interaction and activation method affects the extent to which the TSC provides passive support to the controller's limbs. A tapping task for example forces the controller to move limbs through free space before a finger lands on the TSC. A dragging task requires continuous inputs on the TSC, during which the the TSC supports the finger. As it was seen that even small changes in posture and control strategies could dramatically change BDFT, one might conclude that the execution of each of these interaction methods under influence of turbulence deserves its own research.

Some of the research found focused on the effects of reaching out toward a target on a touch screen, i.e. a tapping task, whilst being exposed to motion disturbances. In such case, the BDFT on the unsupported arm whilst moving toward an on-screen target plays a significant role. The experiment of Rider [18] mentioned in subsection 4-5-1 is an example of such task. In addition to the various target locations, vibration levels were changed as well during that particular experiment, and it was shown that increasing levels of vibration negatively affected speed and accuracy of these reaching tasks. A similar experiment was performed by Avsar [53], who investigated the use of touch screen technology under varying amounts of positive acceleration force. In this experiment, the acceleration force was continuous and applied by strapping weights to the controller's limbs. Here too, participants reached out to the screen to tap targets. Results showed that that movement times increased exponentially with increasing weights, whilst throughput decreased [53]. These findings corresponded with findings from Rider. In an attempt to quantify touch error for a reach-and-touch task under influence of turbulence, Bisschop [19] conducted an experiment that proved correlation with the direction of the disturbance motion and the direction of the input error. However, a correlation between acceleration intensity and touch error wasn't found, most likely due technical inaccuracies in the experiment setup.

Van den Berg [22] specifically researched the use of multi-touch gestures under influence of turbulence. Two-finger drag and pinch gestures were used to pan, zoom and re-positioning route maps under influence of three different turbulence profiles. Performance parameters included task completion time and gesture count. A significant relation between task completion time and turbulence was already found for low levels of turbulence.

Research towards the use of touch screen technology in turbulent environments was also performed outside the realms of the aerospace industry. Bjrneseth [21] assessed the use of multi-touch gestures versus traditional touch-screen button- and menu interaction under influence of disturbance motions applicable to the maritime environment. This research revealed that traditional TSC interaction, i.e. tapping gestures with a button-like interface, was better suitable for a moving environment when compared to multi-touch gestures, whereas multi-touch gestures seemed to increase situation awareness .

Goode et al. [23] investigated the effect of vehicle motion on performance, usability and workload with TSC applications for in-vehicle Battle Management Systems using several types of input gestures for two different motion disturbances: smooth- and rough road conditions. Tapping, multi-touch panning- and zooming, hold and drawing using a continuous drag input gestures were evaluated. For all input methods, workload increased whilst performance decreased due to the additional time required to complete tasks. Dodd's experiment [17] too evaluated tapping and dragging gestures. For increased levels of vibration, participants again committed more errors and needed more time to complete the task.

Research that looked at a trade off between activation methods under the influence of turbulence has also been performed. Bauersfeld specifically looked at the first-contact and lift-off methods, as they seemed the most suitable for flightdeck applications for reasons described in Subsection 4-3-2. Significant relations were found between intensity of turbulence and path length before target activation. Furthermore, a trade-off between the two activation functions and the level of turbulence was found. Finally, the level of turbulence did not impair pilot's ability to perform their task [35].

4-6 Summary

Advantages and disadvantages of the use of TSCs have been discussed in this chapter. Touchscreens proved to be especially useful on the flightdeck because of the ability to show more information in a limited amount of physical space, whilst increasing situation awareness [20]. Lack of tactile feedback [41] and parallax errors [42] proved to be important disadvantages of the use of TSCs. However, the accidental triggering of control actions [44] might be the largest disadvantage when using TSCs on the flightdeck, as BDFT is likely to be induced in these types of vibrating environments.

Furthermore, several TSC interaction methods were discussed, where a distinction was made between Single- and Multi-Touch gestures, and between Continuous and Discrete gestures. Discrete gestures, such as tapping, are already used for TSC systems [11], whilst the use of continuous gestures has been proposed [47, 48, 51, 52]. Finally, activation methods were discussed. Although activation methods that mitigate unwanted inputs do exist, they tend to consist of sequential touches that take up much time. It is for that reason that TSCs are less suitable for the control of actions that are of critical nature.

It was seen that efforts have been made to investigate the effects of BDFT on the use of TSCs. In general, increasing levels of motion disturbances caused an increase in task completion time and decreased performance for all types of gestures [17, 22, 18, 23]. TSCs located right in front and slightly right to the controller provided best performance for two experiments, whereas overhead displays and TSCs on the location of the CDU caused worst performance [17, 18].

Chapter 5

Conclusion and Recommendations

Although the use of touch screen technology is wide spread, a number of unsolved challenges still stand in the way of successful implementation in the flight deck environment. One of the main challenges is to mitigate the effects of BDFT in such dynamic environment, involuntary screen inputs caused by the highly dynamic environment [35]. A literature study was performed to identify shortcomings in current research regarding this topic.

To guide the literature study, research questions were posed in Chapter 1. With the background information that was gathered in the previous chapters, these questions can now be answered in Section 5-1 which serves as a conclusion. Eventual shortcomings from current research that emerge are used for the recommendations towards further research in Section 5-2.

5-1 Answers to Research Questions

> "How are touch sensitive displays currently implemented in the cockpit environment and what developments are to be expected?"

Touchscreen technology is currently used for a multitude of applications. In the cockpit environment, however, usage of the technology proved is still very limited. So far, only few systems manufactured by Garmin, Rockwell Collins and Honeywell intended for the business segment do have implemented TSCs, allowing data entry using tapping gestures, swiping gestures for menu navigation and dragging gestures for map displacement [11, 12, 51].

Boeing, Thales and Rockwell Collins have announced implementation of more advanced systems in future flight decks which are also aimed at the commercial market [1, 52]. These systems allow for more intuitive multi-touch gestures and route manipulation. Proposals with similar functions have been made in literature. With increasing amounts of subsystems, and therefore increasing amounts of data that has to be managed from the cockpit, increased use of touchscreen technology is expected as it provides maximum use of the limited physical real-estate available [20] whilst simultaneously increasing situation awareness of the pilot [15].

"For what applications in the cockpit are touch screen displays best used, and for which tasks are TSCs not suitable?"

It was seen that Touch Screen Controllers improve situation awareness if natural interaction is possible, for example using intuitive gestures [15]. Multiple proposals for the use of such gestures in a flightdeck environment have been made, of which interaction with the flight path proved to be the most suggested application [47, 48]. From a situation awareness point of view, this makes sense as current flight path alterations have to be made using the FMS. The FMS currently does not give a direct graphical representation of these alterations but instead uses a separate Navigation Display (ND), decreasing situation awareness.

Touch screens are, however, less suitable for the control of actions that are of critical nature, such as manipulation of engine status. Switching off an engine using an TSC would require for sequential-touch and land on – lift off activation methods to prevent critical errors [35], which would be very time consuming and thereby defeat the purpose of a touch screen.

"How do vibrations present in the cockpit affect the human controller?"

It was seen that vibrations have four effects on the human body [37]. Visual impairment prevents the operator from obtaining an accurate foveal image of the observed information. Neuromuscular interference reduces SNR between intentional muscle activity and inadvertent muscle activity, which may lead to perceptual disorientation. Central effects include voluntary or involuntary changes in control behavior due to interference of vibration with cognitive processes. Finally, vibration feedthrough or biodynamic feedthrough leads to unwanted control inputs due to feedthrough of accelerations through the human body to the input device. Although these types of interference all affected the use of traditional input devices such as buttons and switches before, it is the latter mentioned BDFT that poses the main problem for the use of TSCs, as mitigation of BDFT due to contact with a physical switch is inconceivable.

"How does turbulence affect the usability of touch screens in a flightdeck environment?"

Turbulence affects the use of touchscreens significantly [22, 18, 19, 21, 23]. The previously mentioned BDFT in combination with effects caused by visual impairment and neuromuscular interference adversely affect speed and accuracy of reaching tasks. The extent to which the ability to perform the intended task is affected depends on position and orientation of the screen with respect to the controller and the gestures that are used to interact with the TSC [18]. A trade-off between activation methods has been shown to exist with increasing turbulence levels. [35] Also, traditional button-like layouts were shown to be preferable over interfaces that demand for MT gestures with increasing turbulence [21]. However, interfaces that reflected the state of the aircraft more naturally and allowed for intuitive interaction did increase situation awareness of the pilot. This also allowed for easy continuation of a specific task after an interruption.

The main research question that was posed in Chapter 1-1 can now be answered;

> What is the present state of research in the field of touch screen use in the cockpit environment and how can the understanding of flight deck motion disturbances contribute to the mitigation of challenges associated with this particular use of touch screen technology?

It was seen that research towards the use of touch screens in the cockpit environment has been performed. Even more so, TSCs are already implemented on a small scale [11, 12, 51]. Efforts are being made to develop products for the commercial market and propositions for implementation of certain gestures were also made in literature [47, 48]. There is a good understanding of the pros and cons of such use, intuitive design being one of the biggest advantages [15] and BDFT being the biggest disadvantage. Although the concept of BDFT is well known, mitigation currently only takes place in the form of passive support systems. Mitigation of BDFT using noise signal cancellation was proposed in literature [24], but it requires a good model of the BDFT. Efforts to build such a model for the use of touch screens in a turbulent environment have not been found in existing literature.

5-2 Literature Study Recommendations

Several conclusions can be drawn from the literature study. First of all, more intuitive gestures for purposes such as map zooming, panning and route-dragging tasks are going to play a major role in the design of TSC layout in a flight deck environment [12, 47, 48, 52]. Furthermore, although several researchers aimed to exactly quantify the control errors made when using such input devices in a turbulent environment [18, 19], this seems to be less useful as far too many variables affect the results. Also, observed vibrations in the cockpit are a product of the velocity field and the aircraft dynamics [28]. Therefore, observed vibrations differ per aircraft type. Research should be performed with a focus on continuous touch (CT) tasks, such as a route displacement assignment. This particular gesture proves promising for future use, and little research toward this particular single-touch dragging task has been performed before. As exact quantification of touch errors during such task cannot be extrapolated to out-of-laboratory scenarios, focus should be placed on the general biodynamic feedthrough effects for the task in order to add meaningful contributions to the body of knowledge. Although BDFT too is dependent on many variables, it is believed to provide a better generalization of the effects that occur over a wide frequency range. This analysis is recommended to performed for both vertically and horizontally oriented displays, as literature suggested that effects of turbulence are most noticed if the screen surface is located in the same direction as the perturbations [19]. Given that atmospheric turbulence mainly acts in the vertical direction with respect to the body axis of the aircraft, different BDFT models are to be expected for different screen orientations.

With this specific insight which has been gained from the literature study, the research question posed in Chapter 1-1 can be narrowed down;

> "How do motion disturbances influence pilot control skills and biodynamic feedthrough whilst performing a dragging task on flightdeck-based touch screen positioned at the PFD and FMS locations?"

In order to find an answer to this research question, it is recommended to use the work of Venrooij [24] as a theoretical basis to obtain a general model for the biodynamic feedthrough which occurs whilst conducting a dragging task during turbulence exposure. In order to perform such analysis, continuous TSC inputs of the controller should be measured and recorded which are then to be analyzed in the frequency domain. If the effects of BDFT manifest, the frequencies used as motion disturbance are expected to appear in this frequency analysis. The ratio between power at the disturbance frequencies and the TSC input power at the corresponding frequencies can then be used to obtain an estimate for BDFT.

To observe whether it is possible at all to conduct such experiment, it is recommended to conduct a preliminary experiment. This preliminary experiment would evaluate whether a controller suffers from BDFT during a CT task, or if the friction between finger and TSC, and physical support of the TSC are sufficient to mitigate the effects of BDFT. Furthermore, a preliminary experiment would show if disturbance frequencies manifest in a frequency analysis of TSC inputs, should effects of BDFT occur.

In order to gain a deeper understanding on the pilot control skills, it is recommended that the theoretical basis by Venrooij is used in conjunction with pilot identification techniques to model pilot control behavior. Although human manual control behavior is often seen as inherently non-linear, there are methods to describe carefully designed control tasks with quasi linear pilot models [54]. These quasi linear pilot models consist of both a linear part describing the controllers' response to the signals that he or she perceives, and a remnant signal that accounts for the behavior that cannot be captured by the model. Values for the parameters of the linear part of this model can be estimated using identification techniques. Such techniques have been successfully applied before [55, 56, 57, 58, 59, 60, 61, 62]

Chapter 6

Preliminary Experiment Setup

Based on the recommendations from the literature review, an initial proposal was made to investigate effects of the particular effects of BDFT on a continuous dragging task. Due to the concern that this particular task is not affected by BDFT for reasons described in Section 6-1 and therefore could not be measured, a preliminary experiment was conducted that served as proof of concept. The current chapter describes how this particular experiment was designed and executed. Section 6-2 describes the task that participants were asked to conduct. A more theoretical background behind this experiment is given hereafter, as Sections 6-3, 6-4 and 6-5 describe the theory behind the forcing functions, the apparatus and the implementation of the experiment into the apparatus respectively. Finally an overview of the procedures that were followed will be presented in Section 6-6. The results of this experiment are presented in Chapter 7.

6-1 Experiment Objective

In the literature review part of this report it was fuond that mitigation of BDFT was possible, albeit to a limited extent, either using a model-based BDFT cancellation (in which a BDFT model is used to calculate a real-time cancellation signal) or by providing passive support [24]. The nature of the continuous dragging task in question means by definition that a physical contact between the control element, the finger of the operator, and touch device exists. It is this connection between the finger and the touch device that might lead to sufficient support and friction to mitigate BDFT.

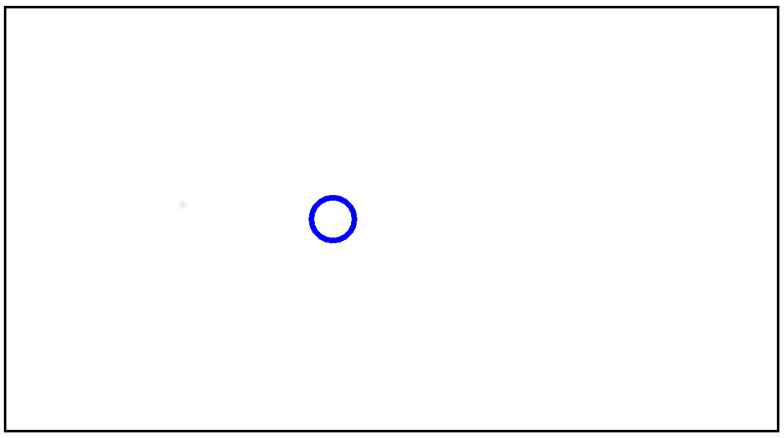

Figure 6-1: Visual representation of the preliminary experiment interface.

To determine whether a research into the proposed touchscreen activation task would yield fruitful results, a preliminary experiment is conducted that acts as proof of concept. In case BDFT can be measured in a continuous dragging task, a research proposal towards more elaborate research can be made.

6-2 Control Task

In order to observe to which extent BDFT influences the control behavior of a pilot whilst performing a continuous drag task, a pursuit tracking experiment was performed. In such a task, subjects are to minimize the error between the current finger position and the position of the target, indicated with a blue hollow circle. By following a target indicated on a touch sensitive display with the controllers finger, a way-point dragging task was simulated. A representation of the interface used is given in Figure 6-1. The target position moved in the horizontal (x) direction only, and its position was determined by a target signal, which is described in detail in Section 6-3.

Motion cues were given to the controller in varying directions whilst performing this tracking task, but in no more than one direction at a time. The four conditions were as follows;

- Surge
- Sway
- Heave
- No Motion

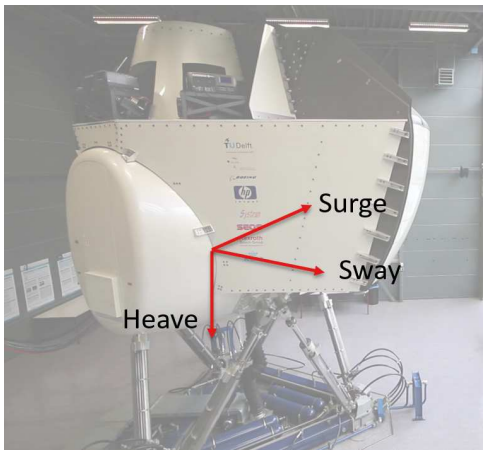

Figure 6-2: Visual representation of motion disturbance directions.

The disturbance signal used in each of the conditions was identical. Information regarding the composition of the signal can be found in Section 6-3. Note that the motion conditions were the only independent variables during this preliminary experiment.

For this experiment a within-subjects design was chosen. All subjects completed the same motion conditions, executed in a different order to prevent possible confounds to the experiment results. The order in which the different conditions are executed are indicated by the latin square in Table 6-1.

Table 6-1: Latin square used for the preliminary experiment.

		Run								
		R1	R2	R3	R4	R5	R6	R7	R8	
Condition	S1	1	2	3	4	1	2	3	4	etc..
	S2	2	3	4	1	2	3	4	1	
	S3	3	4	1	2	3	4	1	2	
	S4	4	1	2	3	4	1	2	3	

6-3 Forcing Functions

Analysis of the effects of BDFT caused by turbulence on touch sensitive display inputs required the need for disturbance signals that simulated atmospheric turbulence. Since the objective was to observe if certain disturbances were fed back into the touch inputs of the participants, these disturbance signals should be well understood by the designer of the signal whilst appearing completely random to the participant. Furthermore, the experiment demanded for a moving target that was to be followed by the human controller. In order to prevent the human controller from developing strategies to counteract motion disturbance, a predictable movement function was to be avoided.

For both purposes, sum-of-sine target and disturbance forcing functions were used, f_t and f_d respectively. The disturbance function properties for heave, sway and surge and the target forcing function properties are given in 6-2. These disturbance frequencies have been based on values found in [55], and have been successfully used in previous experiments [63] [64]. The amplitude distribution of these forcing functions were adapted to fit the motion limits of the SRS (Table 6-3) and determined using a low-pass filter, also used by Pool and Zaal [65]. Furthermore, a cresting technique was used such that peaks in the time domain were prevented [66]. The crest factor (CF) is determined using 6-1, and is defined as the maximum amplitude of a signal divided by the Root Mean Square (RMS) of this signal.

$$CF = \frac{max|f_{d(t)}|}{RMS|f_{d(t)}|} \tag{6-1}$$

From the resulting properties, the forcing functions were generated according to Equation 6-2, in which amplitudes $A_{d,t}$, frequencies $\omega_{d,t}$ and phases $\phi_{d,t}$ are defined for each individual sinusoid.

$$f_{d,t}(t) = \sum_{k=1}^{N_{d,t}} A_{d,t}(k) sin[\omega_{d,t}(k)t + \phi_{d,t}(k)] \tag{6-2}$$

The forcing function f_t that was obtained using Equation 6-2 with properties of the second column in Table 6-2. To prevent a nonzero starting position a fade-in function was introduced, indicated in Equation 6-3. The result of this fade-in function was multiplied with the the forcing function from equation 6-2 to obtain a target function that was faded in, ensuring a zero start. This resulting signal was directly used to drive the target position, in the horizontal direction only.

$$g_{d,t}(t) = (1 - cos(\frac{\pi t}{t_{fade}}) \cdot 0.5) \tag{6-3}$$

The forcing function f_d too was obtained using Equation 6-2 with properties from Table 6-2. This resulted in a position signal for disturbance. The apparatus described in 6-4, however, required acceleration inputs and it too required a zero starting position. Differentiating a faded position signal twice to obtain acceleration inputs for the hexapod simulator would yield motion commands that drift the simulator to the edge of its motion

bounds due to a nonzero mean. Using Equations 6-2 and 6-3 in combination with the chain rule indicated in 6-4 prevented such drift and yielded an acceleration signal that was properly faded whilst preventing a nonzero starting acceleration. This resulting signal is visualized in Figure 6-3.

$$f_{d_{faded}}(t) = f_d \cdot g_d'' + 2 \cdot g_d' \cdot f_d' + f_d'' \cdot g_d \tag{6-4}$$

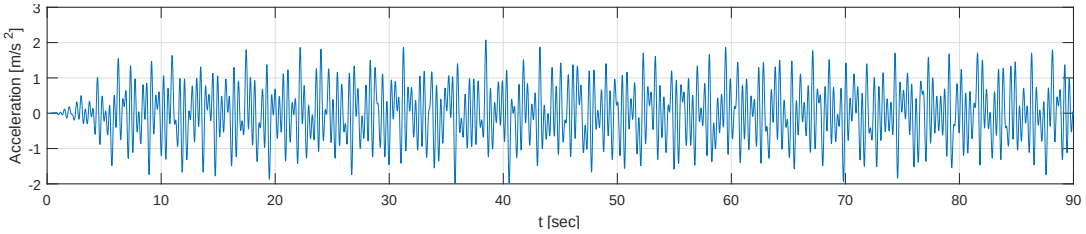

Figure 6-3: Motion disturbance signal $f_{d_{faded}}$

Table 6-2: Target and Disturbance forcing function properties.

disturbance, $f_{d_{xyz}}$				target, f_t			
$n_d, -$	ω_d, rad s^{-1}	A_d, deg	ϕ_d, rad	$n_t, -$	ω_t, rad s^{-1}	A_t, deg	ϕ_t, rad
5	0.3835	1.062e –01	-2.692e –01	3	0.2301	7.897e –01	1.445e +00
11	0.8437	8.029e –02	4.016e +00	7	0.5369	9.587e –01	1.478e –04
23	1.7641	3.999e –02	-8.065e –01	19	1.4573	1.720e +00	-1.825e +00
37	2.8379	2.037e –02	4.938e +00				
51	3.9117	1.240e –02	5.442e +00				
71	5.4456	7.530e –03	2.274e +00				
101	7.7466	4.712e –03	1.636e +00				
137	10.5078	3.407e –03	2.973e +00				
171	13.1155	2.841e –03	3.429e +00				
226	17.3340	2.404e –03	3.486e +00				

6-4 Apparatus

The experiment was performed in the SImulation, MOtion and NAvigation Institute (SIMONA) Research Simulator (SRS) at the faculty of Aerospace Engineering at the Delft University of Technology, Figure 6-4a. This simulator was equipped with a touch screen device which was mounted horizontally on the pedestal as indicated in Figure 6-4b. Besides controlling the target on the touchscreen, no other input methods had to be used. Outside visuals had been disabled to prevent possible visual distractions and cockpit lighting was turned on. Furthermore, motion was enabled to provide the disturbances. This motion was independent from the control inputs and was directly derived from the disturbance function without the use of additional motion filters. The participant was seated on the left side of the input device throughout the experiment.

Table 6-3: Motion limits of the SIMONA Research Simulator [67].

Degree of Freedom	Minimum	Maximum
Surge	-0.981 [m]	1.259 [m]
Sway	-1.031 [m]	1.031 [m]
Heave	-0.636 [m]	0.678 [m]
Roll	-25.9 [°]	25.9 [°]
Pitch	-23.7 [°]	24.3 [°]
Yaw	-41.6 [°]	41.6 [°]

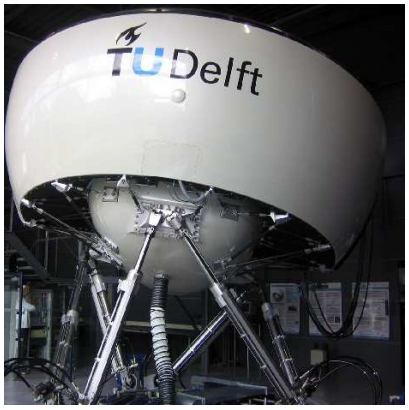

(a) Outside View of the SRS

(b) Touch screen setup in the SRS

Figure 6-4: The SIMONA Research Simulator and the preliminary experiment setup.

6-5 Implementation

The experiment was implemented onto the SRS using a software middleware layer called DUECA (Delft University Environment for Communication and Activation). Implementation using DUECA allows for easy implementation of simulation modules without dealing with the complexities of real-time scheduling [67]. The information between these modules is distributed over channels, indicated by the lines running between the modules. A schematic overview of the experiment modules can be found in Appendix 1, where the modules are indicated by square boxes.

The experiment is initiated from the Experiment Control Interface (ECI), providing a Graphic User Interface (GUI) with the possible experiment settings. Either the Joystick or Touchstreamer modules provide inputs to the experiment, where the Joystick is used for development purposes only. The Forcing Functions module converts the forcing function properties from Table 6-2 to forcing function signals as described in Section 6-3. The System Dynamics module converts the target forcing function to an actual screen position, which is used by the Display module to plot the target onto the touch screen. The Signal Checker is provides a graphical representation of the current disturbance to the simulator engineer. In order to engage the participant to deliver a good performance, the RMS(e) score is indicated between the runs. This score is determined by the Score Calculator module based on the variance of the error between the actual finger position on the screen and the target position, in the horizontal direction only. The DataLogger module finally stores all important data that is to be used for the analysis of the experiment. Note that although the target is moved in the horizontal direction only, the current finger position is logged in both the horizontal and vertical directions.

6-6 Participants and Procedures

In total 6 participants performed the experiment, all of them right-handed males. The average age was 27.7 years with a standard deviation of 3.9 years. None of them had previous experience with this particular control task. The experiment did not call for any set of piloting skills, hence these participants were not required to have any flight experience.

All pilots were instructed to read a two-page briefing before arriving at the SIMONA. The briefing was emailed to pilots before their scheduled experiment session and explained the purpose of the experiment and the overall procedures. Pilots were not given any details about the motion conditions.

At the day of the experiment, pilots initially received a verbal briefing on the experiment, covering the items mentioned in the emailed briefing. Additional questions that pilots may have had were answered during this briefing. Consent forms and other paperwork requiring personal details were filled out by the pilot at this time.

After the experiment briefing pilots received a safety briefing on the SIMONA, explaining the plan of action in the event of an emergency. Pilots were then strapped in and seating position was adjusted such that the they felt as comfortable as possible whilst executing the experiment.

The experiment consisted of four sessions with three runs each according to the latin square as represented in Figure 6-1. The SIMONA engineer on duty mentioned the RMS(e) to the participant to stimulate good performance. The participant was instructed to try and obtain the lowest score possible. No information was given regarding the motion conditions or on how to improve RMS(e) scores at any time. After the final run of the transfer phase, all questions that participants may have had were answered, including details on motion conditions.

Chapter 7

Preliminary Experiment Results

The results obtained from the preliminary experiment, which was conducted as described in Chapter 6, are presented in this chapter.

The goal of the experiment was to observe whether disturbance frequencies were reflected in the screen inputs. To this extent, the Power Spectral Densities (PSD) of the control inputs are compared between different conditions in Section 7-1. From these PSDs an estimation for BDFT in the form of a bode plot can be made, allowing to see at which turbulence frequencies BDFT causes the most adverse inputs. Results of this estimation are presented in Section 7-2. Finally, the performance of the participants is analyzed which allows to observe from which disturbances input errors originate, these results are presented in Section 7-3. A more elaborate discussion regarding the results presented in the preceding sections follows in Section 7-4-2. From this discussion, a conclusion is drawn with recommendations for the research proposal.

7-1 Power Spectral Densities

Chapter 6 described how forcing functions were used to excite the human controller at various disturbance frequencies. Using a set of predefined multisine parameters, a seemingly random yet fully deterministic signal was created in the time-domain that simulated turbulence. Goal was to see how much response was to be found in the input signals onto the Touch Screen Controller (TSC).

In order to visualize at which disturbance frequencies the participant is excited, the disturbance signal in the time domain is converted to the frequency domain using the Fast Fourier Transform (FFT). Here, the average amount of power per unit of frequency generated is determined, yielding the PSD (Power Spectral Density) [68]. The result for the motion and target disturbance signals are given in Figures 7-1b and 7-1a respectively. Both the target and motion disturbances remained constant for all experiment conditions, with exception of motion disturbance for the baseline condition.

This same procedure can be repeated for both the horizontal and vertical screen inputs. This yields a representation of how much of the disturbances are fed through to the TSC by the participant. These results are presented in Subsections 7-1-1 and 7-1-2 respectively. It should be noted that these PSDs have been generated from the the time-averaged horizontal inputs of all participants with a specific condition. Red stars indicate the motion disturbance frequency locations, whereas green stars indicate the target function frequency locations.

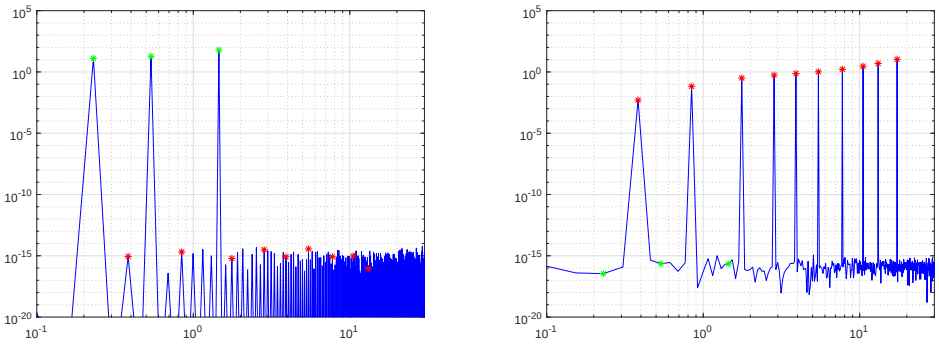

(a) Target disturbance **(b)** Motion disturbance

Figure 7-1: PSDs of the target and motion disturbance signals

7-1-1 PSD: Horizontal input

Figure 7-2 displays the PSDs for the horizontal input under influence of each of the disturbance conditions. For all conditions three large peaks are observed in the lower frequency ranges. These correspond to the target peak locations in Figure 7-1a and Table 6-2, indicating that participants had no trouble following the target signal.

When looking at the figure with the horizontal screen input PSD under influence of **surge** motion disturbances, it can be seen that the frequencies at which motion disturbance excited the participant do not reflect in the touchscreen input signal for lower frequencies. It is only for the higher motion disturbance frequencies that a response is seen in the touchscreen. A similar behavior is observed for the **heave** condition. A response to motion is not observed in the baseline condition, which matches the expectations as motion disturbance for that condition lacks. The figure displaying the PSD of horizontal screen inputs under influence of **sway** motion disturbances does reflect the motion disturbance signal frequencies for all but the lowest frequencies.

7-1-2 PSD: Vertical input

Figure 7-3 displays the PSDs for the vertical input under influence of each of the disturbance conditions. This figure too was generated from the time-averaged vertical inputs of all participants for each specific condition.

This time, the three large peaks at the lower frequencies indicating the response to the target function are less present due to the fact that the target only moved in the horizontal plane of the screen. However, note that these peaks are still clearly visible under influence of heave disturbance and in the baseline condition.

Most response to motion disturbance is observed in the **surge** scenario, indicated by the large peaks. This is consistent with findings in 7-1-1 that the contribution of disturbance motion is largest when acting in the same plane as the control inputs. For both the **sway** and **heave** scenarios, a response to motion in the vertical screen inputs is observed at higher frequencies only. Once again, a response to motion is not observed in the **baseline condition** as expected.

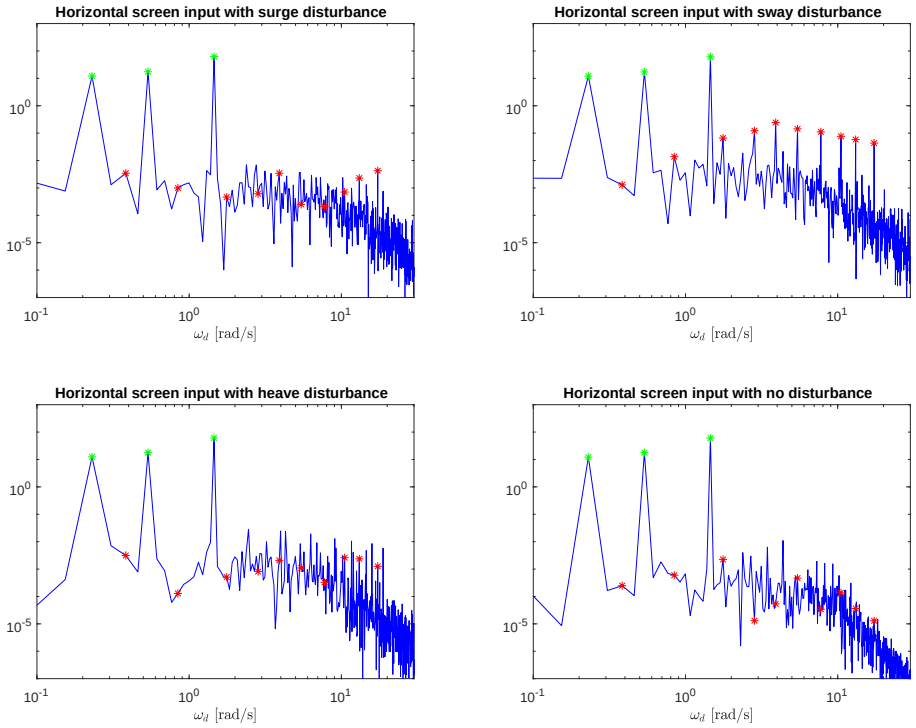

Figure 7-2: Horizontal input PSD, averaged over all participants.

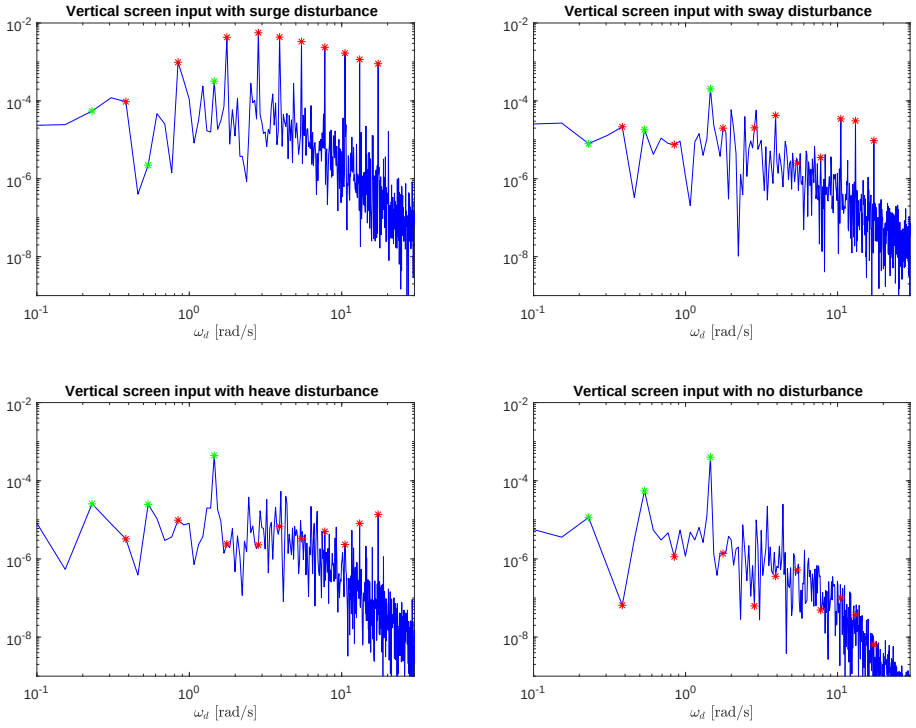

Figure 7-3: Vertical input PSD, averaged over all participants.

7-2 Biodynamic Feedthrough Estimation

The amplitudes for various frequencies in the PSDs presented in Chapter 7-1 do in itself not give an indication of the extent of BDFT for these frequencies. After all, a large disturbance power at a certain frequency is almost guaranteed to cause a large input power for that specific frequency onto the touchscreen.

Instead, a transfer function $H_{BDFT}(j\omega_m)$ describing the BDFT can be estimated using the motion disturbance as input and the touch screen controls as output [24], with ω_m being the frequency range of the disturbance signal and j the imaginary unit. The estimate of this transfer function, $\hat{H}_{BDFT}(j\omega_m)$, is calculated using Equation (7-1) in which $\hat{S}_{f_d,y_{x,y}}$ represents the estimated cross-spectral density between the disturbance signal $f_d(t)$ and screen inputs in the horizontal and vertical direction $y_{x,y}$. $S_{f_d,f_d}(j\omega_m)$ represents the auto-spectral density of the disturbance signal $f_d(t)$.

$$\hat{H}_{BDFT}(j\omega_m) = \frac{\hat{S}_{f_d,y_{x,y}}(j\omega_m)}{\hat{S}_{f_d,f_d}(j\omega_m)} \tag{7-1}$$

The behavior of this obtained transfer function is represented by bode plot in Figure 7-4. In this figure, results of all participants for a specific condition have been averaged. The top figures indicate the BDFT magnitude for horizontal and vertical inputs respectively, whereas bottom figures reveal the BDFT phase plots. Whiskers illustrate the spread of individual participant results.

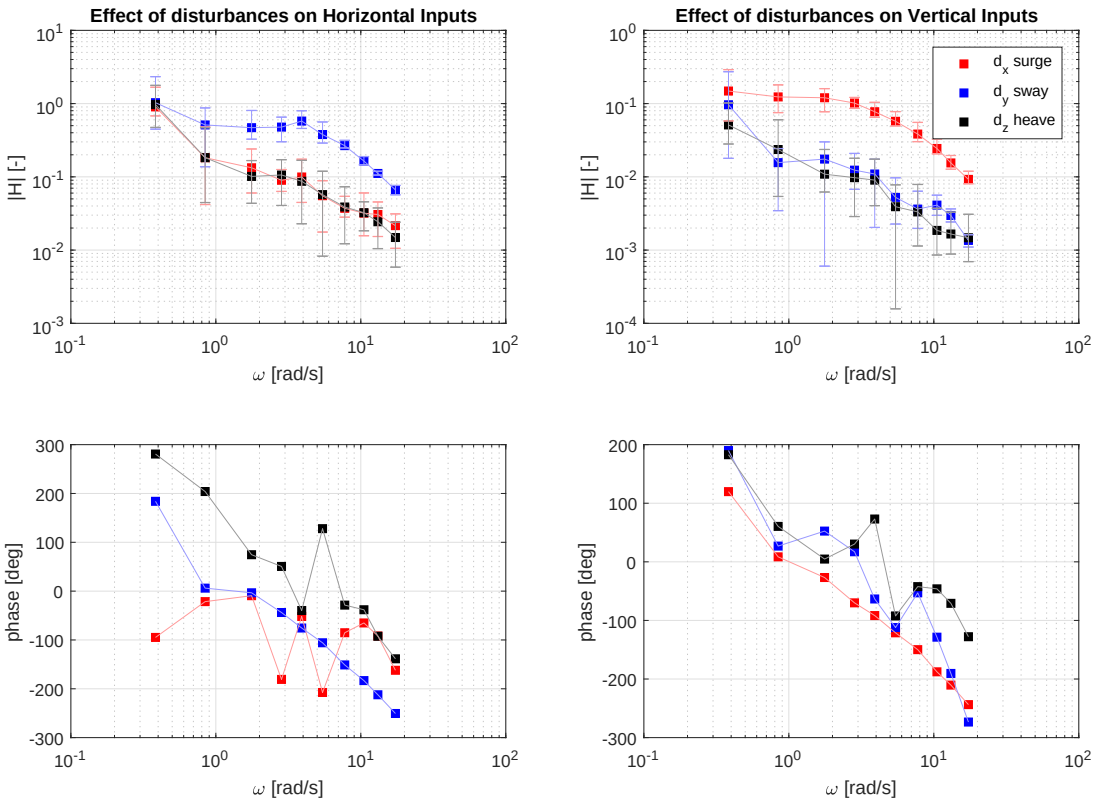

Figure 7-4: Estimated Biodynamic Feedthrough, averaged over all participants.

7-3 Performance

To compare the effect of different disturbance directions onto the performance of the continuous dragging task, the variance of the error signals ($\sigma^2_{e_{x,y}}$) was calculated from the spectral analysis of the signals measured. This error signal was defined as the difference between the target position and the actual finger position. The performance was determined for both horizontal ($\sigma^2_{e_x}$) and vertical position ($\sigma^2_{e_y}$) over the screen. As indicated in Section 6-5, the control inputs were logged in both the horizontal and vertical position over the screen. As there was no target signal present in the vertical direction of the screen, the error in vertical direction was simply determined by the difference of the vertical control input with respect to the horizontal centerline of the screen. After determining the variances in both directions, individual contributions of both the disturbance and target signals can be determined as all of these signals provide power at independent frequencies [69].

Figure 7-5 displays the tracking error variance decomposition for horizontal screen inputs, under influence of surge, sway, heave and no disturbances. Each column represents the time averaged results of a single participant for a specific disturbance condition. The same procedure is followed for the vertical tracking error variance decomposition in Figure 7-6. Due to the small magnitude of the total variance under influence of sway, heave and no disturbance in this direction, a detailed image is given in Figure 7-7. Blue segments of each bar indicate the contribution of the target signal towards the total variance of the error, whereas the green segments indicate the contribution of motion disturbance. The yellow bars indicate the remainder of the variance, i.e. the total variance minus the contributions of the target and disturbance functions and is called the remnant. The remnant is therefore a measure of the variance that is not correlated with the forcing functions, e.g. due to distraction of the participant or noise in their neuromuscular system.

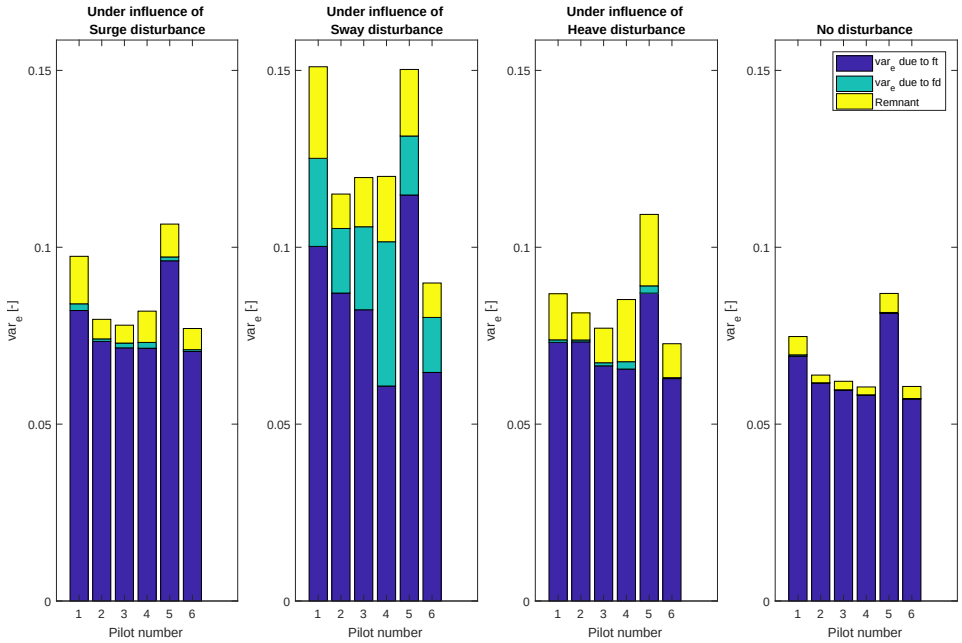

Figure 7-5: Tracking error variance decomposition for horizontal inputs.

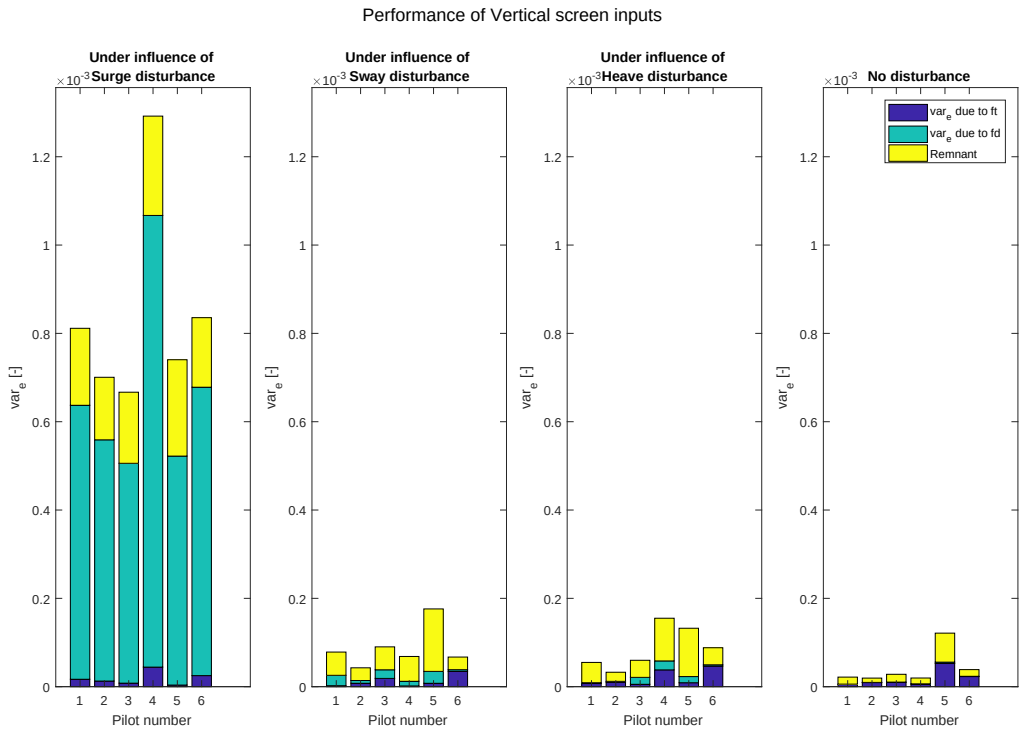

Figure 7-6: Vertical tracking error variance decomposition

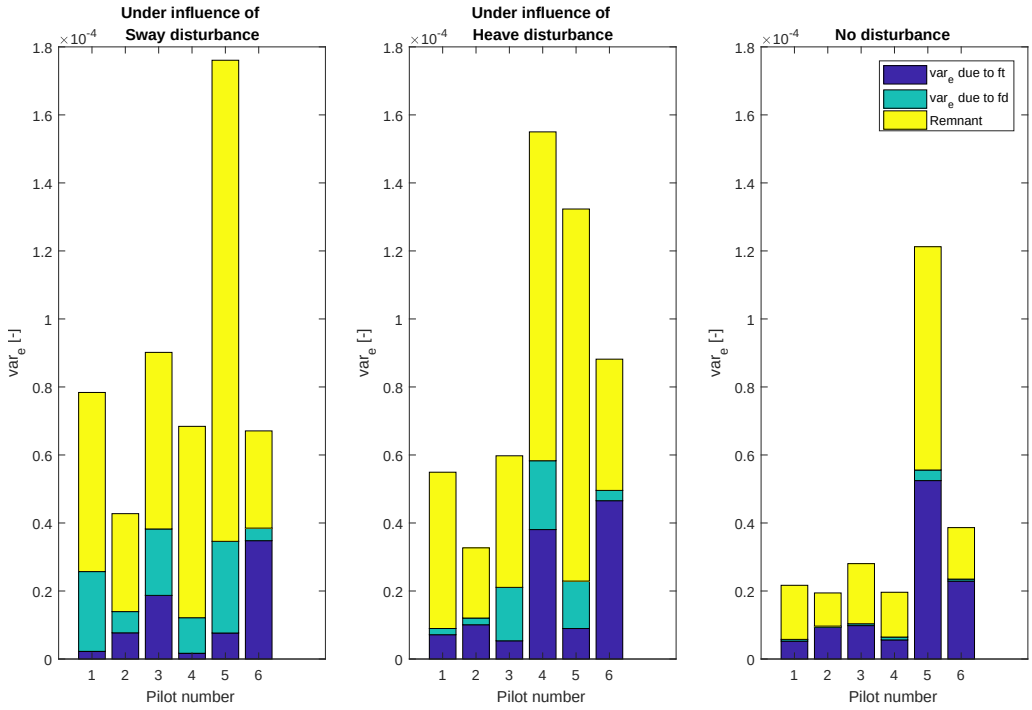

Figure 7-7: Vertical tracking error variance decomposition, detailed image of baseline, sway and heave conditions.

7-4 Experiment Discussions & Recommendations

Results of this experiment where shown using Power Spectral Density (PSD) plots, a BDFT estimation and performance measures. Those plots are discussed in Subsection 7-4-1, from which recommendations are drawn in Subsection 7-4-2

7-4-1 Results Discussion

The PSDs indicated that motion disturbances indeed led to BDFT causing involuntary touchscreen inputs. Figure 7-2 showed that sway disturbances mainly cause involuntary horizontal touch inputs, whereas Figure 7-3 proved that surge had the largest effect on vertical touch inputs. In other words, the disturbances proved to have largest impact when they acted in the same plane as the control inputs. These findings are in line with previous research [19].

The PSDs also revealed power at input frequencies corresponding with frequencies of out of plane motion disturbances, for both input directions. For the horizontal input direction, input frequencies corresponded with surge and heave motion disturbance frequencies above 10 rad/s. This same behavior was observed for vertical screen inputs with sway and heave disturbances. Both give a clear indication of a coupling between the participant's control behavior in both axes. This coupling is, however, not limited to situations with motion disturbance. Power at frequencies from the target function, which moved in the horizontal screen position only, was also observed in vertical input plane for all conditions (Figure 7-3). This clearly shows that human controllers have problems isolating control inputs to a single axis only. From here on, this effect will be referred to as 'crossfeed'. In all PSDs peaks are observed which do not match any of the excitation frequencies. A possible explanation is that movement of participant's finger over the screen was not always smooth, as fingers 'stick' to the screen.

A distinct difference in magnitude can be observed between the horizontal input PSD from Figure 7-2 and the vertical input PSD from Figure 7-3. A possible explanation is that the control behavior of the participants differed for each input direction, as a target function in the vertical screen direction was missing. As the subject was instructed to move in horizontal direction only, the subject was likely using a more compliant control behavior for that direction whilst having a stiff behavior in the vertical direction to prevent deviation from the horizontal center line of the screen. Previous research has shown that different control strategies affect BDFT significantly [24].

This difference in PSD magnitude between the two input directions is also reflected in the biodynamic feed-through estimate, as the estimate is a product of the aforementioned PSDs (Section 7-2). From Figure 7-4 in which these estimates are given as a bode plot for both input directions, it becomes clear that all motion disturbances affect input for any control direction.

The magnitude plot in Figure 7-4 of the horizontal inputs points out that BDFT for **sway** (d_y and represented by the blue line) is largest. Furthermore the peak of the BDFT lies at 3 rad/s, after which the magnitude quickly degrades. This behavior is seen for **surge** and **heave** as well, as the magnitude only starts to drop quickly after this frequency. The magnitude for those disturbance cases are mutually comparable but notably lower than the sway feedthrough. The corresponding phase plot shows decreasing phases as the frequency increases for all disturbances.

The right side of the plots in Figure 7-4 presents the effect of BDFT on vertical screen inputs. Here **surge** disturbance causes the highest BDFT magnitude. This magnitude remains constant up to a frequency of 2 rad/s after which the BDFT gradually

decreases. The BDFT due to **sway** and **heave** are comparable, but again notably smaller in magnitude. The phase plot corresponding to the vertical input bode shows decreasing phases as the frequency increases for all disturbances too.

Hence, the BDFT is especially large in magnitude for sway in the horizontal input direction and for surge in the vertical input direction, confirming the disturbances' largest impact when acting in the same plane as the control inputs. Presence of BDFT with out of plane disturbances also confirms crossfeed.

Finally the performance plots were given. Figure 7-5 also clearly indicated that sway movements had the largest effect on horizontal screen input performance. This indicates once more that the contribution of disturbance motion is largest when acting in the same plane as the control inputs. From the figure it also becomes apparent that the target function contributes to the error variance significantly. This can be explained due to a delay between the logged finger position and the target indicator. Because the input frequencies are exactly the same as the target frequency but with a constant delay, there is a constant error that is attributed to f_t. The contribution of this target function to the error variance seems to be fairly constant across all motion disturbance conditions. To get a rough indication of this delay, the horizontal screen input of all participants and their runs was time shifted such that the error between this input and the target signal was minimized. This yielded a delay with a mean of 0.149 seconds and standard deviation of 0.017 seconds. The origin of this time delay can be attributed to both mechanical delays, such as screen response time, computational and communication delays, and neuromuscular delays in the human system.

The remnant components in Figure 7-5 proved to be smallest in the baseline condition without motion disturbance, and largest for the disturbance condition in plane with the control input. Surprisingly, the remnant was of similar large size during heave disturbance. Participants indicated that control dynamics during this particular disturbance direction varied as pressure between the screen and the finger constantly changed due to BDFT, which might lead to this result.

Figure 7-6 indicated the tracking error variance decomposition for vertical screen inputs, under influence of the four motion disturbance settings. Note that the scale of the error variance is much smaller for the vertical screen inputs when compared to the horizontal input case. This can be explained due to the absence of a target function in the vertical direction, the variance indicated is therefore directly a measure of deviation from the horizontal center line of the screen.

As expected, it is the motion disturbance in surge direction that evidently contributes most to the error variance for the vertical inputs. Although vertical screen input error variances are significantly smaller with sway and heave motion disturbances when compared to surge, influences of these motion disturbances on vertical inputs are still clearly observable. This can especially be seen in the detail image (Figure 7-7) where the f_d contributions are significant, again clearly indicating presence of crossfeed. Motion disturbance contributions to the error variance in the no disturbance case can be explained as pure coincidence, as part of the input errors are bound to be in the same frequency spectrum as the disturbances.

For all motion disturbance conditions the target function contributes to the error variance to a similar extent, indicating that the ability to perform the tracking task wasn't affected by the motion disturbances. Once again, the remnant proved to be smallest for the baseline condition. For sway and heave the remnant was of similar size, and remnant proved to be largest during surge disturbances.

7-4-2 Experiment Conclusion and Recommendations

A preliminary experiment was conducted that served as proof of concept to observe whether it was possible to observe effects of BDFT onto dragging inputs made on a touchscreen whilst experiencing motion disturbances. The results of this experiment proved that it was indeed possible to observe and measure these effects.

The PSDs, BDFT estimate and performance results all showed that motion disturbances have largest impact on BDFT when acting in the same plane as the control inputs. It is for this reason that, although heave disturbance did not contribute to the input error during this preliminary experiment, it is expected that heave does have a significant effect on dragging tasks when vertical mounted touch screens are used. As many of the present displays are vertically mounted in modern-age flight decks, further research is required with multiple screen positions of which at least one is vertically mounted to learn the effects of heave components on performing dragging tasks.

Furthermore, all results showed evidence of crossfeed, a phenomenon that causes control inputs intended for a certain control axis to be made into another control axis. In order to investigate the extent to which this crossfeed takes place, an experiment should be conducted with target functions in both axes of the screen. However, from the error variance decomposition it was learned that a significant delay was present between target and the inputs of the participant. The mechanical parts of this delay should be fully understood, as it allows for a more precise modeling of the delays within the human controller. Noise in the PSDs might be partially mitigated if participants use touchscreen gloves, decreasing random movement accelerations and sore finger tips. Before deciding if these touch screen gloves are to be used, a small experiment should be conducted to determine whether or not BDFT is affected by the use of such gloves.

For future research it is also recommended that the target signal is adapted such, that it allows quantification of the effects of different modalities on participant's control behavior. Much research has been conducted in the past using higher frequency target signals to fit parameters onto a human controller model [55, 56, 57, 58, 59, 60, 61, 62]. Future experiment should in such case balance between resembling a realistic dragging task (e.g. a route change) and being an experiment with the objective to obtain the best possible pilot control model.

Conclusions:

- Effects of BDFT measurable with touch screen dragging task
- Evidence of crossfeed was found

Recommendations:

- Investigate use of vertically mounted touchscreens
- Investigate the effects of crossfeed whilst performing a dragging task
- Identify sources of delay between target and the screen inputs
- Investigate the use of touchscreen gloves
- Adapt target positions such, that it allows for human controller modeling

Chapter 8

Research Proposal

After performing a literature study it was found that research towards execution of a dragging task on a touch screen in a turbulent cockpit environment was lacking, although several initiatives exist to implement these features in future cockpits [47, 48, 52]. A preliminary experiment was therefore conducted to determine whether evidence could be found that in-flight turbulence affect performance of such dragging tasks. Not only did the results of this experiment confirm these expectations, but indications of crossfeed were also found.

In order to perform a more comprehensive analysis towards the effects of motion disturbance on this specific task, a research is proposed. Its supporting research question is posed in Section 8-1, after which the proposed design of this experiment is discussed in section 8-2. Note that this experiment is still under consideration, small amendments to this chapter for the actual experiment are therefore likely. The results, expected outcomes and relevance of this experiment are finally discussed in Section 8-3.

8-1 Research Question

Now that a good understanding of the present state of research in the field of touch screen use in the cockpit environment has been obtained, the research question posed in Chapter 1 can be narrowed down. Following a literature study and preliminary experiment, the objective of the research is to answer the research question posed below;

> "How do motion disturbances influence pilot control skills and biodynamic feedthrough whilst performing a dragging task on flightdeck-based touch screen positioned at the PFD and FMS locations?"

8-2 Experimental Setup

To evaluate how motion disturbances influence pilot control skills whilst performing a dragging task on a flightdeck-based touch screen, a human in the loop experiment is conducted using the SRS. The proposed design of this experiment is explained in this chapter.

8-2-1 Control Variables

Participants are instructed to conduct a route change using a touch sensitive display. The position to which the route needs to be changed to will be indicated by means of a target marker. The position of this target marker will continuously change during the run, each run lasting 90 seconds. Participants are required to keep their finger in contact with the screen during the duration of this run. Whilst performing the task, the participant will be exposed to turbulence. A representation of the control interface is given by Figure 8-1, where the target is indicated by the white triangle, and the current finger position indicator with the magenta marker.

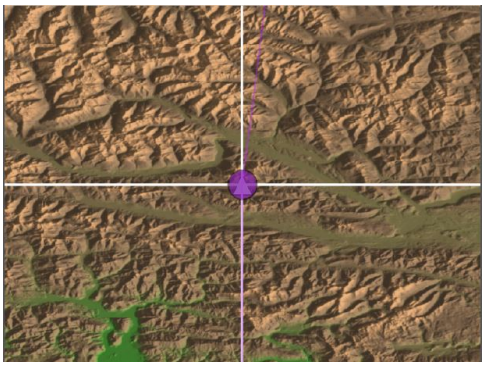

Figure 8-1: Visual representation of the experiment control interface.

Section 7-4-2 discussed that the use of gloves could lead to smoother results and therefore better frequency responses. Furthermore, participants could conduct the experiment for a prolonged time with reduced strain to the finger tops. To avoid possible pollution of results, a mini test should be conducted to see whether this is the case. Should the results be favorable, all participants wear gloves during the experiment. If the gloves do affect results significantly, none of the participants will wear gloves and the length of the experiment will be reduced.

Control Variables:

- Control Task
- Use of gloves

8-2-2 Independent Variables

Displays in cockpits are currently mainly located in both the horizontal (CDU) and vertical (PFD, ND, EICAS) planes. To observe the effects of motion disturbance on dragging tasks, both of these screen orientations should be evaluated. Furthermore, from previous research [19] and the preliminary experiment that was conducted for this research, it was proven that BDFT mainly occurs if motion disturbances act in plane with the control direction. As atmospheric turbulence mainly results in vertical displacement of the aircraft, one expects most BDFT effects when control inputs are made in the direction of the heave component. Since the preliminary experiment proved that direction of motion disturbance has a distinct effect on BDFT, it is important that the directions of motion disturbance are uncoupled. This allows for analysis of effects on BDFT from different turbulence components. Next to a baseline condition without motion, pure heave, pure sway and pure surge will be evaluated. Roll, yaw and pitch movements are considered to be outside the scope of this research. These two independent variables (i.e. screen position and disturbance direction) yield a total of eight different conditions, which are summarized in table 8-1. To observe the effect of each of these conditions on the BDFT for a single participant, the experiment has a within-subjects design.

Table 8-1: Experimental conditions used for the experiment.

Condition	Screen Orientation	Disturbance
1	Horizontal	Baseline
2	Horizontal	Sway
3	Horizontal	Surge
4	Horizontal	Heave
5	Vertical	Baseline
6	Vertical	Sway
7	Vertical	Surge
8	Vertical	Heave

Independent Variables:

- Screen locations
- Direction of motion disturbance

8-2-3 Dependent Variables

To answer the research question how motion disturbance influence pilot control skills whilst performing a dragging task, it is necessary to record the inputs that participants make onto the touch screen. From these inputs, it is possible to analyze PSDs and therefore obtain an approximation of BDFT using methods described in Sections 7-1 and 7-2.

Following recommendations from Section 7-4-2, the target frequencies are adapted such that they allow for pilot model identification. Figure 8-2 provides a schematic representation of the experiment where H_P indicates the transfer function describing the control behavior of the participant. The participant is presented a target position by the target forcing functions f_{t_x} and f_{t_y}, after which the error (e_x and e_y) between the current finger position (y_x and y_y) and the target is to be minimized whilst being exposed to disturbance f_d from a certain direction based on the selected condition. Since the values for $f_{t_{x,y}}$ are known, the pilot model too can be determined using touch input $y_{x,y}$.

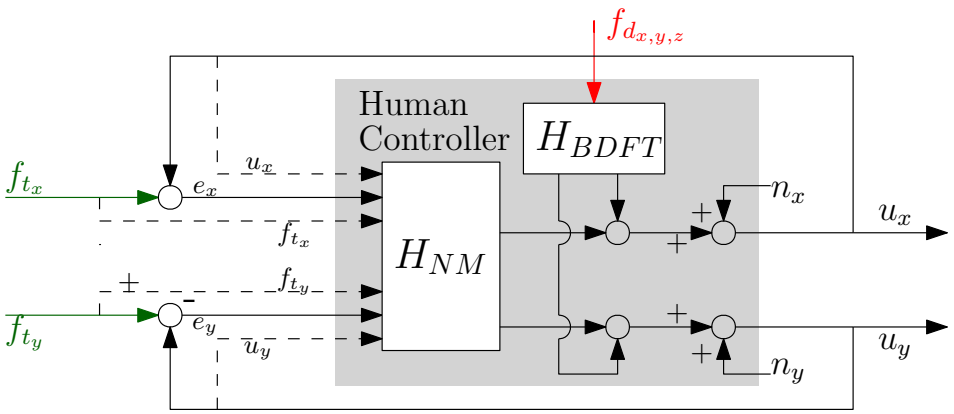

Figure 8-2: A schematic representation of the experiment.

Dependent Variables:

- Screen input

8-2-4 Participants

Participants are required to be right handed. Previous research has shown that handedness has a significant effect on BDFT and input errors [17]. Investigation of handedness for a continuous dragging task is certainly of interest, but would require groups of both left- and right-handed participants of similar size. Due to the limited availability of the experiment apparatus and the amount of independent variables, effects of handedness are considered to be outside the scope of the research.

Due to the nature of the experiment, which replicates the input of route changes in a moving cockpit environment, participants should have good hand-eye coordination and should also be physically fit similar to what is to be expected from commercial pilots. There will not be a particular test selecting for fitness, but results may be rejected after bad performance if it was evident that the subject did not meet the written criteria above.

Participants:

- Right handed
- Fit to participate

8-2-5 Experimental Procedure

Participants will receive a thorough briefing prior to the experiment, covering the explanation of the task at hand and how the touch screen is to be operated. After the briefing, participants will be seated and strapped in the SRS (Section 8-2-6. If the participant indicates to be ready for the experiment, the runs are started. Participant will be instructed to continuously improve on the RMS score that will be verbally communicated at the end of each run.

Each run lasts 90 seconds. Participants are offered to take their time until they feel ready to perform the next run. Depending on the use of gloves (Section 8-2-1), either four or eight runs of each condition (Table 8-1 are collected. Without gloves, only four runs per condition are collected to limit strain on participant's finger, whereas eight are to be completed with gloves. Therefore, as the experiment has a within-subjects design, either 32 or 64 runs are completed in total. After 16 or 32 runs respectively, the participant is offered a break in which they can leave the SRS.

8-2-6 Apparatus

In order for the participants to receive a controlled disturbance signal throughout the experiment, the experiment will be conducted in the (SRS) located at the University of Delft in the faculty of Aerospace Engineering. The SRS is equipped with a hydraulic motion system, capable of providing motion cues in six degrees-of-freedom [67]. Participants do not have influence on the motion cues they receive, as manoeuvring the aircraft is not part of the experiment. Whilst seated at the left side of the pedestal, participants are asked to make inputs on two touch sensitive displays located at both the pedestal and at the location where normally the Primary Flight Display (PFD) is located. An impression of the setup can be seen in Figure 8-3.

(a) SRS exterior.

(b) Experiment setup.

Figure 8-3: The SIMONA Research Simulator and the experiment setup

8-3 Results, Outcome and Relevance

Recommendations that were made following the literature study called to use the work of Venrooij as basis for the research at hand. The objective is to analyze "how motion disturbances influence pilot control skills and biodynamic feedthrough whilst performing a dragging task for flightdeck-based touch screens positioned at the PFD and FMS locations". In order to perform this analysis, the input data that participants are to make on the TSC whilst performing the experiment will serve as basis. Based on this data, the following outcomes can be determined;

- **Power Spectral Densities**: Using the method described in Section 7-1, PSDs of the input data can be obtained from which can be determined which frequencies manifest in the TSC input signal. As target frequencies differ for vertical and horizontal directions over the screen, it might also be possible to detect cross coupling if horizontal target frequencies manifest in vertical screen inputs, and vice-versa.

- **Biodynamic feedthrough**: An estimate of the BDFT is the main priority, as it indicates for which disturbance frequencies the pilot is sensitive whilst making TSC inputs. Although many variables affect the BDFT model, estimation is still very relevant as the plots may reveal a general trend that can be extrapolated to the integration of flightdecks in general.
- **Performance**: When the TSC input signals are known, the error signal is easily determined as it is known which target signal the controller was to follow. The variance of this error can be determined as well, allowing to observe individual contributions of both the disturbance and target signals to the error, since all of these signals provide power at independent frequencies. This is important, as it shows whether most of the TSC input errors originate from the fact that the controller has difficulty tracking the target signal, or if the controller experiences difficulties from the motion disturbance.
- **Pilot identification parameters**: Using a known signal into the controller with a measured output signal allows for identification of the controller model. This is important, since it shows whether the controller is changing strategies during execution of the task.

Next to measurable data from the participant TSC inputs, metadata is gathered. These variables include;

- **Participant Mass and Length**: The extent to which BDFT manifests is dependent of controller mass and length. Whether the difference in BDFT between subjects with different lengths and mass is significant, can be measured.
- **Participant Age**: Although BDFT effects do not necessarily change with controller age directly, different control strategies do. Recording the participant's age may hint at the use of different strategies for controllers with varying age.

Chapter 9

Conclusions & Future Steps

The purpose of this preliminary report was to construct a basis for new research: to investigate how motion disturbances influence pilot control skills and biodynamic feedthrough whilst performing a dragging task for flightdeck-based touch screens positioned at both the PFD and FMS locations. This basis was established in three parts; a literature study, a preliminary experiment and an experiment proposal.

9-1 Conclusions

Literature Study The foundation for this construction started with a literature study, which was guided by the research questions as posed in the introduction as a guide. Several conclusions were drawn from the literature study. It was found that several proposals exist that integrate the use of single-touch (ST) and multi-touch(MT) gestures in the design of a TSC for the use of navigation. Effects of turbulence on the execution of some of these gestures was performed, but research towards continuous touch (CT), ST gestures is lacking. Although the use of TSC was favorable in general, the biggest disadvantage of its use proved to be BDFT. Although the concept of BDFT is well known, mitigation currently only takes place in the form of passive support systems. Mitigation of BDFT using noise signal cancellation was proposed in literature, but it requires a good model of the BDFT. Efforts to build such a model for the use of touch screens in a turbulent environment have not been found in existing literature.

These findings led to a couple of recommendations. First, the research question was adapted to "How do motion disturbances influence pilot control skills and biodynamic feedthrough whilst performing a dragging task on flightdeck-based touch screen positioned at the PFD and FMS locations". In order to find an answer to this research question, it is recommended to use the work of Venrooij as a theoretical basis to obtain a general model for the biodynamic feedthrough, whilst using pilot identification techniques to model pilot control behavior.

Preliminary Experiment To determine whether it was actually possible to measure and model biodynamic feedthrough, a preliminary experiment was performed in the SRS.

Participants task was to track a target that moved over the screen, in horizontal direction only, whilst being exposed to motion disturbances. Results of this experiment confirmed that estimation of BDFT was possible. Findings in literature were also confirmed, as it was shown that motion disturbances proved to have largest impact on BDFT when acting in the same plane as the control inputs. This will especially be of importance for the use of vertically mounted TSCs as the most prominent motion disturbance, heave, is expected to impact manipulations on this screen most. Furthermore, evidence of crossfeed was found.

Recommendations which followed from this experiment include the use of two screens, each oriented in a different orientation. Furthermore, the target should move in two directions over the screen to identify the extend to which crossfeed takes place. Third, the use of gloves was recommended. In addition to the recommendations from the literature report, these recommendations led to the experiment proposal.

Experiment Proposal In order to answer the new research question, a human-in-the-loop experiment is proposed that will take place on the SRS. During this experiment, participants are to track a target on a touchscreen whilst being perturbed by motion disturbances. The direction of these motion disturbances is varied throughout the experiment. The screen which is used to execute the task is the second independent variable. One screen will be located on the pedestal to simulate the use of a CDU. A second TSC is to be placed in front of the controller, at the location where usually the PFD is located. The control variables consist of the tracking task and the use of gloves. The resulting data from the experiment consists of touch location data and target positions. Based on this information, PSDs, BDFT models, performance data and Pilot model parameters can be determined. Furthermore, participant mass, length and age are collected for two purposes. First, they serve for statistical purposes. Second, they will be collected to determine whether a significant correlation exists between these parameters and BDFT models. Participants are not selected based on these parameters, but do need to be right-handed to have a homogeneous group as research suggested that BDFT is suggested significantly by handedness. A group of 16 participants minimum will perform the experiment.

9-2 Future Steps

This preliminary report covers three of the in total seven parts that have to be performed in order to complete the research in light of the master of science thesis: a literature study, a preliminary experiment and an experiment proposal. Four more steps follow;

1. Development and implementation of the experiment proposal in DUECA, allowing to perform a human-in-the-loop experiment on the SRS.
2. Conducting the experiment according to the proposal.
3. Analysis of the resulting data as suggested in the experiment proposal.
4. Reporting of the findings in a research paper, which is to be included in the final MSc. thesis.

Part III

Appendices

Appendix A

Motion Disturbance

In order to observe the effects of BDFT on performing continuous dragging tasks on the TSC, and to model its behavior, a motion disturbance signal was required. This appendix discusses the efforts that have been made to obtain the motion disturbance signals as described in the AIAA paper, Part I.

This disturbance motion signal f_d had to meet multiple criteria in order to be useful for the experiment;

1. **Cover a wide frequency range:** It has been shown that BDFT is heavily affected by the frequency of motion disturbance [18, 19]. To observe the participant's response to the motion disturbance, the disturbance signal should at least contain the frequencies to which the human controller has been shown to be sensitive for [27].

2. **Appear random to participant:** Humans can adapt their neuromuscular dynamics to motion disturbances that they are about to experience [70]. One example is to stiffen the limbs when a bump in the road ahead appears. To prevent the participant from anticipating on particular motion disturbances that he or she remembers from previous runs, it is key that the signal appears random.

3. **Discrete frequencies:** In order to determine the BDFT as described in the AIAA paper, Part I, it is required to know both the motion disturbance power and the TSC input power for the motion frequencies. These motion disturbance frequencies can however not overlap the target frequencies, as it would be impossible to isolate power from the motion disturbance at these frequencies.

4. **Sufficient Power**: The disturbance signal should hold sufficient power at all frequencies measured in order to determine a human response.

In an effort to obtain a disturbance signal that meets these criteria whilst appearing as realistic as possible, a Boeing 747 Simulink model was used. Using this model, ten time traces of surge, sway and heave accelerations were generated for a Boeing 747, flying in a trimmed state at 35,000 feet with 490 knots IAS in clean configuration.

These obtained time traces were converted to a PSD using the FFT algorithm. The ten PSDs for each motion disturbance direction were finally averaged to filter out noise and obtain a single FFT in which the frequency response of a Boeing 747 was visualized. These responses can be observed in Figure A-1 by the dashed lines. Using these responses, a first order model was fitted. Similarly to previous experiments, a second-order low pass filter was subsequently used to determine the amplitudes of the individual motion disturbance sines in the forcing function [71, 72]. A cresting technique was used such to determine the phases, preventing peaks in the time domain [66]. This resulted in a multisine disturbance signal that was tested in the SRS.

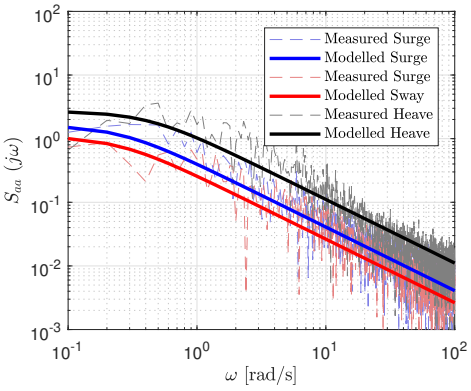

Figure A-1: Estimated Boeing 747 turbulence model.

It was determined that this signal did not meet the fourth requirement. Since amplitudes in the low frequencies were highest, the signal was adjusted such that the available physical motion space of the SRS was fully used by those frequencies. This, because the SRS motion is limited by the range to which the pistons can extend. As the amplitudes at higher frequencies were significantly lower, it resulted in a motion in which only the lowest frequencies were felt.

To approximate the turbulence of a Boeing 747 nonetheless, efforts were made to divide the PSD of the Boeing 747 turbulence response in equally sized bins and work out the total power per bin. Remember that the PSD of this response is logarithmic, and may therefore contain more power at higher frequencies than that the PSD suggests. This process is graphically represented by Figure A-2.

The resulting values have been by the black squares in Figure A-2c. Again, a model is fitted and its results are displayed by the blue line in Figure A-2d. It can be seen that the dynamics of this model are similar to those found earlier in Figure A-1. The resulting multisine parameters, which had been obtained using the same procedure as with the earlier model, indeed showed a large variation in amplitudes again (Table A-1).

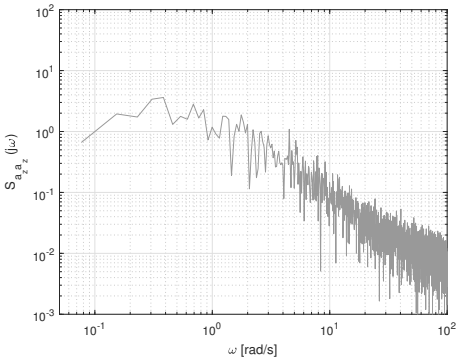

(a) PSD of the B747 heave response, cruise condition.

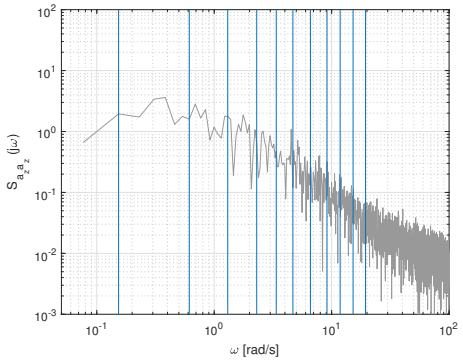

(b) Separation of the PSD in equally sized bins.

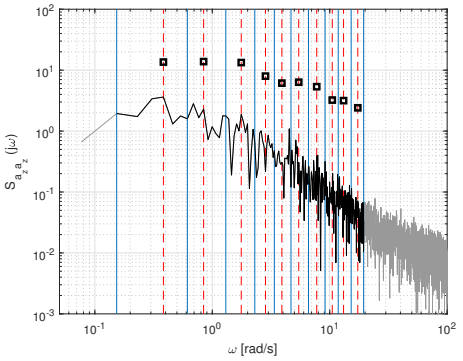

(c) Determining the total bin power by integration.

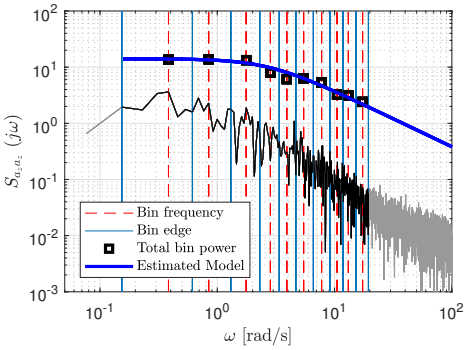

(d) New estimated Boeing 747 turbulence model.

Figure A-2: Determining realistic turbulence

The same analysis was been performed for the Boeing 747 in approach configuration at an altitude of 3,000 feet with 180 knots IAS, flaps 20° and landing gear retracted. No considerable differences were found. As the signal did not meet the requirements as set out, it was decided to use the parameters as used in the AIAA paper, Part I.

Disturbance, f_{d_z}			
N_d	ω_d	A_d	ϕ_d
–	rad s^{-1}	deg	rad
5	0.3835	$9.493 \cdot 10^{1}$	-2.716
11	0.8437	$1.892 \cdot 10^{1}$	-9.631
23	1.7641	$3.799 \cdot 10^{0}$	2.154
37	2.8379	$1.210 \cdot 10^{0}$	-1.544
51	3.9117	$5.254 \cdot 10^{-1}$	-2.702
71	5.4456	$2.121 \cdot 10^{-1}$	9.970
101	7.7466	$7.771 \cdot 10^{-2}$	-1.912
137	10.5078	$3.195 \cdot 10^{-2}$	-2.816
171	13.1155	$1.661 \cdot 10^{-2}$	-1.093
226	17.3340	$7.261 \cdot 10^{-3}$	-3.020

Table A-1: Parameters of the estimated multisine Boeing 747 motion disturbance signal.

Appendix B

Experiment Briefing

This appendix shows the experiment briefing that was handed out to participants prior to the experiment.

Effects of Atmospheric Turbulence on a Continuous Dragging Task

Experiment Briefing

Thank you for taking the time to participate in this research. This document will explain about the purpose of the experiment at hand, and what is expected from you as a participant. Before starting the experiment we will discuss the contents of this briefing once more. Feel free to ask any questions you may have at that time.

Purpose

The purpose of this experiment is to investigate how turbulence and the resulting aircraft dynamics influence the ability for pilots to perform continuous route dragging tasks using a touch sensitive display in a flightdeck environment.

Apparatus

The experiment will be performed in the SImulation, MOtion and NAvigation Institute (SIMONA) Research Simulator (SRS) at the faculty of Aerospace Engineering at the Delft University of Technology, Figure 1a. This simulator is equipped with two touch screens that are to be used for the route dragging task (Figure 1b). One of these displays is located right in front of you, where normally the Primary Flight Display (PFD) would have been located. The second screen is mounted on the pedestal, just below the location where normally the Control Display Unit (CDU) is located. No other input methods have to be used. Outside visuals have been disabled but motion is enabled to provide motion stimuli. This motion is independent from the inputs that are made into the touchscreen. Whilst performing the experiment, you will be seated in the left seat of the cockpit.

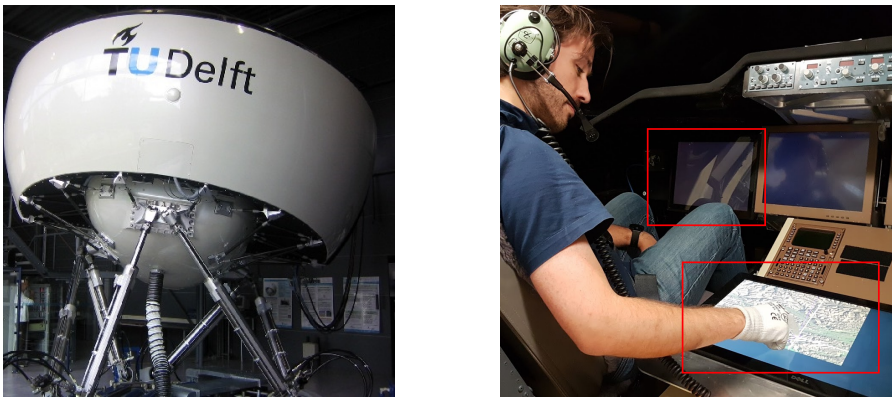

(a) Outside View of the SRS (b) Touch screen setup in the SRS

Figure 1: The SIMONA Research Simulator and the experiment setup used for the experiment

Experiment Task

In order to observe the effects of turbulence components on touch screen inputs, a compensatory tracking task is to be performed whilst being exposed to a turbulent motion. The tracking tasks consists of minimizing the error between the current finger position, indicated by the purple marker, and the position of the target indicated with the white triangle. This target will constantly be moving in both the horizontal and vertical directions over the screen, and it should be followed with your finger at all times without loosing contact with the screen. An example of the interface that you will use to perform the task can be seen in Figure 2. Note that it is important that you only touch the target position on the screen with the index finger, without supporting your hand elsewhere on the screen.

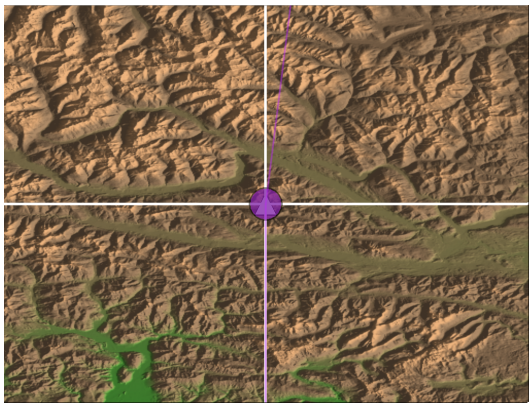

Figure 2: Experiment Display.

Experiment Procedures

You are welcomed in the coffee corner on the first floor of the SIMONA building at the Faculty of Aerospace Engineering of the Delft University of Technology. First, the contents of this briefing will be discussed once more and any questions that you may have regarding the procedures will be answered. Hereafter, you will be asked to sign a consent form of which the conditions are discussed in the following section. A safety briefing of the simulator will be given before seats are adjusted to ensure a comfortable seating position.

Hereafter, the experiment will begin. You are exposed to different kinds of turbulence in a random order during which you will have to perform the aforementioned tracking task. Although you will be exposed to different turbulence conditions, your task will remain the same. The monitor that lights up will have to be used for the tracking task, this too will happen in a random order. A total of 64 runs are to be completed, each run lasting 90 seconds. The complete experiment should take around 2.5 hours, including a break after 32 runs.

Your rights

Participation in the experiment is voluntary. Although unlikely, the disturbances can induce motion sickness, it is perfectly fine to request for a break at any time during the experiment. If you do not feel comfortable continuing the experiment you can terminate your cooperation at any time. The data collected during the experiment is considered confidential and only the experimenter is able to link results to a particular participant. By participating, you agree that your data may be published. The data will be anonymized before publication in such case.

Finally we would like to ask you not to disclose any particular details of the experiment to other participants of the experiment before the experiment has finished, to prevent biased results. By signing the consent form you agree that you have understood these terms and conditions.

Thank you for participating in this study!

Appendix C

BDFT Parameter Estimation Results

In order to describe BDFT dynamics of a continuous TSC dragging task in a linear model, efforts have been made to estimate parameters on the model as proposed in (C-1), and described in the AIAA paper (Part I).

$$\hat{H}_{BDFT}(s) = G_{BDFT} \cdot \frac{1}{m_{BDFT} \cdot s^2 + b_{BDFT} \cdot s + k_{BDFT}} \tag{C-1}$$

Model parameters presented in this paper were averaged over participants. Results of the genetic algorithm, followed by a Newton-Gauss optimization algorithm, have however been generated for each individual run before these averaged parameters were determined. This appendix shows results of the individual parameter estimation.

Results of each run have been color coded and correspond to the numeric values below the bode plots, given in the same color. The average value over four runs was determined and given below the line in black writing. Its corresponding bode plot is given by the dashed black line.

Figure C-1: Parameters Estimates: Participant 2, Horizontal Inputs on CDU

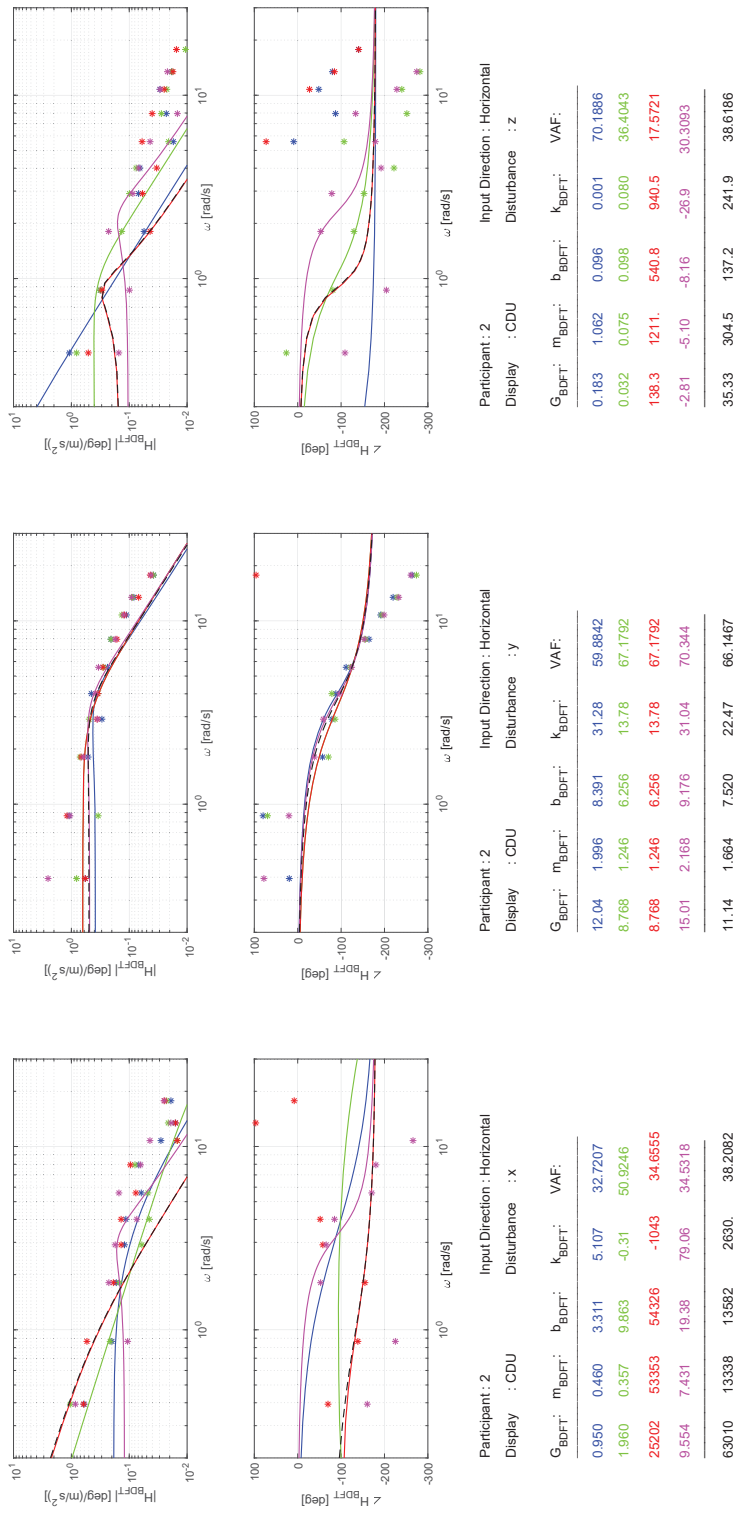

Figure C-2: Parameters Estimates: Participant 2, Vertical Inputs on CDU

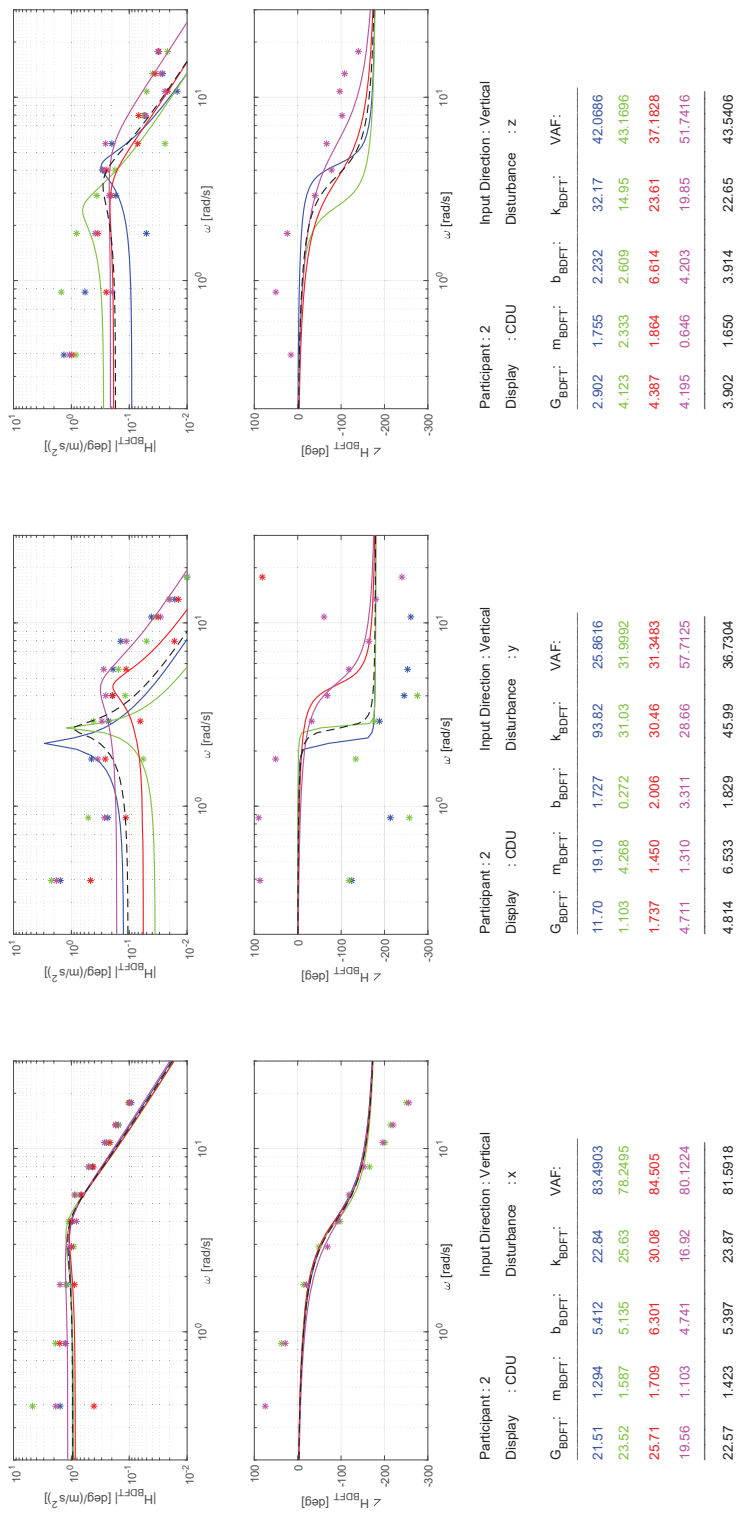

Figure C-3: Parameters Estimates: Participant 2, Horizontal Inputs on PFD

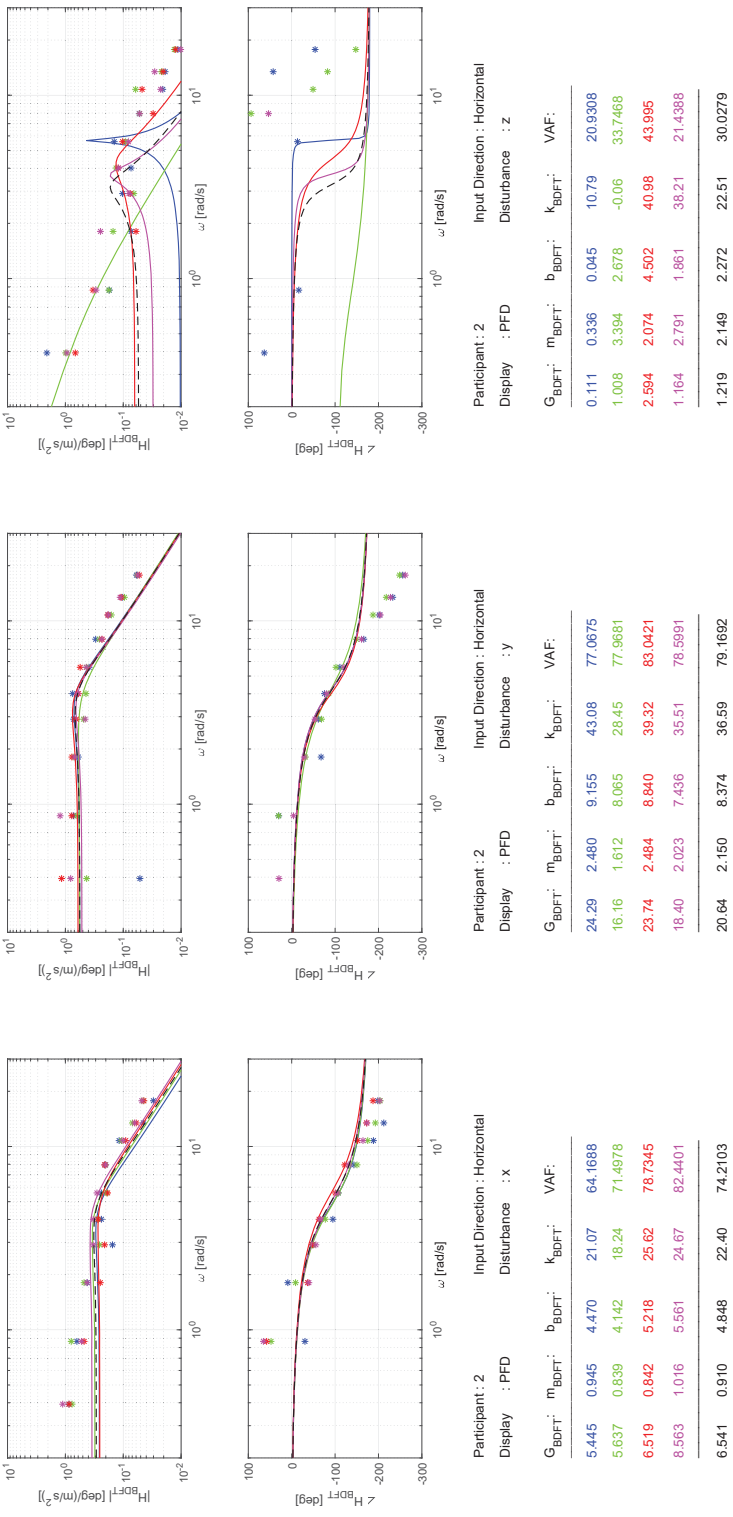

Figure C-4: Parameters Estimates: Participant 2, Vertical Inputs on PFD

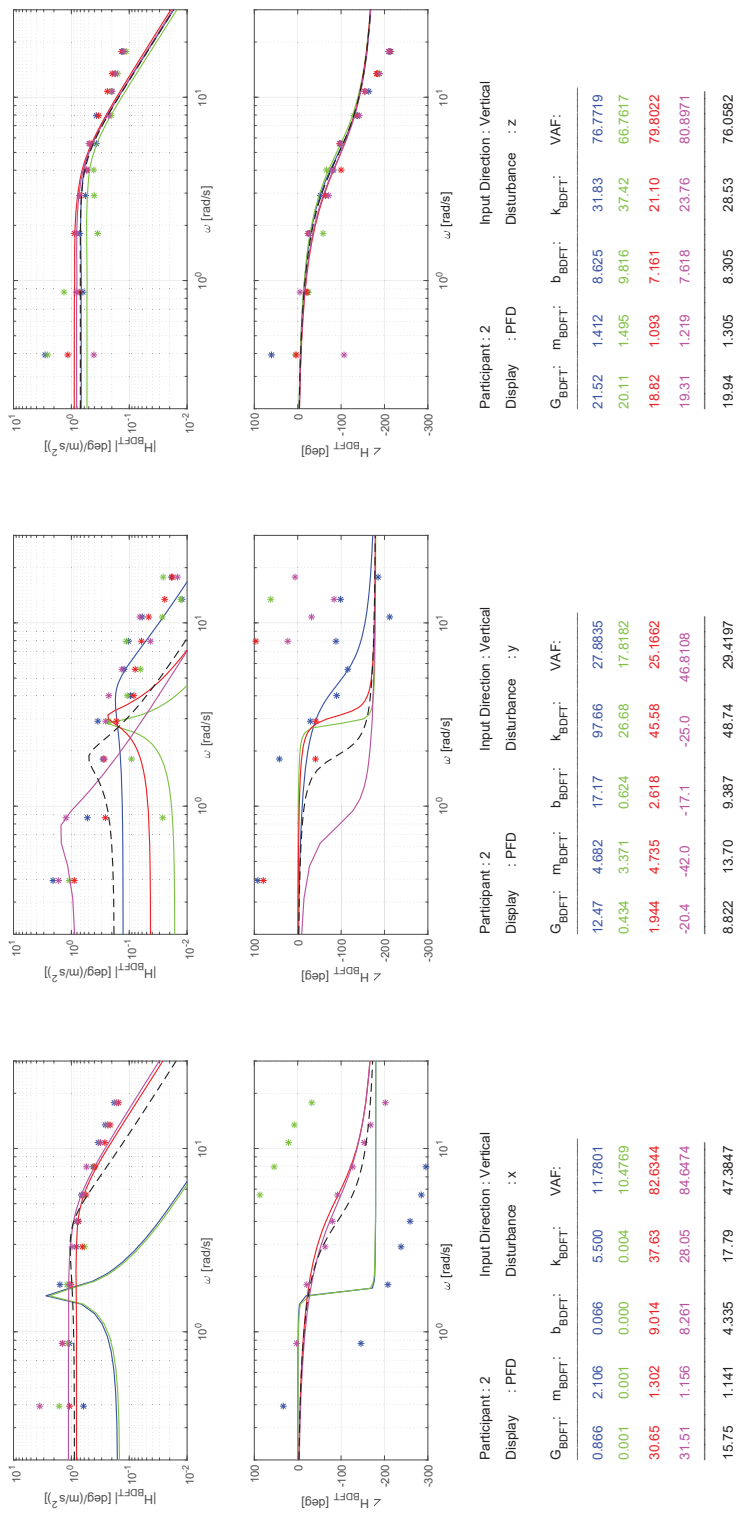

Figure C-5: Parameters Estimates: Participant 3, Horizontal Inputs on CDU

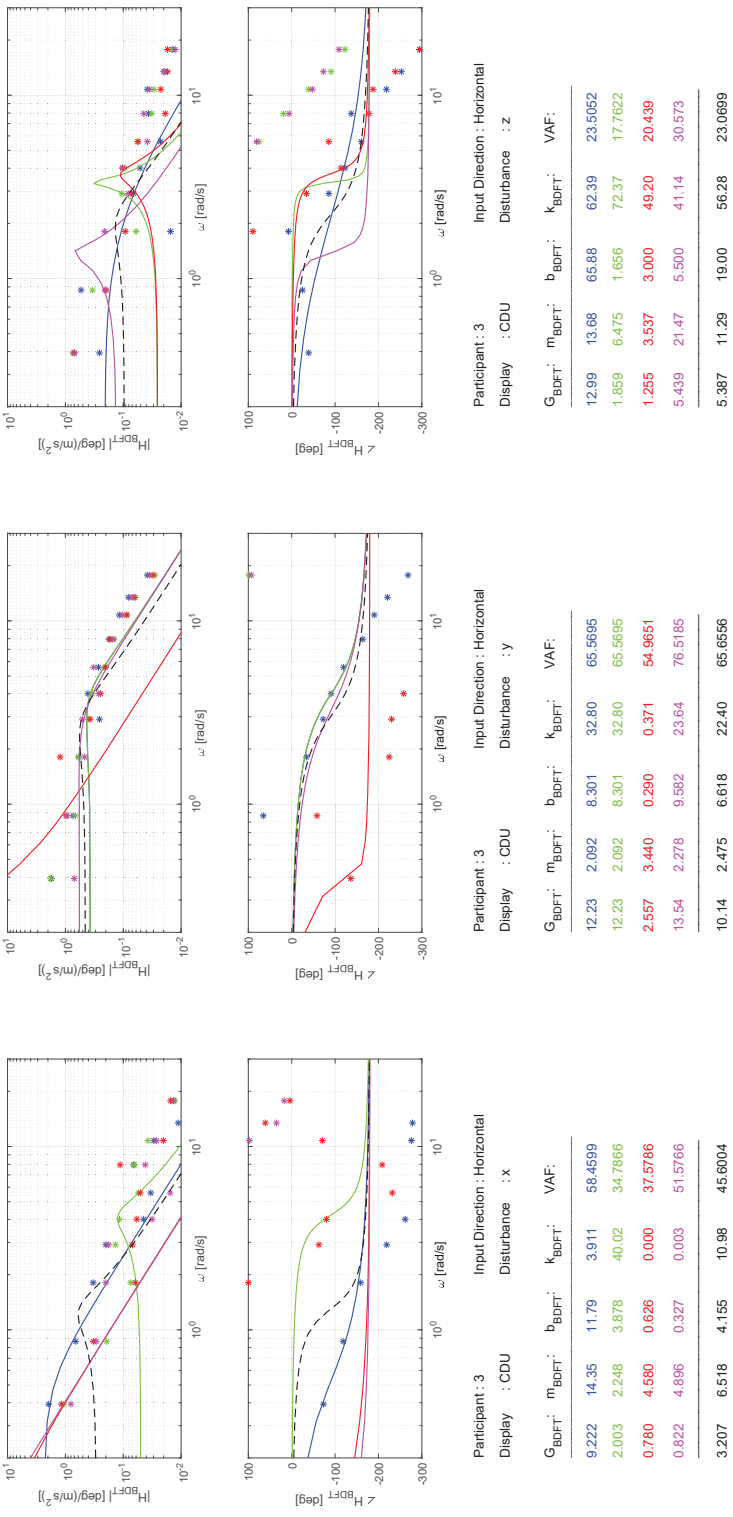

Figure C-6: Parameters Estimates: Participant 3, Vertical Inputs on CDU

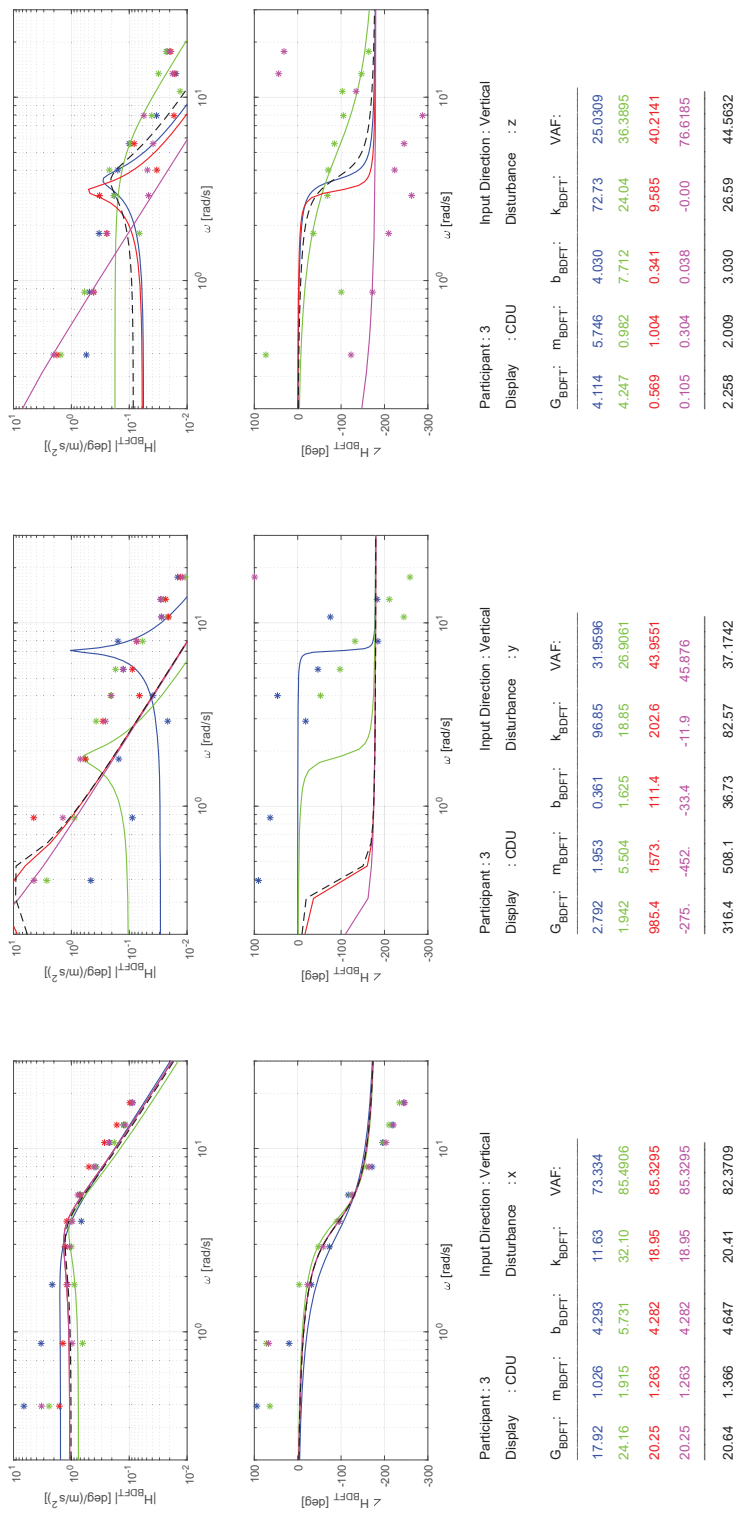

Figure C-7: Parameters Estimates: Participant 3, Horizontal Inputs on PFD

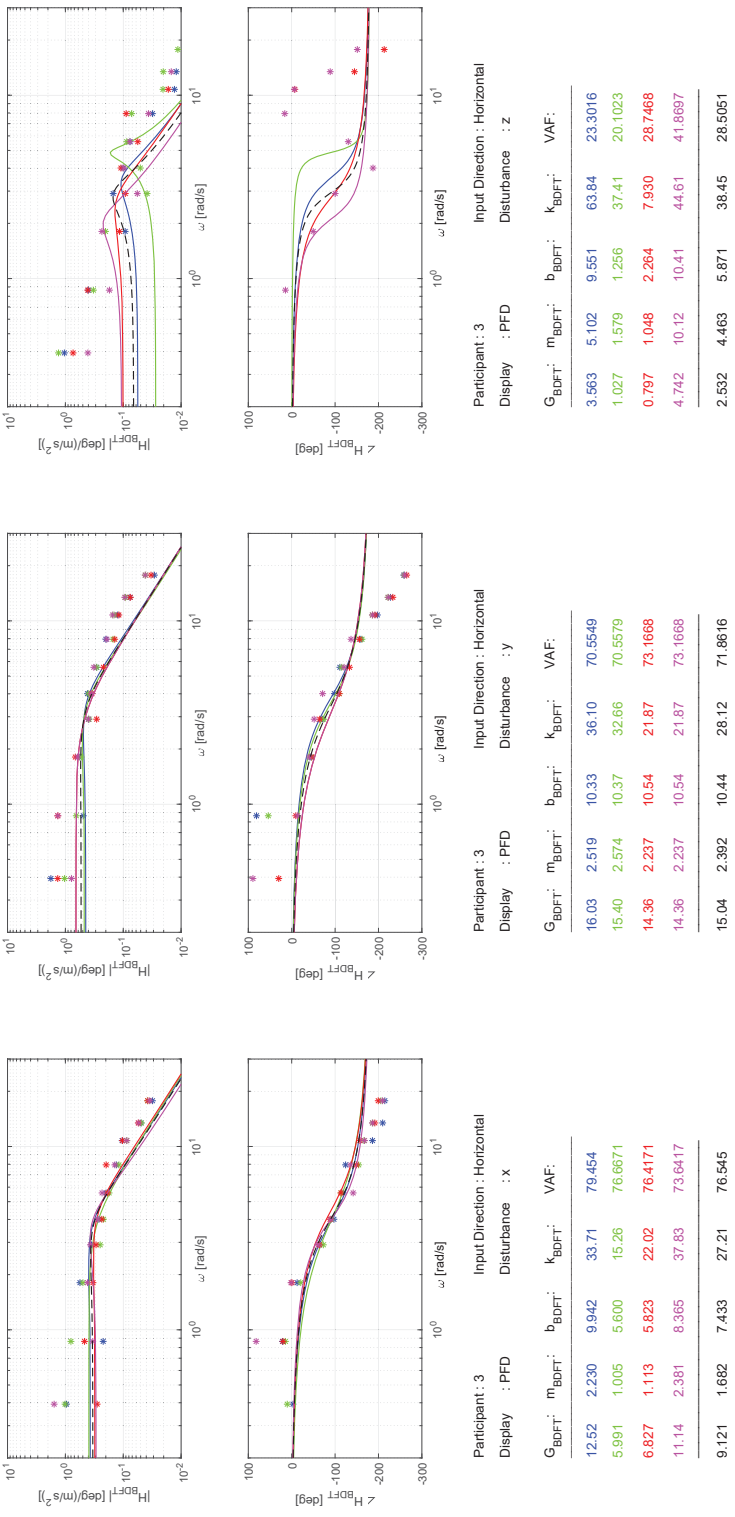

Figure C-8: Parameters Estimates: Participant 3, Vertical Inputs on PFD

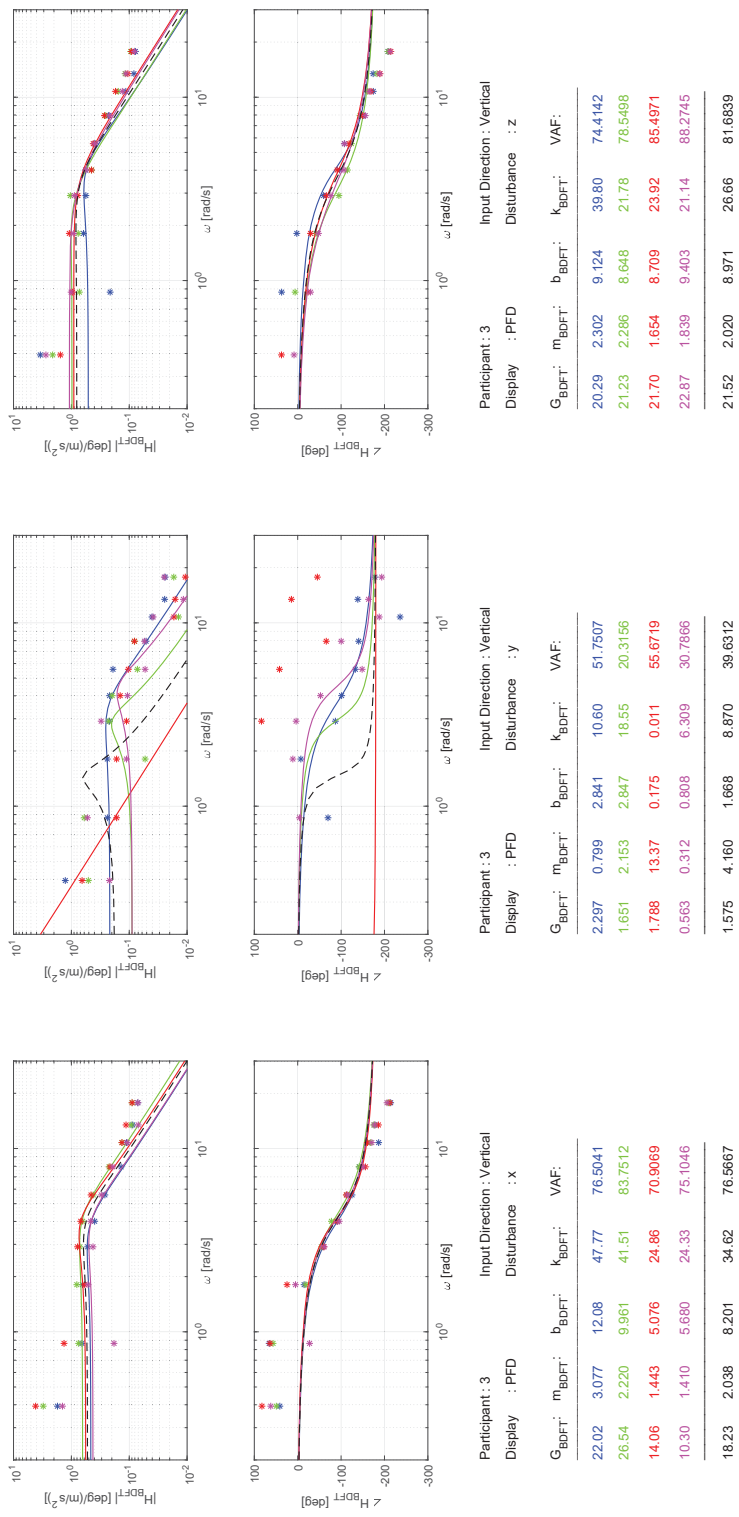

Figure C-9: Parameters Estimates: Participant 4, Horizontal Inputs on CDU

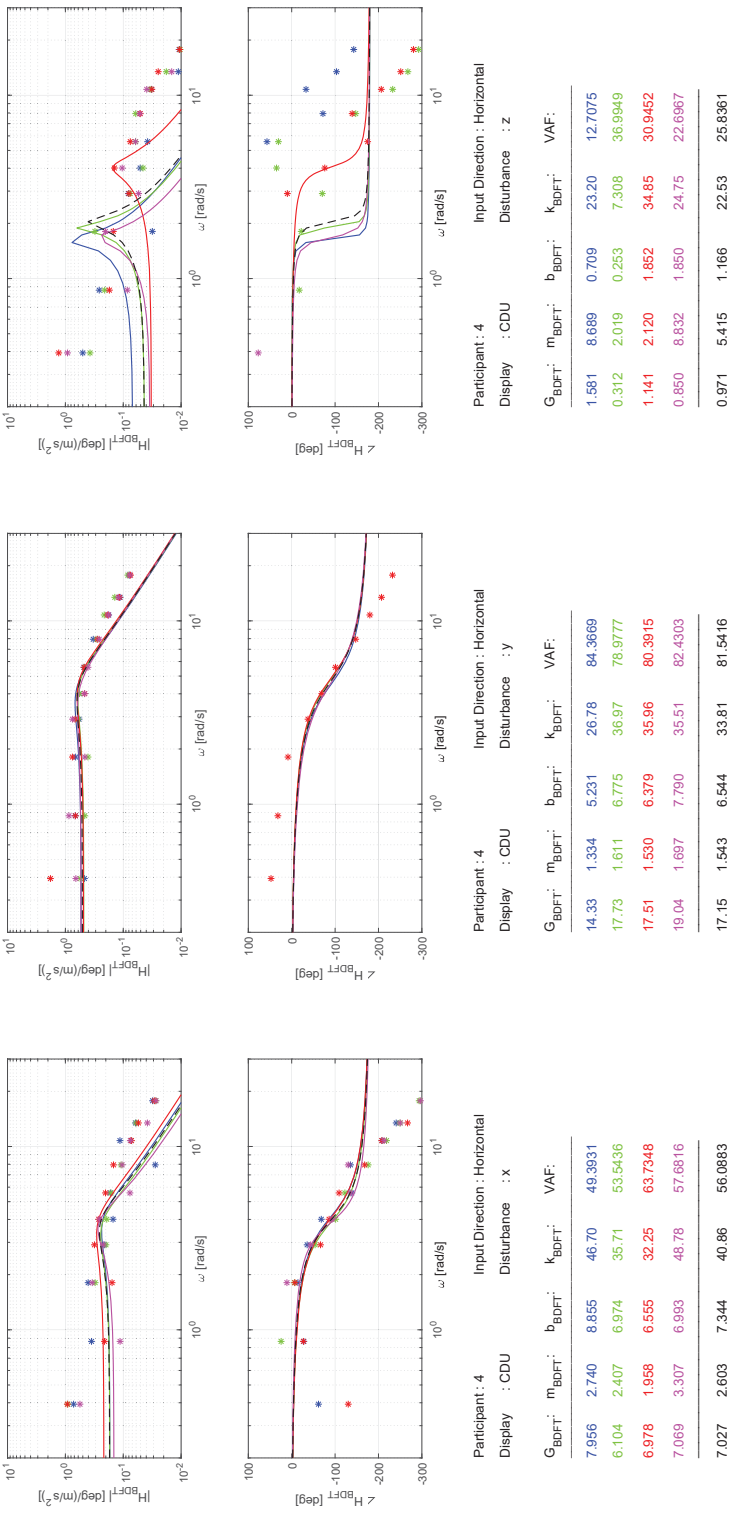

Figure C-10: Parameters Estimates: Participant 4, Vertical Inputs on CDU

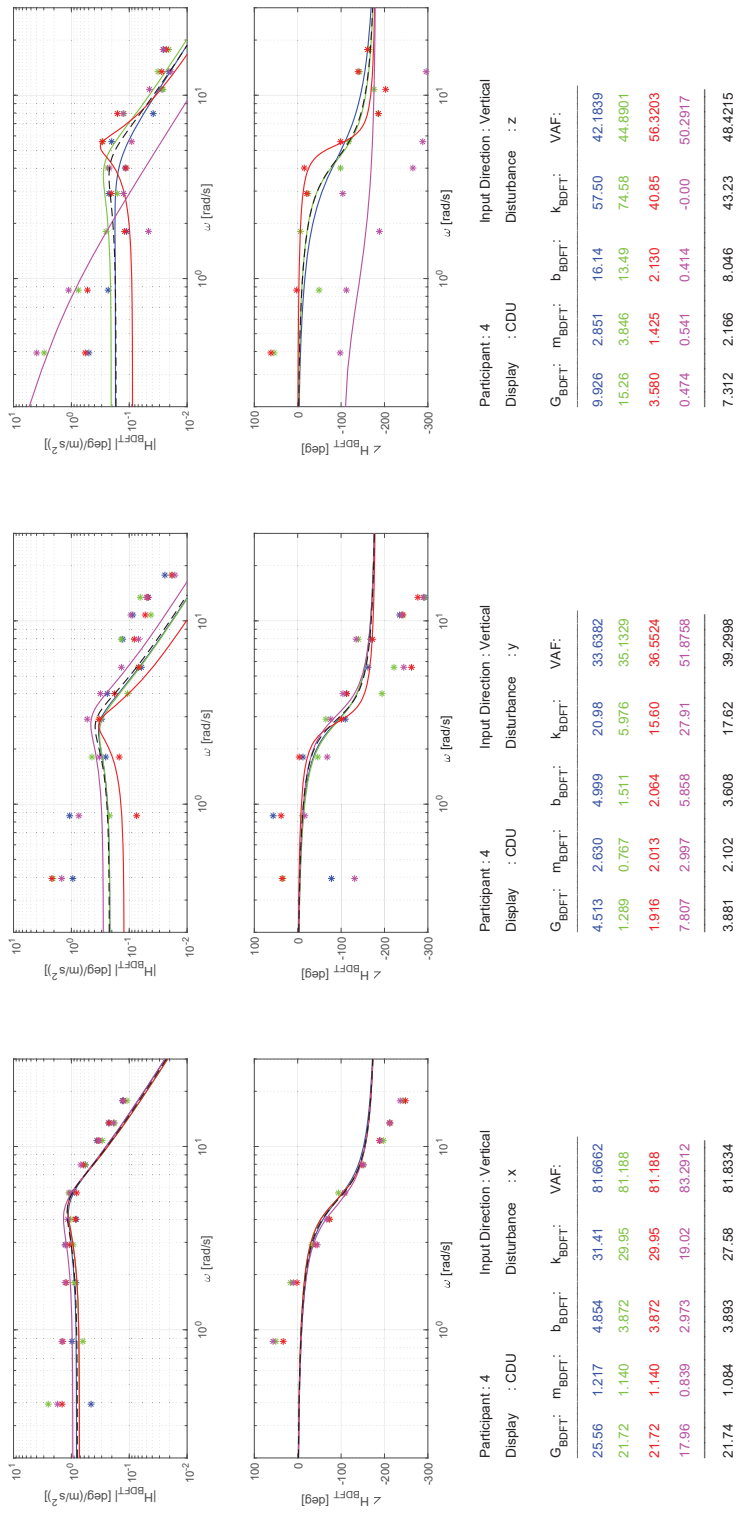

Figure C-11: Parameters Estimates: Participant 4, Horizontal Inputs on PFD

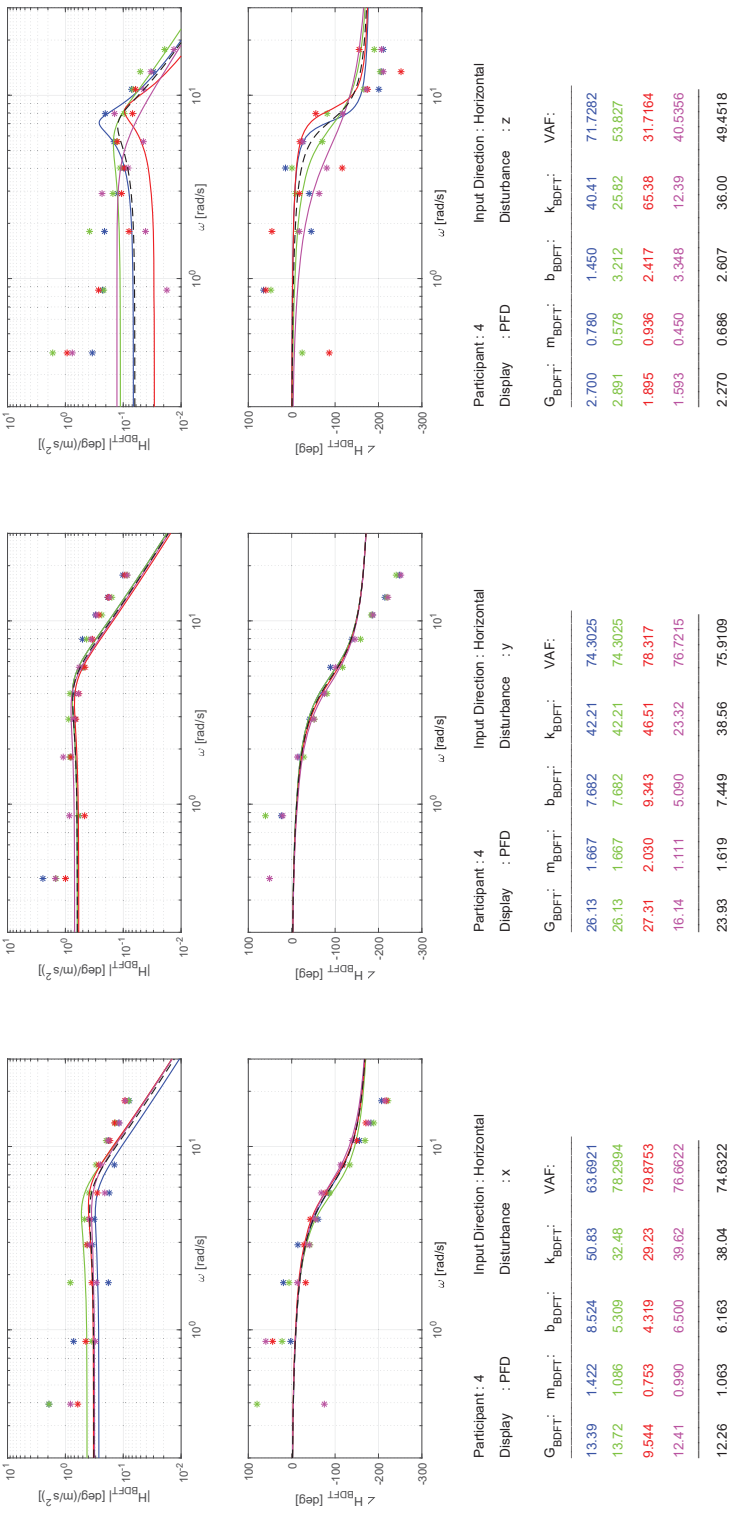

Figure C-12: Parameters Estimates: Participant 4, Vertical Inputs on PFD

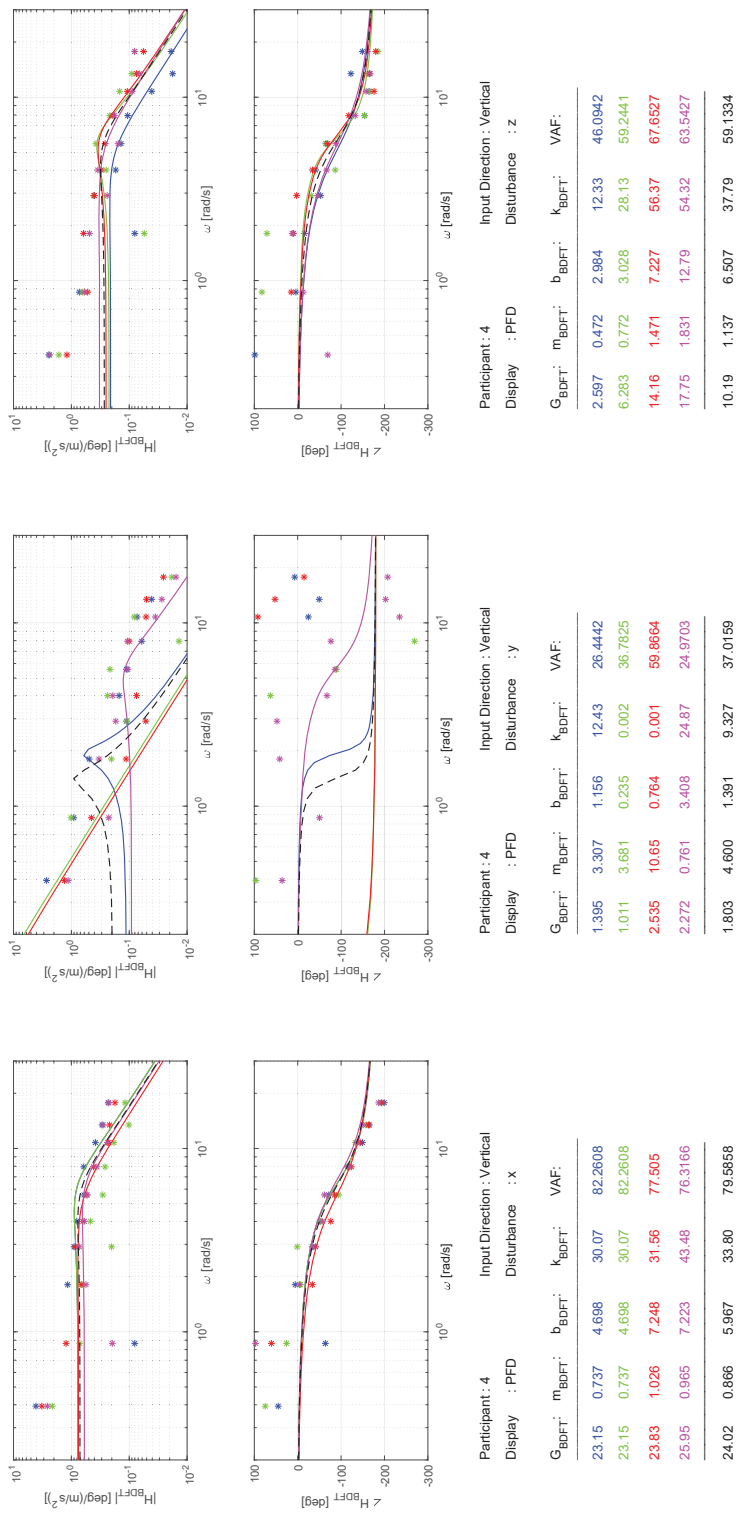

Figure C-13: Parameters Estimates: Participant 5, Horizontal Inputs on CDU

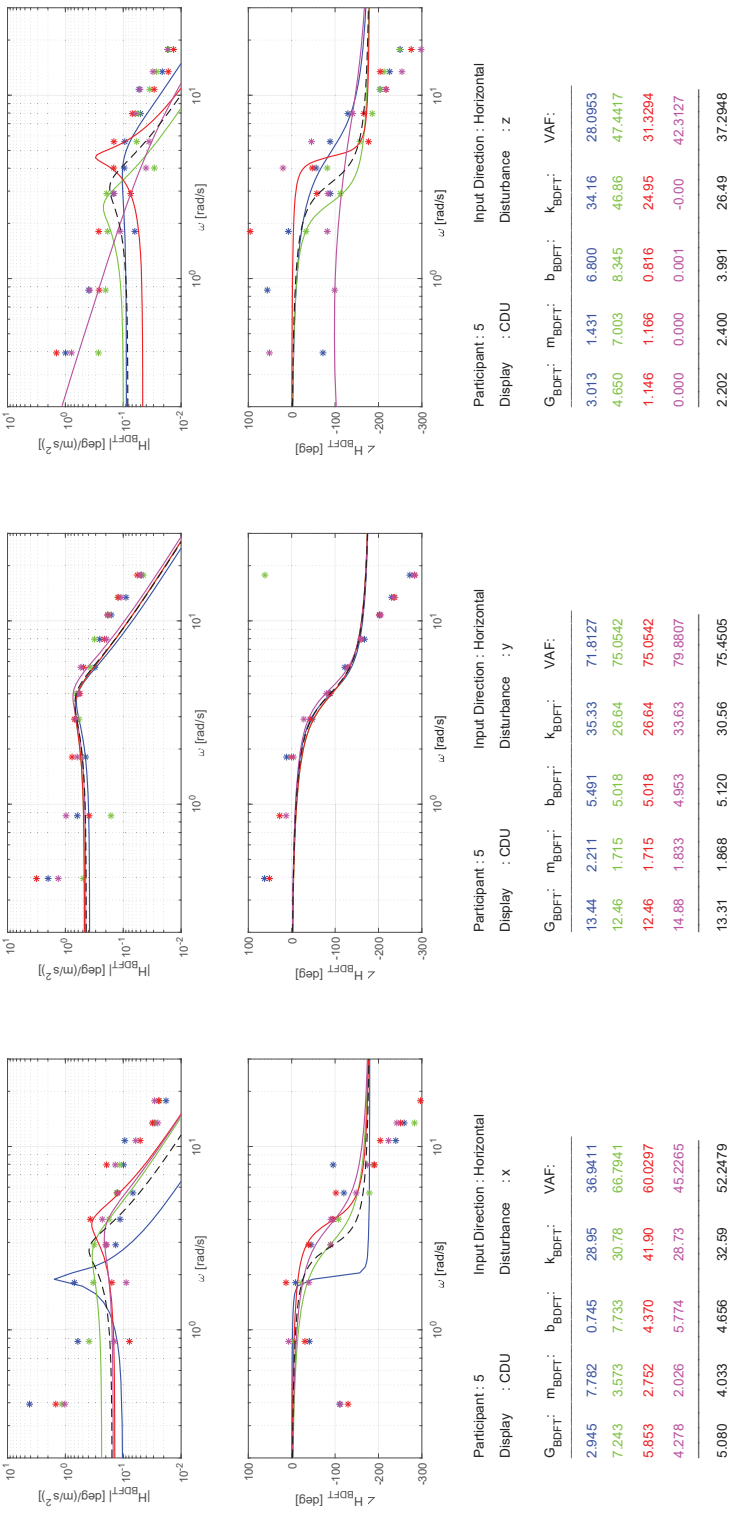

Figure C-14: Parameters Estimates: Participant 5, Vertical Inputs on CDU

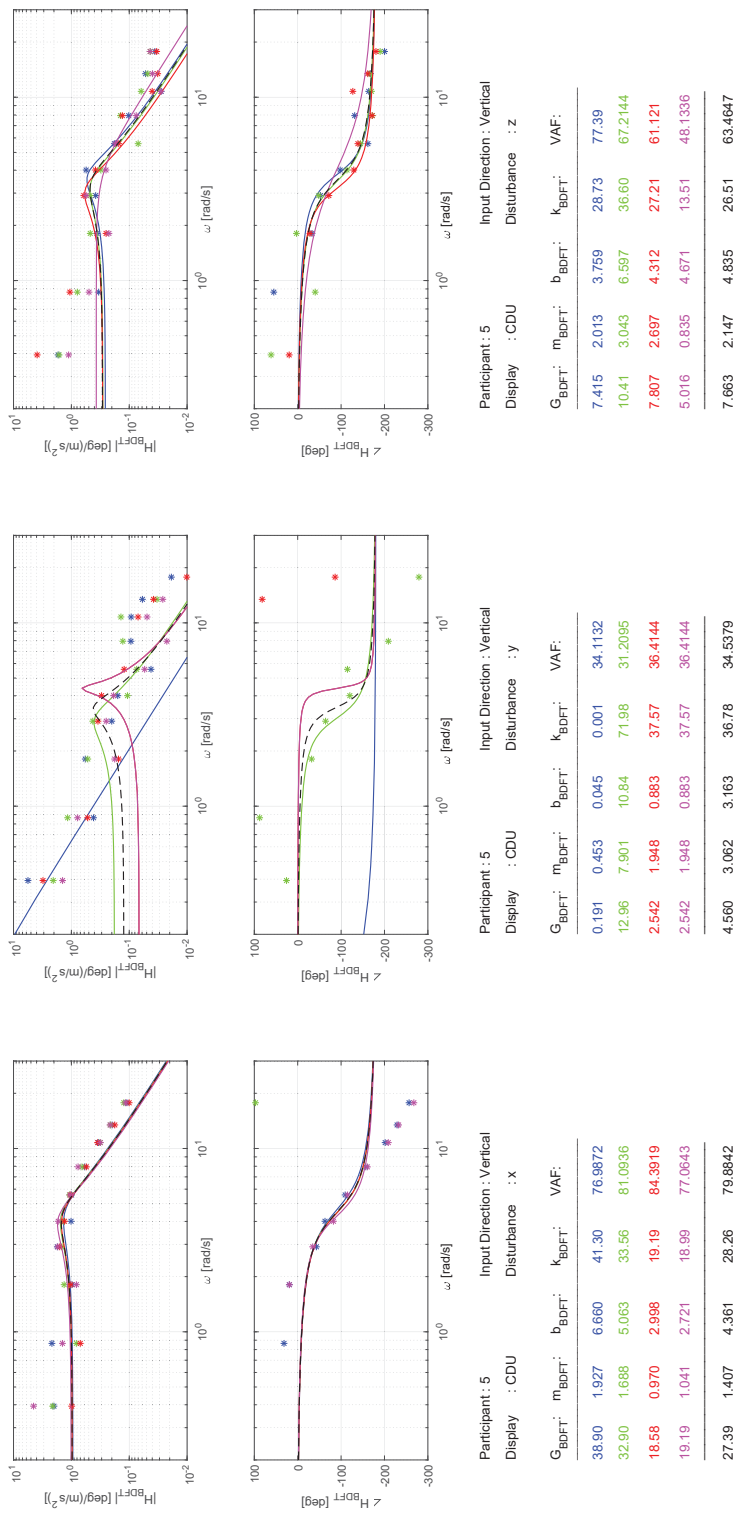

Figure C-15: Parameters Estimates: Participant 5, Horizontal Inputs on PFD

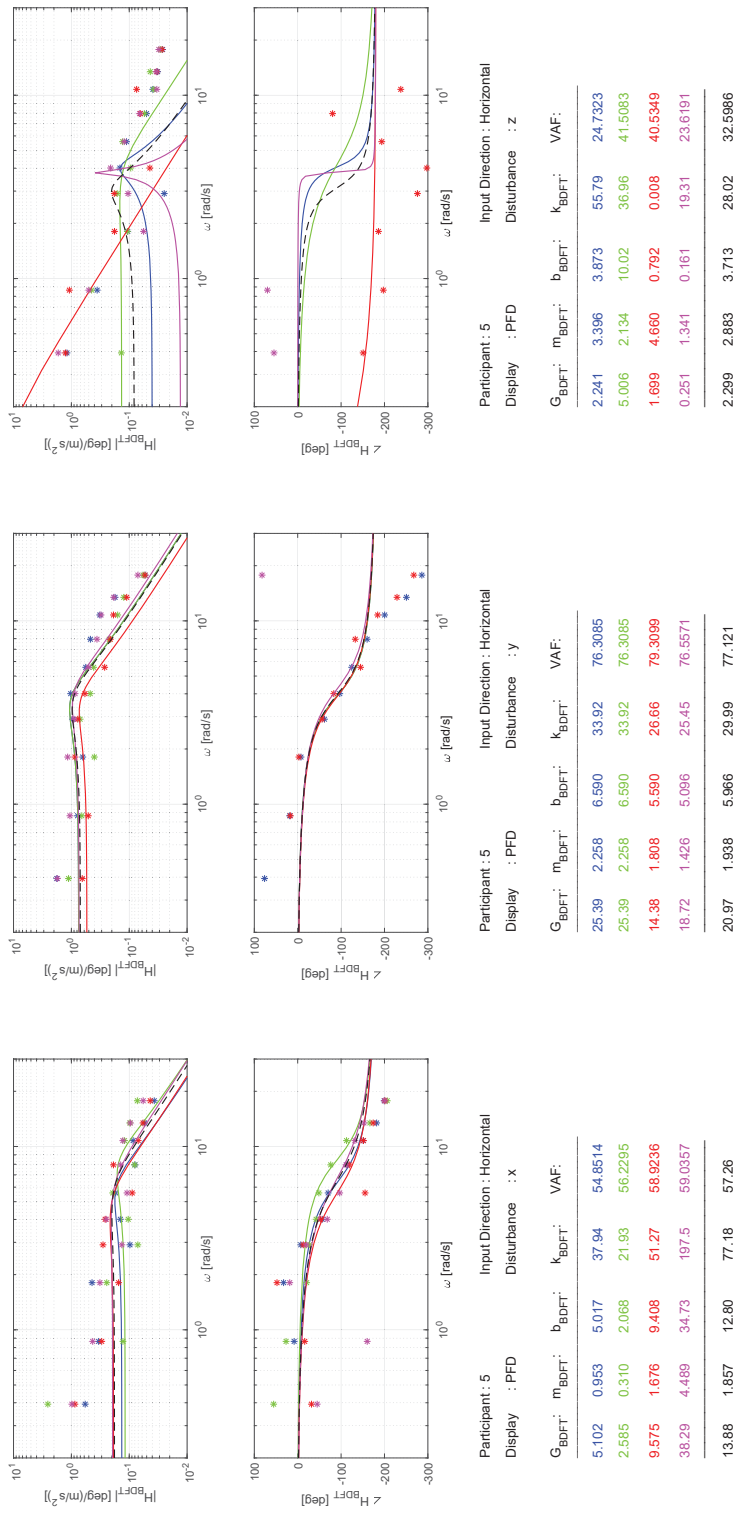

Figure C-16: Parameters Estimates: Participant 5, Vertical Inputs on PFD

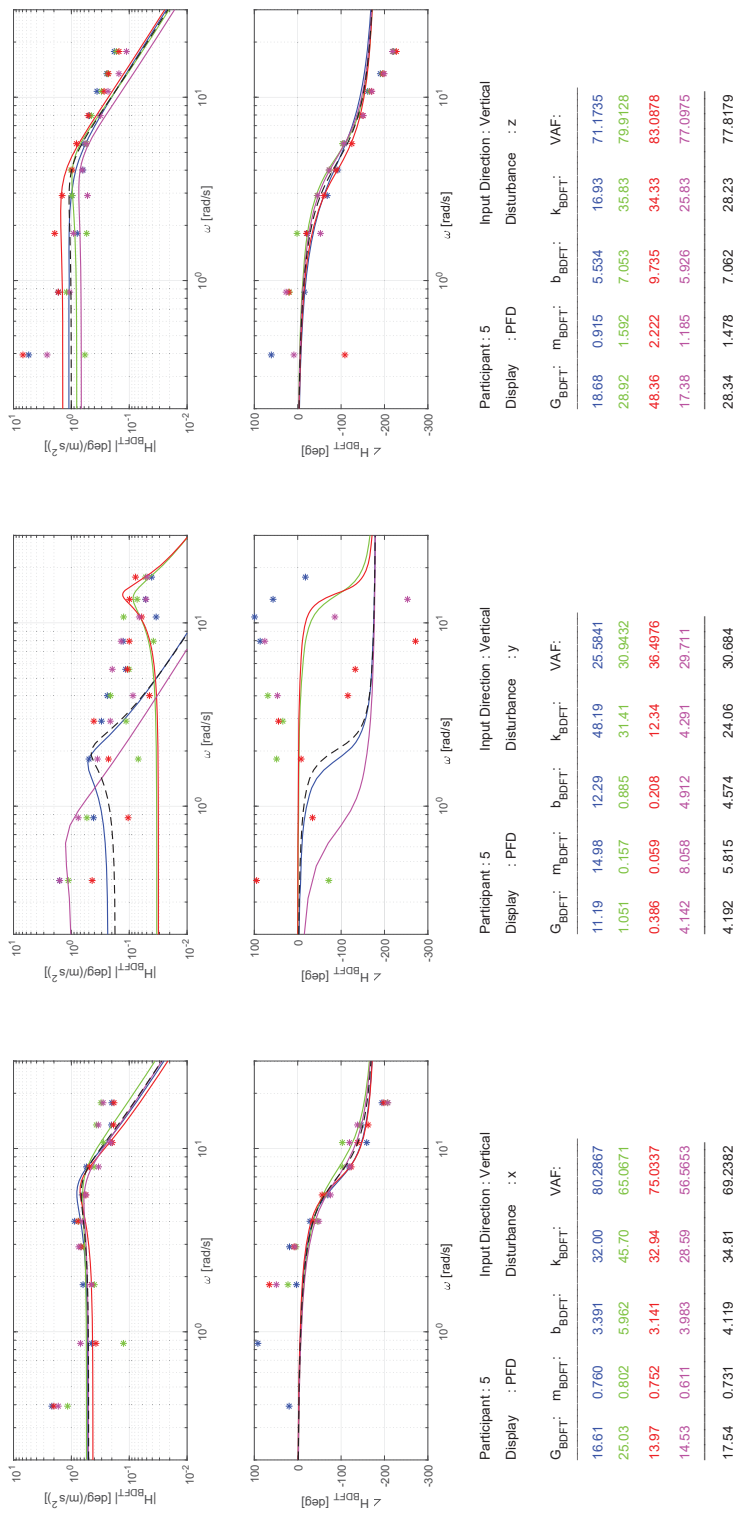

Figure C-17: Parameters Estimates: Participant 6, Horizontal Inputs on CDU

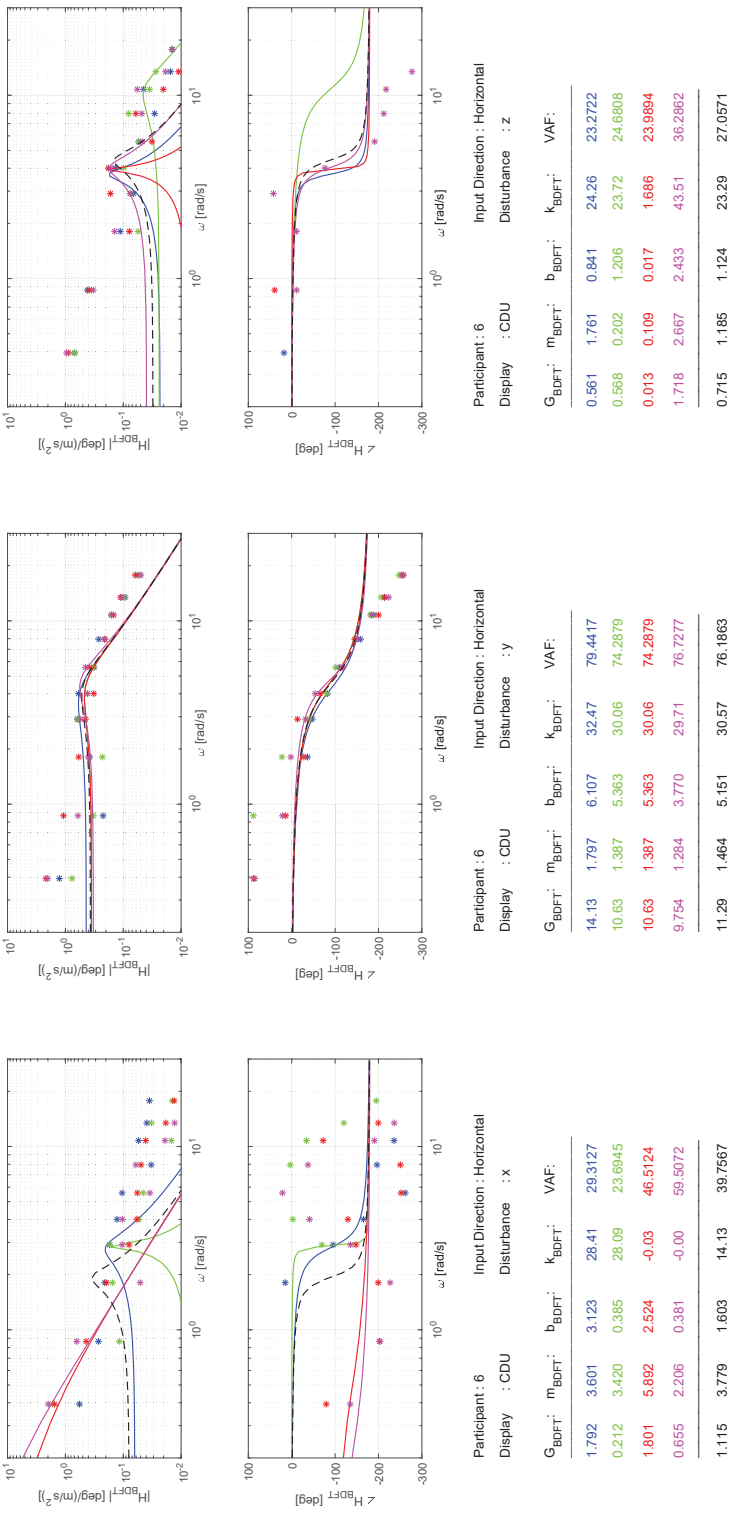

Figure C-18: Parameters Estimates: Participant 6, Vertical Inputs on CDU

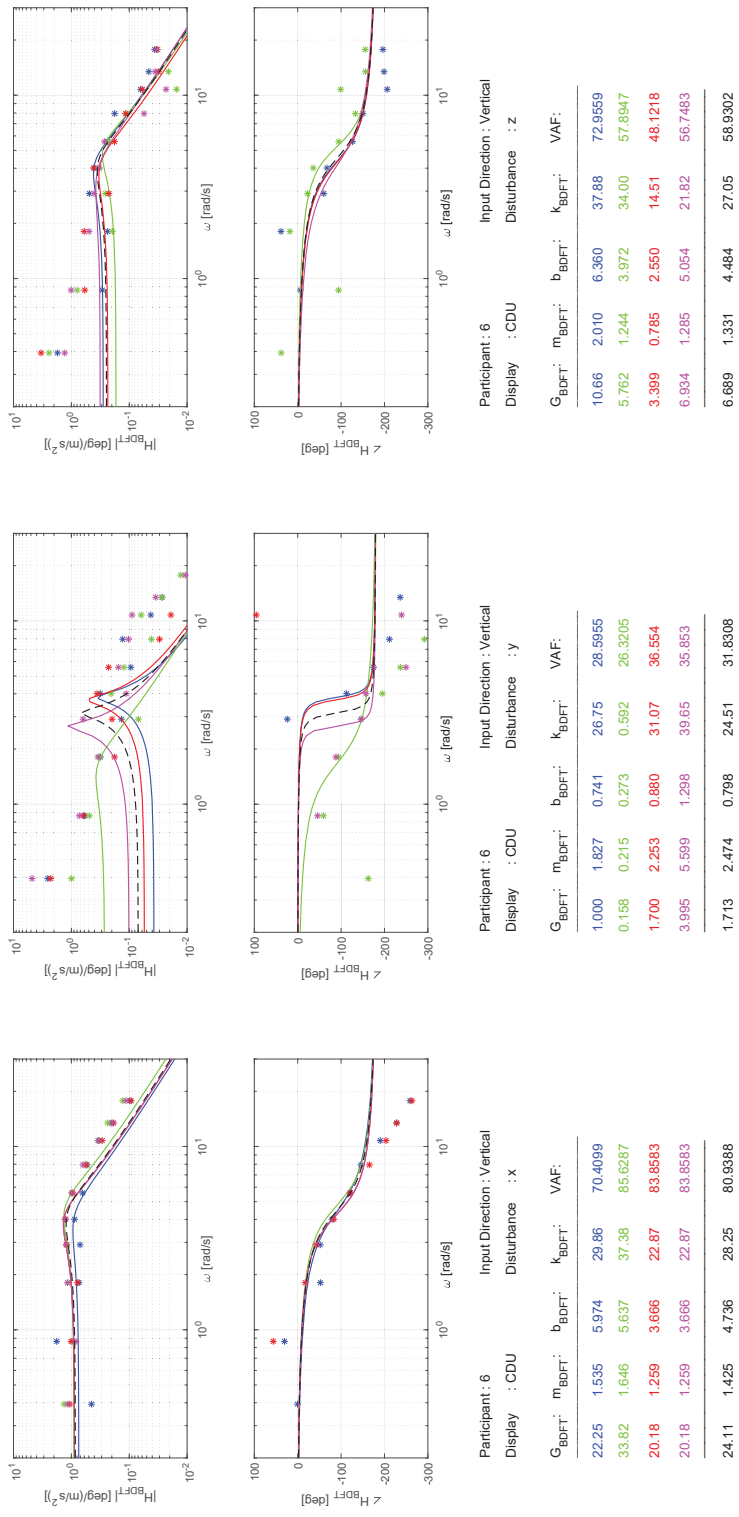

Figure C-19: Parameters Estimates: Participant 6, Horizontal Inputs on PFD

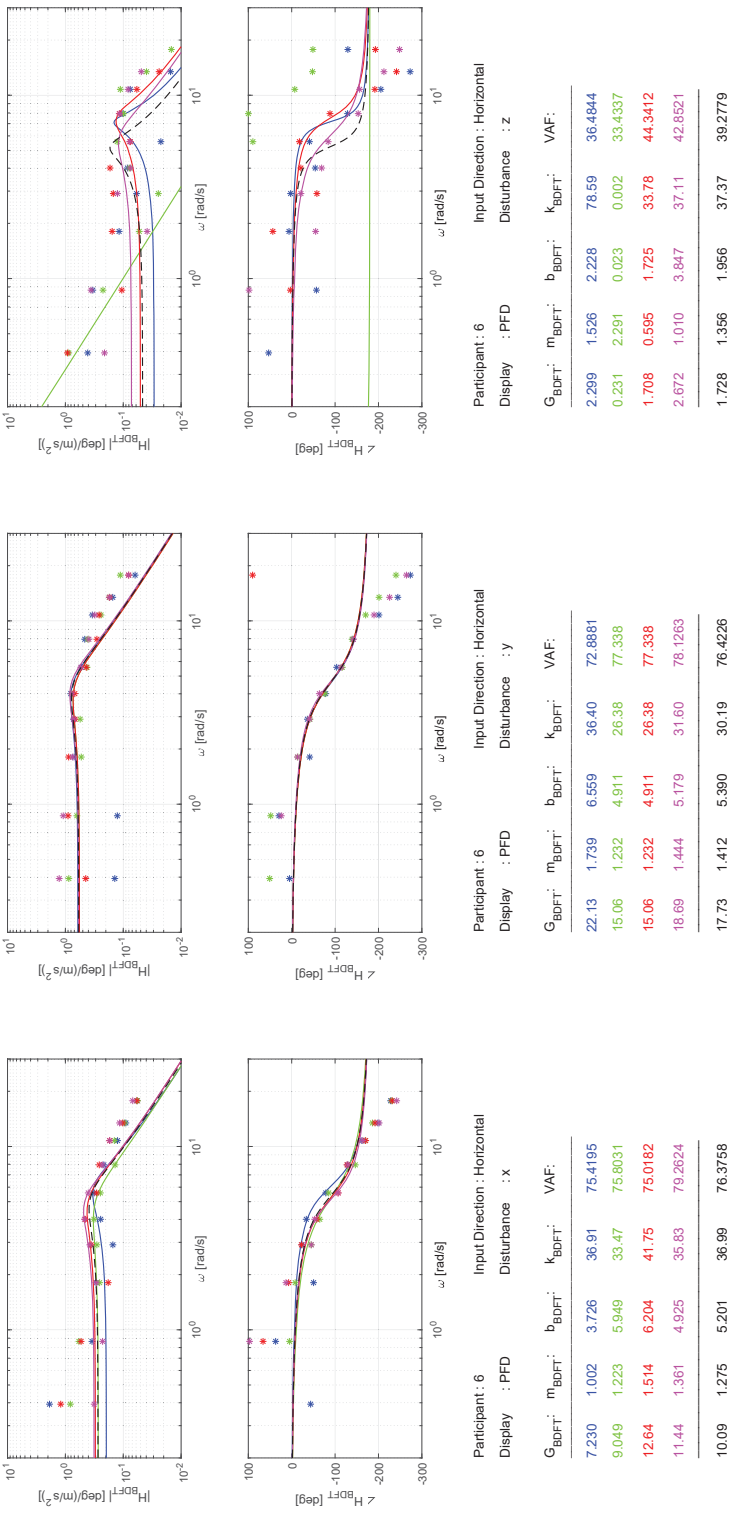

Figure C-20: Parameters Estimates: Participant 6, Vertical Inputs on PFD

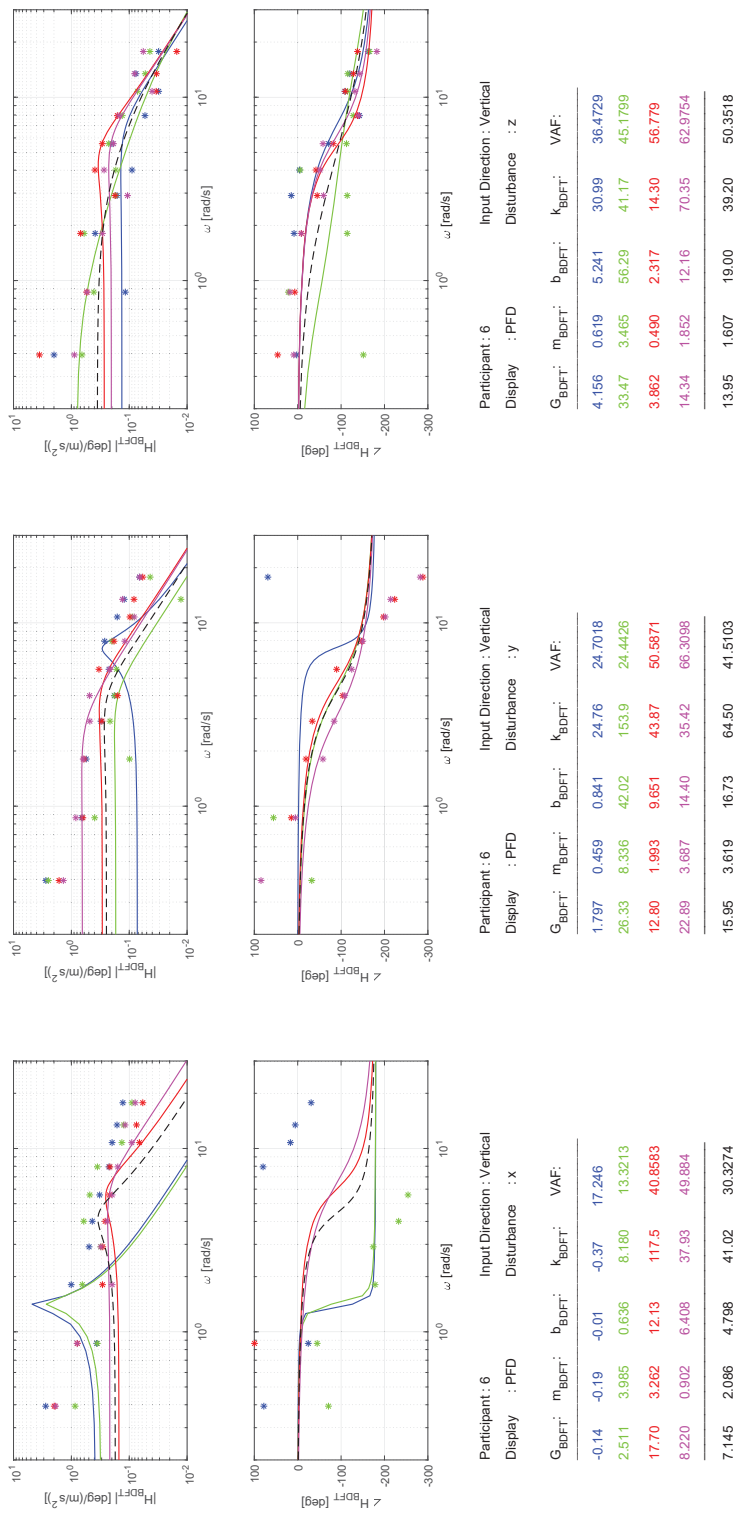

Figure C-21: Parameters Estimates: Participant 7, Horizontal Inputs on CDU

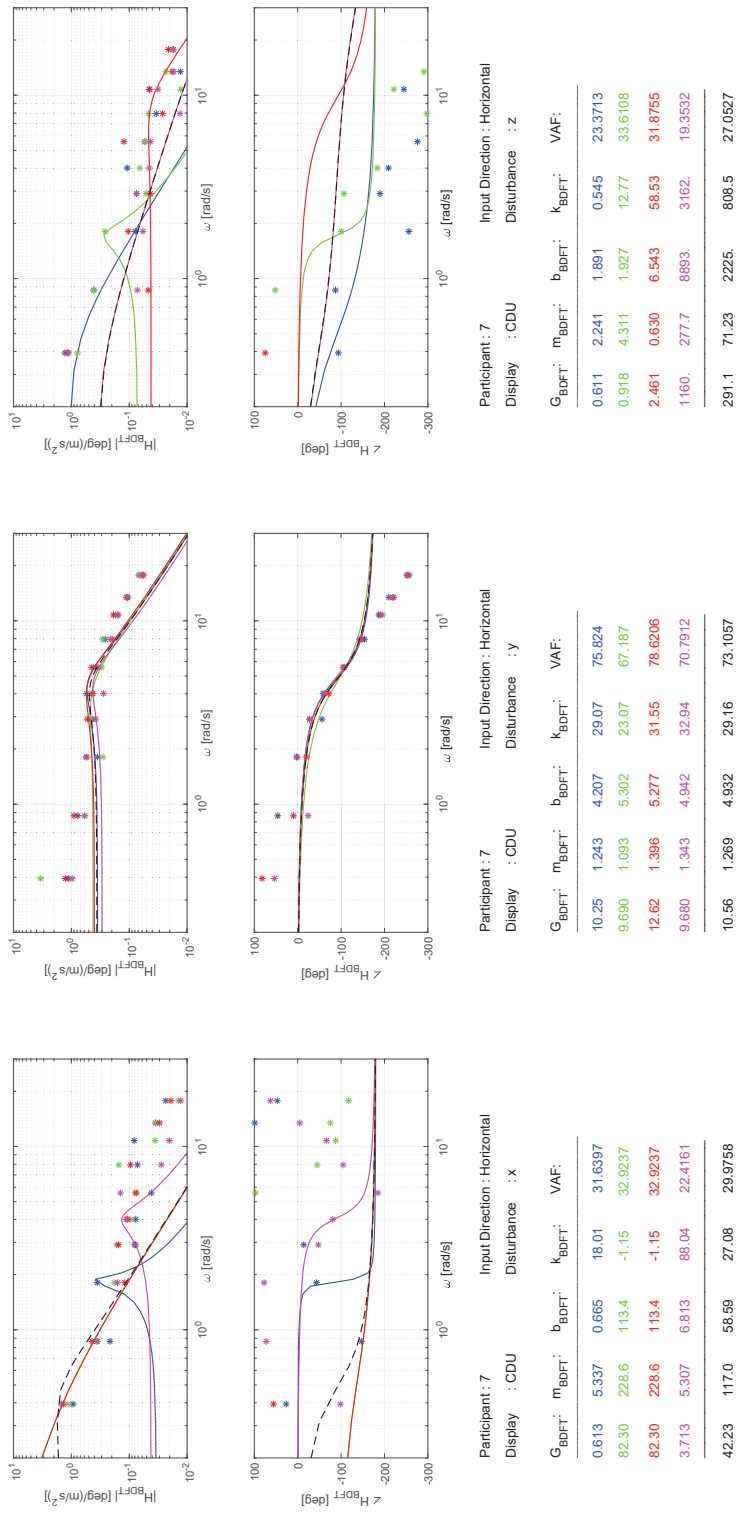

Figure C-22: Parameters Estimates: Participant 7, Vertical Inputs on CDU

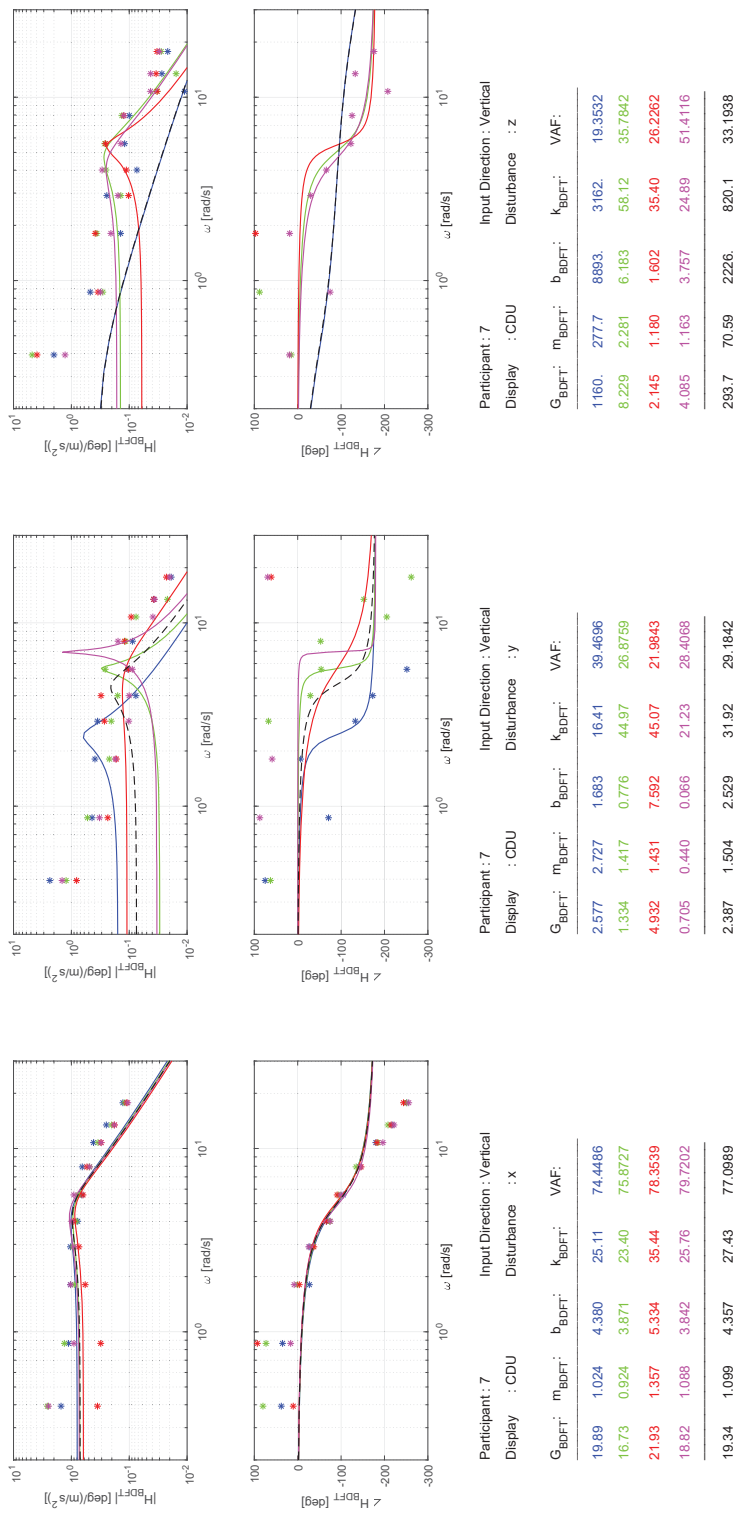

Figure C-23: Parameters Estimates: Participant 7, Horizontal Inputs on PFD

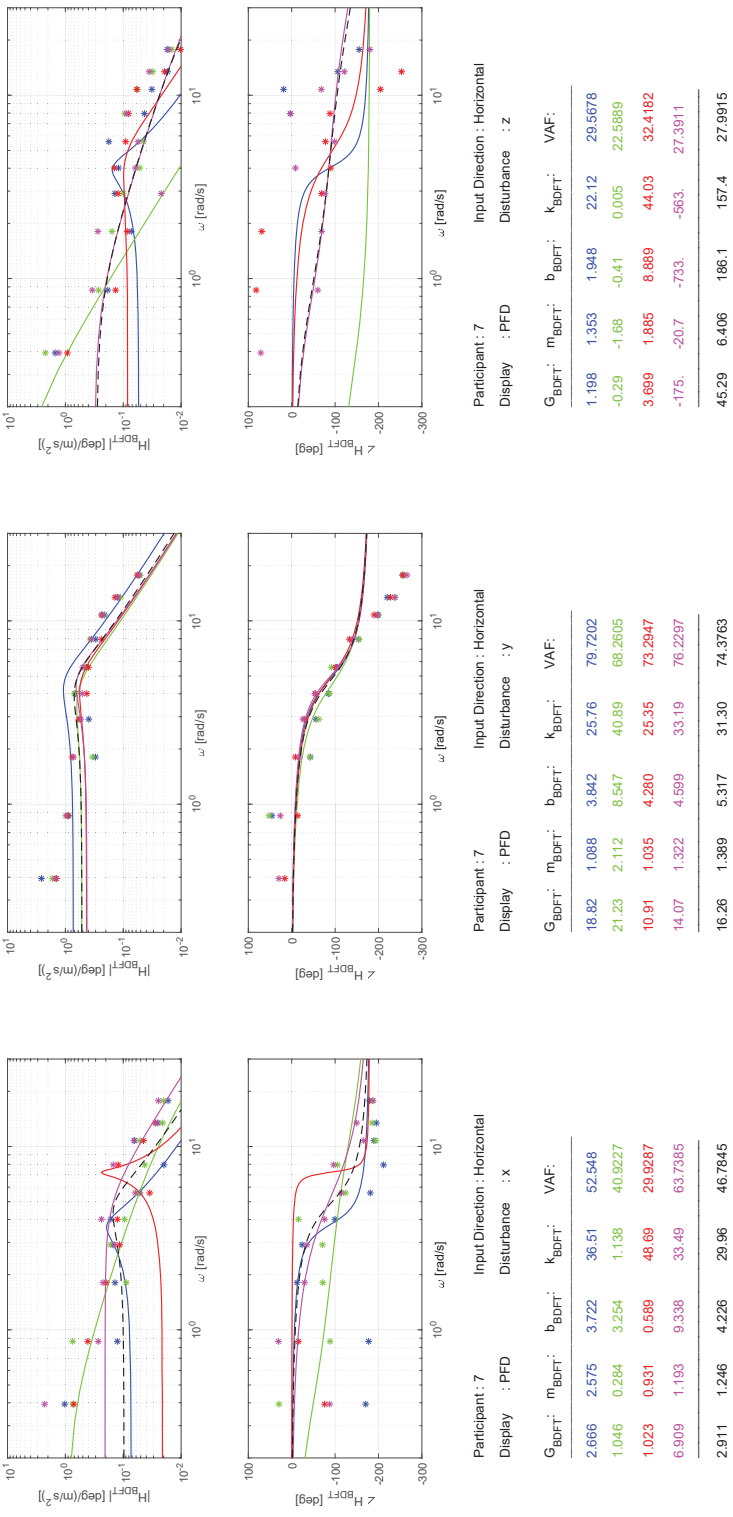

Figure C-24: Parameters Estimates: Participant 7, Vertical Inputs on PFD

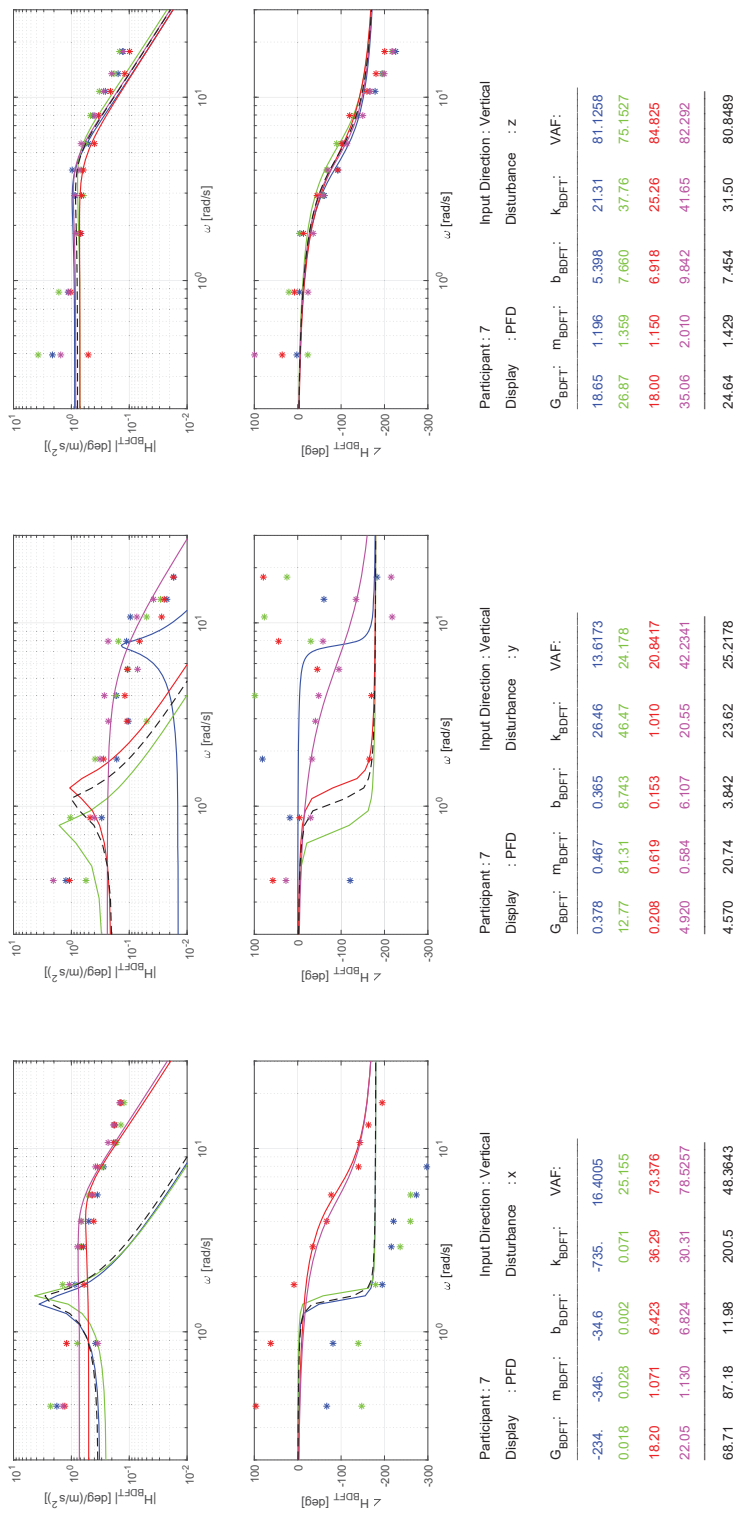

Figure C-25: Parameters Estimates: Participant 8, Horizontal Inputs on CDU

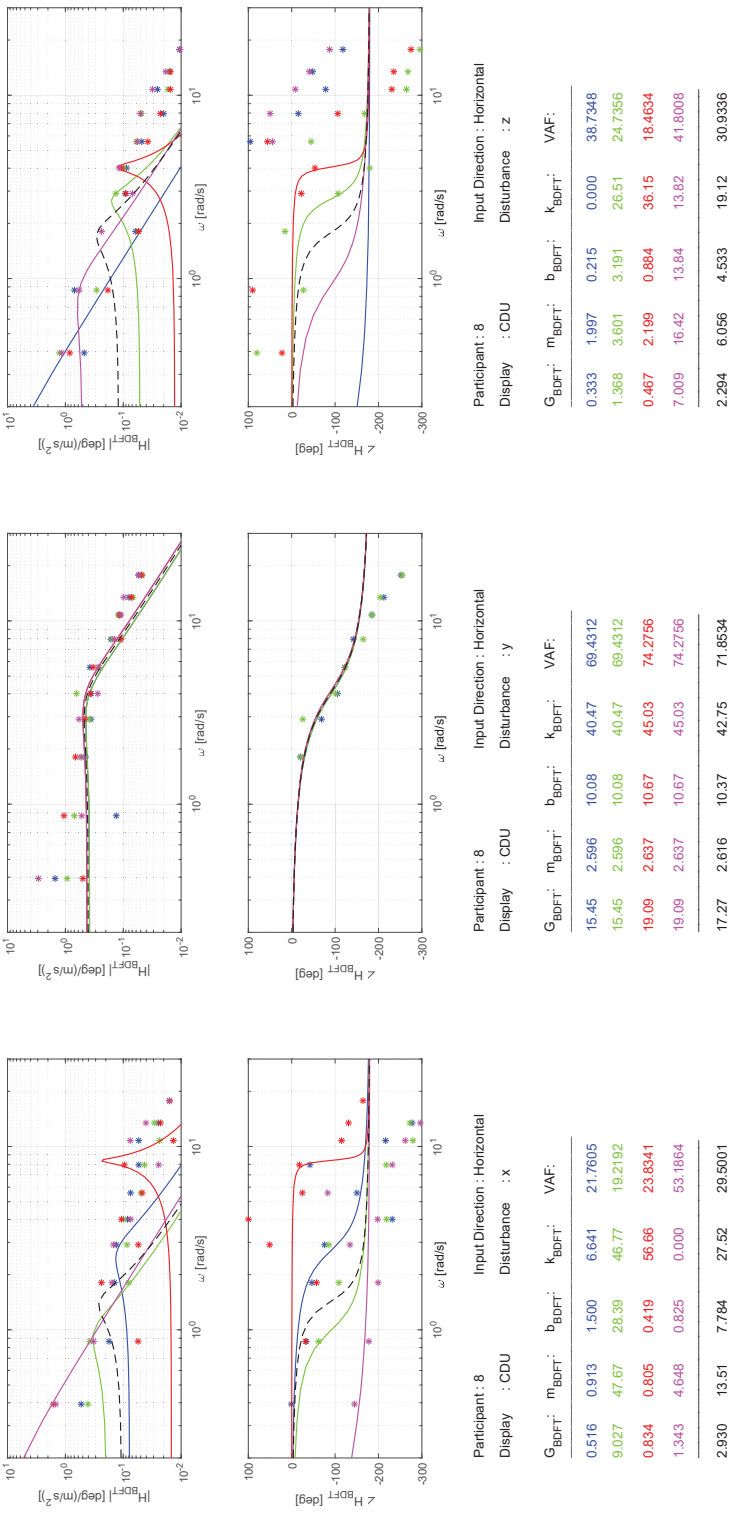

Figure C-26: Parameters Estimates: Participant 8, Vertical Inputs on CDU

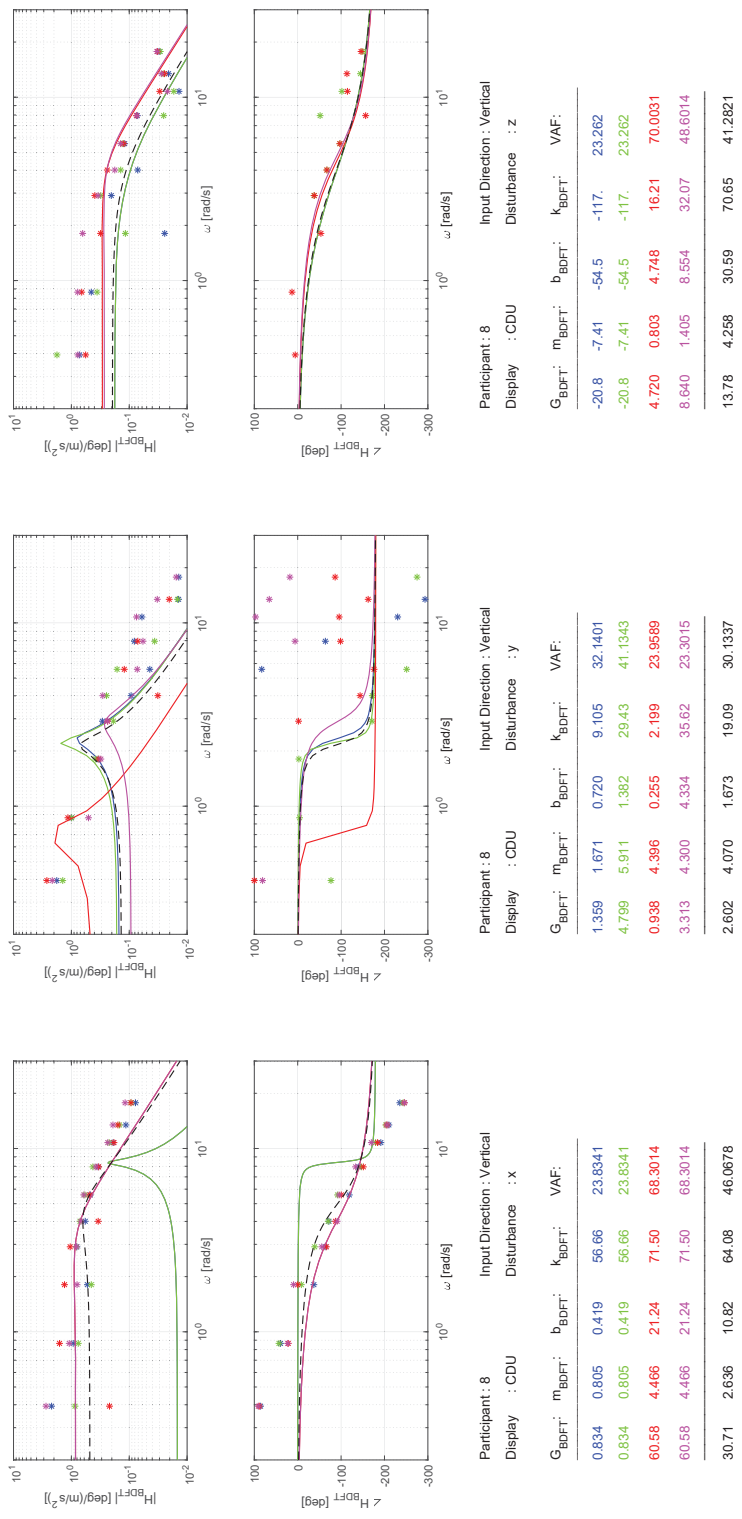

Figure C-27: Parameters Estimates: Participant 8, Horizontal Inputs on PFD

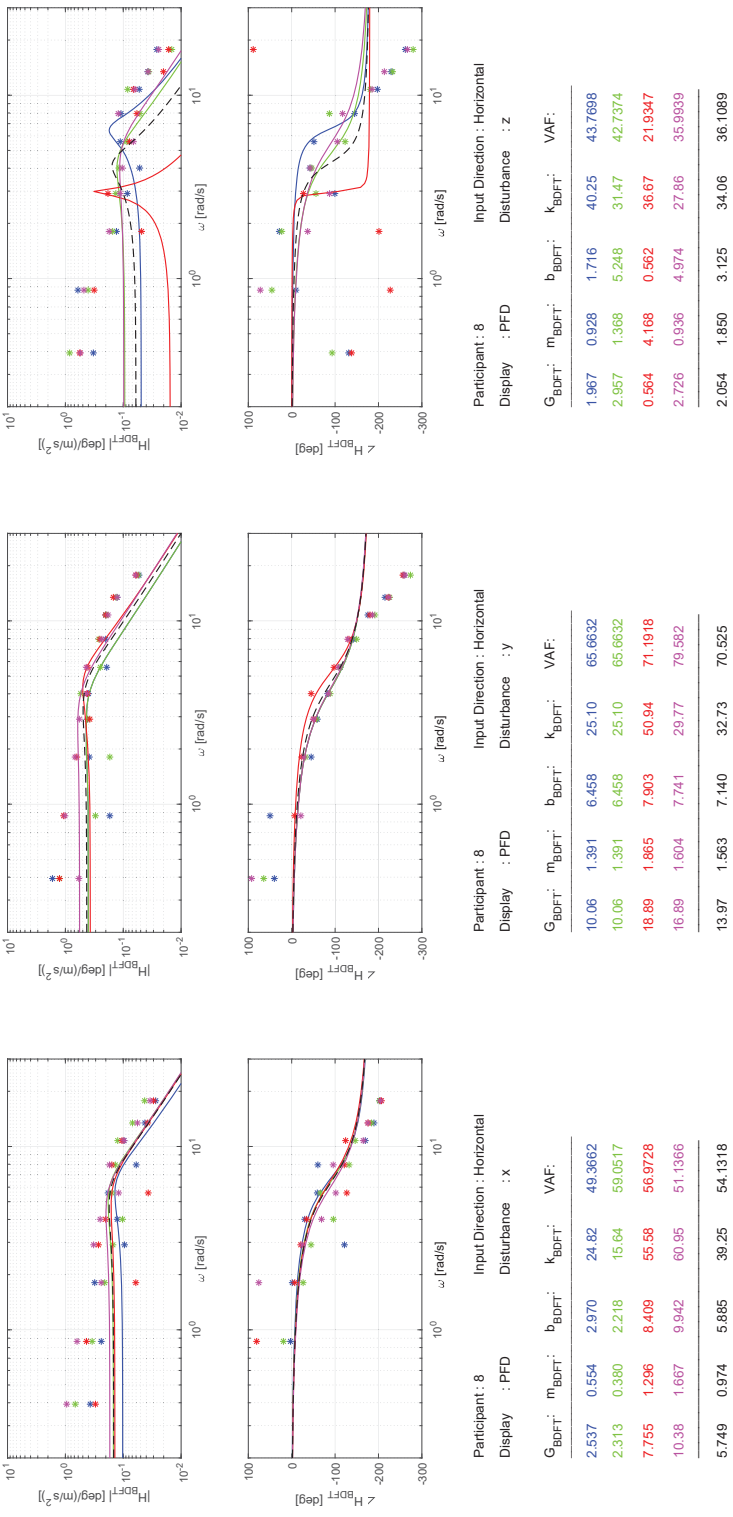

Figure C-28: Parameters Estimates: Participant 8, Vertical Inputs on PFD

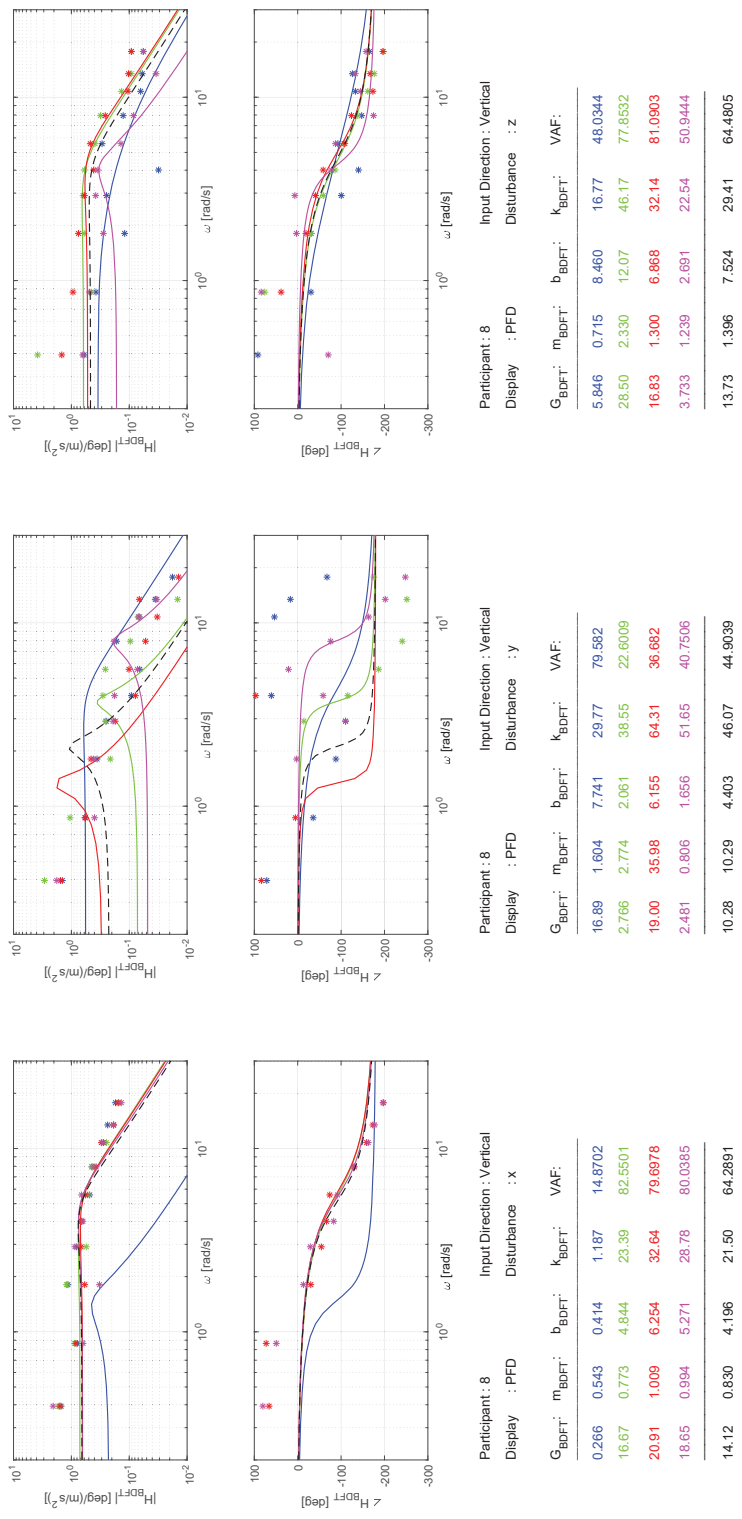

Figure C-29: Parameters Estimates: Participant 9, Horizontal Inputs on CDU

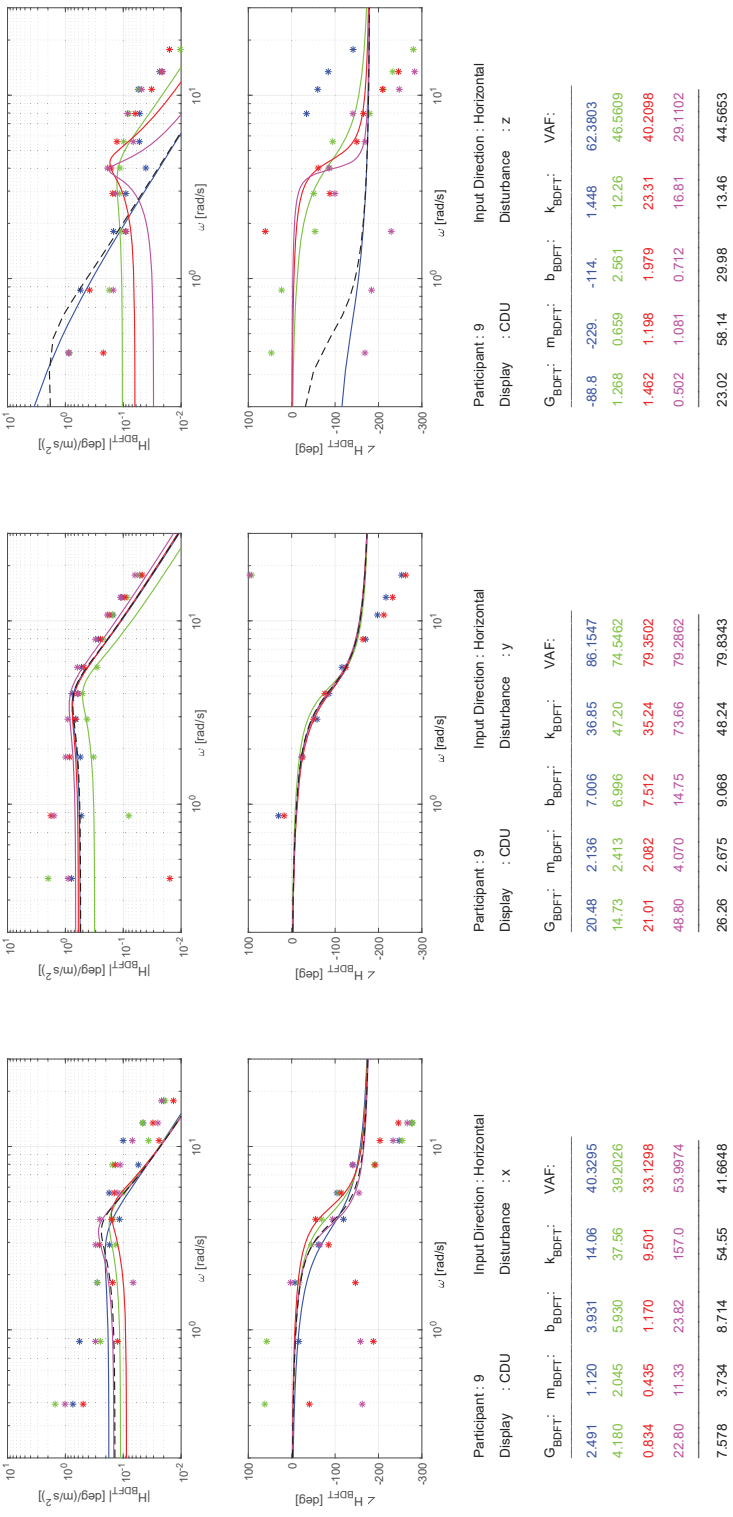

Figure C-30: Parameters Estimates: Participant 9, Vertical Inputs on CDU

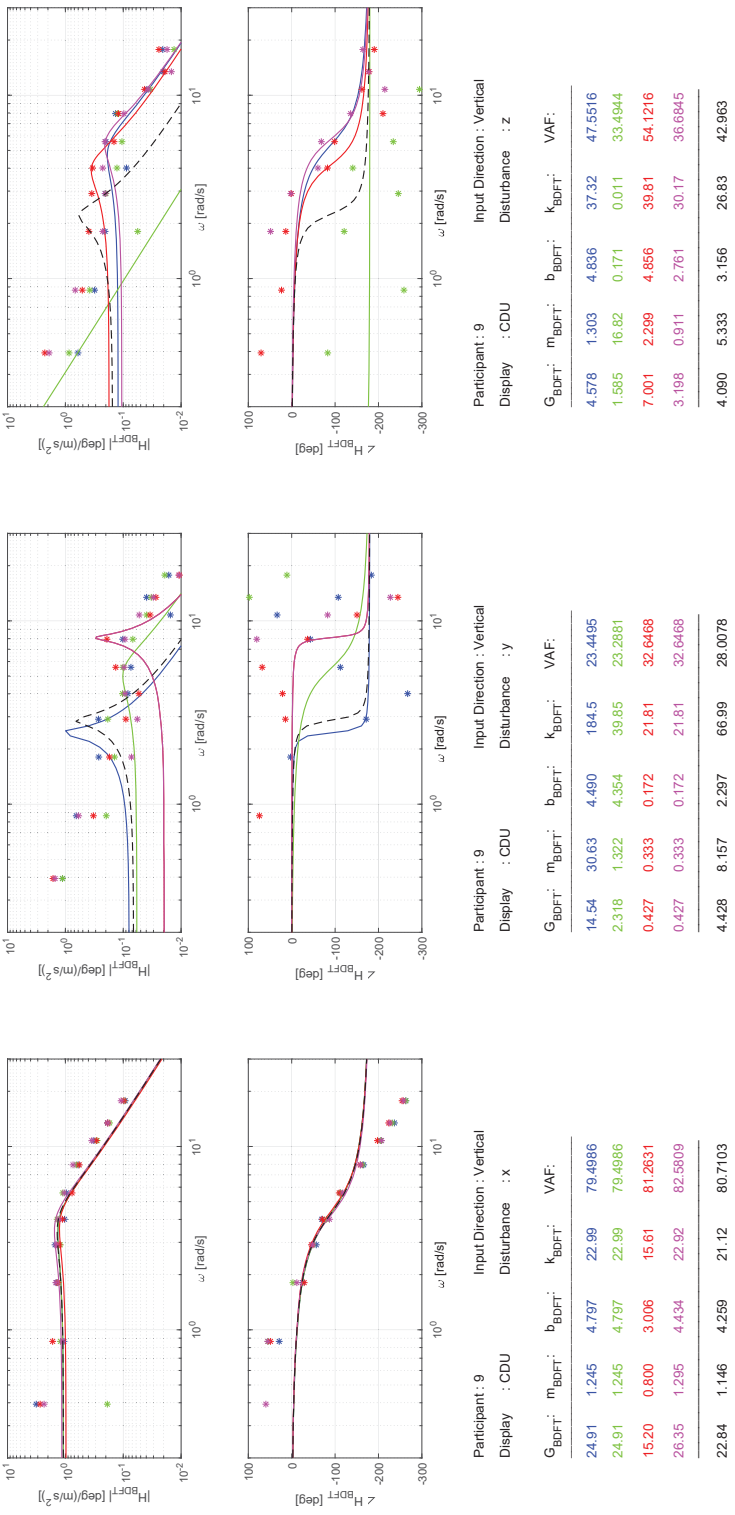

Figure C-31: Parameters Estimates: Participant 9, Horizontal Inputs on PFD

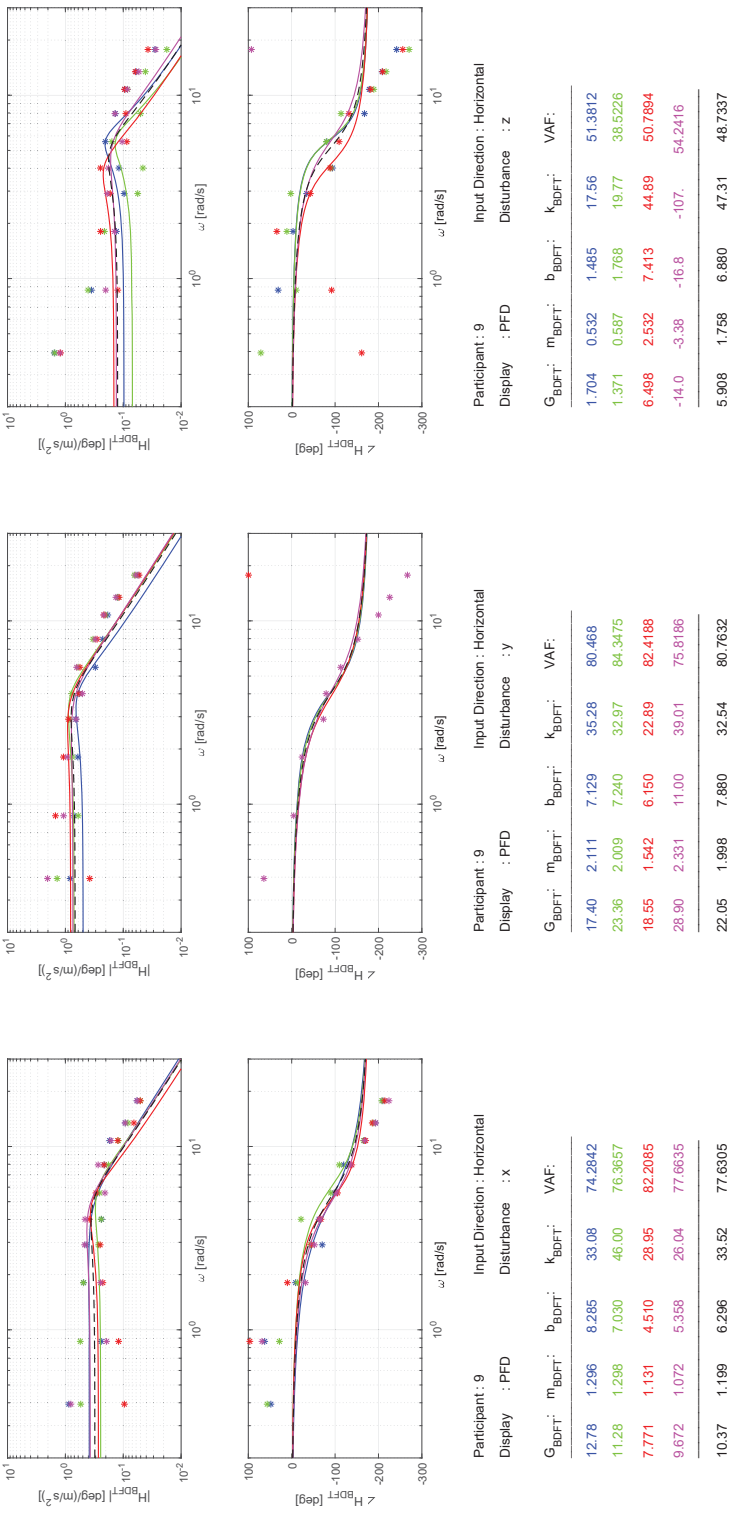

Figure C-32: Parameters Estimates: Participant 9, Vertical Inputs on PFD

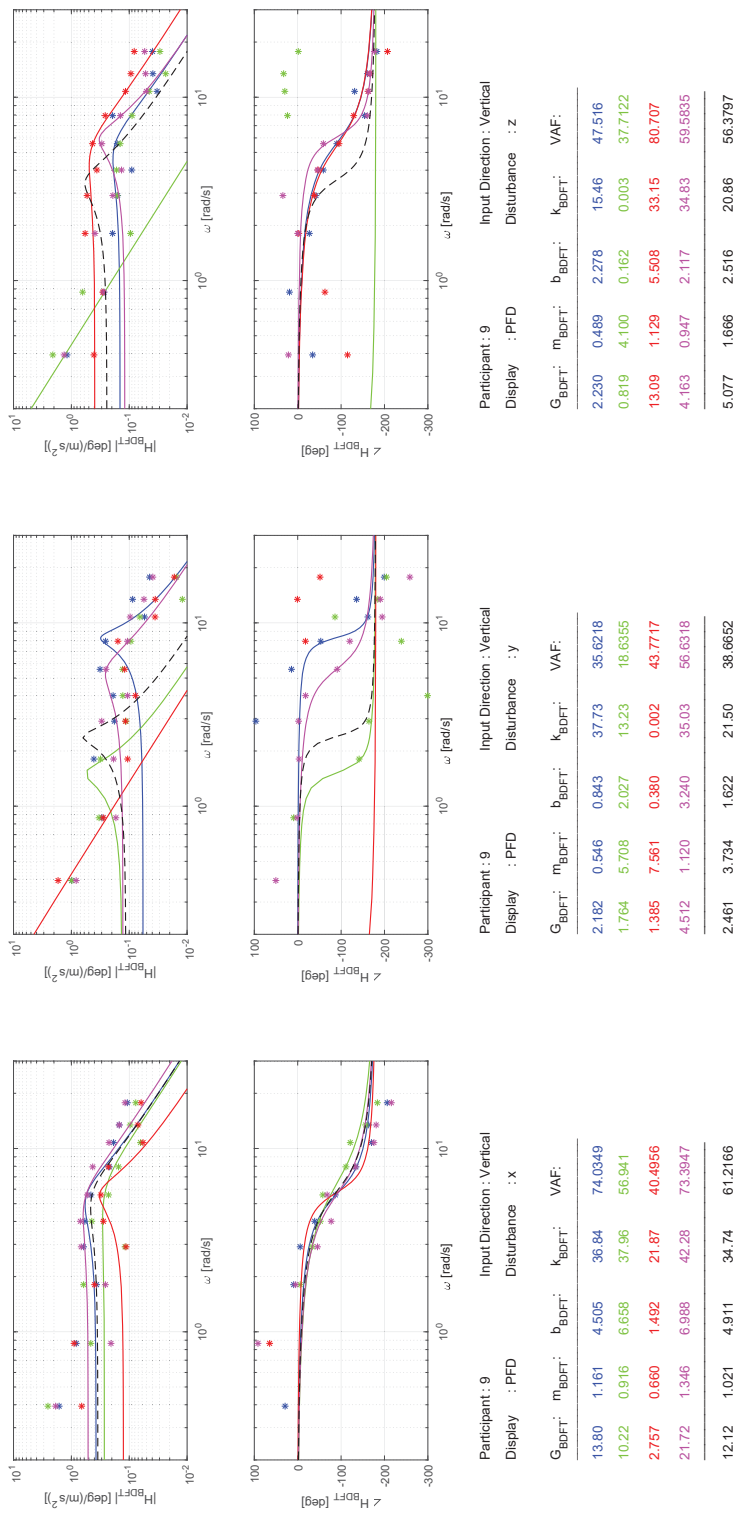

Figure C-33: Parameters Estimates: Participant 10, Horizontal Inputs on CDU

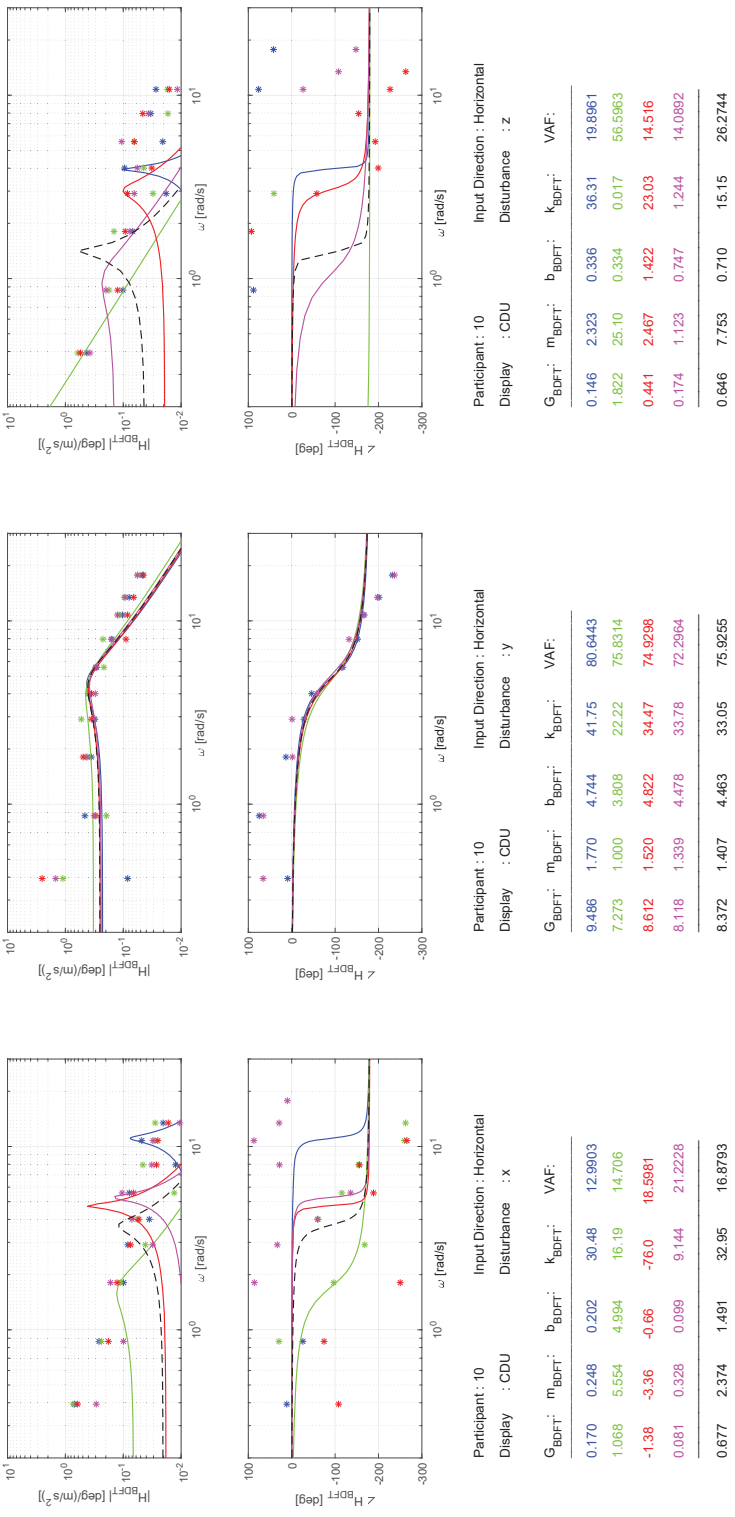

Figure C-34: Parameters Estimates: Participant 10, Vertical Inputs on CDU

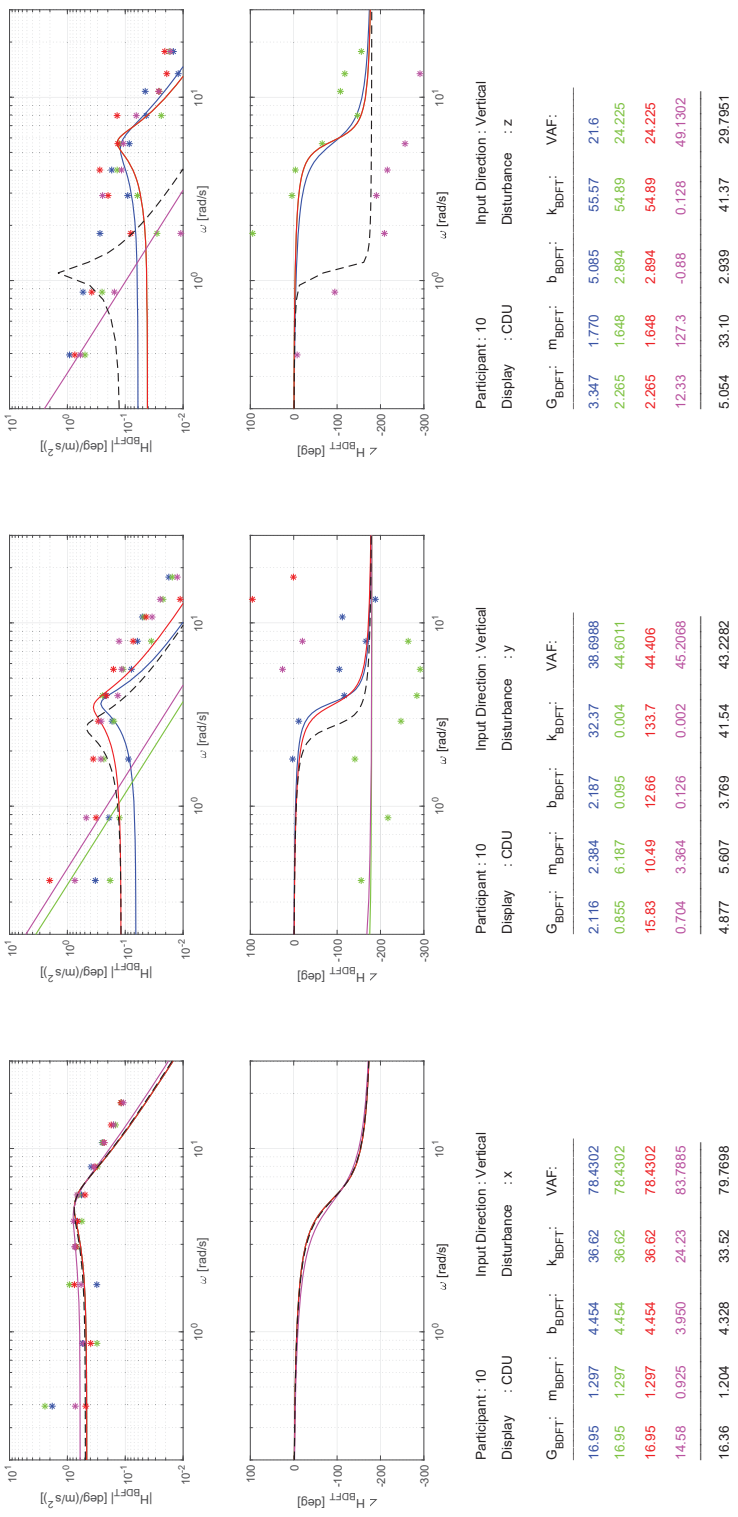

Figure C-35: Parameters Estimates: Participant 10, Horizontal Inputs on PFD

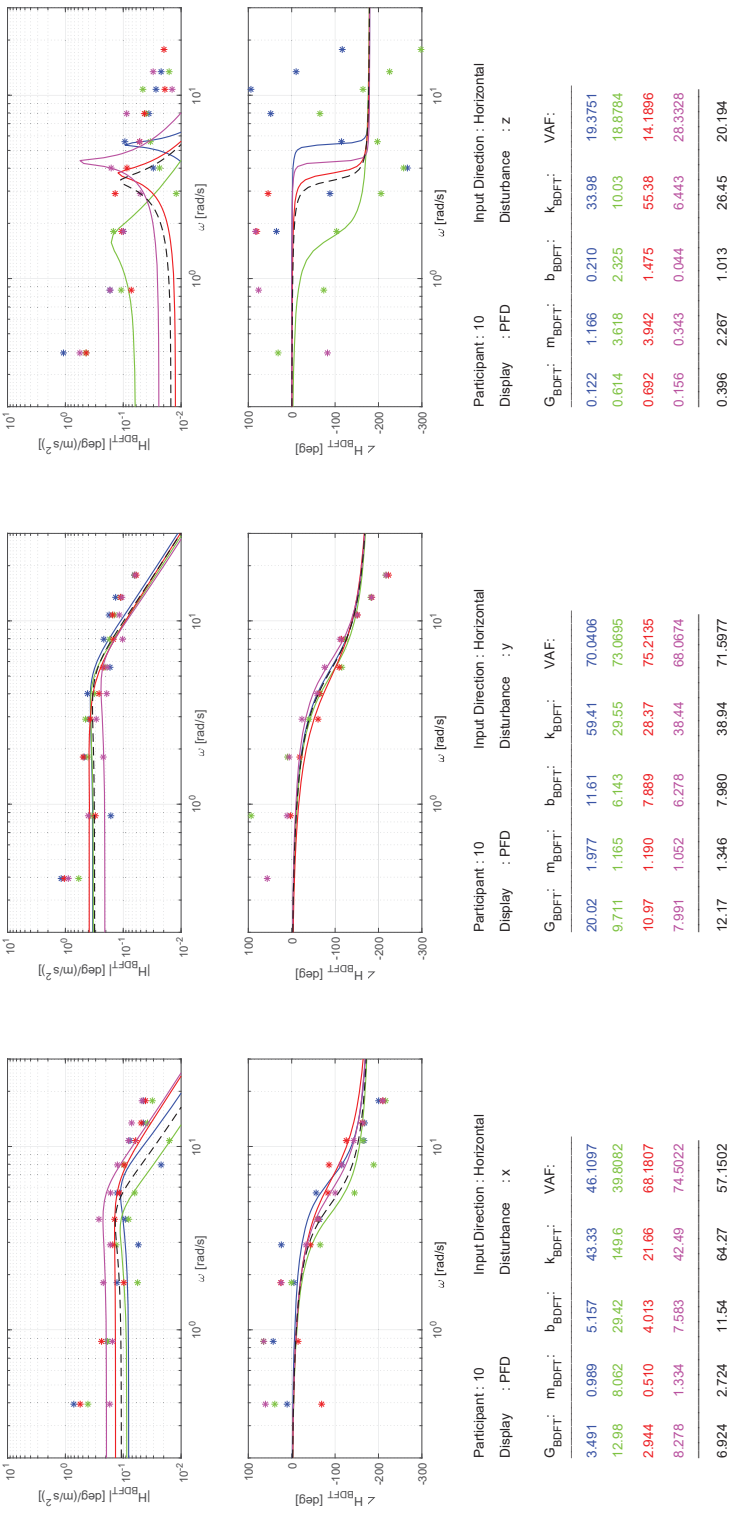

Figure C-36: Parameters Estimates: Participant 10, Vertical Inputs on PFD

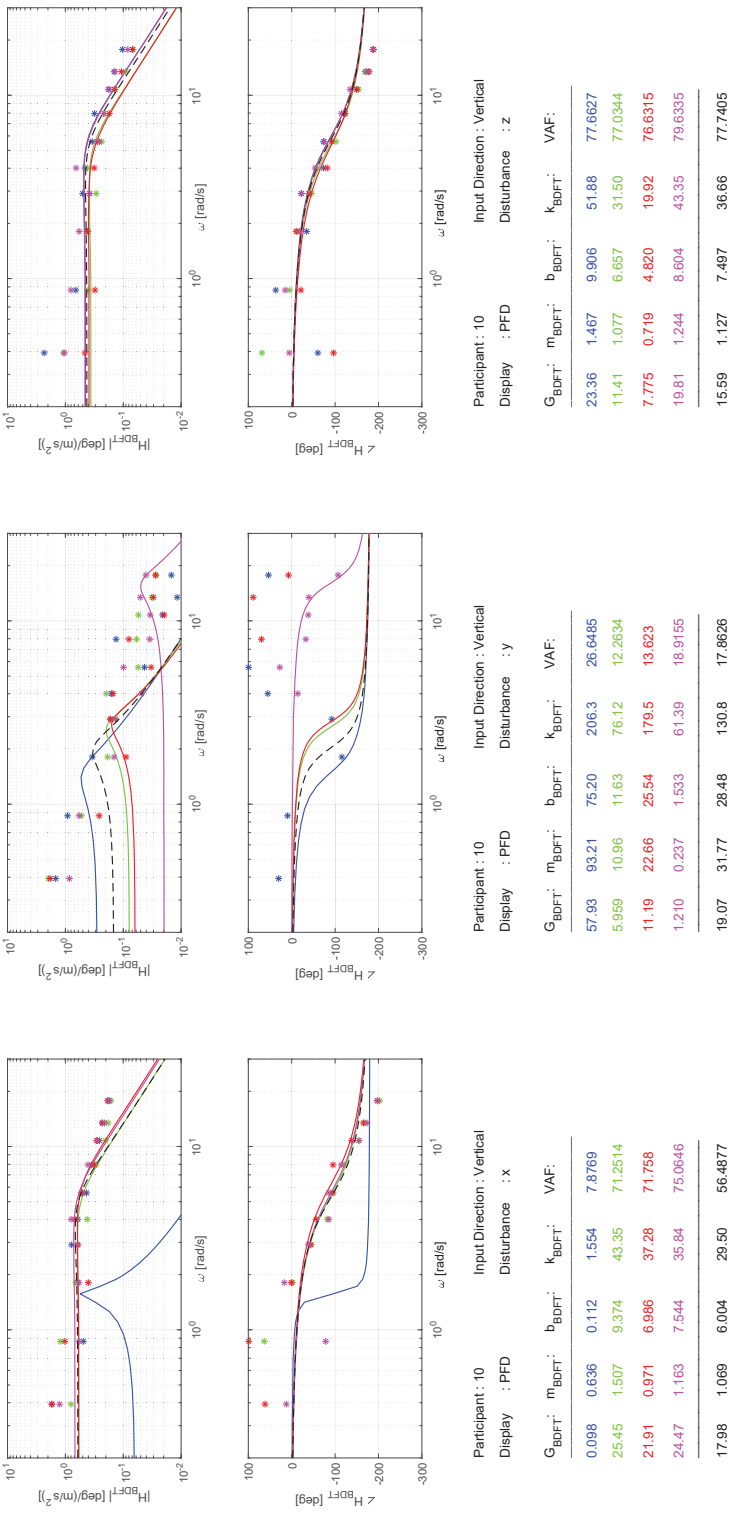

Figure C-37: Parameters Estimates: Participant 11, Horizontal Inputs on CDU

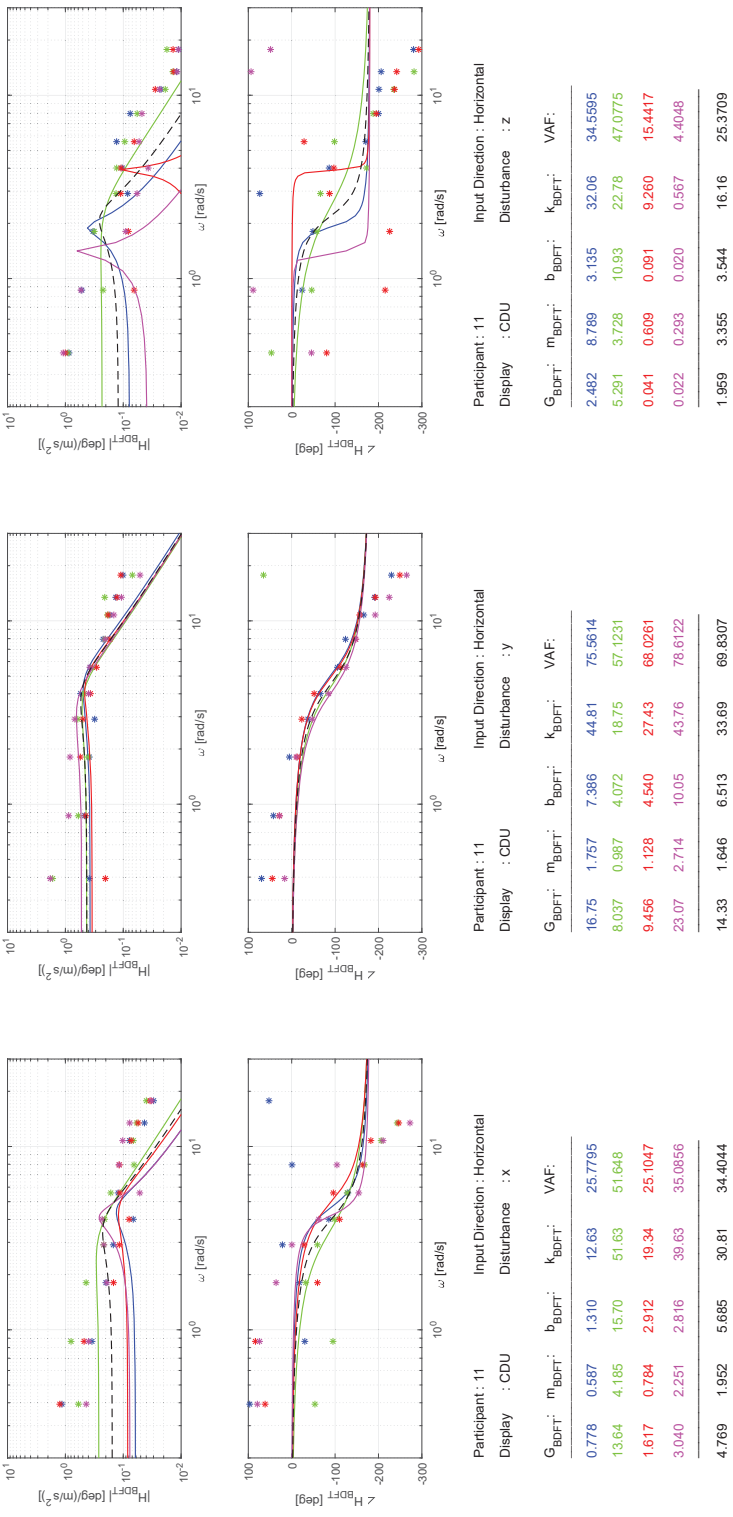

Figure C-38: Parameters Estimates: Participant 11, Vertical Inputs on CDU

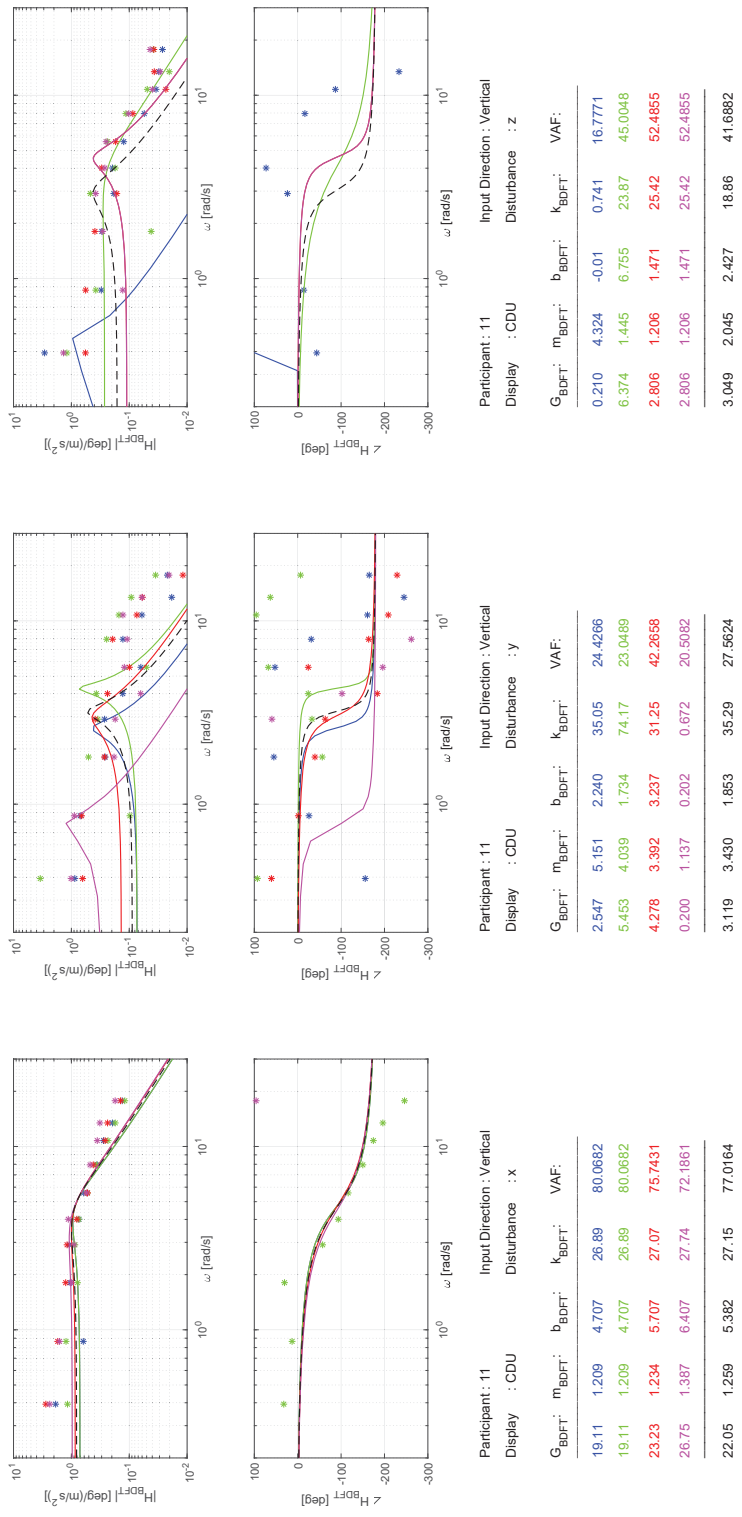

Figure C-39: Parameters Estimates: Participant 11, Horizontal Inputs on PFD

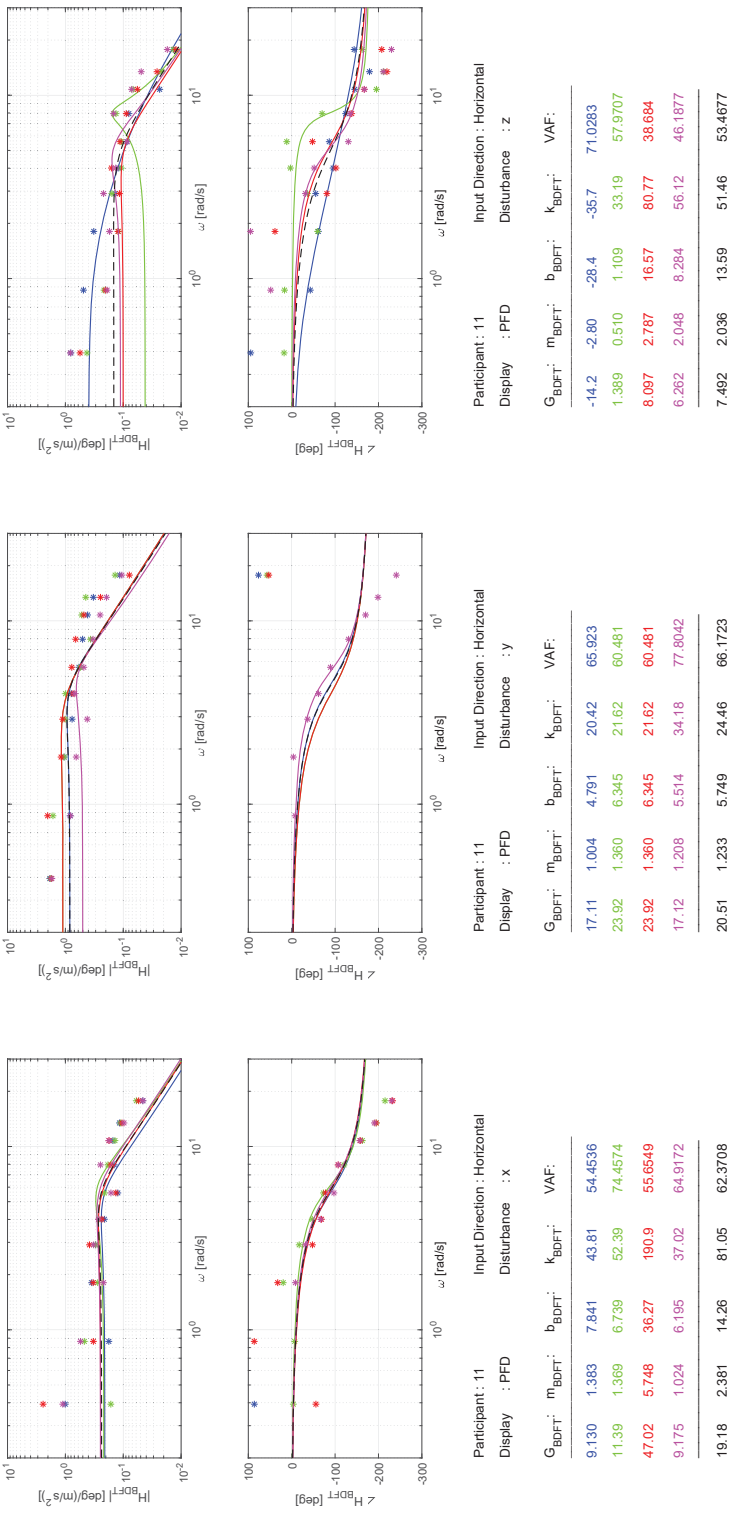

Figure C-40: Parameters Estimates: Participant 11, Vertical Inputs on PFD

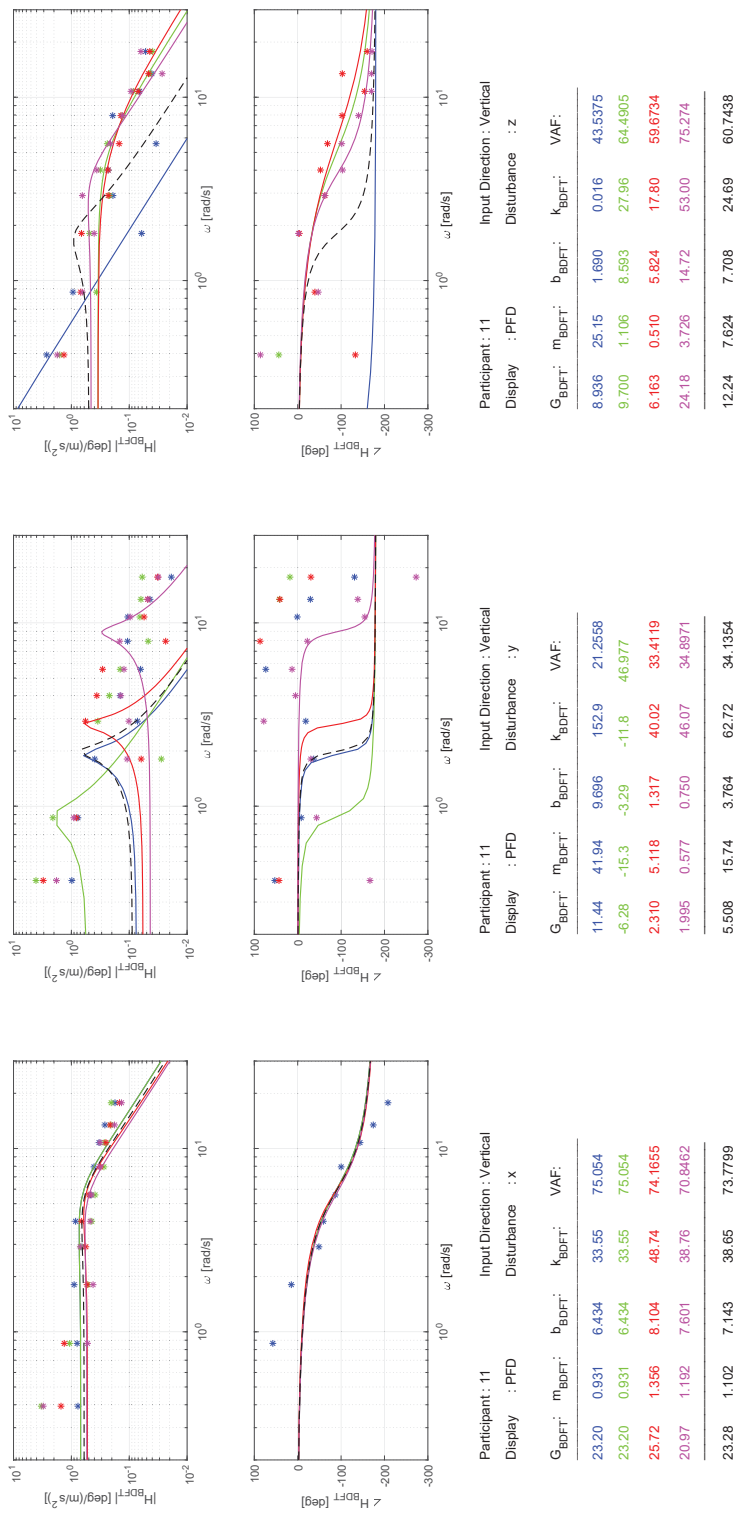

Figure C-41: Parameters Estimates: Participant 12, Horizontal Inputs on CDU

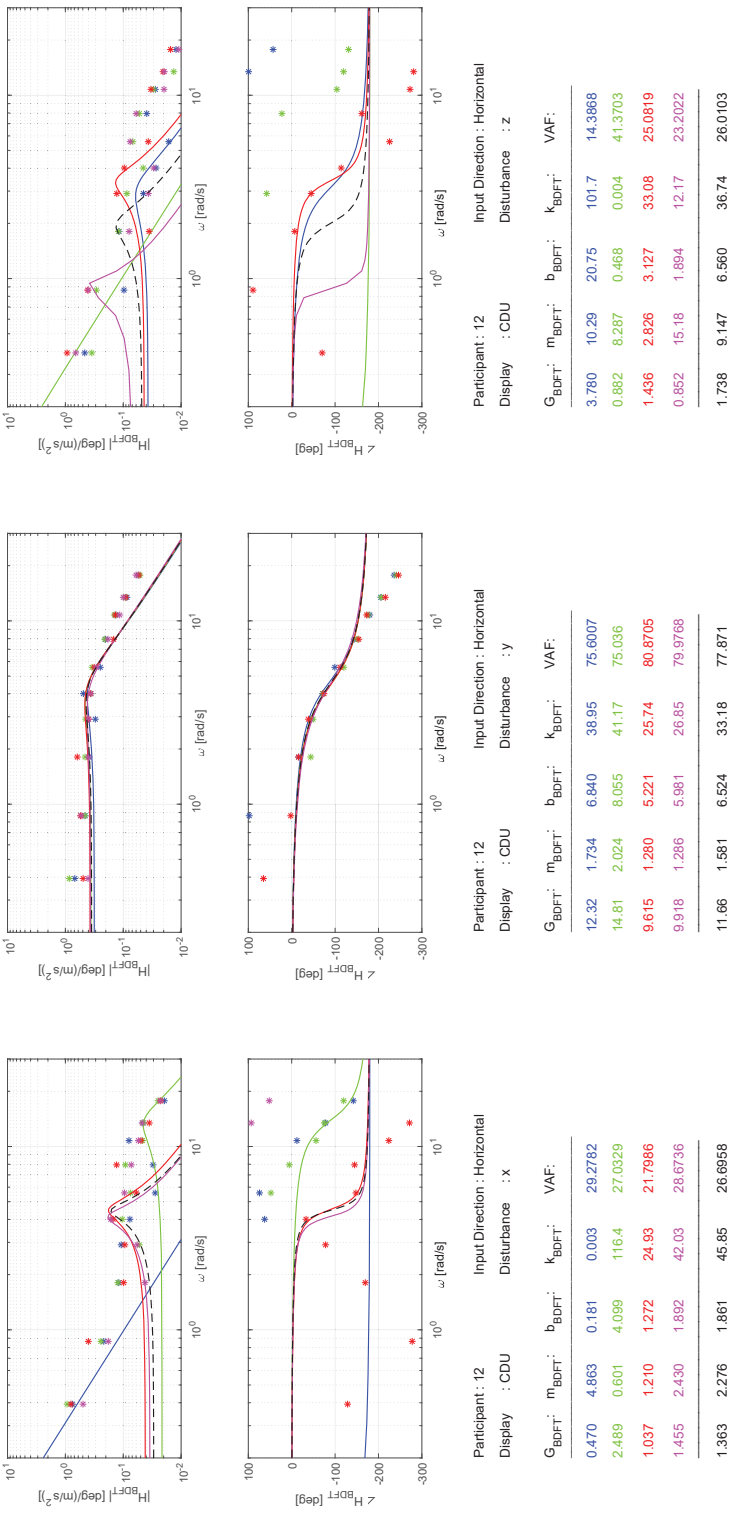

Figure C-42: Parameters Estimates: Participant 12, Vertical Inputs on CDU

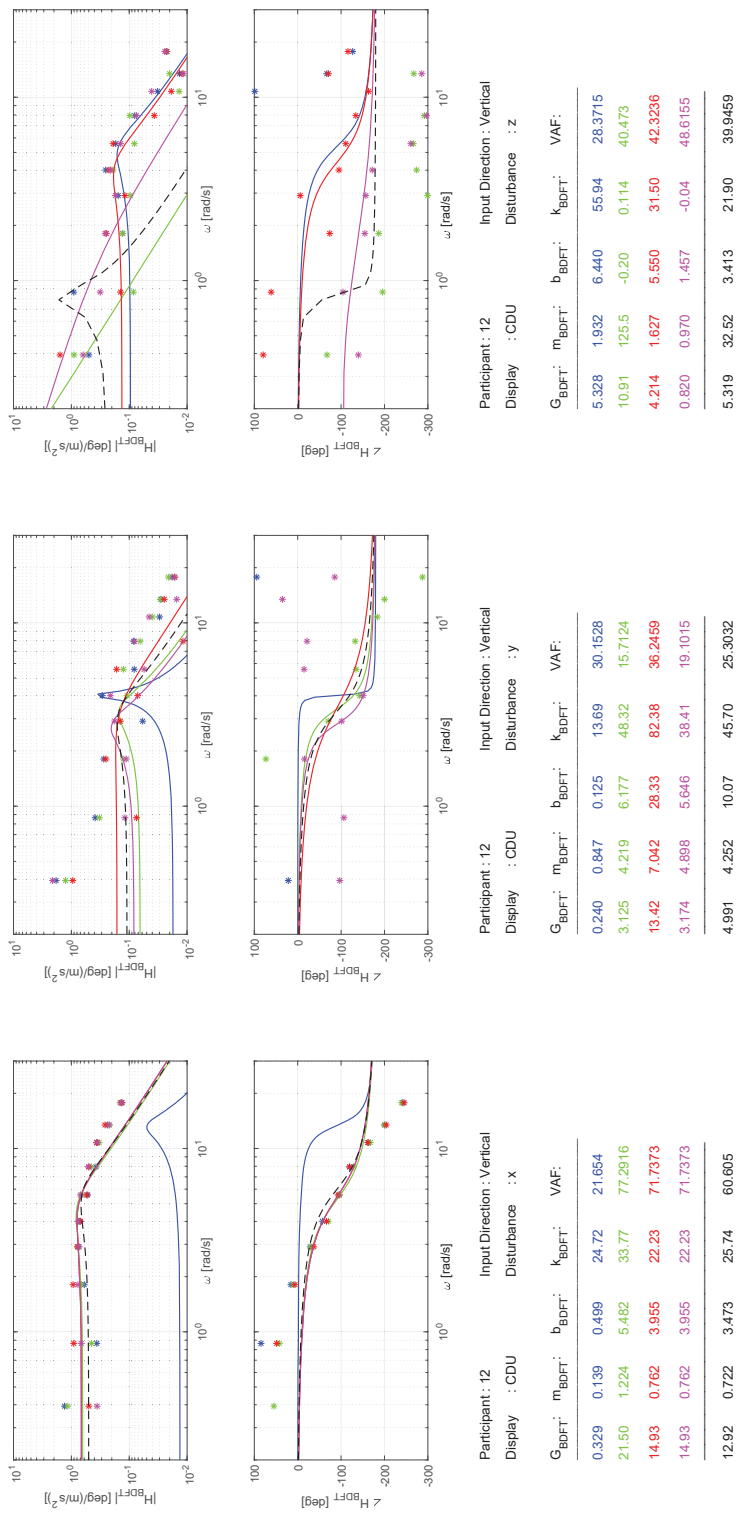

Figure C-43: Parameters Estimates: Participant 12, Horizontal Inputs on PFD

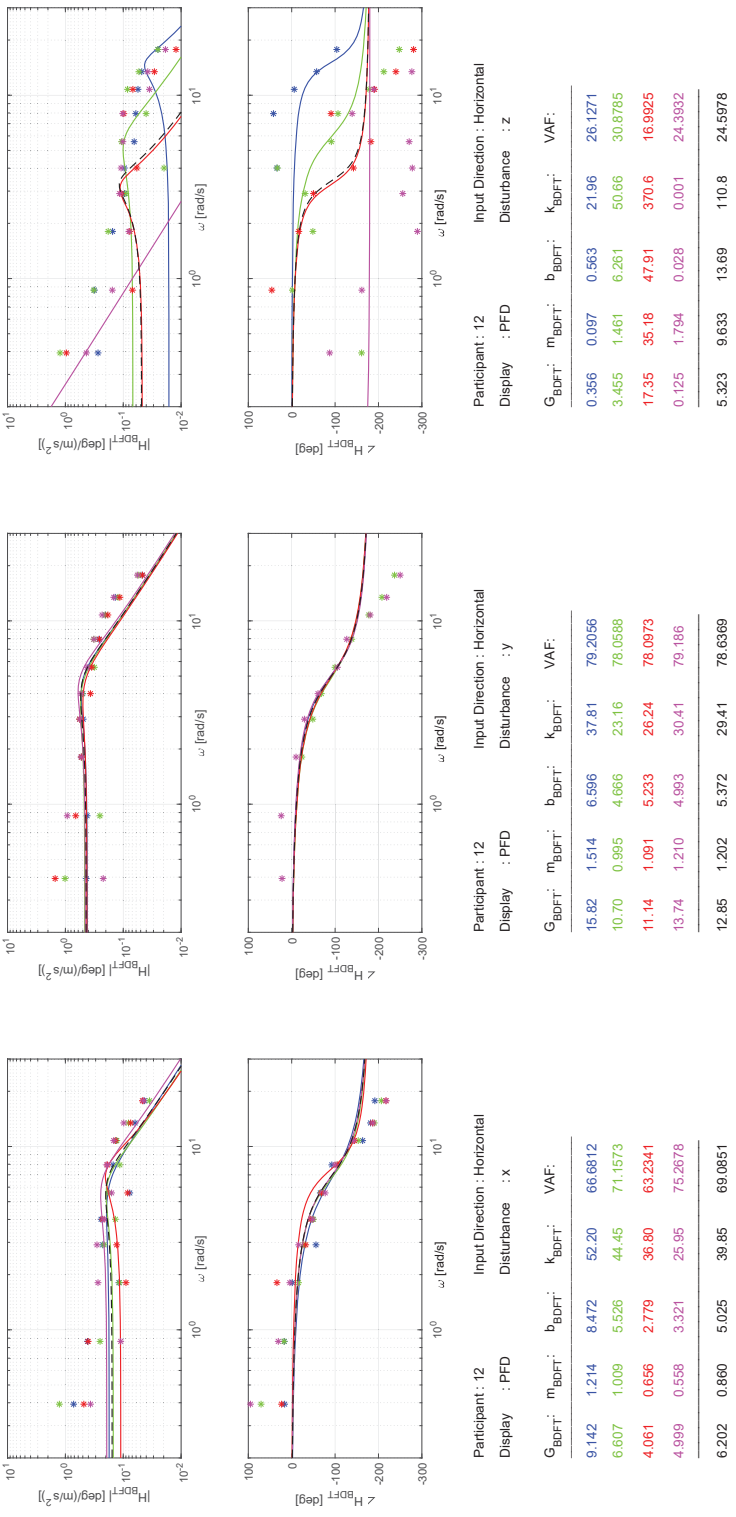

Figure C-44: Parameters Estimates: Participant 12, Vertical Inputs on PFD

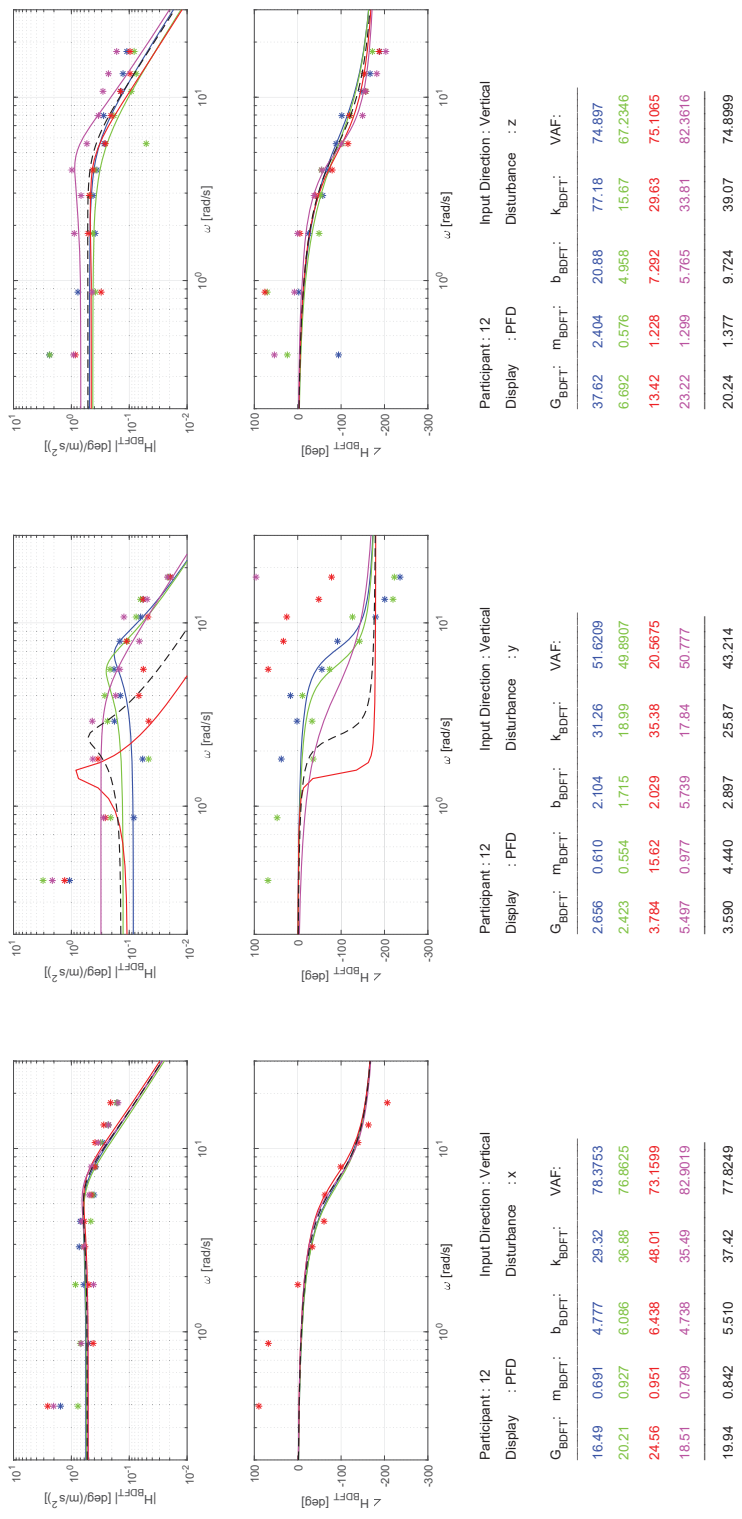

Figure C-45: Parameters Estimates: Participant 13, Horizontal Inputs on CDU

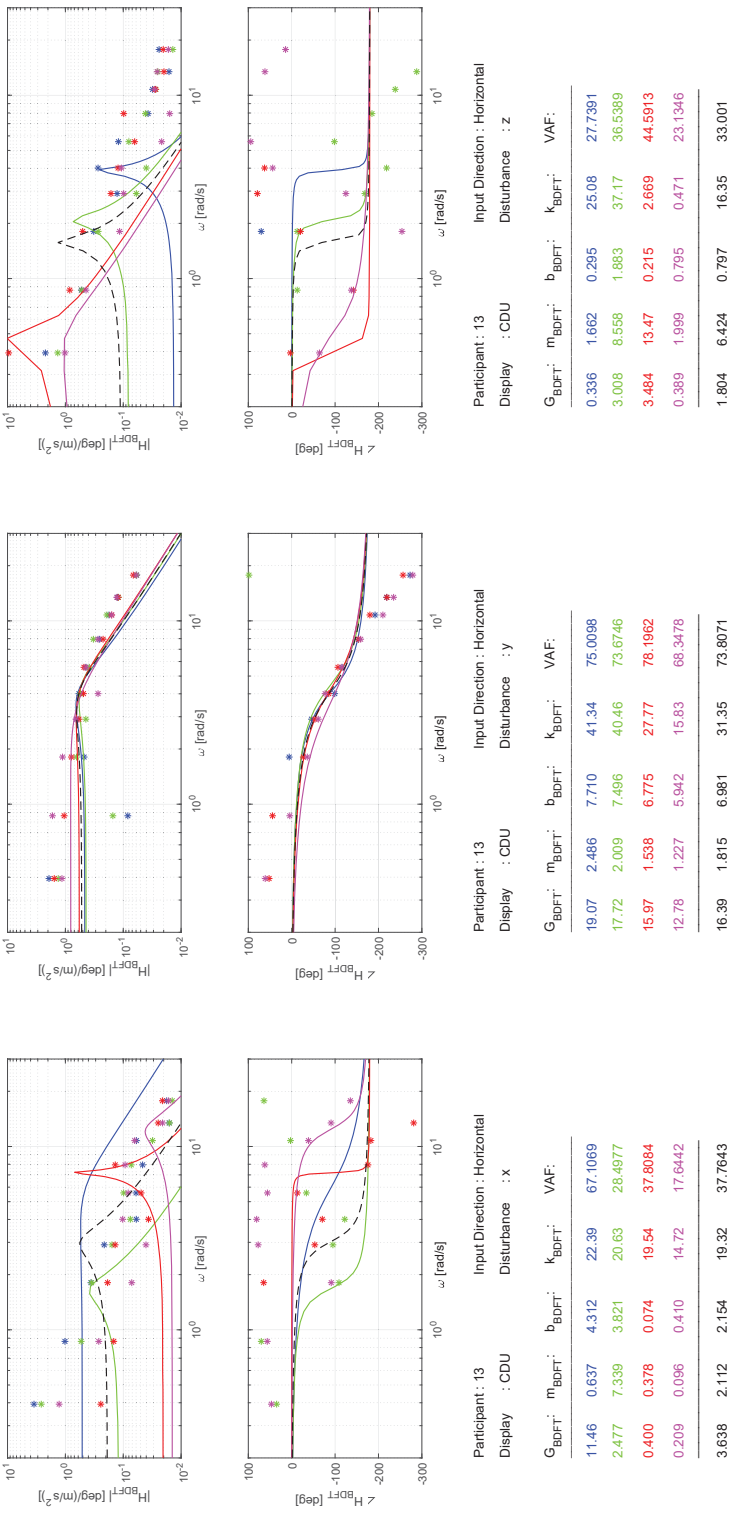

Figure C-46: Parameters Estimates: Participant 13, Vertical Inputs on CDU

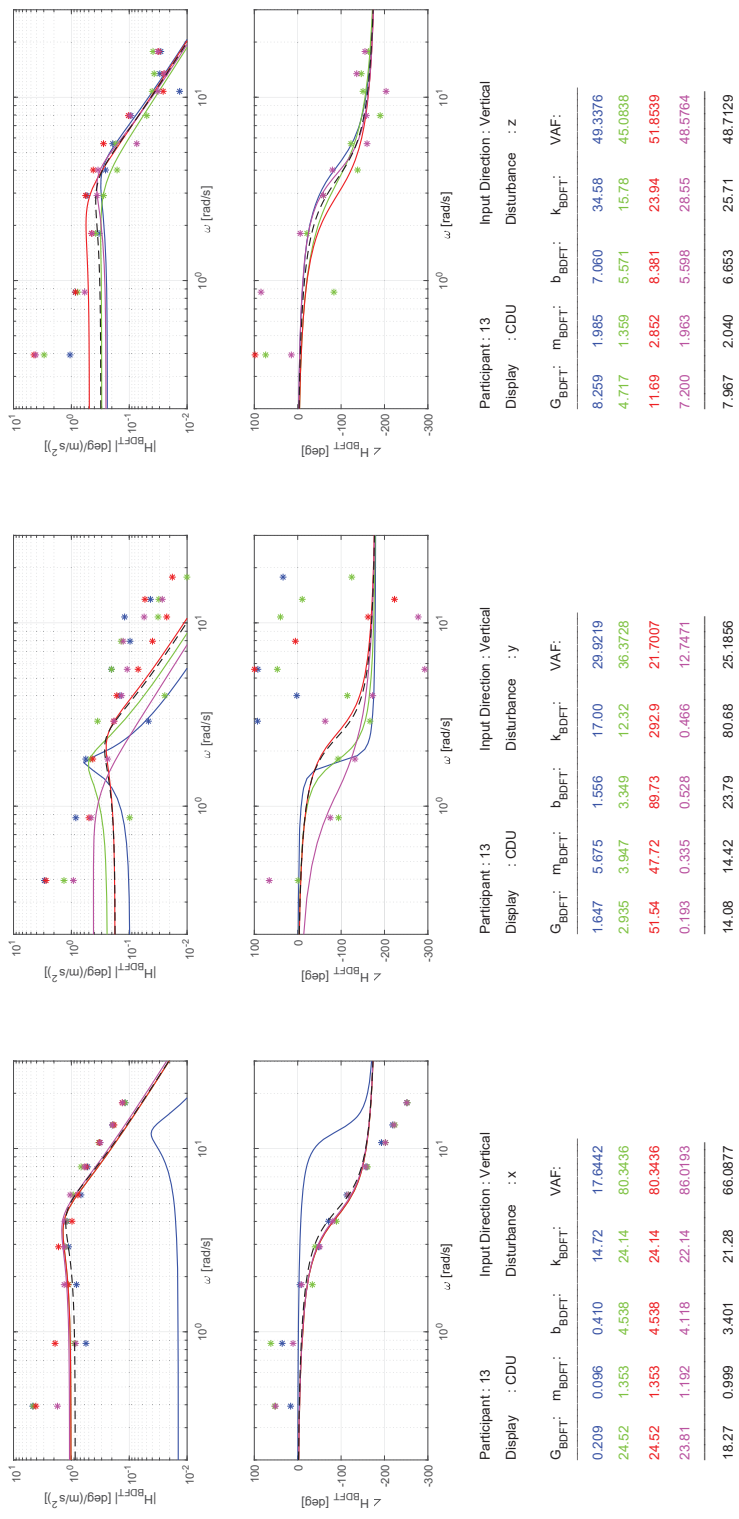

Figure C-47: Parameters Estimates: Participant 13, Horizontal Inputs on PFD

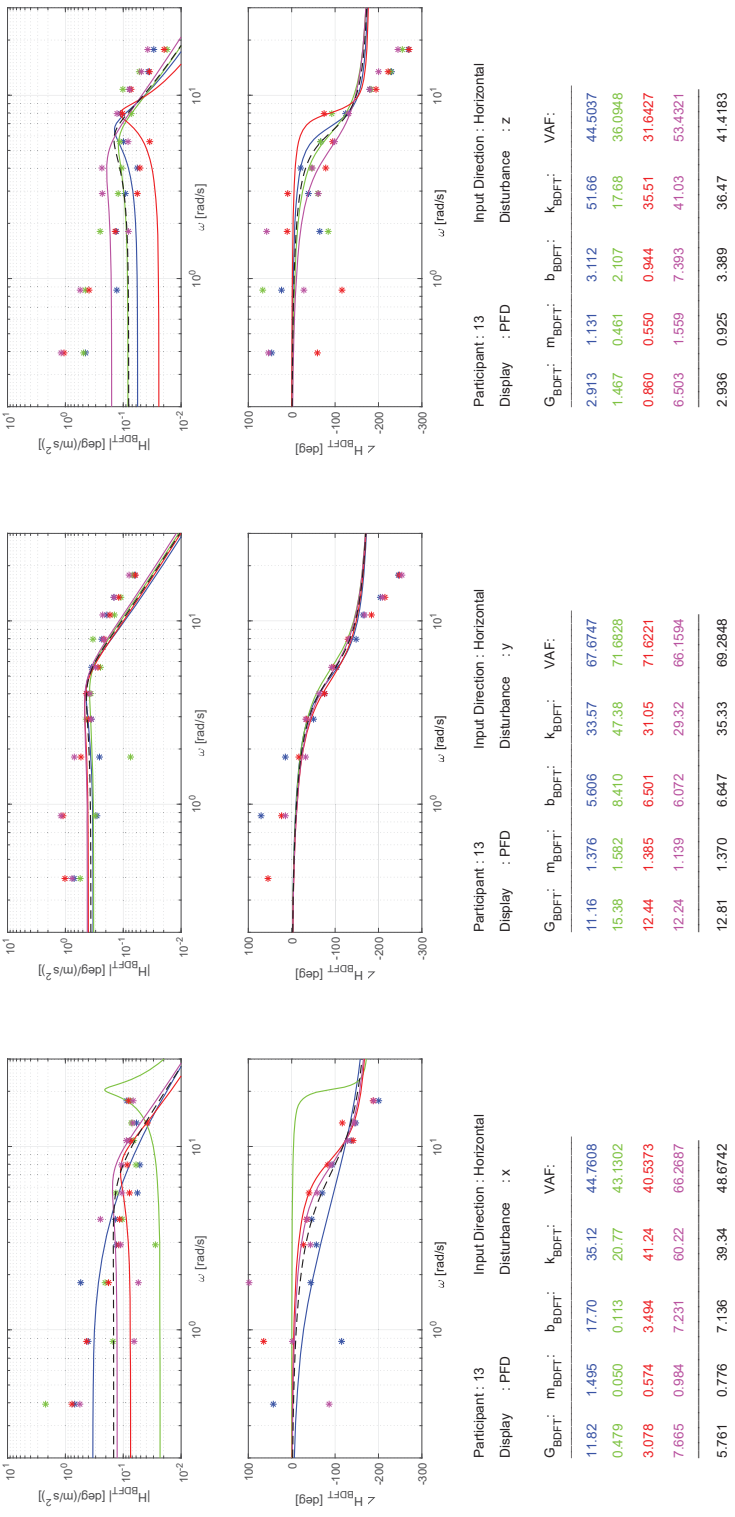

Figure C-48: Parameters Estimates: Participant 13, Vertical Inputs on PFD

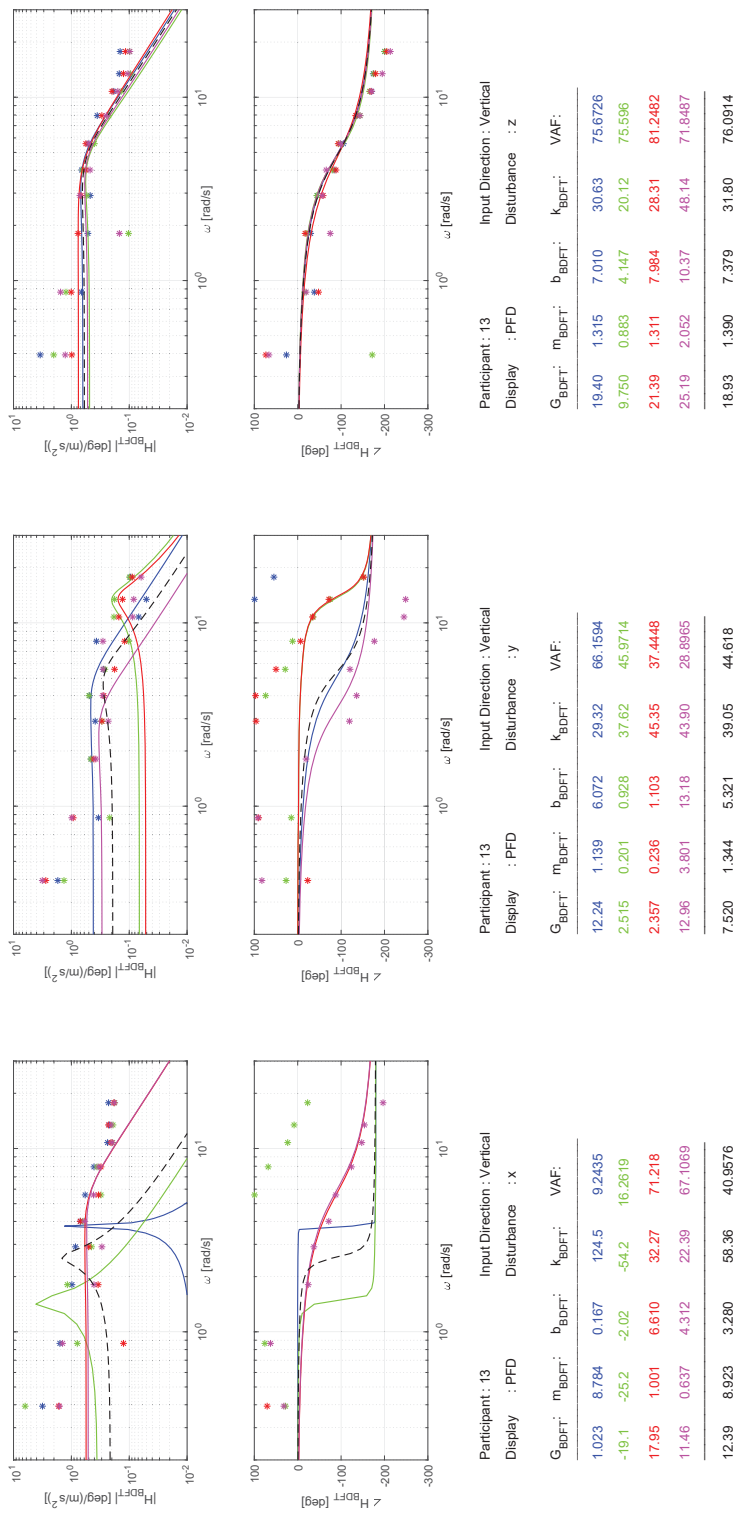

Figure C-49: Parameters Estimates: Participant 14, Horizontal Inputs on CDU

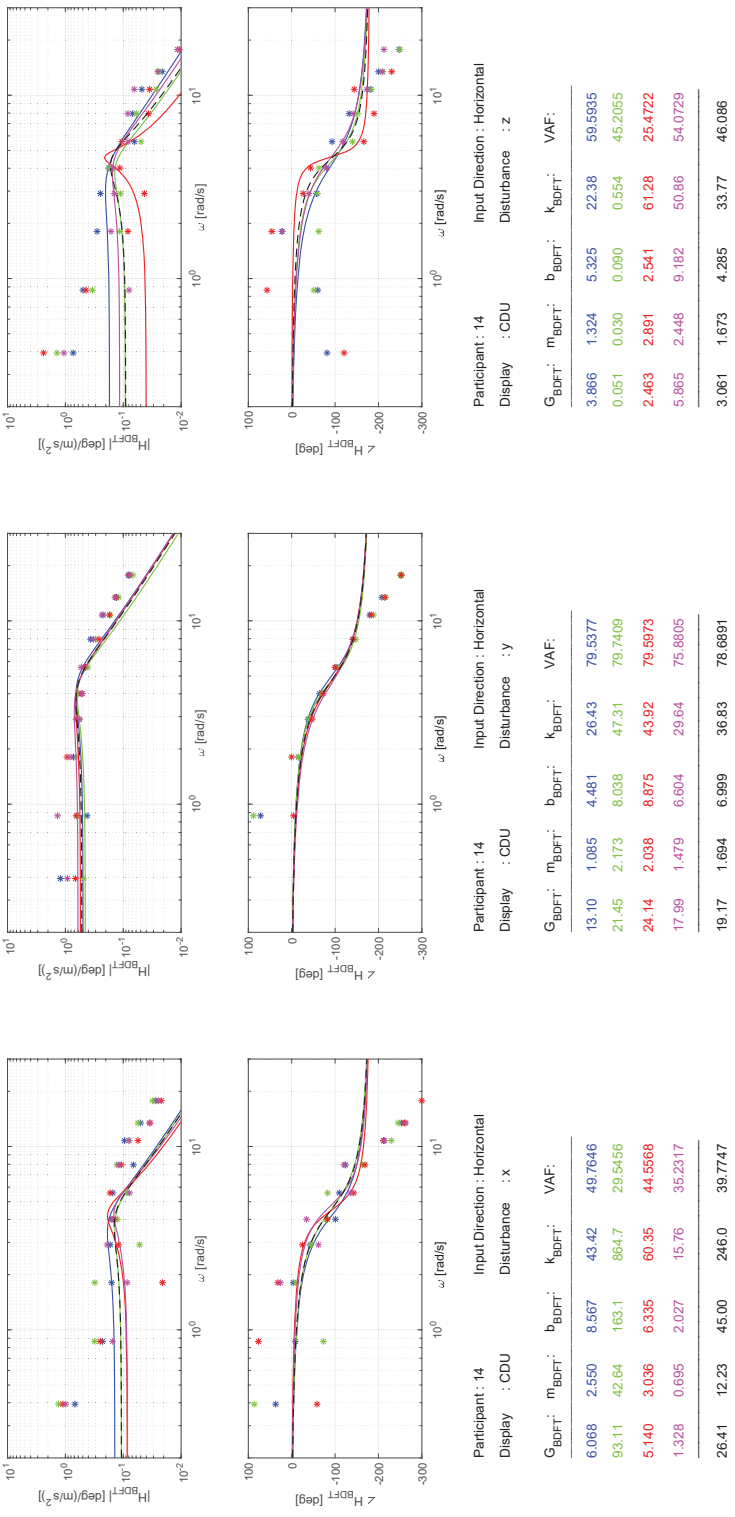

Figure C-50: Parameters Estimates: Participant 14, Vertical Inputs on CDU

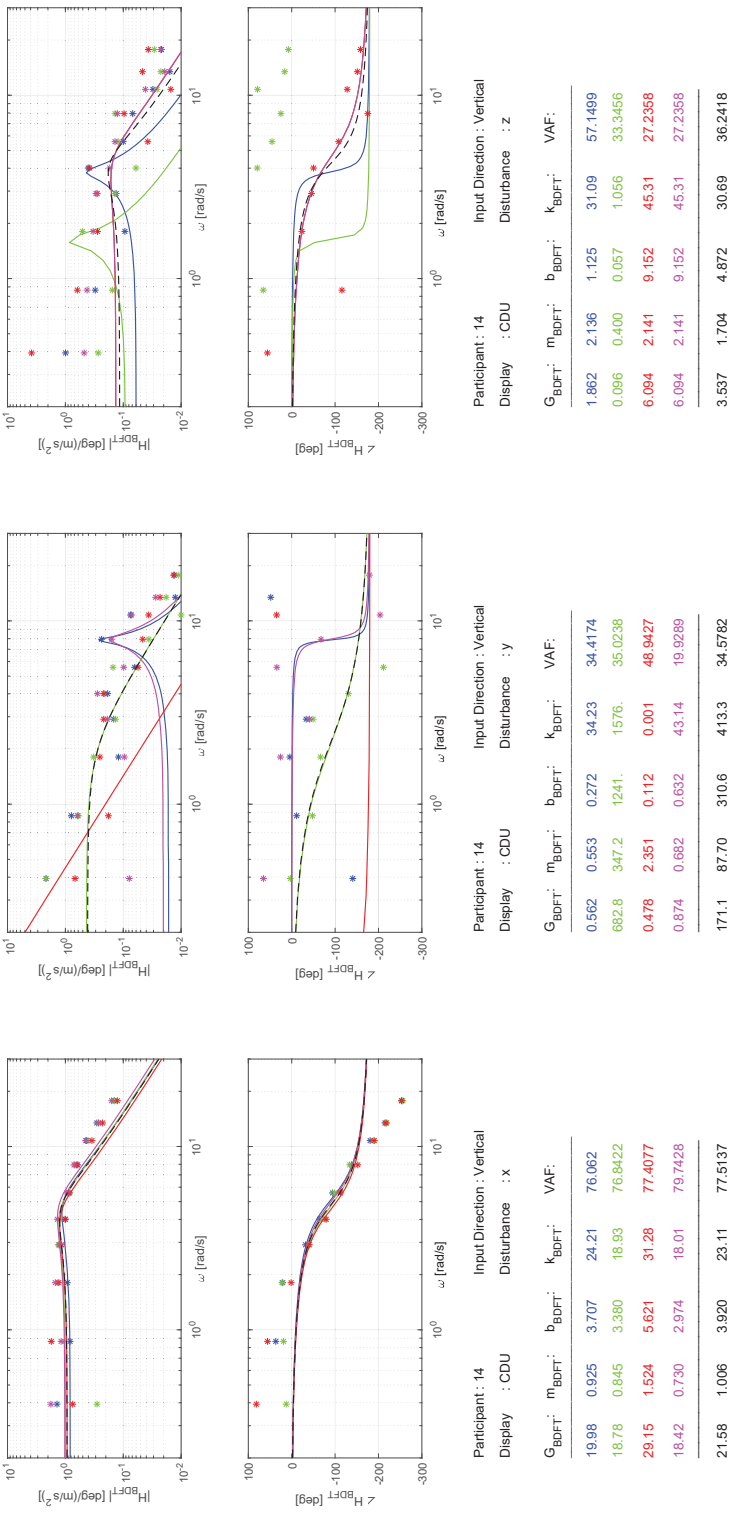

Figure C-51: Parameters Estimates: Participant 14, Horizontal Inputs on PFD

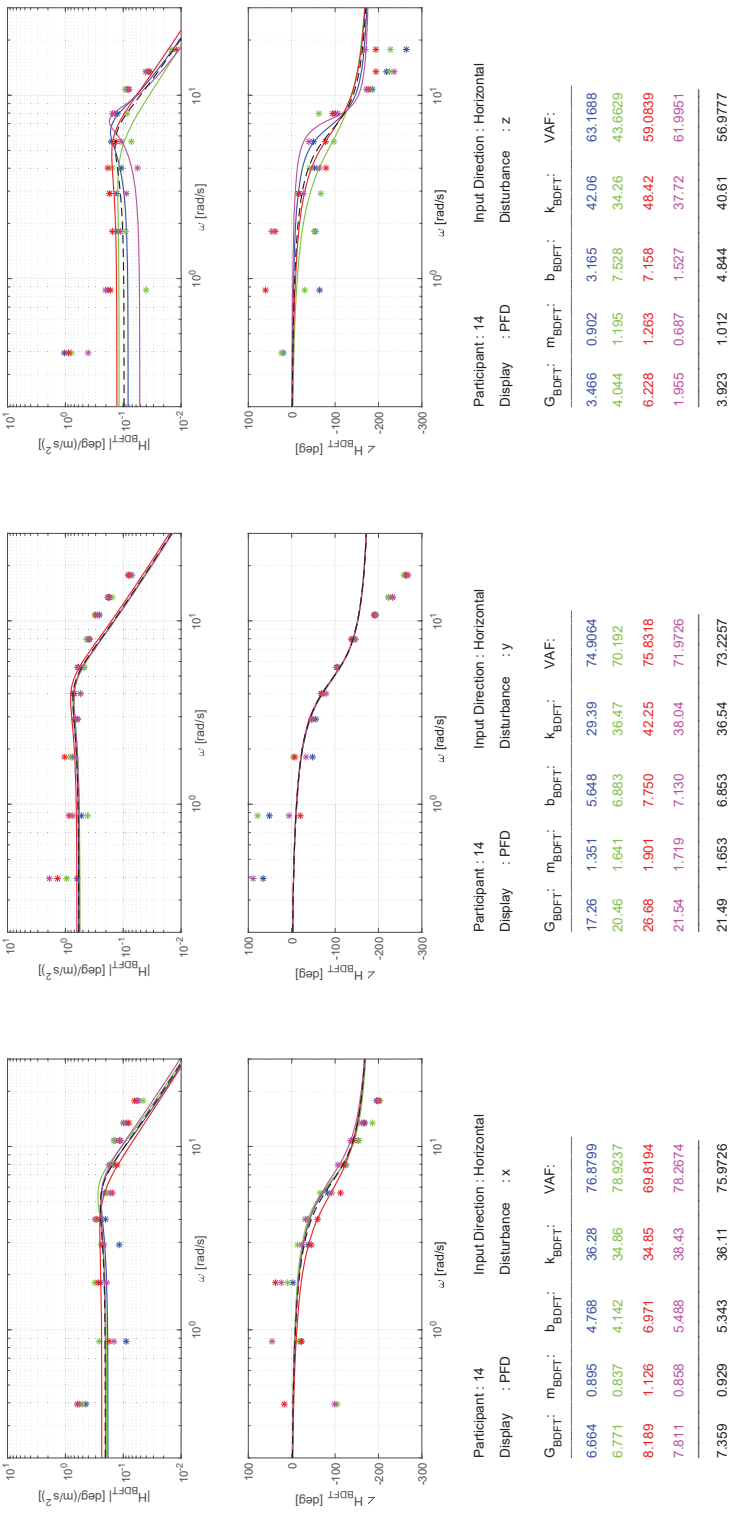

Figure C-52: Parameters Estimates: Participant 14, Vertical Inputs on PFD

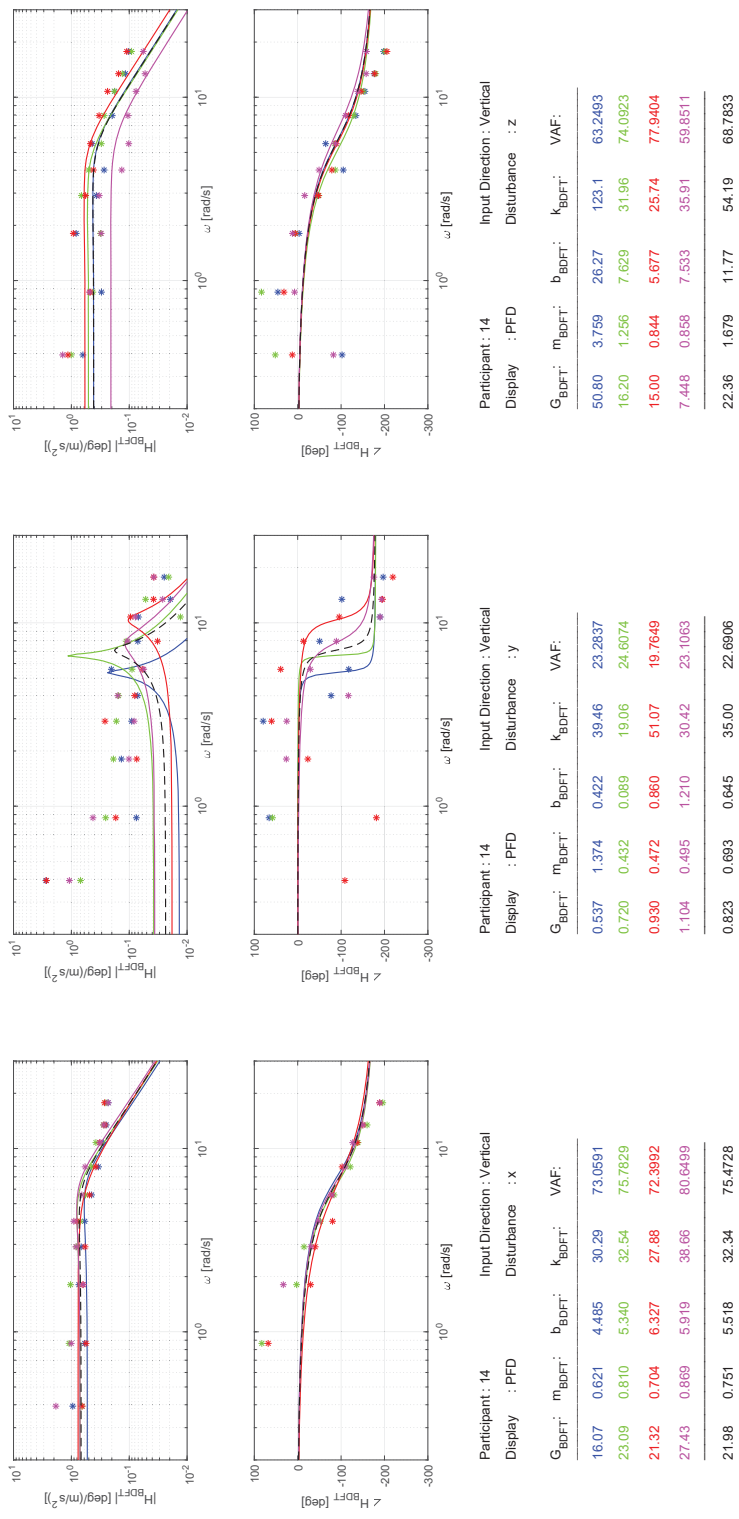

Figure C-53: Parameters Estimates: Participant 15, Horizontal Inputs on CDU

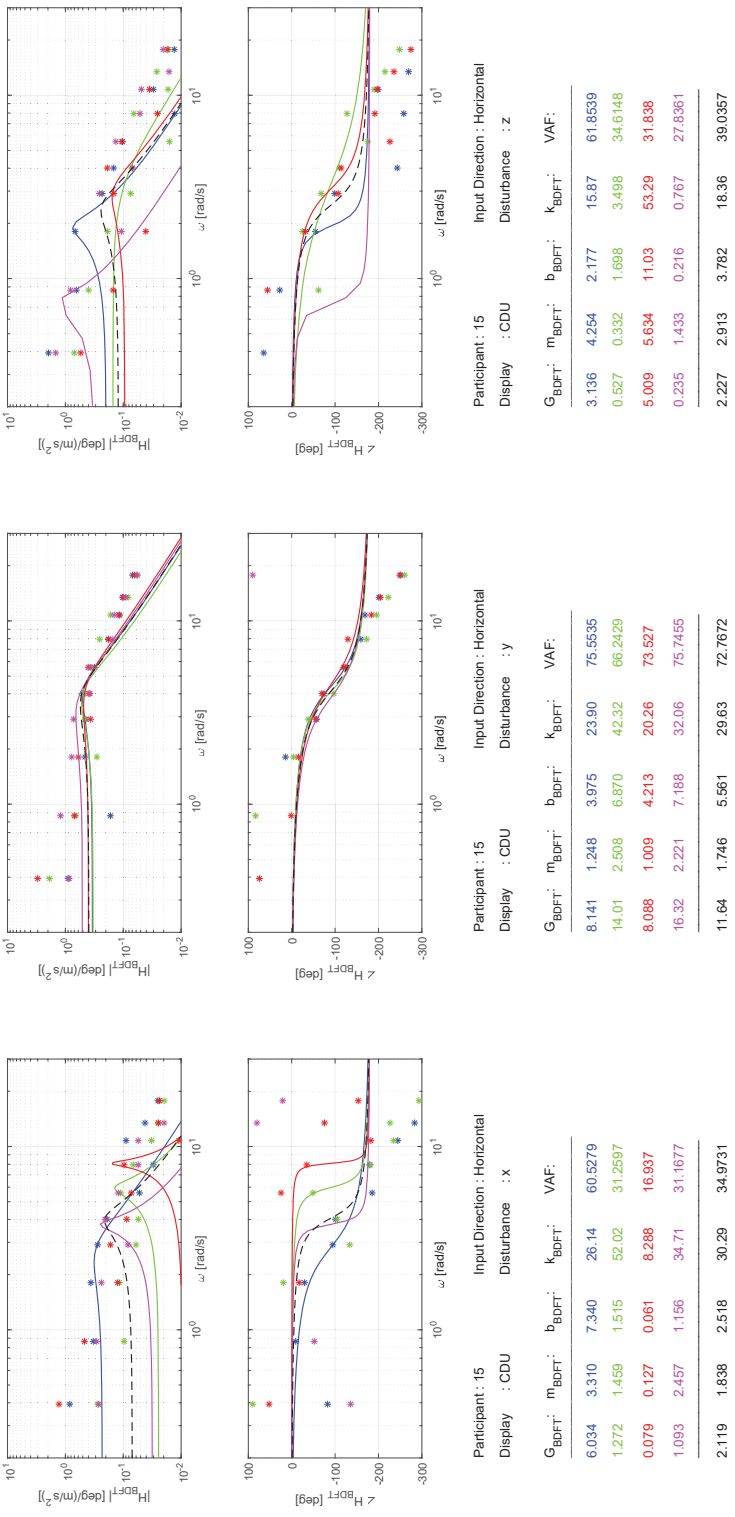

Figure C-54: Parameters Estimates: Participant 15, Vertical Inputs on CDU

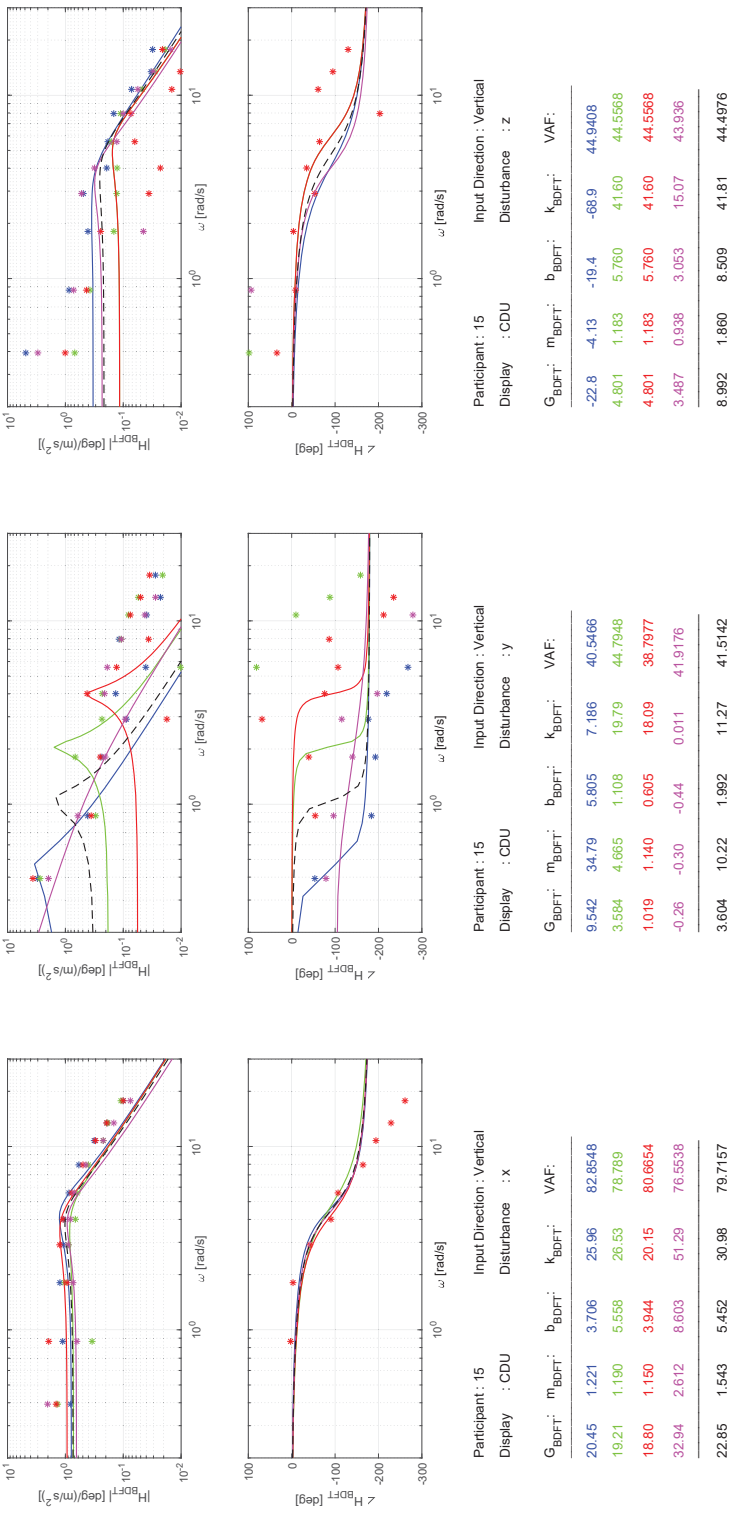

Figure C-55: Parameters Estimates: Participant 15, Horizontal Inputs on PFD

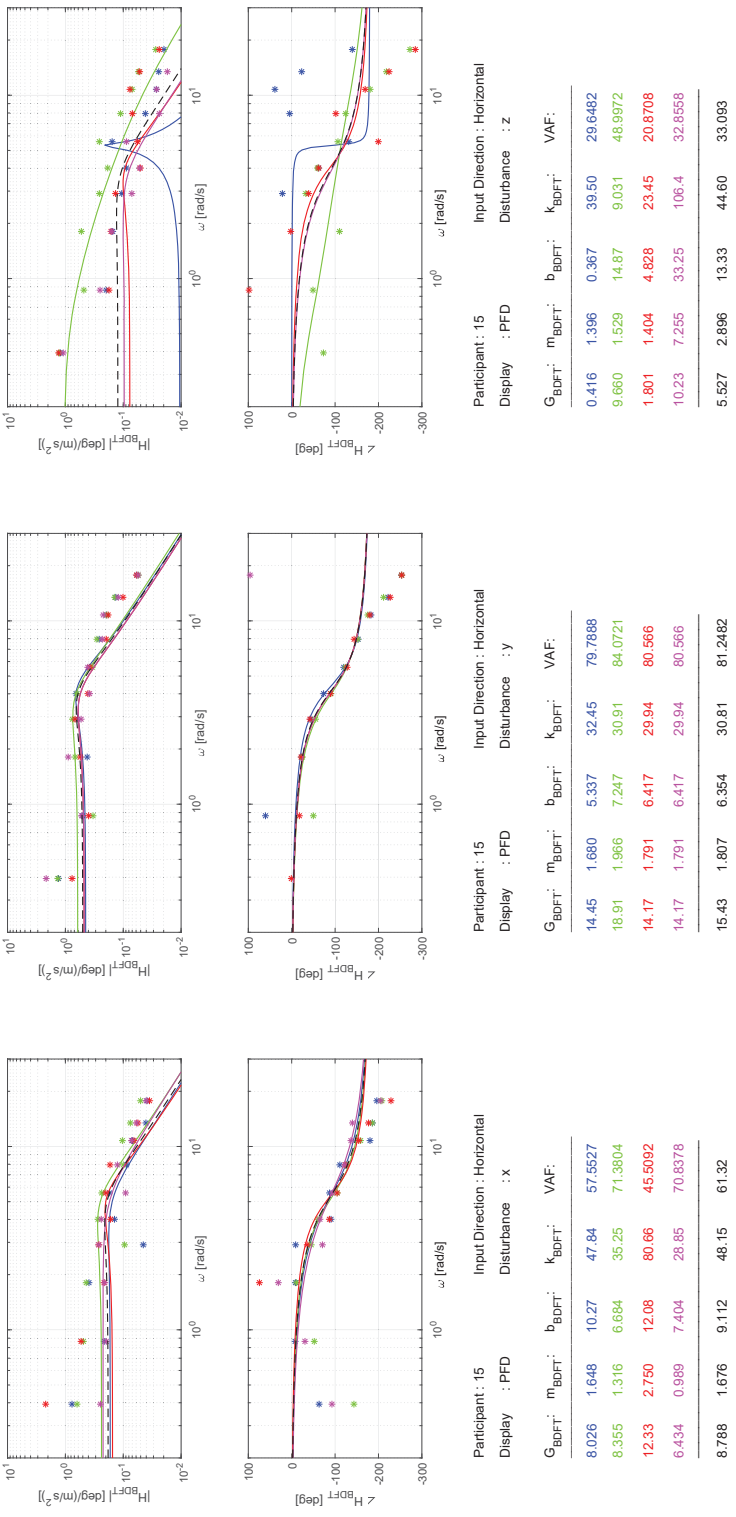

Figure C-56: Parameters Estimates: Participant 15, Vertical Inputs on PFD

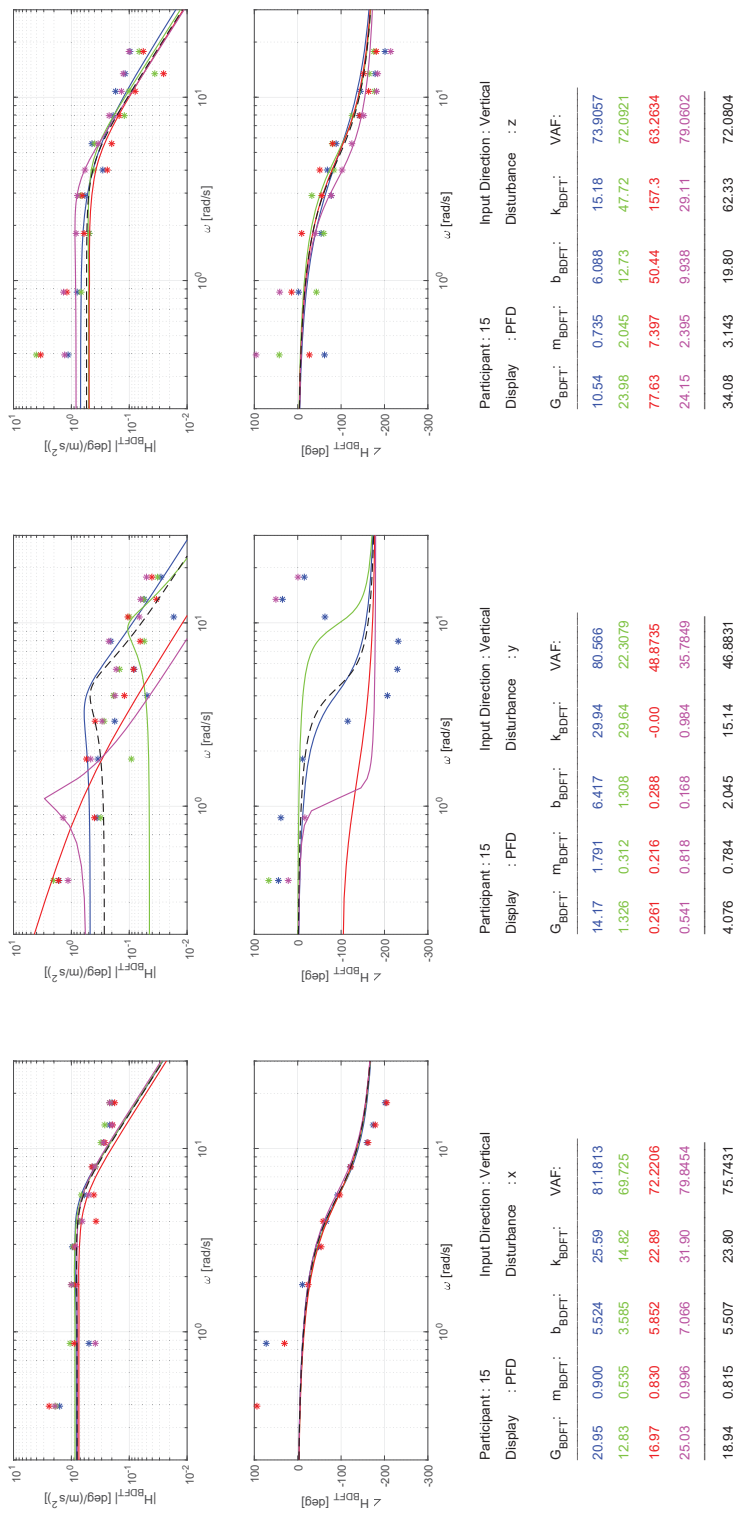

Figure C-57: Parameters Estimates: Participant 16, Horizontal Inputs on CDU

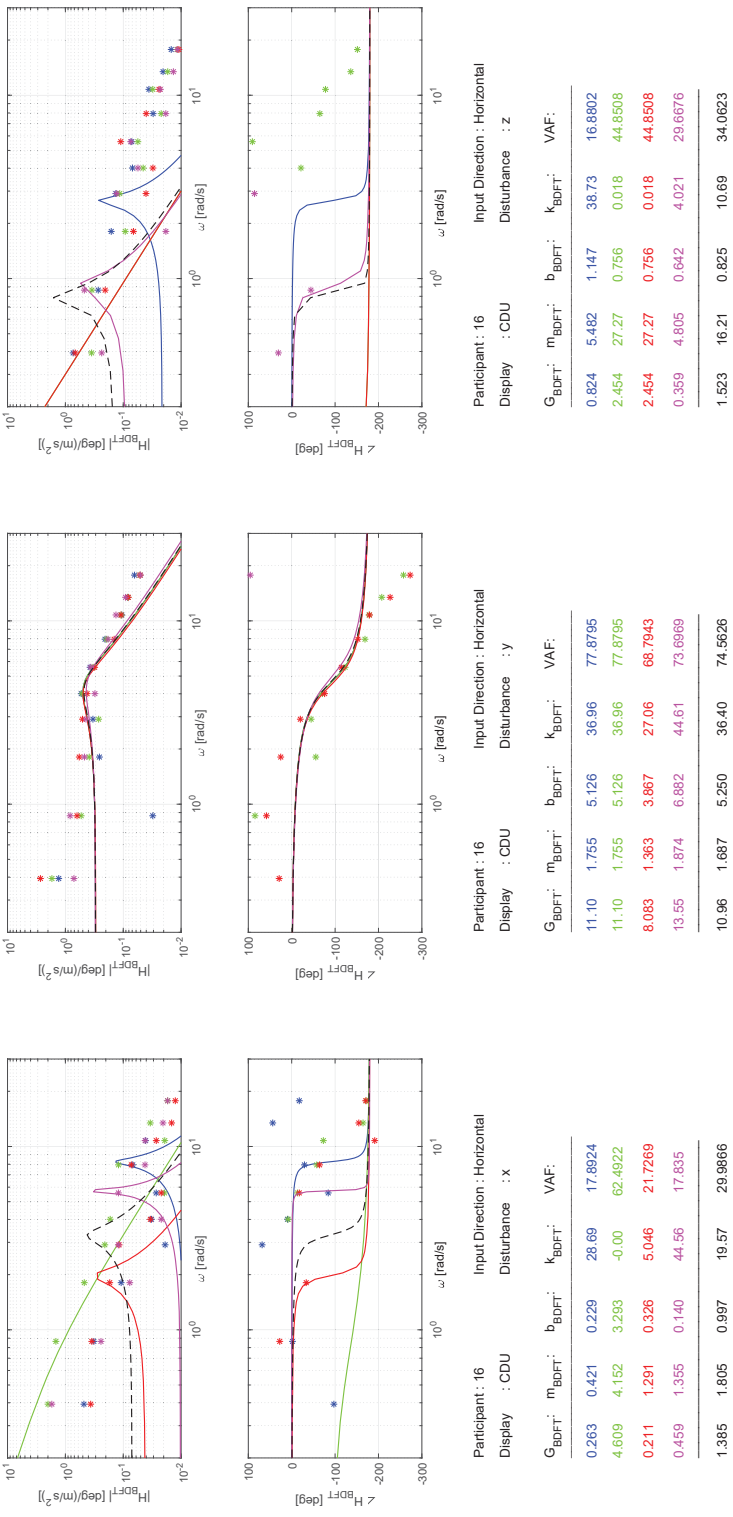

Figure C-58: Parameters Estimates: Participant 16, Vertical Inputs on CDU

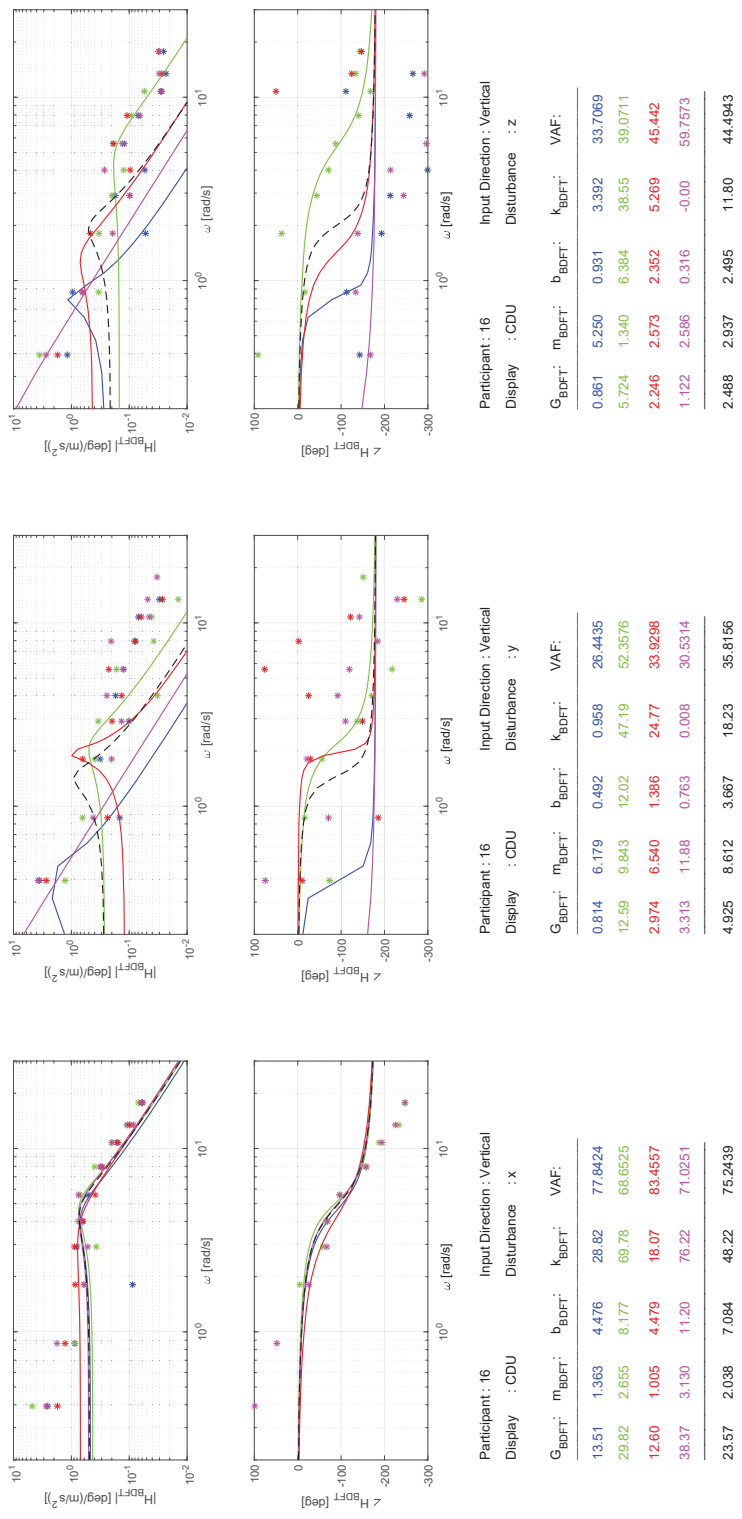

Figure C-59: Parameters Estimates: Participant 16, Horizontal Inputs on PFD

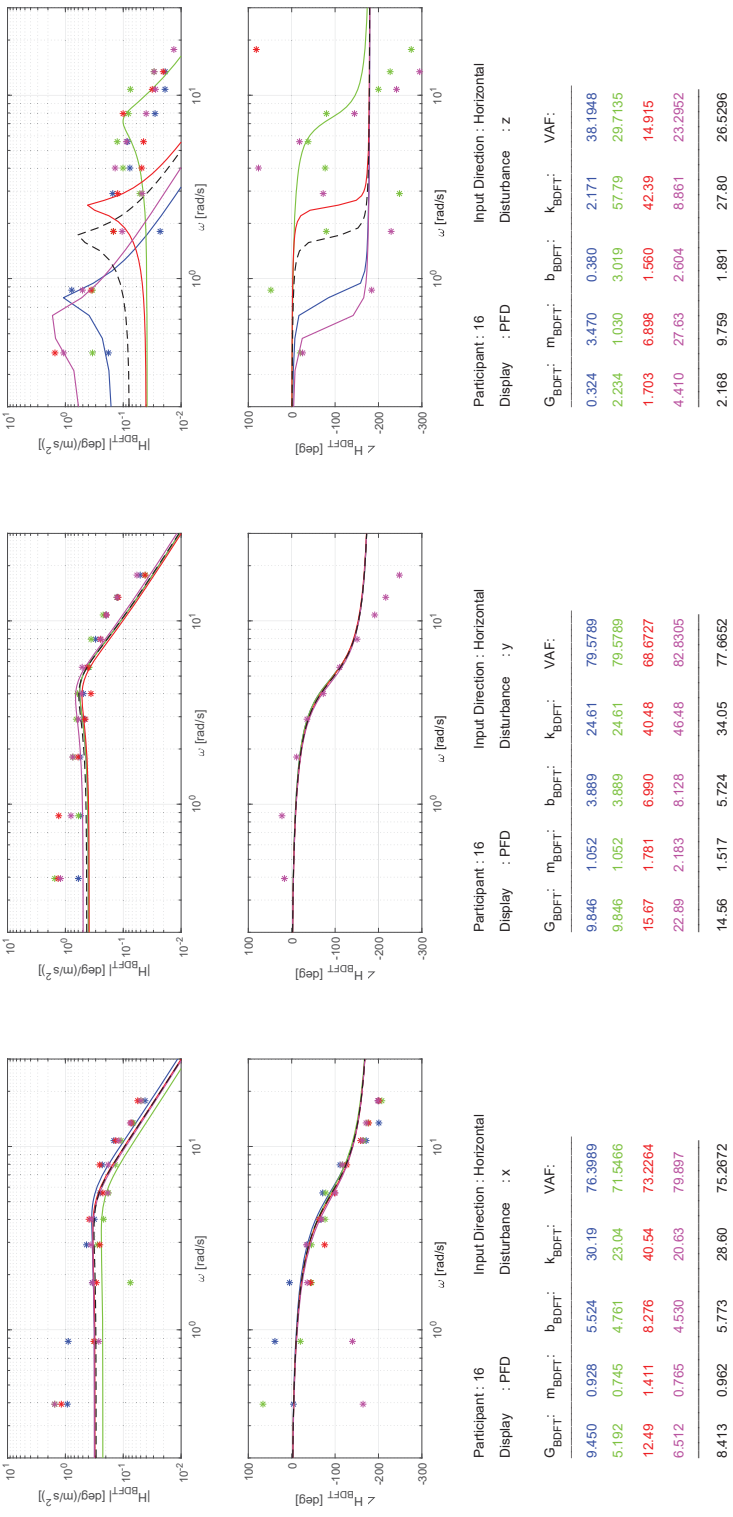

Figure C-60: Parameters Estimates: Participant 16, Vertical Inputs on PFD

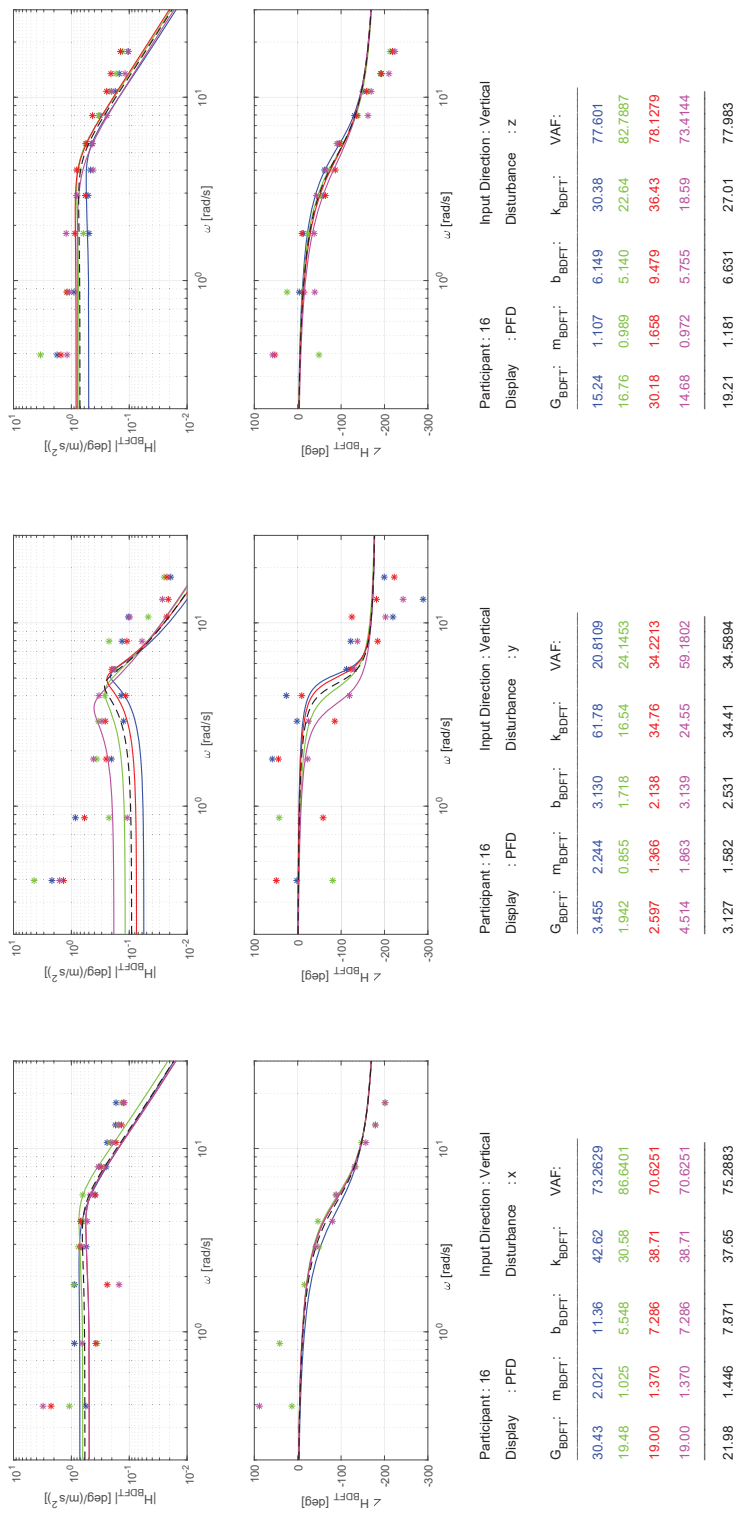

Figure C-61: Parameters Estimates: Participant 17, Horizontal Inputs on CDU

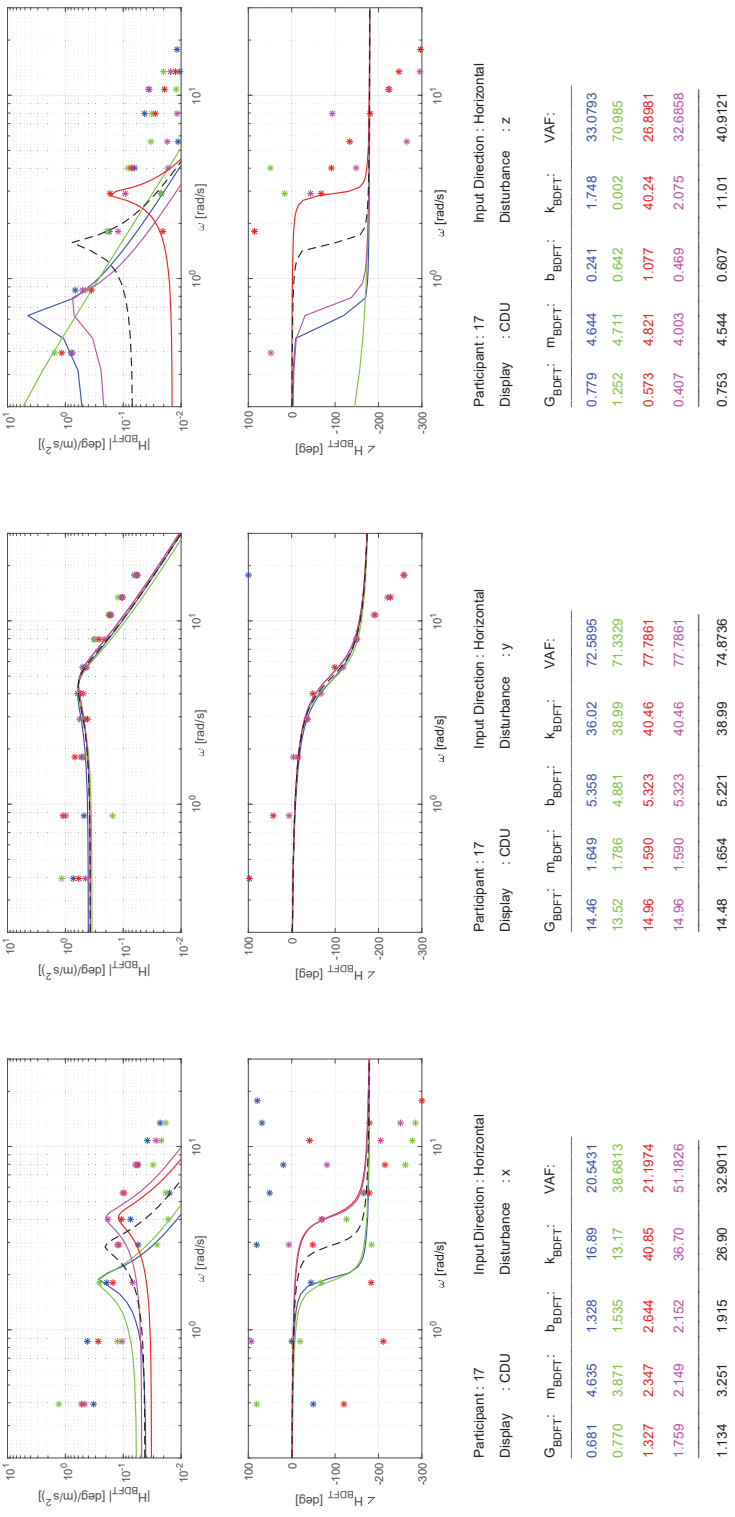

Figure C-62: Parameters Estimates: Participant 17, Vertical Inputs on CDU

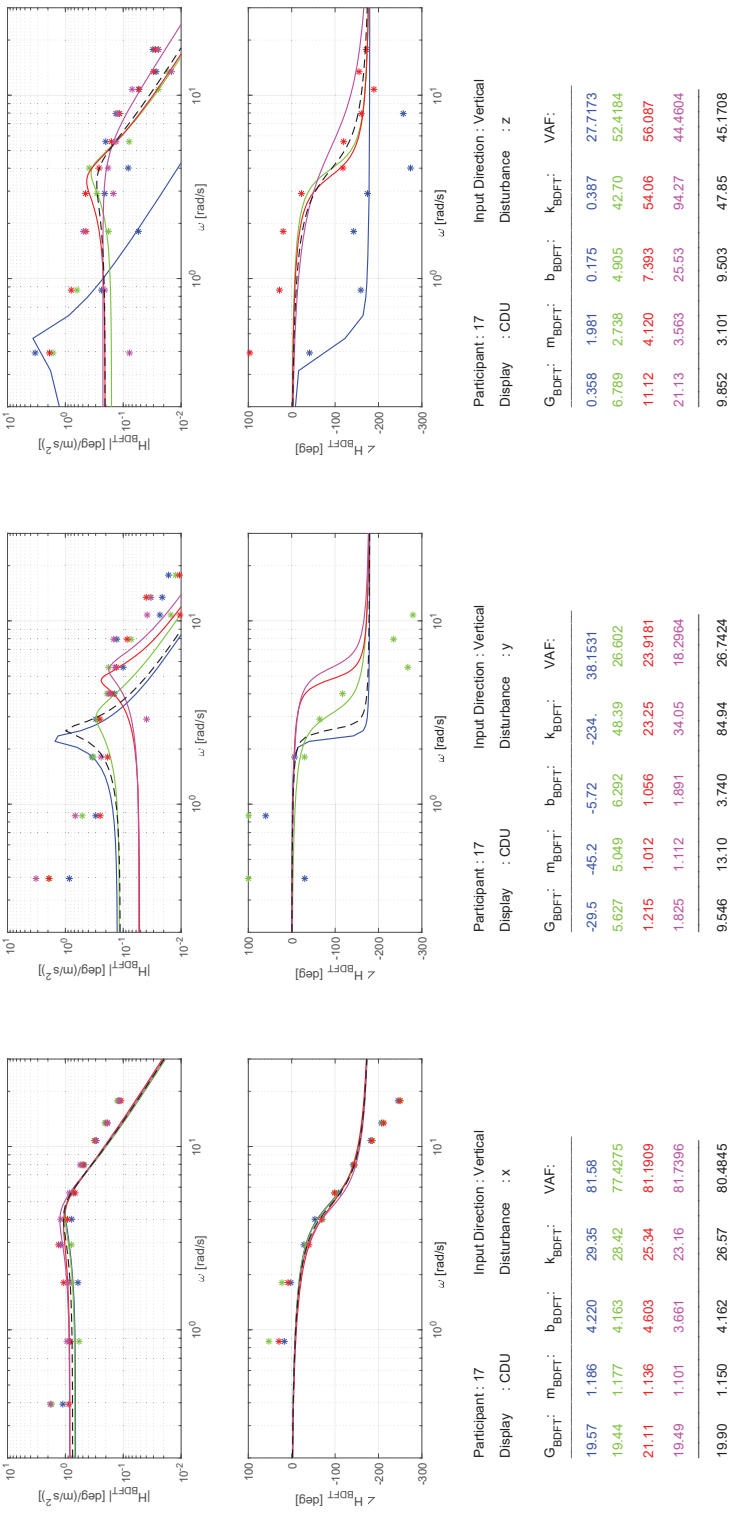

Figure C-63: Parameters Estimates: Participant 17, Horizontal Inputs on PFD

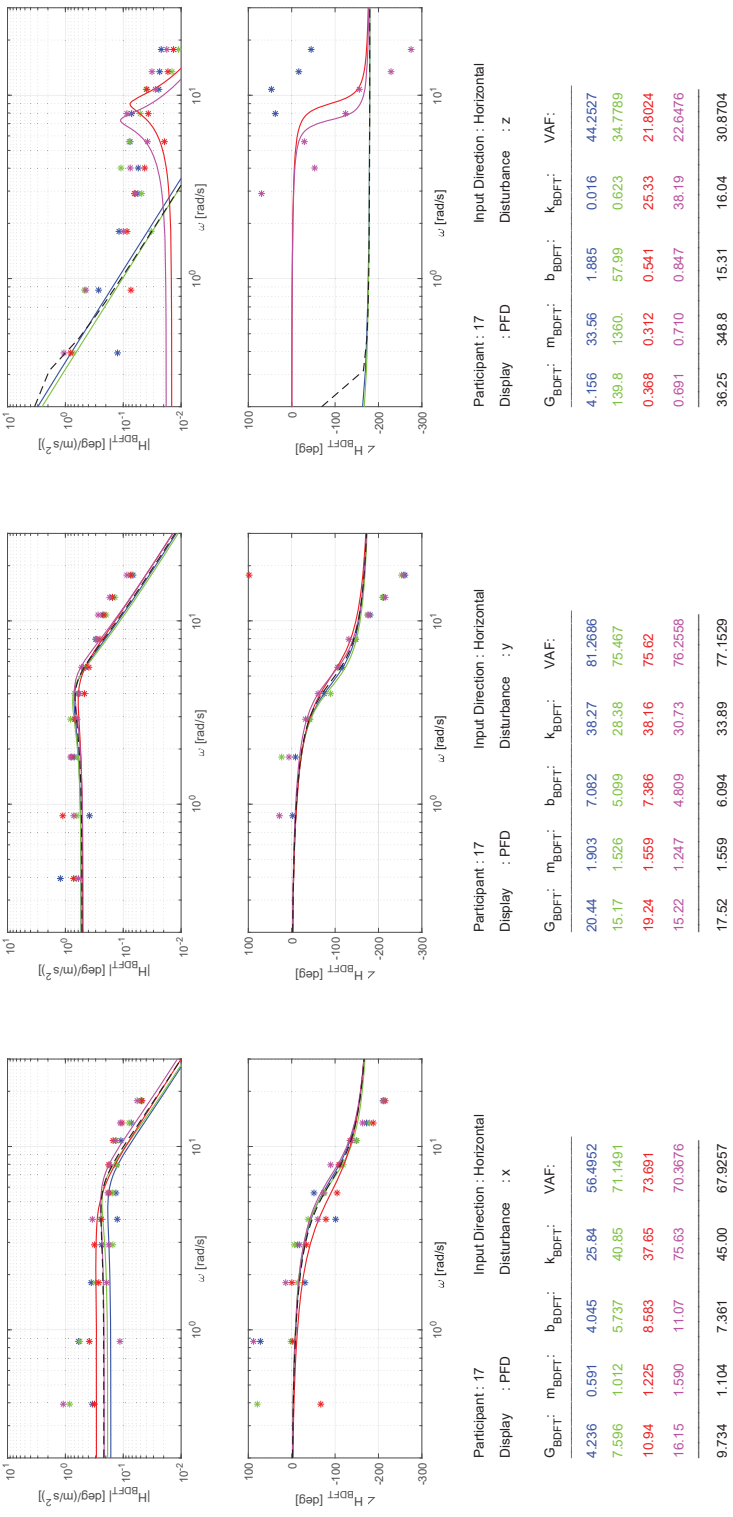

Figure C-64: Parameters Estimates: Participant 17, Vertical Inputs on PFD

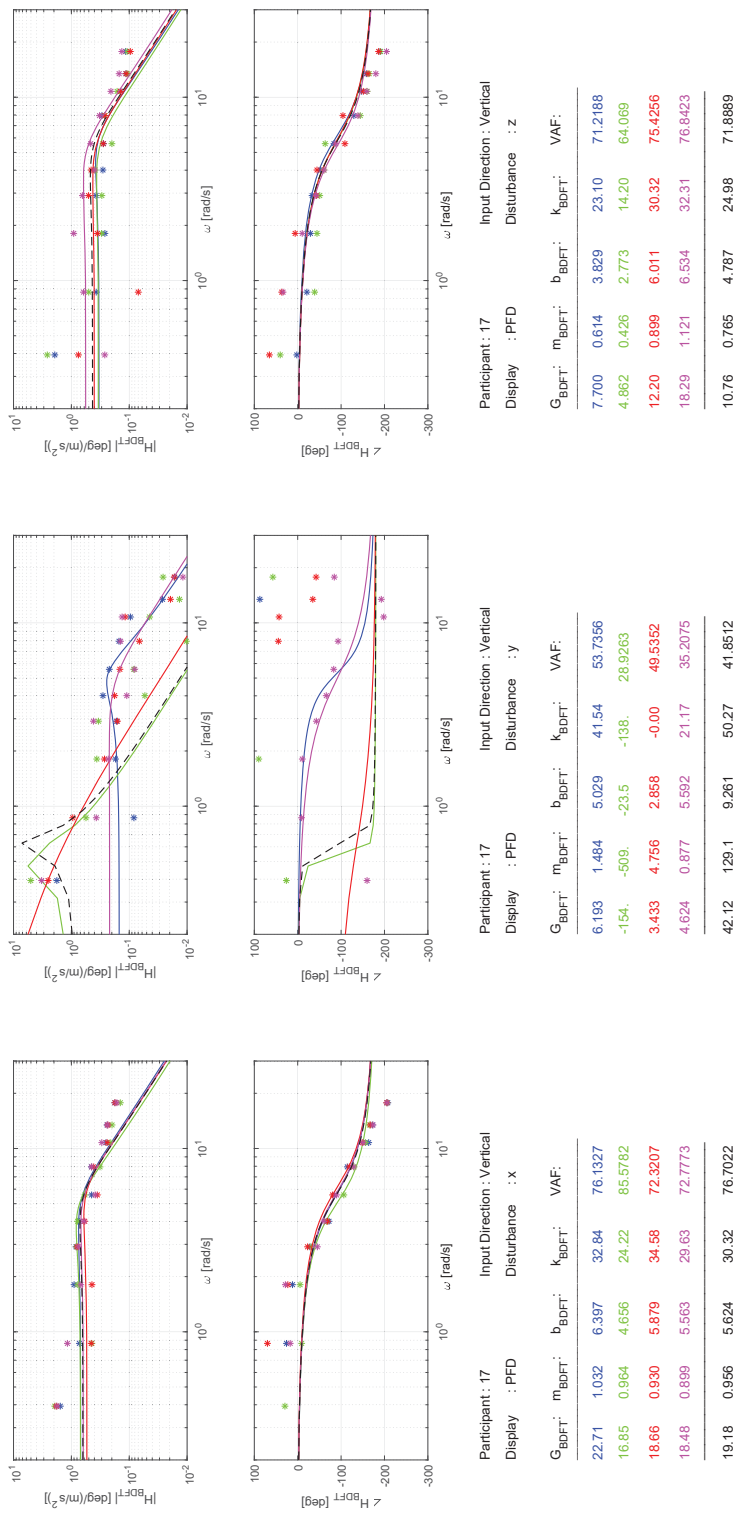

Appendix D

Performance

To obtain a quantitative measure for the control performance of the participant, the TSC input error was determined. This error was determined for each direction by subtracting the target signal for each corresponding direction with the TSC input signals. The variance was directly determined from this error signal, which served as measure for performance of the participants. For the sake of clarity, the variance was converted to $[mm^2]$ in this appendix.

With the total error variance obtained, it was possible to account parts of the total error variance to the known disturbances as the frequencies of those components were known [69]. This allowed to identify participant's sources of tracking error. The AIAA paper in Part I presented average performance figures. This appendix, however, provides the performance figures per participant.

Each bar gives the total error variance of a single participant, for a certain condition. The dark blue, light blue, green and yellow parts represent horizontal- and vertical target, disturbance and remnant components, respectively. The left figure presents error variances for the horizontal input direction, whereas the right figure presents error variances for the vertical input direction.

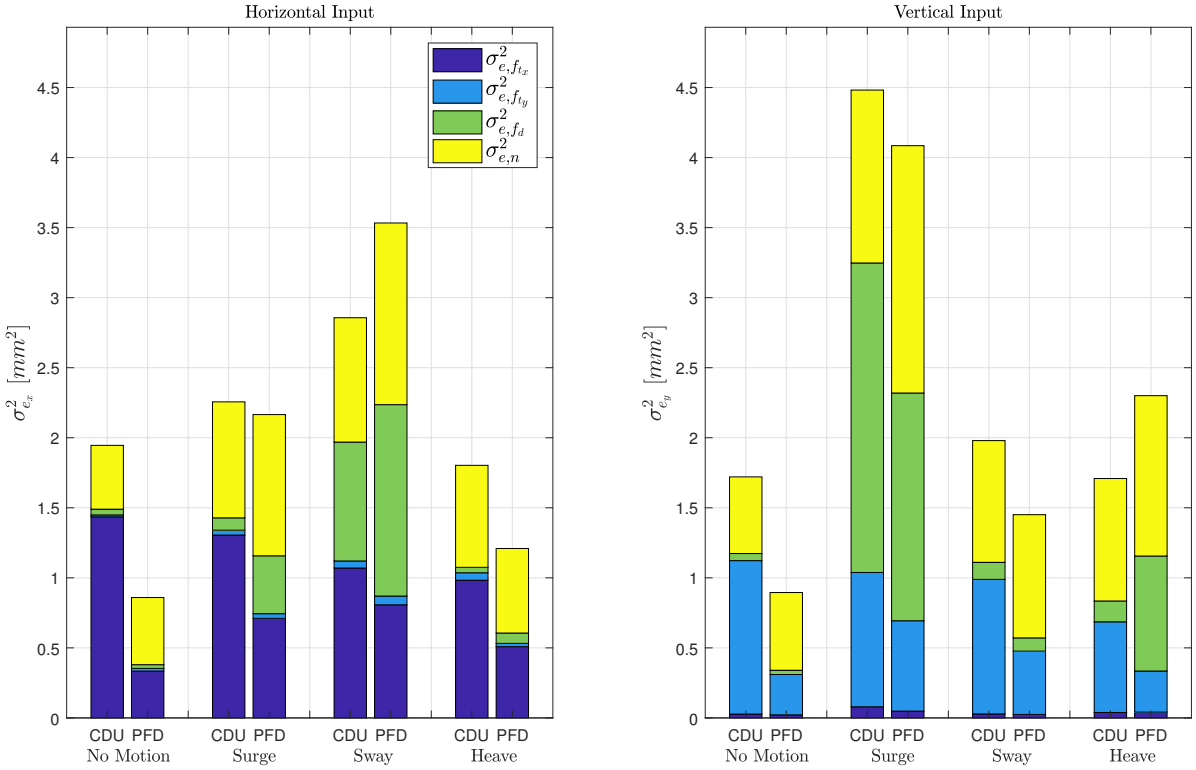

Figure D-1: Error variance components for Participant 2

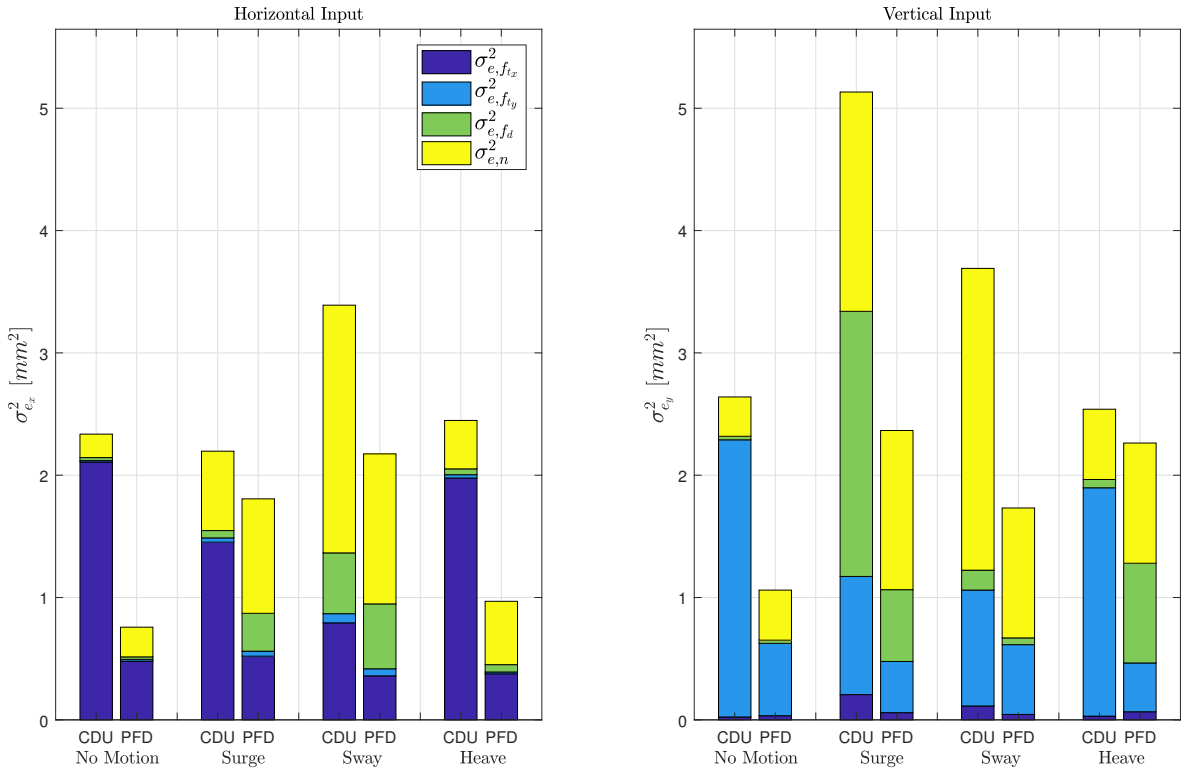

Figure D-2: Error variance components for Participant 3

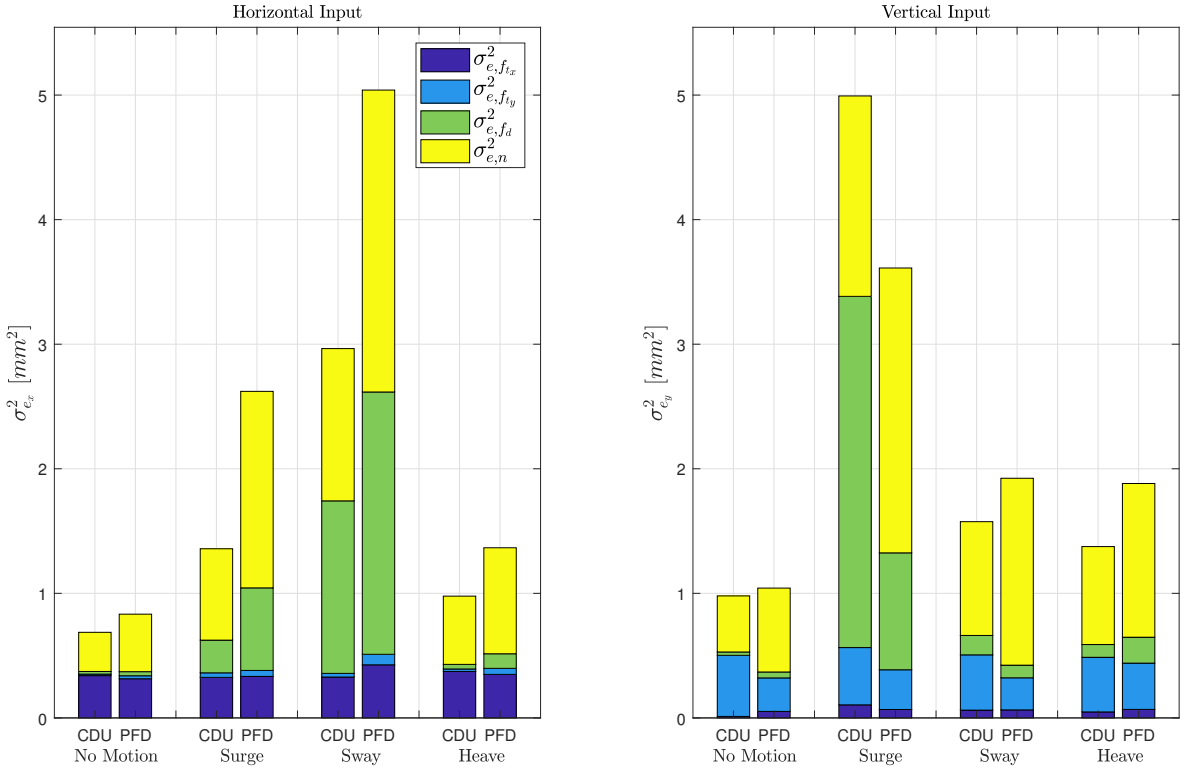

Figure D-3: Error variance components for Participant 4

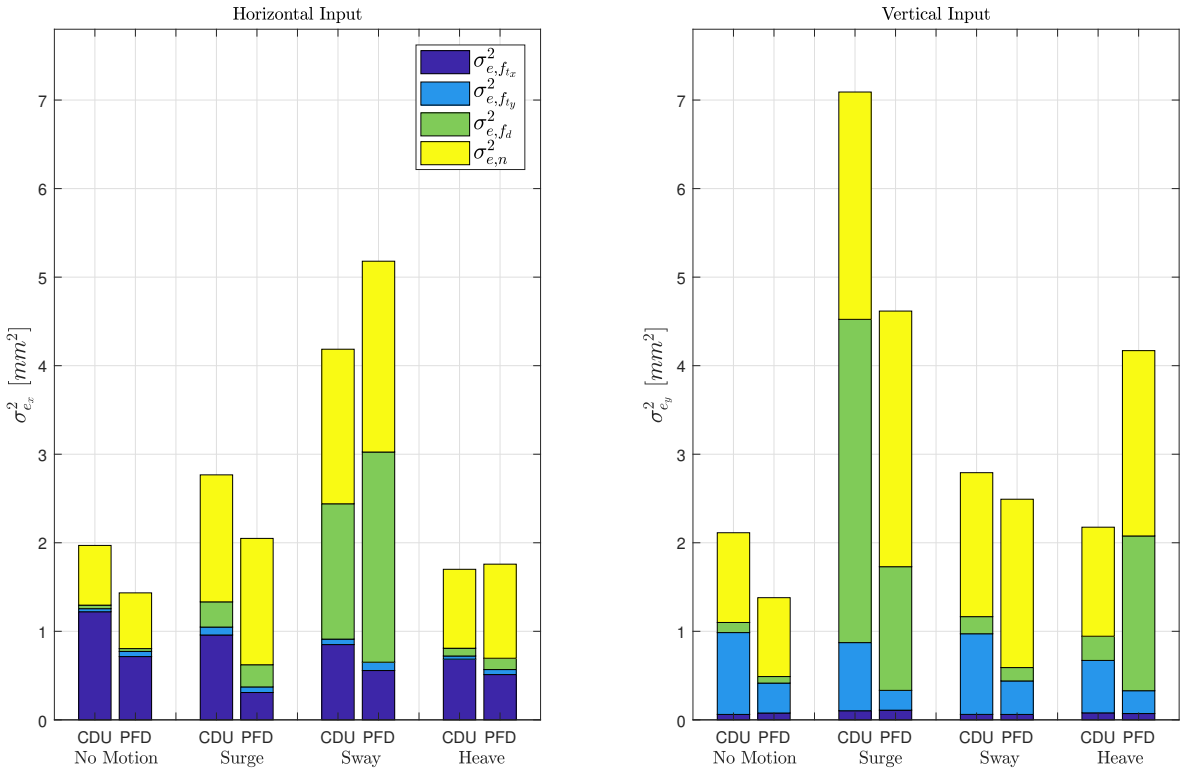

Figure D-4: Error variance components for Participant 5

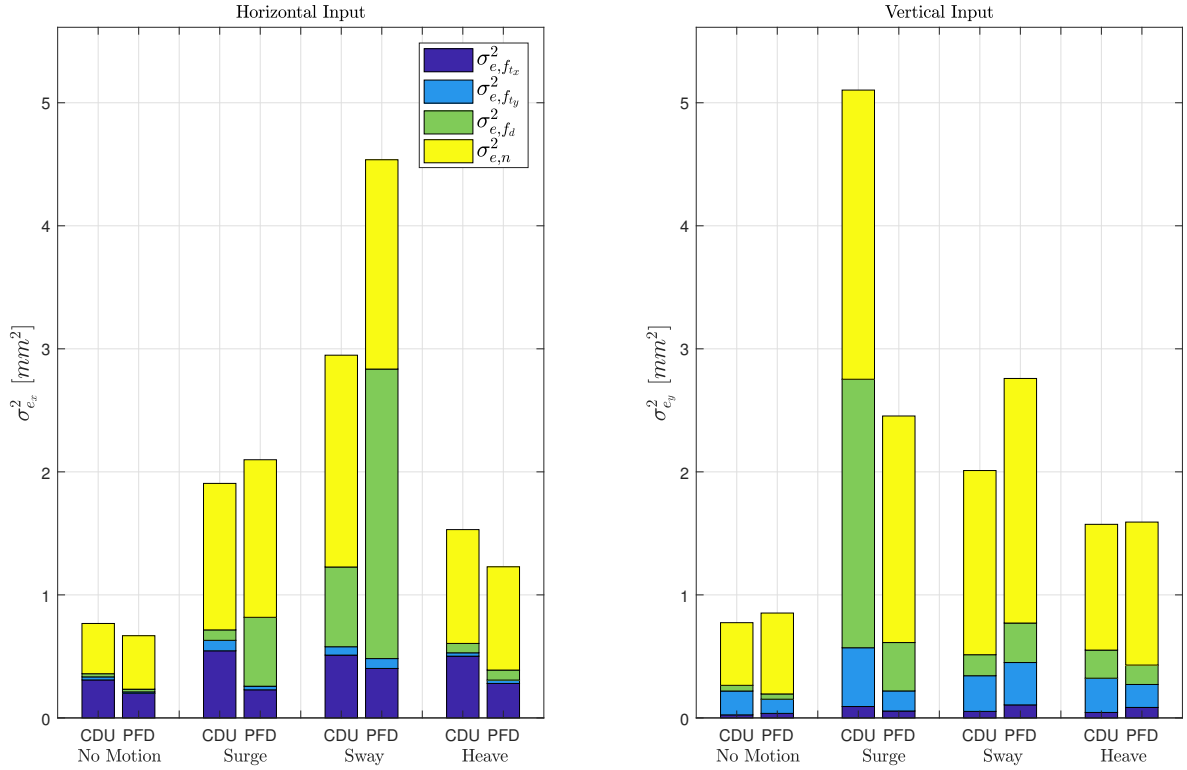

Figure D-5: Error variance components for Participant 6

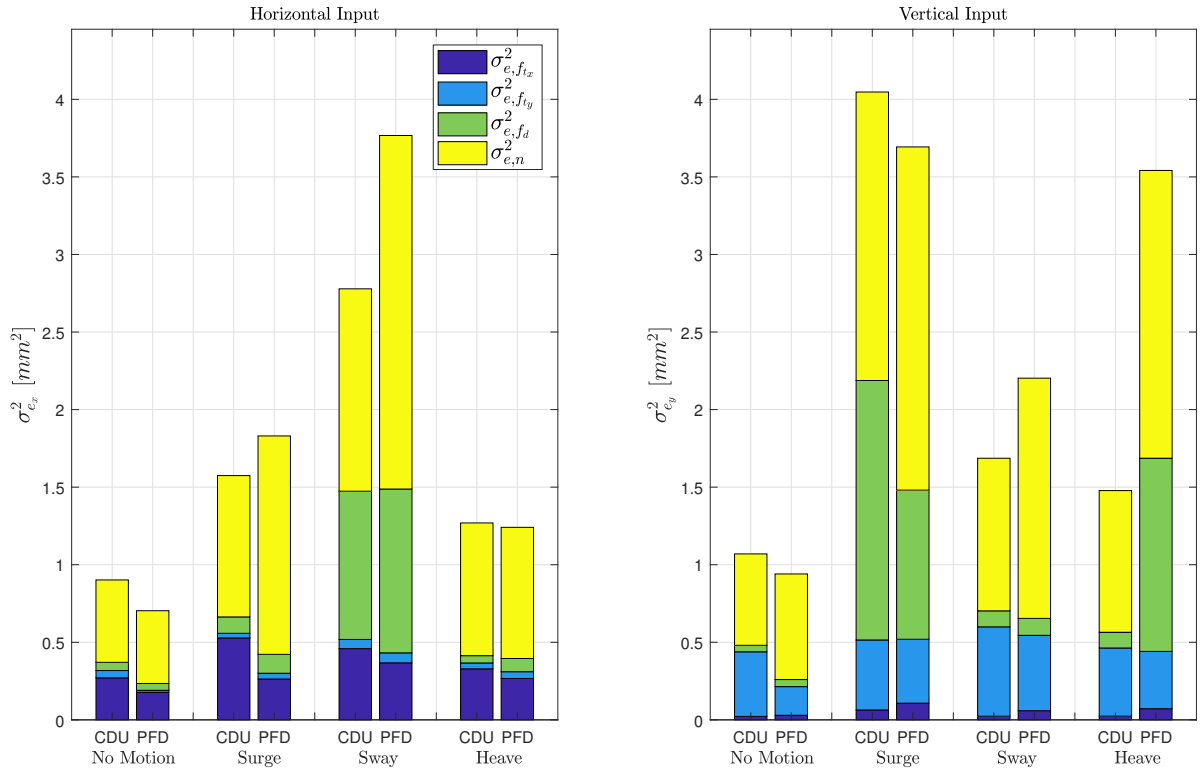

Figure D-6: Error variance components for Participant 7

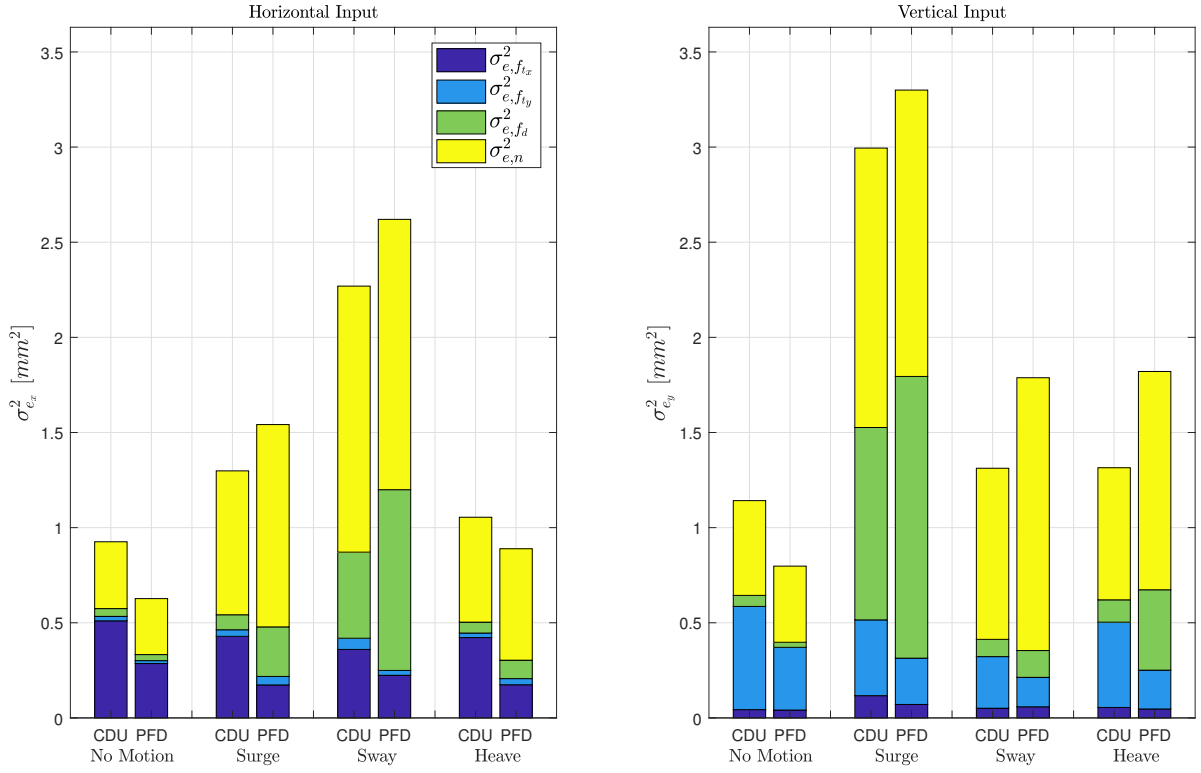

Figure D-7: Error variance components for Participant 8

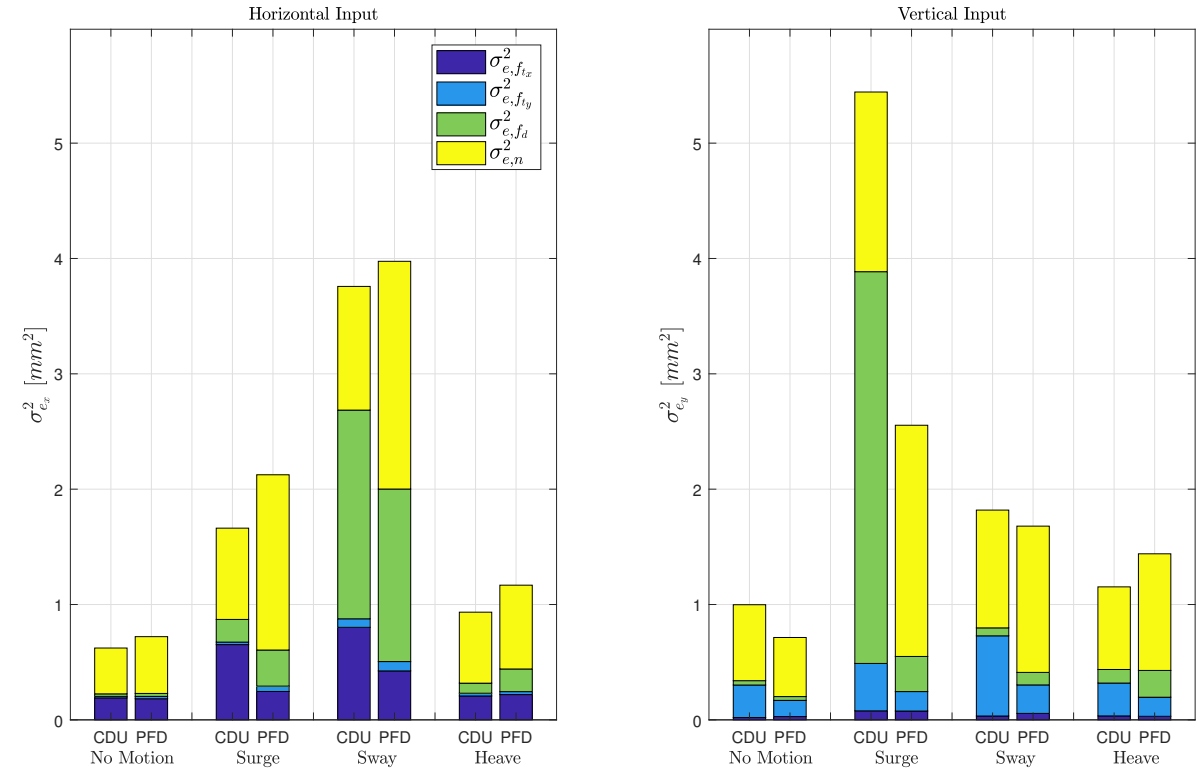

Figure D-8: Error variance components for Participant 9

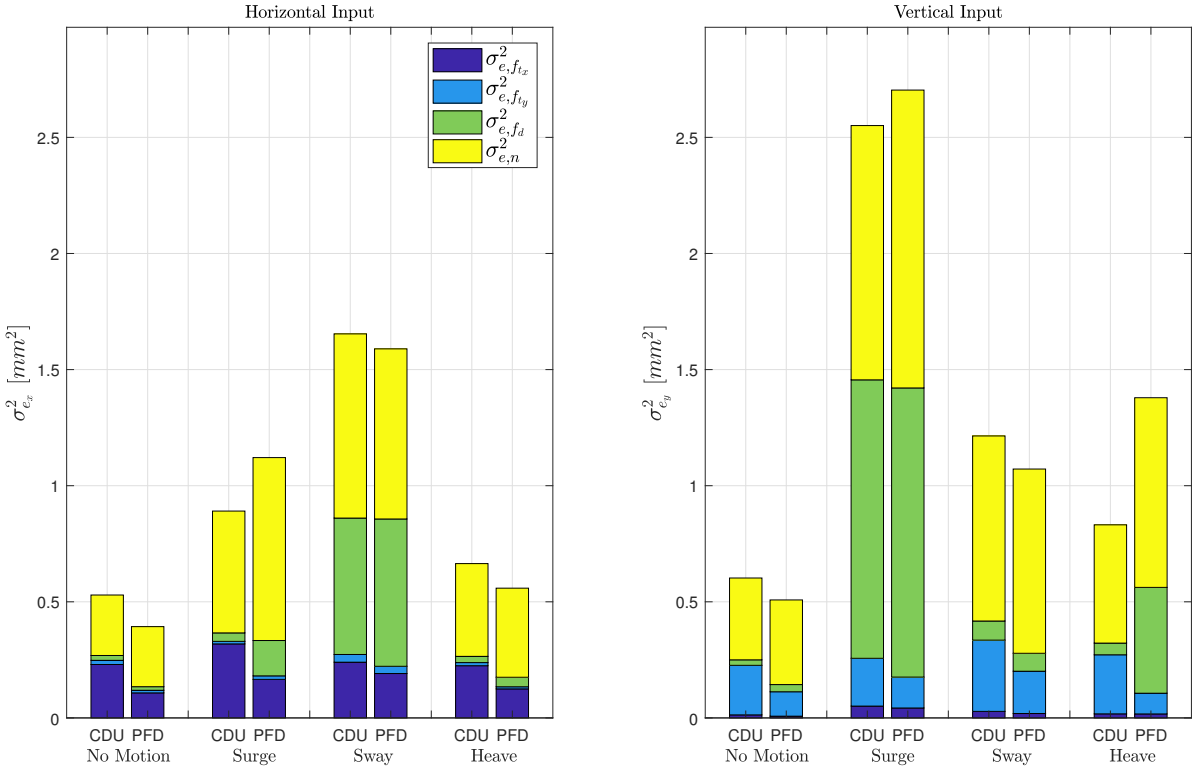

Figure D-9: Error variance components for Participant 10

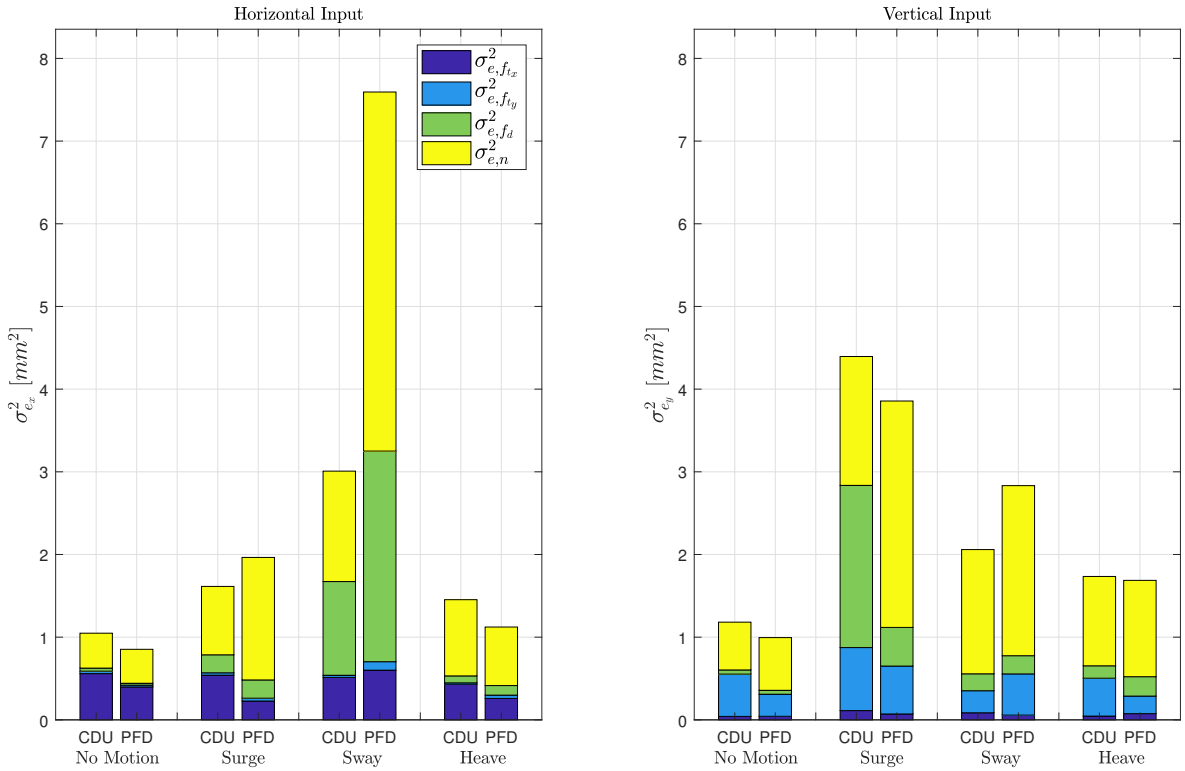

Figure D-10: Error variance components for Participant 11

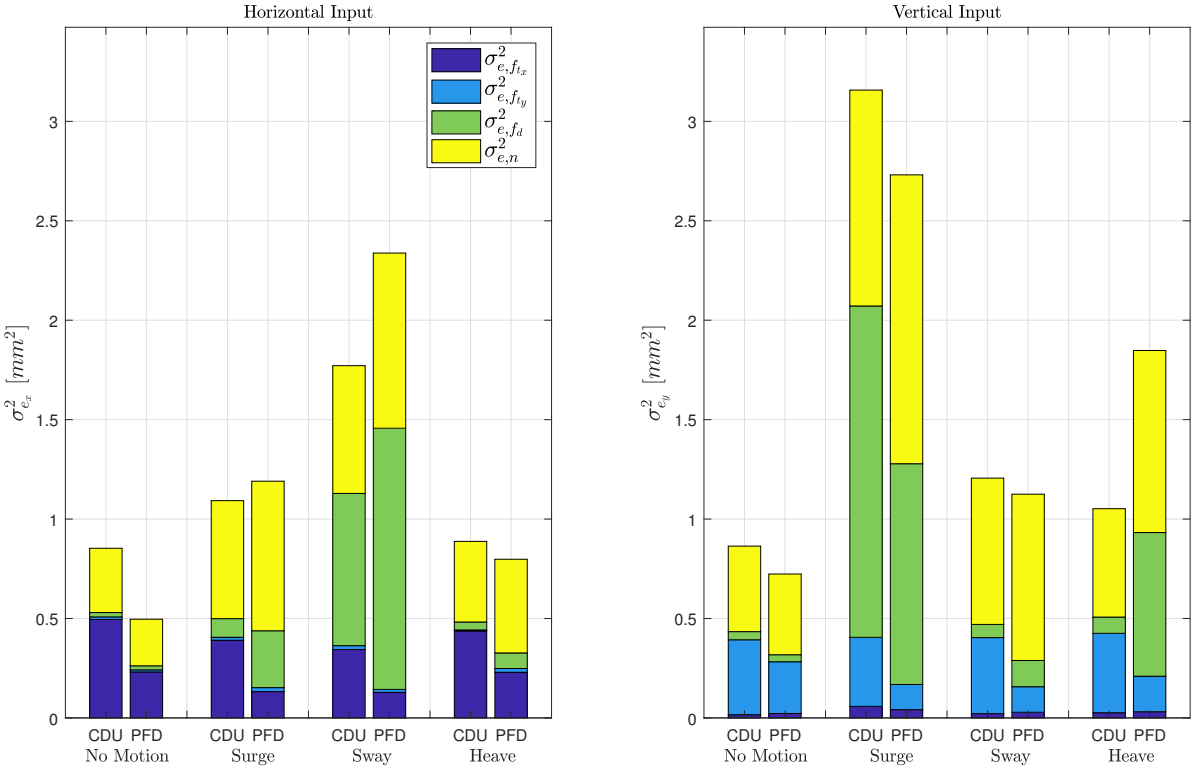

Figure D-11: Error variance components for Participant 12

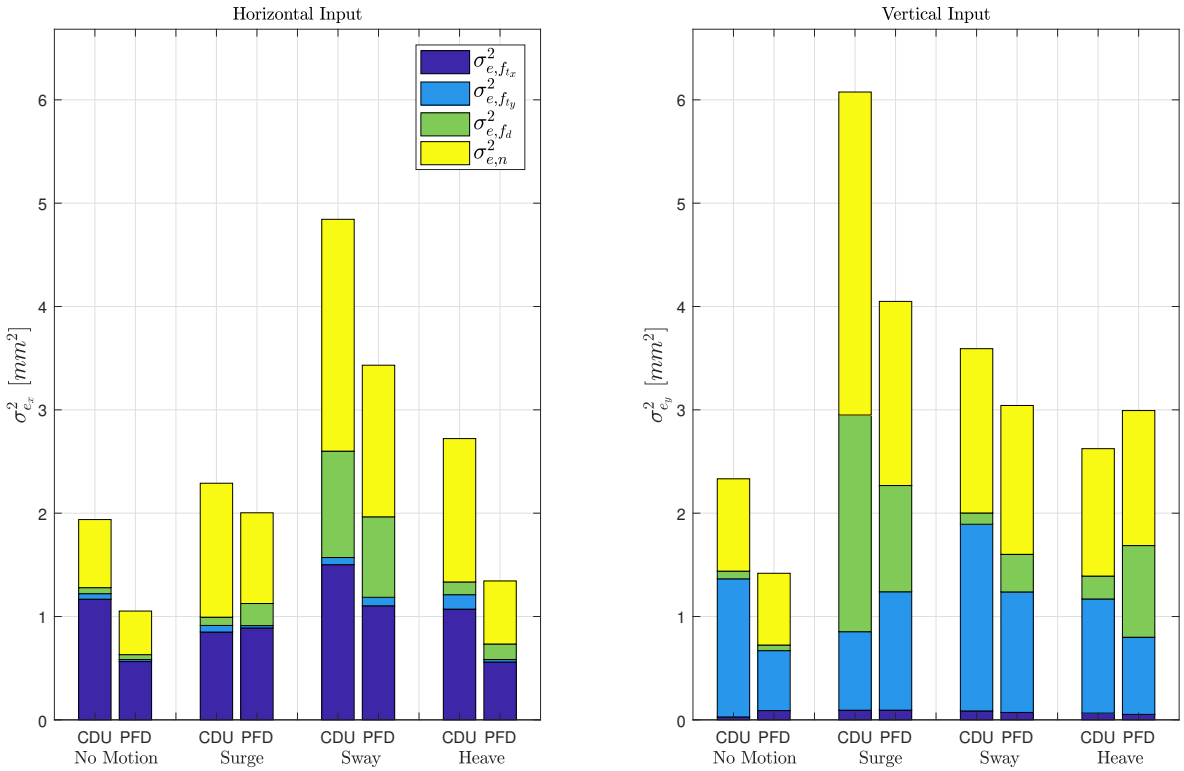

Figure D-12: Error variance components for Participant 13

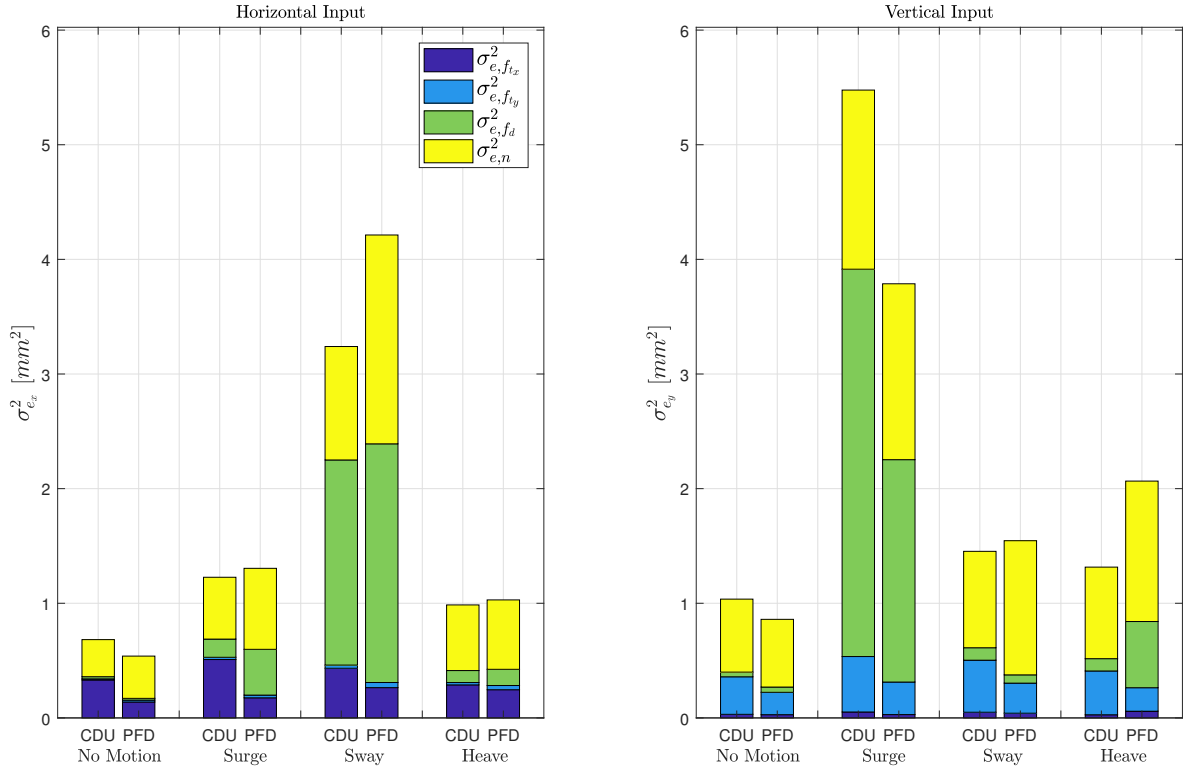

Figure D-13: Error variance components for Participant 14

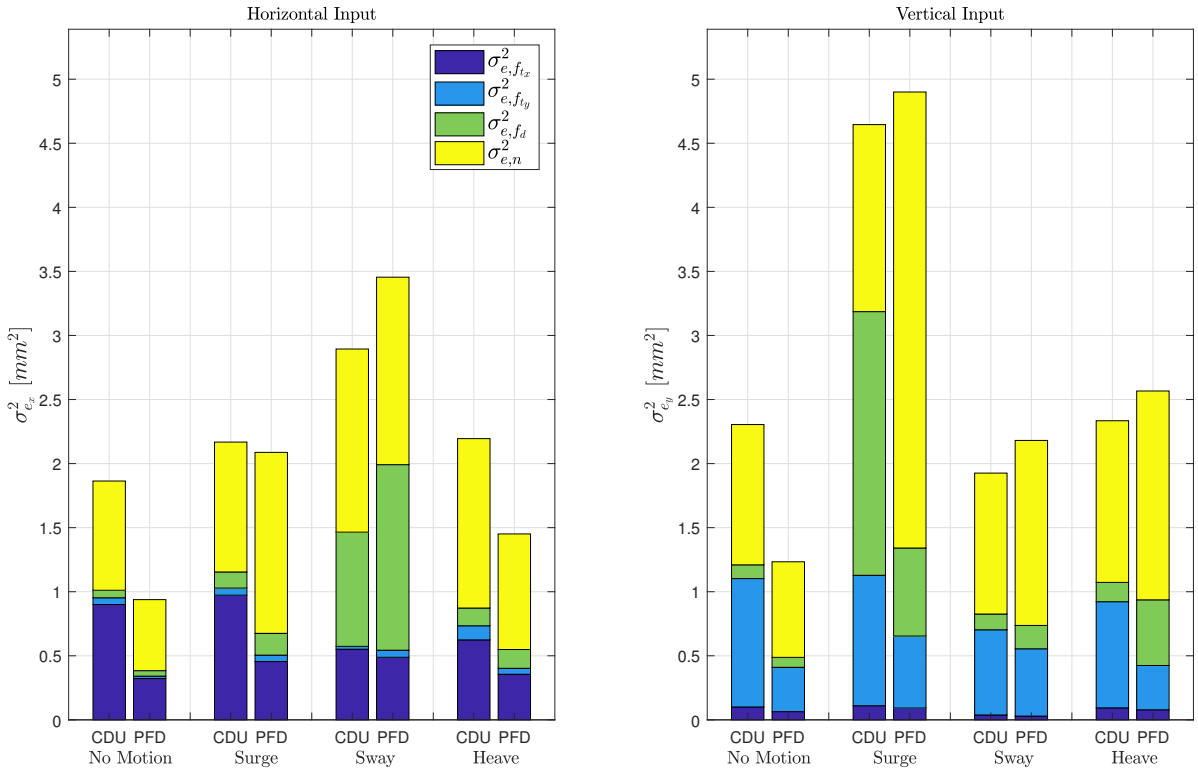

Figure D-14: Error variance components for Participant 15

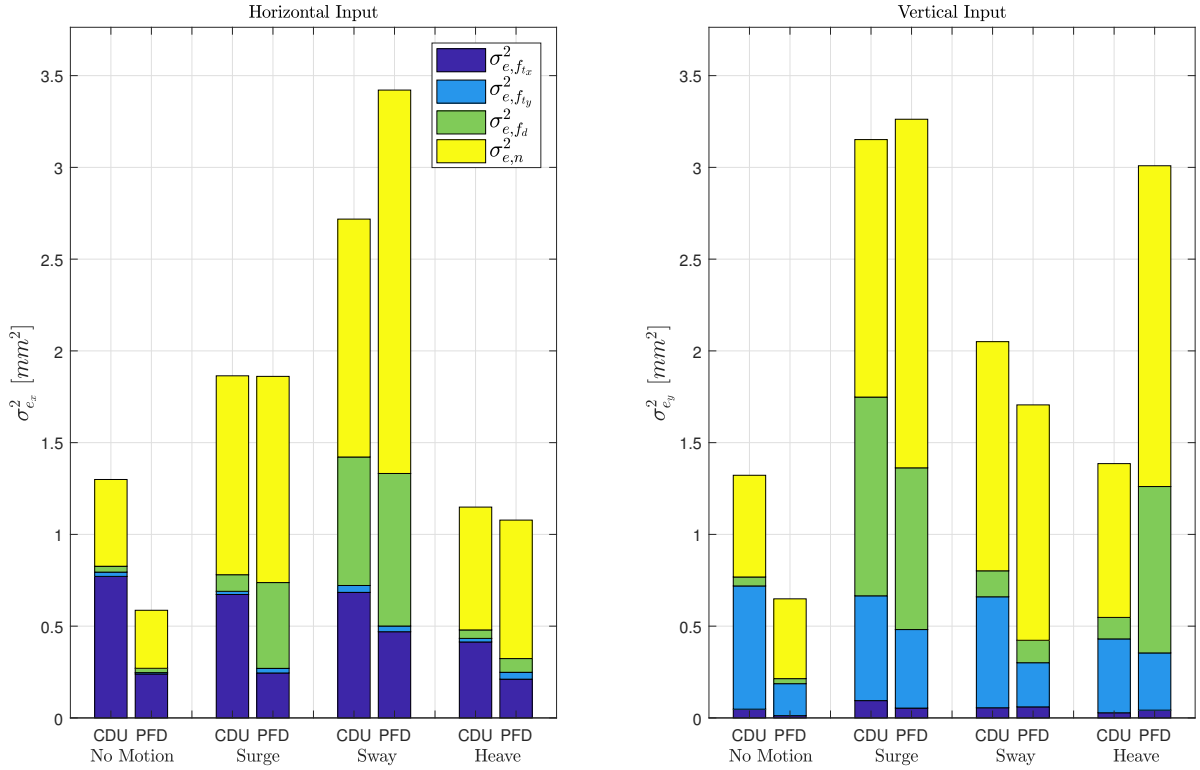

Figure D-15: Error variance components for Participant 16

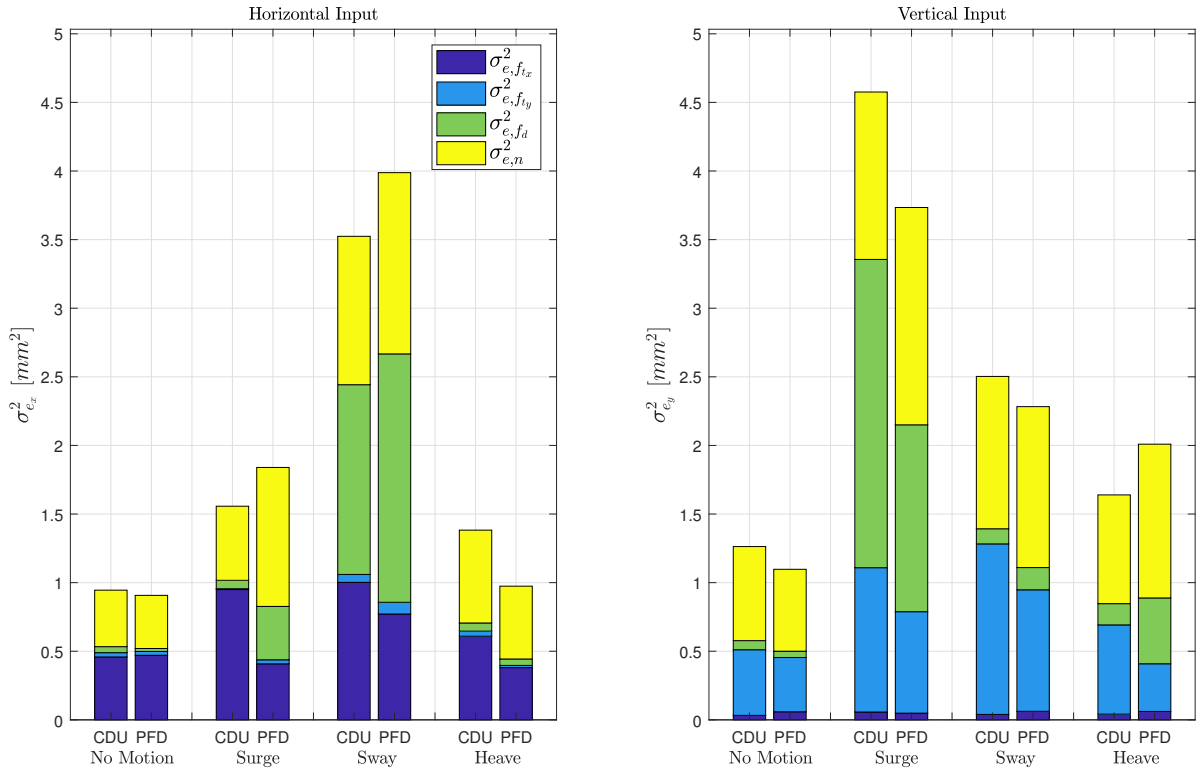

Figure D-16: Error variance components for Participant 17

Appendix E

Experiment Curiosities

• For the main experiment, 17 participants:
  - Performed a total of 1088 successful runs.
  - Dragged a total of 9.846 kilometers.
  - Used a total of 0 sickness bags.
  - Crashed the SIMONA 60 times.

• 4.67 GB's of data collected.

• 20 packages of chocolate were purchased as gratitude gifts for a total of 3.6 kilograms, of which:
  - 18 were handed out to 17 participants.
  - 1 was stolen.
  - 1 was for own consumption.

• The whole graduation project took 208 working days, of which are excluded:
  - 94 weekend days.
  - 6 days taken off for holiday.
  - 22 days taken off for other courses.

Bibliography

[1] Collins, R., "Boeing 777X to feature touchscreen flight displays from Rockwell Collins," `https://www.rockwellcollins.com/Data/News/2016-Cal-Yr/CS/FY16CSNR51-777x.aspx`, 2016, [Online; accessed November 30, 2016].

[2] Wallace, L. E., *Airborne Trailblazer: Two decades with NASA Langley's 737 flying laboratory*, 1994.

[3] Rininger, T. V., "A view of the instrument panel inside a DC-2 in TWA livery, N1943D," `https://www.photoshelter.com`, 2010, [Online; accessed April 9, 2017].

[4] Daniel and Fall, R., "707-329 series cockpit," `www.airliners.net`, [Online; accessed April 9, 2017].

[5] McLellan, A., "Cockpit of a Boeing 737-300 LN-KKU operated by Norwegian Air Shuttle," `www.airliners.net`, 2010, [Online; accessed April 9, 2017].

[6] Naddsy, "A380 cockpit," `www.flickr.com/photos/83823904@N00/64156219`, 2010, [Online; accessed April 9, 2017].

[7] Sarter, N. B. and Woods, D. D., "Pilot Interaction With Cockpit Automation: Operational Experiences With the Flight Management System," *The International Journal of Aviation Psychology*, Vol. 2, No. 4, 1992, pp. 303–321.

[8] Wiener, L., Service, U. S. N. T. I., and Center, A. R., *Human Factors of Advanced Technology ("Glass Cockpit") Transport Aircraft*, NASA contractor report, NASA Ames research Center, 1989.

[9] Johnson, E. A., "Touch display novel input/output device for computers," *Electronics Letters*, Vol. 1, No. 8, October 1965, pp. 219–220.

[10] Avsar, H., Fischer, J. E., and Rodden, T., "Designing Touch-enabled Electronic Flight Bags in SAR Helicopter Operations," *Proceedings of the International Conference on Human-Computer Interaction in Aerospace*, HCI-Aero '16, ACM, New York, NY, USA, 2016, pp. 14:1–14:11.

[11] Garmin, "Garmins G3000 Integrated Flightdeck Brings Touchscreen and Widescreens to the Cockpit," `http://newsroom.garmin.com/press-release/aviation/garmins-g3000-integrated-flightdeck-brings-touchscreen-and-widescreens-cockpi`, October 2009, [Online; accessed January 30, 2017].

[12] Collins, R., "Rockwell Collins unveils touch-control flight displays to enable natural," `http://www.rockwellcollins.com/sitecore/content/Data/News/2011_Cal_Yr/CS/FY11CSNR50-touch-controlled-flight-display.aspx`, July 2011, [Online; accessed January 30, 2017].

[13] Boeing, "Touchscreens come to 777X flight deck," `www.boeing.com`, 2016, [Online; accessed April 9, 2017].

[14] Thales, "Thales Furthers Future Cockpit Functionality," `www.airtrafficmanagement.net`, 2012, [Online; accessed April 9, 2017].

[15] Albinsson, P.-A. and Zhai, S., "High Precision Touch Screen Interaction," *Proceedings of the SIGCHI Conference on Human Factors in Computing Systems*, CHI '03, ACM, New York, NY, USA, 2003, pp. 105–112.

[16] MacKenzie, I. S., Sellen, A., and Buxton, W. A. S., "A Comparison of Input Devices in Element Pointing and Dragging Tasks," *Proceedings of the SIGCHI Conference on Human Factors in Computing Systems*, CHI '91, ACM, New York, NY, USA, 1991, pp. 161–166.

[17] Dodd, S. R., Lancaster, J., Grothe, S., DeMers, B., Rogers, B., and Miranda, A., "Touch on the flight deck: The impact of display location, size, touch technology and turbulence on pilot performance," *Proceedings of the IEEE/AIAA 33rd Digital Avionics Systems Conference (DASC)*, 2014.

[18] Rider, K. A., "Effects of ride motion perturbations on the speed and accuracy of in-vehicle reaching tasks," 2006, pp. 1–180.

[19] Bisschop, J. F., *The effects of motion induced interference on the use of touch interfaces in a cockpit*, Master's thesis, Delft University of Technology, Faculty of Aerospace Engineering, July 2012.

[20] Bonelli, S. et all, "The usability evaluation of a touch screen in the flight deck," *Cases on Usability Engineering*, Vol. 53, IGI Global, 2013, p. 270297.

[21] Bjørneseth, F. B., Dunlop, M. D., and Hornecker, E., "Assessing the effectiveness of direct gesture interaction for a safety critical maritime application," *International Journal of Human Computer Studies*, Vol. 70, No. 10, 2012, pp. 729–745.

[22] Berg, V. D., Damveld, H. J., Borst, C., Paassen, M. M. V., and Mulder, M., "Investigating the Effects of Turbulence and Spatial Gesture Thresholds on Multi-Touch Interaction," 2017.

[23] N. Goode, M. G. Lenn and P. Salmon, "The impact of on-road motion on BMS touch screen device operation," *Ergonomics*, Vol. 55, No. 9, 2012, pp. 986–996.

[24] Venrooij, J., *Measuring, modeling and mitigating biodynamic feedthrough*, Ph.D. thesis, Delft University of Technology, March 2014.

[25] Parks, D., "Defining Human Reaction to Whole-Body Vibration," *Human Factors*, Vol. 4, 1962, pp. 305–314.

[26] McLeod, R. and Griffin, M. J., "A design guide for visual displays and manual tasks in vibration environments. Part 2: Manual tasks," 1986.

[27] Griffin, M., *Handbook of Human Vibration*, 988 p, Academic Press, 1996.

[28] Mulder, J. A., Van Staveren, W. H. J. J., Van der Vaart, J. C., Mulder, M., and Chu, Q. P., *Aircraft Responses to Atmospheric Turbulence Lecture Notes*, Delft University of Technology, November 2016.

[29] Ruijgrok, G. J. J., *Gegevens van de atmosfeer.*, Technische Hogeschool Delft, 1970.

[30] Andrews, D. G., Holton, J. R., and Leovy, C. B., *Middle atmosphere dynamics*, No. 40, Academic press, 1987.

[31] scientifique et technique internationale du vol à voile, O. and Organization, W. M., *Weather Forecasting for Soaring Flight*, OMM (Collection), World Meteorological Organization, 2009.

[32] Administration, F. A., "Aeronautical Information Manual," 2015.

[33] Pritchard, F. E., "A Statistical Model of Atmospheric Turbulence and a Review of the Assumptions Necessary for Its Use," Tech. Rep. AGARD No. CP.17 Pt.II, Paris: Advisory Group for Aerospace Research and Development, 1966.

[34] Gerlach, O. H., and Schuring, J., "Mathematical Model of External Disturbances Acting on an Aircraft During an ILS Approach and Landing," Tech. Rep. VTH-159, Delft University of Technology, 1970.

[35] Bauersfeld, K., "Effects of turbulence and activation method on touchscreen performance in aviation environments," 1992.

[36] Mansfield, N. J., *Human response to vibration*, CRC press, 2004.

[37] McLeod, R. and Griffin, M. J., "Mechanisms of vibration-induced interference with manual control performance," *Ergonomics*, Vol. 38, No. 7, 1995, pp. 1431–1444.

[38] Motortrend.com, "2010 BMW 535i Gran-Turismo menu button," `http://www.motortrend.com/cars/bmw/5-series/2010/2010-bmw-535i-grand-turismo-verdict/`, December 2011, [Online; accessed April 15, 2017].

[39] Karat, J., McDonald, J. E., and Anderson, M., "A comparison of menu selection techniques: Touch panel, mouse and keyboard." *International Journal of Man-Machine Studies*, Vol. 25, No. 1, 1986, pp. 73–88.

[40] ipadpilotnews.com, "Whats the best iPad for pilots?" `http://ipadpilotnews.com/2017/05/whats-best-ipad-pilots-2/`, 2017, [Online; accessed May 30, 2017].

[41] Kaminani, S., "Human computer interaction issues with touch screen interfaces in the flight deck," *AIAA/IEEE Digital Avionics Systems Conference - Proceedings*, 2011.

[42] Sears, A. and Shneiderman, B., "High Precision Touchscreens: Design Strategies and Comparisons with a Mouse," *Int. J. Man-Mach. Stud.*, Vol. 34, No. 4, April 1991, pp. 593–613.

[43] Lin, C. J., Hsieh, Y.-H., Chen, H.-C., and Chen, J. C., "Visual performance and fatigue in reading vibrating numeric displays," *Displays*, Vol. 29, No. 4, 2008, pp. 386 – 392.

[44] Degani, A., Palmer, E. A., and Bauersfeld, K. G., "Soft Controls for Hard Displays: Still a Challenge," *Proceedings of the Human Factors and Ergonomics Society Annual Meeting*, Vol. 36, No. 1, 1992, pp. 52–56.

[45] Apple, "Gesture Recognizer Basics," `https://developer.apple.com/library/content/documentation/EventHandling/Conceptual/EventHandlingiPhoneOS/index.html`, 2017, [Online; accessed April 10, 2017].

[46] Google, "Using Touch Gestures," `https://material.io/guidelines/patterns/gestures.html#`, 2017, [Online; accessed April 10, 2017].

[47] Mertens, M. and Damveld, H. J., "An avionics touch screen-based control display concept," *Proceedings of SPIE - The International Society for Optical Engineering*, Vol. 8383, No. 0, 2012, pp. 83830L.

[48] Stuyven, G., Damveld, H., and Borst, C., "Concept for an Avionics Multi Touch Flight Deck," *SAE Int. J. Aerosp.*, Vol. 5, 10 2012, pp. 164–171.

[49] Beringer, D. and Lee, K., "Parameters influencing the airborne application of touch devices for data entry and retrieval. Phase 1: Technological, positional and chronological effects (Tech Report HFRL-88-2/MDHC-88-1). New Mexico State University, Department of Psychology," *Human Factors Research Laboratory*, 1988.

[50] Honeywell, "New Honeywell Technologies Including Touchscreens in Cockpit Help Gulfstream's Newest Aircraft Take Flight," October 2014, `https://www.honeywell.com/newsroom/pressreleases/2014/10/new-honeywell technologies-including-touchscreens-in-cockpit-help-gulfstream-s-newest-aircraft-take-flight-newest-aircraft-take-flight` [Online; accessed April 17, 2017],.

[51] Gulfstream, "Gulfstream Symmetry Flight Deck," `http://www.gulfstream.com/technology/symmetry-flight-deck`, 2014, [Online; accessed April 17, 2017].

[52] Thales, "Thales Unveils Avionics 2020 Future Cockpit," `https://www.thalesgroup.com/en/worldwide/aerospace/press-release/thales-unveils-avionics-2020-cockpit-future`, June 2013, [Online; accessed April 9, 2017].

[53] Avsar, H., Fischer, J., and Rodden, T., "Future flight decks: impact of +Gz on touchscreen usability," *International Conference on Human Computer Interaction in Aerospace: HCI-Aero*, 2016.

[54] McRuer, D. T., Graham, D., Krendel, E. S., and Reisener, W. J., "Human Pilot Dynamics in Compensatory Systems, Theory Models and Experiments with Controlled Element and Forcing Function Variations," Tech. Rep. AFFDL-TR-65-15, Air Force Flight Dynamics Laboratory, Wright-Patterson Air Force Base (OH), 1965.

[55] Zaal, P. M. T., Pool, D. M., de Bruin, J., Mulder, M., and van Paassen, M. M., "Use of Pitch and Heave Motion Cues in a Pitch Control Task," *Journal of Guidance, Control, and Dynamics*, Vol. 32, No. 2, 2009, pp. 366–377.

[56] Stapleford, R. L., McRuer, D. T., and Magdaleno, R. E., "Pilot Describing Function Measurements in a Multiloop Task," *IEEE Transactions on Human Factors in Electronics*, Vol. 8, No. 2, June 1967, pp. 113–125.

[57] Stapleford, R. L., Peters, R. A., and Alex, F. R., "Experiments and a Model for Pilot Dynamics with Visual and Motion Inputs," Tech. Rep. NASA CR-1325, Systems Technology, Inc., Hawthorne (CA), 1969.

[58] Hess, R. A., "Model for Human Use of Motion Cues in Vehicular Control," *Journal of Guidance, Control, and Dynamics*, Vol. 13, No. 3, 1990, pp. 476–482.

[59] van der Vaart, J. C., *Modelling of Perception and Action in Compensatory Manual Control Tasks*, Ph.D. thesis, Delft University of Technology, Faculty of Aerospace Engineering, 1992.

[60] Hosman, R. J. A. W., *Pilot's Perception and Control of Aircraft Motions*, Ph.D. thesis, Delft University of Technology, Faculty of Aerospace Engineering, 1996.

[61] Nieuwenhuizen, F. M., Zaal, P. M. T., Mulder, M., van Paassen, M. M., and Mulder, J. A., "Modeling Human Multichannel Perception and Control Using Linear Time-Invariant Models," *Journal of Guidance, Control, and Dynamics*, Vol. 31, No. 4, July-August 2008, pp. 999–1013.

[62] Ellerbroek, J., Stroosma, O., Mulder, M., and van Paassen, M. M., "Role Identification of Yaw and Sway Motion in Helicopter Yaw Control Tasks," *Journal of Aircraft*, Vol. 45, No. 4, July/August 2008, pp. 1275–1289.

[63] Barendswaard, S., Pool, D. M., and Mulder, M., "Human Crossfeed in Dual-Axis Manual Control with Motion Feedback," *Proceedings of the 13th IFAC/IFIP/IFORS/IEA Symposium on Analysis, Design, and Evaluation of Human-Machine Systems, Kyoto, Japan*, 2016.

[64] Van Wieringen, A. T., Pool, D. M., van Paassen, M. M., and Mulder, M., "Effects of Heave Washout Filtering on Motion Fidelity and Pilot Control Behavior for a Large Commercial Airliner," *Proceedings of the AIAA Modeling and Simulation Technologies Conference, Portland, Oregon, Aug. 8-11*, No. AIAA-2011-6323, 2011.

[65] Zaal, P. M. T. and Pool, D. M., "Multimodal Pilot Behavior in Multi-Axis Tracking Tasks with Time-Varying Motion Cueing Gains," *Proceedings of the AIAA Modeling and Simulation Technologies Conference, National Harbor (MD)*, No. AIAA-2014-0810, Jan. 2014.

[66] Pintelon, R. and Schoukens, J., *System identification: A frequency domain approach*, IEEE Press, 2001.

[67] Stroosma, O., van Paassen, M. M., and Mulder, M., "Using the SIMONA Research Simulator for Human-machine Interaction Research," *Proceedings of the AIAA Modeling and Simulation Technologies Conference and Exhibit, Austin, Texas, Aug. 11-14, 2003*, No. AIAA-2003-5525, Aug. 2003, pp. 1–8.

[68] Mulder, J. A., Van Staveren, W. H. J. J., Van der Vaart, J. C., Mulder, M., and Chu, Q. P., *AE4304 Flight Dynamics Lecture Notes*, Delft University of Technology, 2016.

[69] Jex, H. R., Magdaleno, R. E., and Junker, A. M., "Roll Tracking Effects of G-vector Tilt and Various Types of Motion Washout," *Proceedings of the Fourteenth Annual Conference on Manual Control*, 1978, pp. 463–502.

[70] Abbink, D. A. and Mulder, M., "Neuromuscular analysis as a guideline in designing shared control," *Advances in haptics*, InTech, 2010.

[71] Zaal, P. M. T. and Mobertz, X. R. I., *Effects of Motion Cues on the Training of Multi-Axis Manual Control Skills*, AIAA AVIATION Forum, American Institute of Aeronautics and Astronautics, Jun 2017, 0.

[72] Zaal, P. M. T., Pool, D. M., de Bruin, J., Mulder, M., and van Paassen, M. M., "Use of Pitch and Heave Motion Cues in a Pitch Control Task," *Journal of Guidance, Control, and Dynamics*, Vol. 32, No. 2, March–April 2009, pp. 366–377.